Factors that Impact Photochemical Cage Escape Yields

Matthew J. Goodwin,[a] John C. Dickenson,[a] Alexia Ripak[b], Alexander M. Deetz,[a] Jackson S. McCarthy, [a] Gerald J. Meyer,[a*] and Ludovic Troian-Gautier[b,c*]

[a]Department of Chemistry, University of North Carolina at Chapel Hill, Chapel Hill, North Carolina, 27599, United States

[b]Université catholique de Louvain (UCLouvain), Institut de la Matière Condensée et des Nanosciences (IMCN), Molecular Chemistry, Materials and Catalysis (MOST), Place Louis Pasteur 1, bte L4.01.02, 1348 Louvain-la-Neuve, Belgium

[c]Wel Research Institute, Avenue Pasteur 6, 1300 Wavre, Belgium

*Correspondence to: ludovic.troian@uclouvain.be, gjmeyer@email.unc.edu

Abstract. The utilization of visible light to mediate chemical reactions in fluid solutions has applications that range from solar fuel production to medicine and organic synthesis. These reactions are typically initiated by electron transfer between a photoexcited dye molecule (a photosensitizer) and a redox active quencher to yield radical pairs that are intimately associated within a solvent cage. Many of these radicals undergo rapid thermodynamically favored "geminate" recombination and do not diffuse out of the solvent cage that surrounds them. Those that do escape the cage are useful reagents that may undergo subsequent reactions important to the above-mentioned applications. The cage-escape process and the factors that determine the yields remain poorly understood despite decades of research motivated by their practical and fundamental importance. Herein, state-of-the-art research on light-induced electron transfer and cage escape that has appeared since the seminal 1972 review by J. P. Lorand entitled "The Cage Effect" is reviewed. This review also provides some background for those new to the field and discusses the cage escape process of both homolytic bond photo-dissociation and bimolecular light induced electron transfer reactions. The review concludes with some key goals and directions for future research that promise to elevate this very vibrant field to even greater heights.

Contents

1) Introduction, Background and Motivation

The use of sunlight or artificial light to drive reactions that would otherwise be thermodynamically uphill is central to energy conversion[1-22] and represents an emerging area in organic synthesis.[23-26] The reaction of photo-excited photosensitizers (PS*) with electron acceptors or donors (quenchers) provide redox equivalents that have been utilized for solar energy conversion applications and to drive subsequent reactions that yield useful products, **Figure 1**. *Oxidative quenching* refers to the oxidation of a PS* by an electron acceptor; conversely, *reductive quenching* corresponds to the reduction of PS* by an electron donor. The importance of these reactions is that they provide a molecular basis for the conversion of the energy present in PS* into free energy in the form of the redox equivalents. Indeed, the reduced or the oxidized PS products are of keen interest as catalysts in organic photoredox catalysis.[23-26] Oxidative and reductive quenching are often collectively referred to as *charge separation* and have been utilized in photoredox catalysis and photobiology as well as to generate electrical power in regenerative solar cells and solar fuels in photo-electrosynthetic cells.

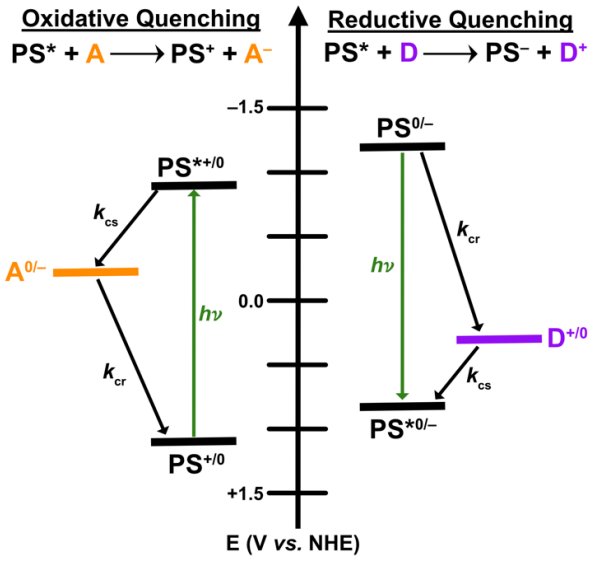

Figure 1. Oxidative (left) and reductive (right) excited-state quenching of PS* with an electron acceptor (A) or electron donor (D) to form the corresponding photoproducts that transiently store free energy in the form of redox equivalents. The rate constants for charge separation (k_{cs}) and charge recombination (k_{cr}) are presented for the given processes. For oxidative quenching, the excited photosensitizer transfers an electron to an acceptor and is hence oxidized; charge recombination occurs by electron transfer from the reduced acceptor to the oxidized photosensitizer. For reductive quenching, the excited photosensitizer accepts an electron from a donor and charge recombination occurs by electron transfer from the reduced photosensitizer to the oxidized donor.

The bimolecular reaction between a PS* and a quencher (Q) is of both fundamental and practical interest. A quencher is a species, typically a molecule or ion, that deactivates (quenches) an excited state by energy transfer, electron transfer, or a chemical mechanism. In this review, the term quencher is used exclusively to describe electron transfer quenching by an acceptor or donor that results in oxidative or reductive quenching, respectively. The accepted mechanism for such bimolecular reactivity involves diffusional interactions between PS* and Q to form what has been historically termed an "encounter complex," comprised of PS* and Q surrounded by solvent molecules that constitute the "solvent cage", shown as brackets in **Figure 2**. It is within this encounter complex that excited-state electron transfer may occur. The encounter complex between PS* and Q is shown in brackets to signify that the structure is poorly understood and loosely envisioned to be solvent molecules that form a "cage" around the PS* and Q reactants.

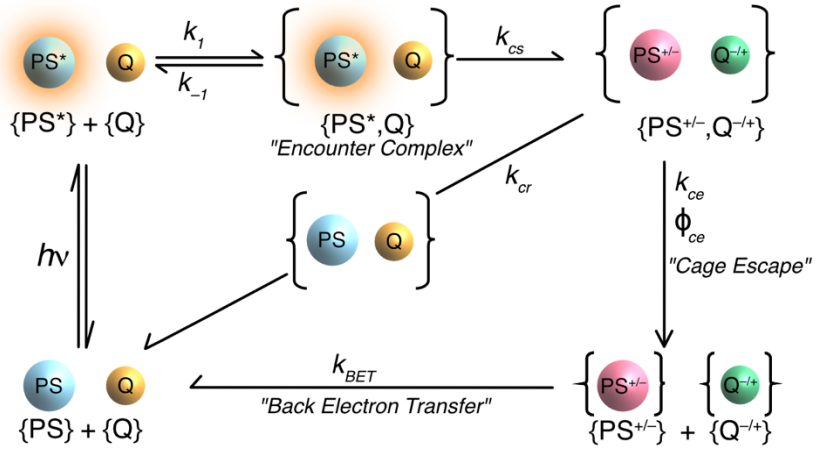

Figure 2. Photophysical scheme used to describe the sequence of events involved in a bimolecular electron transfer reaction between a photosensitizer (PS) and a quencher (Q) triggered by the absorption of a photon (hν). The electron transfer processes are characterized by the corresponding kinetic rate constants: charge separation (k_{cs}), charge recombination (k_{cr}), cage escape (k_{ce}) and back-electron transfer (k_{BET}). Note that this description is for a dynamic quenching process. An alternative mechanism, termed static quenching, occurs when the photosensitizer and quencher form a ground state adduct, thereby precluding the need for diffusion to form the encounter complex. The events following excited-state electron transfer are valid for both static and dynamic quenching mechanisms.

Excited-state quenching reactions have been quantified for over a hundred years employing the time-honored model described by Stern and Volmer.[27-29] Typically the photoluminescence intensity of PS* is measured as a function of the quencher concentration, [Q]. A first-order dependence on [Q] allows extraction of the Stern-Volmer constant, K_{sv}, the reciprocal of which is equal to the quencher concentration necessary to quench half of the excited photosensitizers. Knowledge of the excited-state lifetime of PS*

affords the bimolecular quenching rate constant (k_q). Hence the Stern-Volmer model provides a means to analyze steady state photoluminescence quenching data and extract kinetic and efficiency values whose importance to the field of photochemistry cannot be overstated.[30-38]

A common misconception is that every quenched PS* yields an oxidized or reduced quencher and the corresponding reduced or oxidized PS that are useful for subsequent redox reaction(s) of interest.[27] In other words, it is often concluded that if one completely quenches PS* such that there is no significant photoluminescence from the photosensitizers, the fully solvated oxidized or reduced quencher will be formed in quantitative yield and will carry on subsequent reaction(s). This, however, is rarely the case. Instead, complete quenching simply means that all the PS* are quenched to form the corresponding charge-separated products that are trapped within the same solvent cage as the encounter complex. This species is often called the *geminate radical pair* or the *primary radical ion-pair*. The cage-escape process, *i.e.* the physical separation of the geminate radical pair, is a prerequisite for these products to be useful and typically only a small fraction is able to escape. Product yields are typically much less than unity and as such, a better understanding of this process would allow for much more efficient applications in which light plays a role. *Our understanding of the factors that impact the yield of charge-separated products is the subject of this review.*

The accepted and common explanation for small yields of solvated products when quenching of PS* seems quantitative is that a fraction of the geminate radical pair products recombines within the same "solvent cage" that they were created in. This process is termed *geminate charge recombination* and leads to the recovery of the initial ground-state reactants. To better visualize this, consider again the accepted mechanism for diffusional quenching shown in **Figure 2**.[39-41] An important consequence of the solvent cage is that entrapped reactants undergo multiple collisions within the cage. This has the detrimental effect of enhancing the unwanted geminate charge recombination reaction of the radical pair that is necessarily thermodynamically downhill. As a result, the geminate charge recombination rate constant, k_{cr}, often kinetically outcompetes cage escape, thereby lowering the yield of sought-after products. Hence a PS* quenched by Q quantitatively forms the charge-separated products in a geminate radical pair, but only *within a solvent cage.* The yield of useful products therefore corresponds only to those that escape the solvent cage. Unfortunately, most reported cage escape yields are far less than unity. As reactivity in solvent cages is not well understood, non-zero yields may be viewed as encouraging because they suggest that a deeper knowledge of encounter complexes may one day allow the rational design of 'windows' through which the caged products can escape.

The kinetic rate constants (k_x) indicated in **Figure 2** govern the overall cage escape yield and have in some cases been determined experimentally. Cage-escape occurs with the rate constant (k_{ce}) that competes kinetically with geminate charge recombination (k_{cr}). Most often it is the cage escape yield (ϕ_{ce}) that is most interesting to experimentalists. We emphasize again that factors that govern the cage escape process are, to date, poorly understood even though they are of paramount relevance to societally desirable photo-induced applications, *i.e.* photoredox catalysis,[23-24, 42-61] solar fuel formation (such as hydrogen gas generation),[43-45, 49, 62-69] and photochemotherapy.[70-78]

In principle, the inherent electron transfer reactivity within the transient encounter complex is described most notably through the work of Rudolph Marcus, who developed the canonical Marcus theory for electron transfer that resulted in the 1992 Nobel prize[32-34] as well as through the advances of Rehm and Weller.[30-31] Yet, there are few experimental means to extract the critical Marcus parameters for electron transfer within an encounter complex. This is particularly true for the diffusional quenching of PS*, but less so for the photodissociative excited states described in Section 3 of this review that, by virtue of the Franck-Condon principle, are formed in the same solvent cage as the ground state.[35-36, 38]

Figure 2 is key to understanding diffusional excited state electron transfer that will be presented within Section 4 of this review in more detail. As such, terms such as: quencher, oxidative and reductive quenching, geminate radical pair, cage effect, charge separation, charge recombination, cage escape and back-electron transfer are of paramount importance for the understanding of this review and have thus been described in **Table 1**. The sheer number of papers related to the topic of "cage escape" clearly demonstrates an appreciation for the importance of this elementary step in photochemistry.[35-36, 38, 79-80] Before presenting these publications and their implications, it is worthwhile to consider carefully what experimental findings underlie the mechanism proposed in **Figure 2**. Below, we first discuss the historical evidence for a solvent cage and the geminate recombination within it.

Table 1. Definitions of useful terms used throughout this review.

Term	Definition
Quencher	A molecular entity that deactivates (quenches) an excited state of another molecular entity, either by energy transfer, electron transfer, or by a chemical mechanism. In this review, this term is used exclusively to describe quenching by reductive or oxidative electron transfer.
Oxidative Quenching	Reaction in which the excited photosensitizer is oxidized by an electron acceptor. $PS^* + Q \longrightarrow PS^{\bullet+} + Q^{\bullet-}$
Reductive Quenching	Reaction in which the excited photosensitizer is reduced by an electron donor.

	$PS^* + Q \longrightarrow PS^{\bullet-} + Q^{\bullet+}$
Charge Separation	In this review, charge separation is used to describe the excited-state electron transfer process leading to a pair or radicals enclosed in the solvent cage. This process is associated with the corresponding kinetic rate constant k_{cs}.
Geminate Radical Pair	A pair of radicals that are formed through the charge separation process and that have not yet escaped the cage. This species is also often called the "primary radical ion-pair" in the literature.
Cage Effect	When in a condensed phase, or in a dense gas, reactant molecules come together, or species are formed in proximity to one another, and are caged in by surrounding molecules, they may undergo a set of collisions known as an encounter; the term 'Cage Effect' is then applied. The cage effect is also known as the Franck–Rabinowitsch effect.
Charge Recombination	In this review, charge recombination is used to describe the process that leads to the ground-state products from the geminate radical pair within the solvent cage. This process is associated with the corresponding kinetic rate constant k_{cr}.
Cage Escape	Process by which the geminate radical pair escapes the solvent cage to form the corresponding radicals that are independently solvated. This process is associated with the corresponding rate constant (k_{ce}) and cage-escape yield ϕ_{ce}. This process is sometimes also referred to as the "free radical ion quantum yield" in the literature.
Back-Electron Transfer	In this review, back-electron transfer is used to describe the process that leads to the ground-state products from the solvent-separated radical pair with a corresponding kinetic rate constant k_{BET}. Back electron transfer is thus different from the charge recombination process described above.

1.1) The Solvent Cage

The concept of a solvent cage was first expressed in 1934 by Franck and Rabinowitsch while studying the photochemical generation of radicals in solution.[38, 81] At that time, lower reaction yields measured in the solution phase relative to the gas phase were not understood. This photochemistry did not involve photosensitizers but rather light absorption by stable diatomic molecules to populate dissociative excited states that resulted in homolytic bond cleavage. As a result, the solvent cage was present in the ground state for the solvated molecule. This differs from the previous example where the solvent cage was generated by diffusional encounter of PS* and Q after light absorption. A simplified scheme for light-initiated photochemistry of a diatomic molecule is shown in **Figure 3**. The originally proposed model asserted that the geminate products had to possess sufficient kinetic energy to "*find their way through the surrounding 'walls' of the solvent and to put more molecular layers between them before coming to rest*".[38] The authors predicted that due to the solvent cage, the yields would be lower in fluid solution than in the gas phase, increase with the photon energy, and decrease with increased solution viscosity. Remarkably, all these predictions were borne out in experiments conducted over the next forty years. Detailed examples are given in Section 3 of this review.

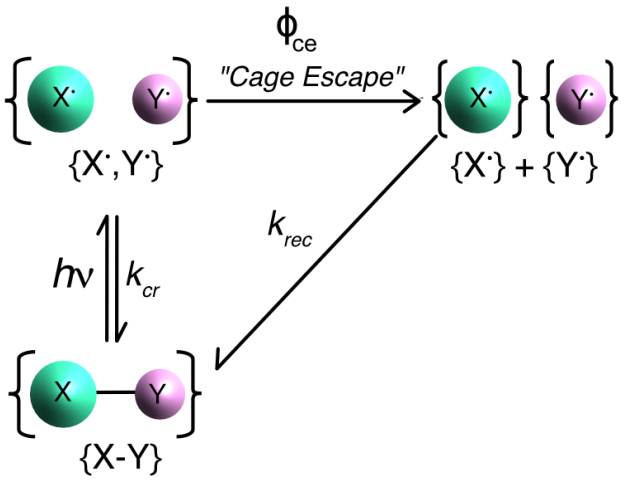

Figure 3. Simplified photochemical scheme for light excitation of a diatomic molecule with a dissociative excited state. Following cage escape, the two radical products undergo recombination to ultimately generate the ground state with a rate constant, k_{rec}.

Rabinowitsch and Wood went on to develop the first mechanical model for the solvent cage.[36] A schematic is shown in **Figure 4**. It was comprised of a conductive brass plate with a zig-zag border placed on a shaker for 'chaotic agitation' that crudely represented the thermal motion of molecules in solution. A conductive pole insulated from the plate was placed in the middle. When a single metallic sphere was placed on the agitated plate it occasionally collided with the conductive pole and closed the electronic circuit providing a light flash that was used to monitor collisions between the 'reactants'. At a given agitation rate, the collisions were isolated in time. When the experimentalists placed wooden spheres, that represented solvent molecules, on the plate their collisions with the conductive pole did not close the circuit and hence were not counted. Curiously, when the number of wooden balls was increased beyond a critical value, collisions with the conductive sphere occurred in "sets" and within each set there was a notable increase in the frequency of collisions. They termed these sets of collisions "encounters" and drew an analogy with the solvent cage (wooden balls) preventing their escape. The wooden balls surrounding the metal ball and the conductive pole provided a crude idea of an 'encounter complex'. The isolated collisions measured in the absence or with a small number of the wooden balls provided a model for gas phase interactions, **Figure 4**

This classical wooden sphere experiment led to three key conclusions that are relevant today. First, the mean number of collisions in the gas phase and between solutes in solution (not their collisions with the solvent molecules) are about the same, ~10^{10} s^{-1}. Second, in solutions, collisions occur in sets called encounters in which the same two species collide multiple times before separating; this occurs because they

are imprisoned in a 'cage' of solvent molecules. Third, the presence of the solvent cage offers the possibility of immediate ("primary") recombination and ordinary recombination that are now referred to herein as (geminate) charge recombination and back electron transfer, with rate constants k_{cr} and k_{BET}, respectively.

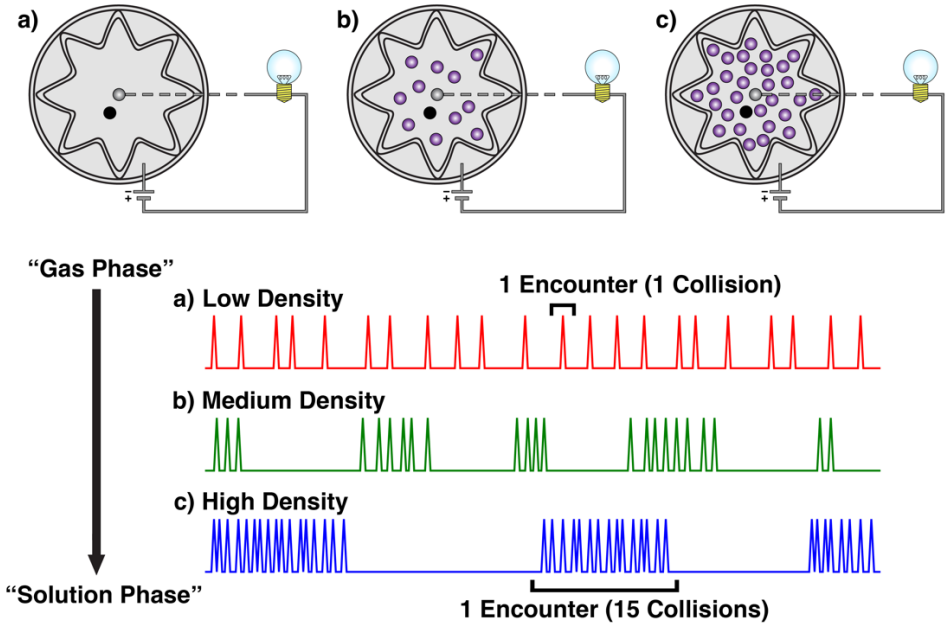

Figure 4. Mechanical model developed by Rabinowitsch and Wood to represent solvent caging. The purple spheres are insulators that represent solvent molecules and a conductive ball (black) and a conductive knob (silver) that represented the photoproducts of interest were placed on a conductive plate that was agitated. Each time the conductive ball collided with the conductive knob the circuit was closed, and a light flashed enabling it to be counted. When the density of insulating balls was small or zero, collisions were isolated like that expected in the gas phase (a). When the density of insulating balls was increased, collisions occurred in sets because the insulating balls prevented escape of the conductive ball from the knob (b-c). The experimentalists termed these sets of collisions 'encounters' and drew analogy with the solvent cage.[36]

A photochemical validation of the solvent cage came from so-called cross-over experiments performed by Levy and Lyon.[35] The photolytic decomposition of mixtures of azomethane and per-deuterated azomethane were quantified in the gas phase and in a condensed solution (**Figure 5**).[35] Photolysis in the gas phase produced an almost perfect 1:2:1 statistical distribution of CH_3CH_3, CH_3CD_3 and CD_3CD_3, respectively. Hence a statistical number of $CH_3^{\bullet}$ radicals 'crossed over' and reacted with $CD_3^{\bullet}$ radicals generated from a different azomethane molecule. In contrast, photolysis in isooctane solutions yielded almost exclusively the in-cage recombination products, CH_3CH_3 and CD_3CD_3. The data provided compelling evidence that the isooctane solvent molecules trapped the photogenerated methyl radicals, preventing their escape, and enabling nearly quantitative radical coupling.

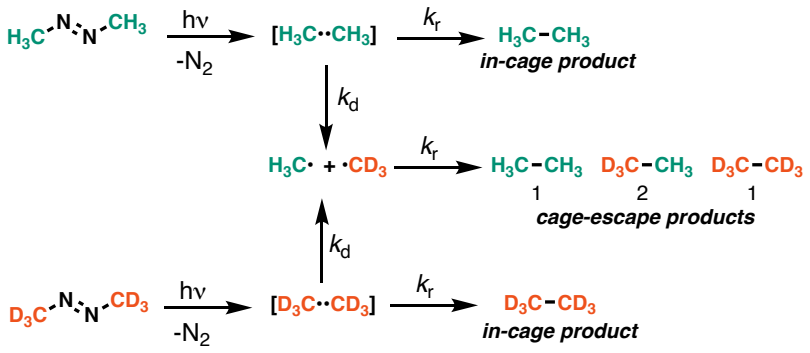

Figure 5. Experimental verification of the cage effect through cross-over experiments in which equal concentrations of azomethane and perdeutero azomethane were photoexcited.[35]

1.2) Methods for Quantifying Cage Escape Yields

An important question that needs to be addressed is: "*How would an experimentalist know what percentage of products formed within the encounter complex escape to yield the sought-after products?*" This is an important question as these products exist for long enough time periods to undergo subsequent diffusional reactions. Historically, the yield was measured by addition of reagents that "trapped" the freely diffusing radicals and formed stable molecules whose concentrations could be determined by ^{1}H NMR or other common spectroscopic techniques. A shortcoming of this approach is that these trapping reagents could themselves become part of the solvent cage, particularly when high reagent concentrations were needed for short lived radicals like chlorine atoms or to test the Noyes cage escape model presented in Section 3.

A closer look at **Figure 2** highlights that the cage escape process is a simple kinetic competition between geminate charge recombination (k_{cr}) and the rate constant for cage-escape (k_{ce}).[82-84] As such, the cage-escape yield can be formulated as:

$$\Phi_{ce} = \frac{k_{ce}}{k_{ce}+k_{cr}} \qquad \text{Eq. 1.1}$$

and a number of authors have used a kinetic approach to determine ϕ_{ce}. The charge recombination rate constant is often estimated through Marcus theory. Alternatively, and in several literature examples described below, the cage escape yield was determined experimentally (*vide infra*) and k_{cr} was extracted from Equation 1.1 with a computed value of k_{ce}. While different equations and formulations have been utilized to estimate k_{ce},[85] the Eigen equation[86] is the most common and highlights that cage escape is a

function of the radius of the solvent cage (r), viscosity (η), dielectric constant (ε), ionic strength (μ), and the charges of the diffusing ion-pair $\boldsymbol{Z_{PS}}$ and $\boldsymbol{Z_Q}$ (Eq. 1.2-1.4) where N is Avogadro's number.

$$k_{ce} = \frac{2kT}{\pi r^3 \eta} \frac{\frac{\omega_r}{RT}}{1-e^{\left(\frac{-\omega_r}{RT}\right)}} \qquad \text{Eq. 1. 2}$$

$$\omega_r = z_{PS} z_Q N \left(\frac{e^2}{\varepsilon r}\right)\left(1 + \beta r \mu^{\frac{1}{2}}\right)^{-1} \qquad \text{Eq.1.3}$$

$$\beta = \left(\frac{8\pi N^2 e^2}{1000 \varepsilon RT}\right)^{\frac{1}{2}} \qquad \text{Eq.1.4}$$

Large uncertainties in ϕ_{ce} are expected when k_{ce} is calculated from the Eigen (or related) Equation 1.2 and k_{cr} is estimated through Marcus theory since: i) the radius of the solvent cage is unknown and is typically approximated as the sum of the reactant radii; ii) the reorganization energy and coupling within the encounter complex are unknown; and iii) the charge of the photosensitizers and quenchers are usually estimated as spherical point charges.[34, 84] Note also that only the overall charge is considered and these models do not account for situations where ions have multiple charges in specific locations. In theory, if the individual partial charge of every atom on the donor and acceptor was known along with the distance between each atom, the calculated partial charge could be used to provide a better understanding of cage escape yields.[87-88] In any event, the kinetic approach for estimating cage escape yields is at best a crude one, most appropriate for comparative studies of homologous series of photosensitizers and quenchers. Our understanding of the encounter complex is simply too rudimentary to accurately predict these rate constants. This review differentiates cage escape yields estimated from rate constants from those determined directly from measuring the concentration of products.

An alternative approach for quantifying cage escape yields is to measure the concentration (or moles) of escaped products divided by the moles of quenched excited states, Equation 1.5.

$$\phi_{ce} = \frac{[moles\ of\ escaped\ products]}{[moles\ of\ quenched\ excited\ states]} \qquad \text{Eq. 1.5}$$

The escaped products in the numerator have been observed by techniques such as NMR, Raman, IR, photoacoustic, and UV-Vis spectroscopy.[89] The latter technique has proven to be the most robust as the absorption changes are directly related to concentrations through the Beer-Lambert Law. Determination of the moles of quenched excited states requires knowledge of the moles of absorbed photons that is typically

determined through the use of actinometers.[90-93] Both electronic and chemical actinometers may suffice, yet most often a chemical actinometer is used such as an excited state with a known extinction coefficient.[90-93] The fraction of the states that are quenched is available from a Stern-Volmer analysis (detailed in Section 2.1).

A representative example of determining the cage escape yield through transient absorbance spectroscopy is described here for oxidative excited-state electron transfer quenching of $[Ru(bpy)_3]^{2+*}$ by an aryl diazonium ($R\text{-}N_2^+$).[94-95] The sequence of relevant light-induced electron transfer follows the equation depicted in Eq. 1.6 and 1.7:

$$[Ru^{II}(bpy)_3]^{2+} \xrightarrow{h\nu} [Ru^{III}(bpy)_2(bpy^{\bullet-})]^{2+*} \qquad \text{Eq. 1.6: Excitation}$$

$$[Ru^{III}(bpy)_2(bpy^{\bullet-})]^{2+*} + R-N_2^+ \xrightarrow{et} [Ru^{III}(bpy)_3]^{3+} + R-N_2^{\bullet} \qquad \text{Eq. 1.7: Electron transfer}$$

Figure 6a shows the time-resolved PL quenching of $[Ru(bpy)_3]^{2+*}$ by 4-methoxybenzene diazonium in acetonitrile. The corresponding absorption change monitored at 450 nm allows the concentration of the oxidized $[Ru(bpy)_3]^{3+}$ product, more generally (ΔA_{PS^+}), to be determined, **Figure 6b**. Note that with the concentrations of products typically formed in a transient absorption study, back electron transfer occurs on a millisecond time scale providing a tens of microsecond window to quantify the concentrations and hence the yield. The extinction coefficients of both the $[Ru(bpy)_3]^{2+}$ ground state and the $[Ru(bpy)_3]^{3+}$ product are needed and are in fact well known.[91-93] In this example, an unquenched $[Ru(bpy)_3]^{2+*}$ was used as the actinometer with a $\Delta\varepsilon$ value of –11,000 $M^{-1}cm^{-1}$ at 450 nm.[91-93]

$$\phi = \left(\frac{\frac{\Delta A_{PS^+}}{\Delta \varepsilon_{PS^+}}}{\frac{\Delta A_{ES_{ref}}}{\Delta \varepsilon_{ES_{ref}}}} \right) \left(\frac{1-10^{-Abs_{ref}(\lambda exc)}}{1-10^{-Abs_{PS}(\lambda exc)}} \right) \qquad \text{Eq. 1.8}$$

The desired cage escape yield (ϕ_{ce}) was obtained by comparing the relative yield of PS^+ produced (ϕ) determined by nanosecond transient absorption spectroscopy and using Eq. 1.8, relative to the percentage of quenched photoluminescence (%PL) determined by the time-resolved photoluminescence in **Figure 6**, Eq. 1.9. A concatenated linear regression of all the data points by constraining the Y-intercept at 0 provided a slope that corresponded to a cage-escape yield of 0.34 (**Figure 6c**).

$$\phi_{ce} = \frac{\Phi}{\%\ PL\ Quenched} \qquad \text{Eq. 1.9}$$

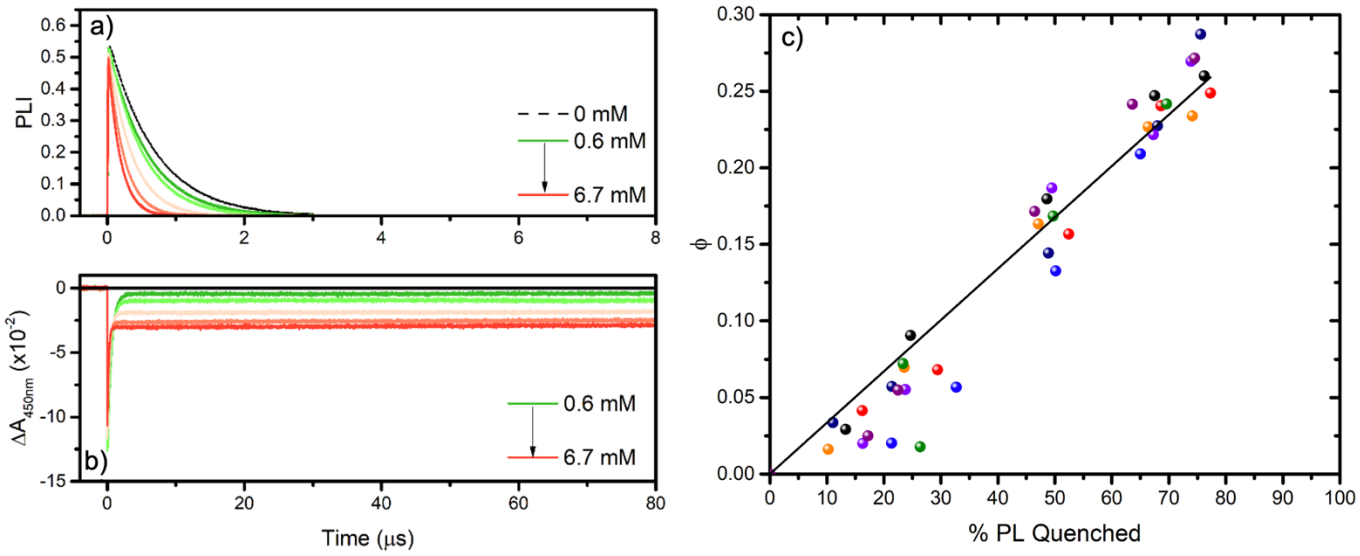

Figure 6. Representative data set for $[Ru(bpy)_3]^{2+}$ quenched by 4-methoxybenzene diazonium in argon-purged acetonitrile at room temperature. a) Excited-state lifetime at different concentrations of 4-methoxybenzene diazonium used to determine the percentage of PL quenched. b) Changes in absorption recorded at 450 nm following pulsed-light excitation at similar concentration of 4-methoxybenzene diazonium as in panel a). c) Plots of the relative yield of PS^+ formed (ϕ) versus the percentage of quenched steady-state photoluminescence (% PL quenched) for $[Ru(bpy)_3]^{2+}$ in the presence of 4-methoxybenzene diazonium tetrafluoroborate. Each color represents a new experiment. The slope was used to extract a cage escape yield of 0.34. Reproduced with permission from references.[94-95] Copyright 2023 Elsevier.

An advantage of this approach is that many quencher concentrations are used to determine the yield. Indeed, literature reports often rely on measurements at a single quencher concentration. In constructing such plots, it is appropriate to weight the higher concentrations more significantly as they typically have less uncertainty in their determination. Indeed, experimentalists often determine ϕ_{ce} with a large excess of quencher to completely quench all excited states and utilize this absorption change to determine the cage-escape yields according to Equation 1.9. Ideally this approach should be repeated at several quencher concentrations where quenching is quantitative and signal-to-noise ratios are most optimal, so that standard deviations can be determined. The method described herein has been previously reported in the literature and allows one to investigate the cage-escape over a wide range of concentrations.[94-95] This is important as the cage-escape yields may be a function of the quencher concentration, especially for ionic photosensitizers and/or quenchers that can undergo ion-pairing or ground state pre-association.[96]

For optimal photophysical studies it is ideal to show that the two photoproducts form in equal concentrations with the same rate constant and undergo back electron transfer with the same k_{BET}; this

requires that the radicals formed are persistent over the time scale of the reaction and that product accumulation is not a confounding issue. For cases where the radicals that escape the cage react before undergoing back electron transfer, it is often necessary to use a pump and flow the solution through the cuvette so that each laser pulse excites a fresh solution.

There are several ways that this particular example could be perfected. First, the concentration of only the oxidized PS^+ was determined spectroscopically. Ideally, both the reduced acceptor concentration and PS^+ should be determined. These should be present in equal concentrations and appear with the same rate constant as the quenching rate constant extracted from Stern-Volmer analysis. Demonstration of the reduced/oxidized forms of the photosensitizer and quencher being formed in equal concentrations indicates that it is a true cage escape process as opposed to irreversible reactivity within the solvent cage. The data shown in **Figure 6** corresponds to single observation wavelength that was utilized to determine the concentrations. A more robust analysis would be to exploit a broader spectral window and perform a global kinetic analysis at all relevant wavelengths, particularly when the products absorb light at multiple wavelengths.

Finally, the actinometer utilized required knowledge of an excited-state extinction coefficient. It is indeed difficult to convincingly demonstrate that molecular excited states even follow Beer-Lambert's law. Nevertheless, for well-known photosensitizers like $[Ru(bpy)_3]^{2+}$, the absorption spectrum and extinction of the metal-to-ligand charge transfer (MLCT) excited states have been rigorously measured through irradiance dependent and energy transfer studies.[91-93] Yet, uncertainties in these changes in molar extinction coefficient often set a limit of two significant figures in the reported ϕ_{ce}. When better estimates of excited state extinction coefficients or alternative actinometers become available, the data reported could be scaled and a more precise yield determined. Indeed, at some level all reported ϕ_{ce} values reflect *relative* quantum yields and considering them as absolute values requires a critical evaluation of all the underlying data.

In summary, this representative example shows some of the strengths and weaknesses of the transient absorption technique for quantifying cage escape yields. It is possible to measure cage escape yields within a few percent, but only when the cage escape yields are significant ($\phi_{ce} > 0.1$) and persistent radical products are formed that absorb light strongly and undergo quantitative back electron transfer. Indeed, careful consideration of the photosensitizer and the quencher are necessary for precise determination of yields. Very often, inherent shortcomings are present in photosystem of interest that result in large uncertainties in cage escape yield determination. Hence there is an opportunity for future research to provide a means to quantify cage escape yields more rigorously through the development of spectroscopic

methods that enable precise transient concentration determinations as well as new quenchers and photosensitizers that provide defined spectroscopic handles with large changes in the extinction coefficients when reduced and/or oxidized.

2) Key Concepts

2.1) Dynamic and Static Electron Transfer

2.1.1) Stern-Vomer Model

Section 4 of this review describes the research that has been published regarding cage escape yields for bimolecular photoredox reactions. Prior to the discussion of cage escape yields, the fundamental mechanism for bimolecular electron transfer reactions is introduced. Oxidative and reductive electron transfer may occur by two different electron transfer quenching mechanisms. The first one is termed *dynamic* quenching and implies that diffusion processes occur before excited-state electron transfer. Such dynamic quenching is also referred to as "diffusional" or "collisional" quenching and was highlighted in **Figure 2**. The second mechanism is termed *static* quenching, where a ground-state adduct is formed between the photosensitizer and the quencher, typically through non-covalent interactions or by forming aggregates with a large number of quenchers. Because the photosensitizer and quencher are associated in the ground state, the charge separation rate constant often becomes larger than the rate constant for radiative decay, often yielding the formation of a "non-luminescent" adduct.[29] Both static and dynamic quenching mechanisms may be operative and can be disentangled using the model developed in 1919 by Otto Stern and Max Volmer.[97] This is accomplished by measuring both the steady-state photoluminescence intensity, PLI, and the excited-state lifetime, τ, as a function of the quencher concentration. When such data plotted as PLI_0/PLI and τ_0/τ (PLI_0 and τ_0 being the steady-state PL intensity and the excited-state lifetime in the absence of quencher) versus the quencher concentration are linear and coincident, dynamic quenching is the primarily operable mechanism. The Stern-Volmer constant, K_{SV}, extracted from the slope (Eq. 2.1) provides access to the bimolecular quenching rate constant (k_q) using the excited-state lifetime in the absence of quencher, τ_0.

$$\frac{(PLI_0)}{(PLI)} = \frac{\tau_0}{\tau} = 1 + K_{SV}[Q] \; = 1 + k_q\tau_0[Q] \qquad \text{Eq. 2.1}$$

Static quenching is assigned as the sole mechanism when the steady state PLI is quenched, yet the excited state lifetime is independent of the quencher concentration. In this case, the change in the initial amplitude, α_0, of the time-resolved photoluminescence decays provides an estimate of the ground state

equilibrium constant for adduct formation.[29] Plots of α_0/α and PLI_0/PLI versus the quencher concentration provide the equilibrium constant, K_s, for quencher-chromophore adduct, Eq. 2.2**.** Such adducts may be quantified through other spectroscopic measurements and the corresponding equilibrium constant determined through a Benesi-Hildebrand type analysis.[98-99]

$$\frac{(PLI_0)}{(PLI)} = \frac{\alpha_0}{\alpha} = 1 + K_s[Q] \qquad \text{Eq. 2.2}$$

In many cases however, excited-state quenching occurs by a combination of both static and dynamic quenching mechanisms. In this case, upward curvature in a Stern−Volmer plot of PLI_0/PLI versus the concentration of quencher is typically observed. Such data has been accurately modeled using Eq. 2.3 which displays a quadratic dependence on the quencher concentration.

$$\frac{(PLI_0)}{(PLI)} = \frac{\alpha_0}{\alpha} \times \frac{\tau_0}{\tau} = 1 + (K_{SV} + K_s)[Q] + K_{SV}K_s[Q]^2 \qquad \text{Eq. 2.3}$$

The model developed by Otto Stern and Max Volmer has withstood the test of time and represents the standard model to investigate excited-state reactivity that is probed either by steady-state or time-resolved photoluminescence measurements or both. It is often assumed that only those photosensitizers with nanosecond or longer excited-state lifetimes are useful for excited-state electron transfer. However, static quenching via pre-association of the PS and the Q, often times through aggregates formed at high Q concentrations, enables quantitative excited-state electron transfer even with short lived excited states.[100-106]

2.1.2) Extraction of Elementary Rate Constants from Quenching Data

As described previously, the quenching rate constant, k_q, is often obtained from Stern-Volmer analysis (Eq. 2.1), however PL quenching is an indirect measurement and does not in itself establish that excited-state electron transfer is operative. Often times in the literature an electron transfer mechanism is assumed with well-established acceptors, such as quinones or pyridiniums, and donors, like amines or phenothiazines, however additional spectroscopic techniques are needed to firmly establish electron transfer quenching.[55, 89] In addition, the k_q value extracted from Stern-Volmer analysis of the quenching data is not an elementary rate constant but rather an observed rate constant for a composite reaction. The underlying charge separation rate constant, k_{cs}, is of tremendous importance for fundamental study and for many practical applications.

It is hence of great interest to relate k_q to k_{cs} for quenching processes that are known to occur by oxidative or reductive excited-state electron transfer. This has historically been accomplished with the well-established model for bimolecular excited state quenching shown generically in **Figure 2**. A steady-state kinetic assumption relating k_q to the desired k_{cs} through the diffusional rate constant, k_{diff}, and the equilibrium constant for encounter complex formation, K_a, has been derived in the literature and yields Eq. 2.4.[44, 107]

$$\frac{1}{k_q} = \frac{1}{k_{diff}} + \frac{1}{K_a k_{cs}} \qquad \text{Eq.2.4}$$

Therefore, in order to determine k_{cs}, it is necessary to consider the diffusional rate constant, k_{diff}, and the association constant for the formation of the encounter complex, K_a. The diffusional rate constant can be estimated using of Equation 2.5,[40]

$$k_{diff} = 4\pi N_A (D_a + D_b)\beta \qquad \text{Eq.2.5}$$

where N_A is Avogadro's number, D_a and D_b are the diffusion coefficients of the reactants, which are accessible experimentally by NMR spectroscopy and electrochemical methods or can be estimated through the Stokes-Einstein relationship.[108-110] The final term, β, is the effective reaction radius. For neutral species, this is typically taken as the sum of the reactants' van der Waals radii. However, if both species are charged, this term must account for the attractive (or repulsive) forces that modulate the diffusional rate constant. Multiple methods to account for diffusion of charged species have been evaluated extensively in the literature, both in dilute aqueous solutions, where simplified models are applicable, and in low dielectric constant organic solvents. The interested reader is directed to these references for a more detailed discussion.[107, 111-112]

The second parameter needed to extract the charge separation rate constant from quenching data is the association constant, K_a.[113] In addition, association constants may be determined experimentally through the use of spectroscopic techniques such as NMR, UV-Vis, IR or static PL quenching data. It is important to note, however, that these techniques report on the ground-state equilibrium, whereas the encounter complex K_a involves the photosensitizer excited-state. Deviations in the excited state are generally small but, in some cases, may be significant and have been studied quantitatively.[44, 114-117] In the common case where the encounter complex is only transiently formed in low concentrations and is hence not directly observed experimentally, theoretical models such as those in the Fuoss expression have been used to estimate the magnitude of the association constant.[107, 118 44, 114-117] Given the uncertainty that often exists in determining K_a, Sutin has suggested the term "activation controlled rate constant" k_{act} with units of M^{-1} s^{-1}, where $k_{act} = k_{cs}K_a$.[119]

2.2) Marcus Theory

The theoretical work of Rudy Marcus provides a conceptual method by which the rate constants for electron transfer occurring in an encounter complex can be understood and even predicted.[33-34, 120-122] Equation 2.6 is the canonical semiclassical expression that many refer to simply as "Marcus Theory". Of course, Marcus had many theories, yet this expression is certainly the most celebrated as it applies to many classes of electron transfer reactions. An important aspect is that the electron transfer rate constant, k_{cs}, is a function of only three variables that may be computed or determined experimentally: the Gibbs Free Energy change (ΔG^o), the reorganization energy (λ), and the electronic coupling or the degree of quantum mechanical mixing between D and A (H_{DA}). The semiclassical expression is valid when H_{DA} is small relative to the thermal energy, kT, and is termed non-adiabatic or weakly adiabatic electron transfer. While educational and highly detailed reviews of Marcus Theory are available in the literature,[32, 34, 120, 123-124] we provide here a brief overview with particular focus on electron transfer reactions occurring in solvent cages.

$$k_{cs} = \frac{2\pi}{\hbar}\frac{{H_{DA}}^2}{\sqrt{4\pi\lambda k_b T}}\exp\left(-\frac{(\Delta G^o+\lambda)^2}{4\lambda k_b T}\right) \quad \text{Eq.2.6}$$

An important pedagogical tool for visualizing electron transfer reactions is the Gibbs free energy surface, sometimes called the potential energy surface.[125-129] Marcus suggested that inherently complex electron transfer reactions can be well modelled by only two potential energy surfaces, one for the reactants (R) and one for the products (P). These are plotted as a function of a nuclear coordinate in **Figure 7**. In one extreme the two reactants in the solvent cage are weakly interacting and undergo *non-adiabatic* electron transfer. In this extreme, an electron 'hops' from the reactant to product surface at the intersection point of the two potential energy surfaces when the free energies of the product and reactant are equal. Non-adiabatic reactions are constrained by the Born-Oppenheimer approximation, electron transfer is faster than nuclear translational, rotational, and vibrational motion.[130]

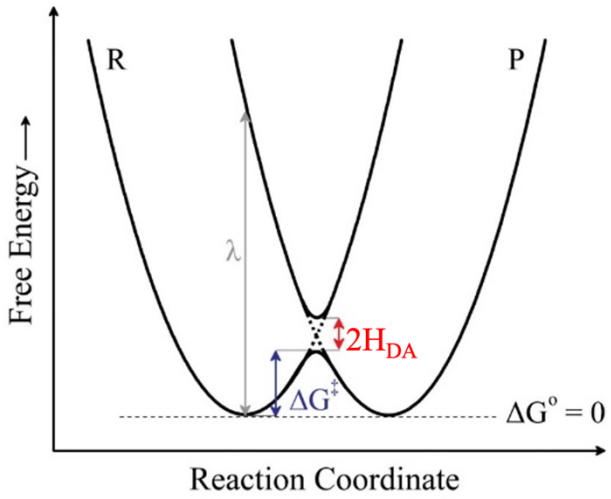

Figure 7. Isoenergetic Gibbs free energy surfaces for a Reactant R and Product P. The reorganization energy, λ, is shown as the vertical energy difference between the product and reactant surfaces. The electronic coupling matrix element, H_{DA}, is a quantitative measure of the overlap of the wavefunctions at the instance of electron transfer. For this self-exchange reaction, where the reactants and products are identical, the free energy barrier is $\Delta G^{\ddagger} = \lambda/4$.

Marcus used a single force constant to determine the free energy surfaces and related them directly to the *reorganization energy*, λ, that is typically computed as a sum of 'outer-sphere' and 'inner-sphere' contributions, $\lambda = \lambda_i + \lambda_o$.[129, 131] The inner-sphere components are the changes in bond lengths and bond angles that accompany electron transfer. Outer-sphere contributions represent the solvent dielectric response to electron transfer. The static dielectric properties of the solvent and the distance between the reactants determine the outer-sphere reorganization energy, which is often computed with dielectric continuum theory, Equation 2.7.[33, 132-133]

$$\lambda_o = \frac{e^2}{4\pi\varepsilon_o}\left(\frac{1}{2r_D} - \frac{1}{2r_A} + \frac{1}{R}\right)\left(\frac{1}{\varepsilon_{op}} - \frac{1}{\varepsilon_s}\right) \qquad \text{Eq.2.7}$$

For many electron transfer reactions occurring within solvent cages, the inner-sphere changes are minimal such that $\lambda = \lambda_i + \lambda_o \sim \lambda_o$. Exceptions exist and one that is highly relevant to cage escape involves changes in the spin quantum number that are accompanied by significant changes in the bond lengths.[134-138]

Electron delocalization and mixing between the molecular orbital wavefunctions of the reactants and products impact the electron transfer kinetics.[139-145] This phenomenon is referred to as electronic coupling, H_{DA}. The wavefunctions are expected to decay exponentially with distance as defined by an attenuation factor, β, that is diagnostic of the media between the reactant and product, Equation 2.8.[146-148]

$$H_{DA} = H_{DA}^{o} \exp\left(-\frac{\beta}{2}(R_{DA} - R_0)\right) \qquad \text{Eq.2.8}$$

The electronic coupling $H_{DA}{}^{o}$ when the reactant and product are at van der Waals separation, R_0, is a maximum and decreases exponentially as the separation increases. After electron transfer in the solvent cage, the separation is expected to be small favoring charge recombination due to the strong coupling and the small reorganization energy. Indeed, since both λ and H_{DA} are distance dependent it is often difficult to experimentally separate their relative contributions to the electron transfer rate constant.

Marcus theory predicts that the rate constant should be dependent on the Gibbs free energy change, ΔG^{o}, and in a very novel way. Note in **Figure 7** the midpoint of the nuclear configuration corresponds to the Gibbs free energy of activation, $\Delta G^{\ddagger}$, which is the thermodynamic barrier for thermal electron transfer. For the self-exchange rate constant shown, $\Delta G^{\ddagger} = \lambda/4$. It can be shown that the activation barrier is a function of the driving force, ΔG^{o}, and reorganization energy as given in Equation 2.9.

$$\Delta G^{\ddagger} = \frac{(\Delta G^{0}+\lambda)^{2}}{4\lambda} \qquad \text{Eq.2.9}$$

Hence a parabolic dependence of $\Delta G^{\ddagger}$ on ΔG^{o} is predicted, which results in a barrier that decreases with increased driving force, $-\Delta G^{o}$ until it is zero when $-\Delta G^{o} = \lambda$ and then subsequently increase as the driving force become more favorable. This gives rise to three kinetic regimes of electron transfer: 1) normal, $|-\Delta G^{o}| < \lambda$; 2) activationless, $|-\Delta G^{o}| = \lambda$; and 3) inverted, $|-\Delta G^{o}| > \lambda$, **Figure 8**. Hence Marcus theory predicts that very exergonic reactions slow down relative to lower driving forces and a maximum rate constant is achieved when the reaction becomes *barrierless*, at $-\Delta G^{0} = \lambda$ so $\Delta G^{\ddagger} = 0$. In solar energy conversion applications, the initial charge separation reactions are often optimized to store the maximum free energy that results in a highly favored charge recombination reaction in the solvent cage that has often been shown to fall in the Marcus kinetic inverted region.[149-150]

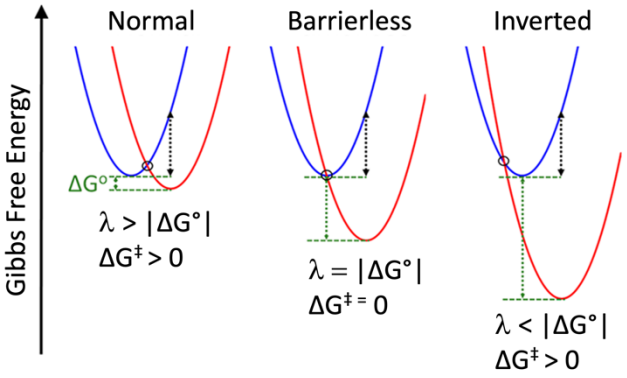

Figure 8. Types of electron transfer reactions as defined by the reaction free energy, ΔG^{o}, and reorganization energy, λ. (From left to right) 'Normal' electron transfer reactions, 'Barrierless' electron transfer reactions and 'Inverted' electron transfer reactions.

As stated at the outset, Marcus theory is appropriate for weak coupling at the non-adiabatic limit or for weakly adiabatic electron transfer. When the electronic coupling becomes very large, adiabatic electron transfer mechanisms become operative that require a different level of theory. [151-154] This raises the question: *how does one know if electron transfer in the solvent cage is adiabatic or non-adiabatic*? The answer is that one generally does not know and the answer will likely depend on the identity of the reactants; however, there is a large body of data that indicates Marcus theory will be applicable in the vast majority of cases. This data comes from thermal electron transfer reactions that also occur within an encounter complex surrounded by a solvent cage. Self-exchange rate constants, typically measured through line broadening experiments, are generally predicted by Marcus theory and are consistent with non-adiabatic transfer.[155-157] In addition, thermal electron transfer reactions between a reactant that differs from the product can often be predicted by the Marcus cross-relation, Equation 2.10.[158-161]

$$k_{cs} = (Kk_{aa}k_{dd}f)^{\frac{1}{2}} \qquad \text{Eq. 2.10}$$

Here k_{aa} and k_{dd} are the self-exchange rate constants, K is the equilibrium constant, and f is a factor often taken to be one. The phenomenal success of the cross-relation indicates that reorganization energy and the electronic coupling for the self-exchange reactions are very similar to that for the cross reaction. Indeed, measured rate constants that differ significantly from that predicted by the Marcus cross-relationship are often taken as evidence of enhanced electronic coupling within the encounter complex.

2.3) Spin and Magnetic Field Effects

2.3.1) Spin Effects

Spin is a quantum number that defines the directionality and magnitude of the angular momentum a species experiences. As presented in this review, electron spin is one parameter that has clearly been shown to impact cage escape yields. Most photosensitizers and quenchers have diamagnetic singlet ground states but there are certainly exceptions, the most important being molecular oxygen which has a triplet ground state. Quantum mechanical spin selection rules demand that the total spin is maintained upon light absorption and electron transfer. Hence, a photosensitizer with an excited singlet state is expected to generate a singlet radical pair that can either escape the cage or rapidly recombine to re-form the singlet ground-state products. On the other hand, a triplet excited state reacts to yield a triplet radical pair that introduces spin forbiddenness to geminate charge recombination to the singlet ground state in the solvent

cage. The result of this spin-forbidden nature of geminate charge recombination for triplet charge separated states within the encounter complex is an enhanced cage escape under many conditions (**Figure 9**). The early model for cage escape developed by Noyes and highlighted in Section 3 does not include spin multiplicity as a factor impacting cage escape yields.[162] Lyon's studies of azomethane were amongst the first to include some sort of spin correction.[35] However, there is now clear evidence that the spin state is important for cage escape in chemistry and biology.[24, 163-176]

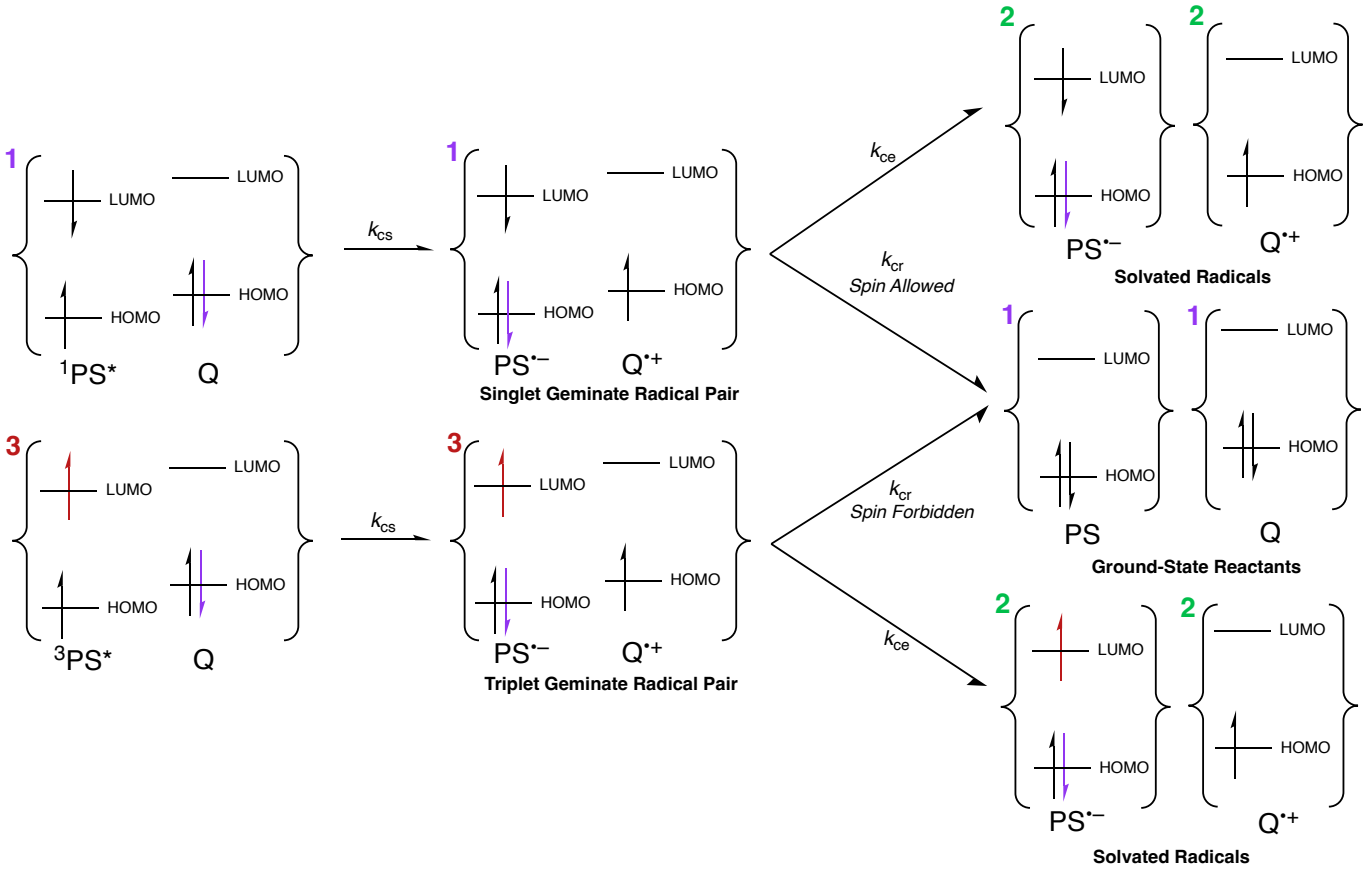

Figure 9. Scheme depicting the fate of the triplet and singlet spin correlated geminate radical pairs following reductive electron transfer using the frontier highest occupied (HOMO) and lowest unoccupied (LUMO) molecular orbitals of the ground state as an approximation for the excited state. Geminate charge recombination generates the ground-state products. In the case on the triplet geminate radical pair, this recombination process is spin forbidden, leading to larger cage-escape yields than in the case of the singlet geminate radical pair.

Transitions between pure spin states of different multiplicity are forbidden by the spin selection rule; however, electron spin can be a poor quantum number, particularly for photosensitizers that contain a second or third row transition metal. This is a result of quantum mechanical mixing of the spin states through spin-orbit coupling termed the internal heavy atom effect. The spin-orbit coupling constant of an atom scales

as Z_{eff}^4 , where Z_{eff} is the effective nuclear charge, and is hence most important for heavy atoms.[177] Indeed, early photophysical studies of organic chromophores revealed that spin-disallowed phosphorescence was enhanced by heavy atoms present in the external solution in what has been termed the external heavy atom effect.[178-180] Theoretical studies have shown that external heavy atoms enhance spin disallowed transitions by the same mechanisms as internal heavy atoms and has also been the subject of several cage escape studies.[173, 175-176] In addition to spin-orbit coupling affecting the spin state of a PS and Q, magnetic fields have been shown to cause variations in spin transforming transitions. Hence there has been great interest in understanding the role(s) heavy atoms and magnetic fields have on fundamental cage escape yields that deserve further elaboration.[179]

2.3.2) Magnetic Field Effects

Interests in the impact of magnetic fields on radical chemistry emerged with the development of chemically induced dynamic nuclear polarization (CIDNP) as an analytical tool to quantify non-Boltzmann distributions of spin states formed during radical reactions. There are several reviews on CIDNP that include light-driven reactions of relevance to cage escape and provide a basis for understanding why electron spin and magnetic fields impact photo-initiated electron transfer reaction mechanisms and their yields.[181-189]

Fundamental insights have emerged from the study of magnetic fields on spin-correlated radical pairs. This spin correlation is the main reason invoked for the distinct difference in cage escape yields measured after quenching of singlet and triplet excited states. Thus, the relative rate of the spin flip reaction versus the rate of cage escape dictates cage escape yields that are perturbed by the application of an external magnetic field.[190] From studies of magnetic field effects on cage escape yields, three underlying mechanisms have been invoked: 1) hyperfine (*hf*): 2) Δg, and 3) triplet. As is detailed below, these mechanisms impact the rate of singlet-triplet transitions. Other mechanisms that have not been applied to the field of cage escape are highlighted in several reviews and textbooks, and are not discussed here.[189-190]

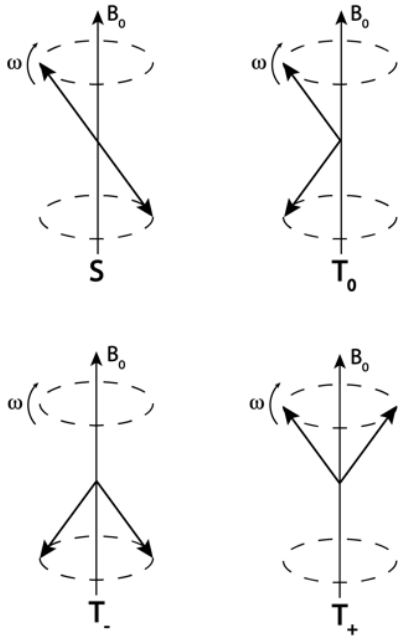

Figure 10. Vector representations of the different spin states that can be occupied under an external magnetic field.

Consider first the *hf* and the Δg mechanisms for spin-correlated radical pairs. An external magnetic field splits the three triplet substates (T_x, T_y, T_z) into the three different spin states, T_0, T_+, T_-, depicted in **Figure 10**.[189-190] The transition rates between these triplet substates and the singlet spin state (S) are unique to each mechanism and are invoked to rationalize magnetic field effects on the cage escape yield.

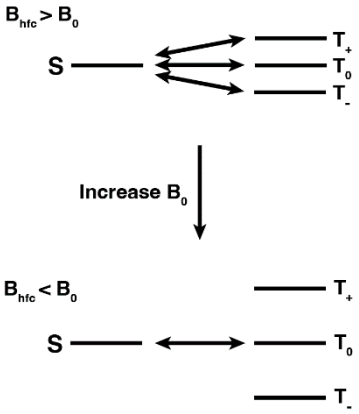

Figure 11. Scheme depicting the *hf*-mechanism. When the hyperfine field is greater than the external field, transitions between the S and all three T states are possible. When the external field is greater than the hyperfine field, the splitting between these states is too large and transitions between only the S and T_0 state are allowed.

The *hf* mechanism considers spin correlated radical pairs with nuclear spin interactions[189] and the balance between the internal and external magnetic fields via Equation 2.11.

$$B = B_0 + B_{hfc} \qquad \text{Eq. 2.11}$$

Here B is the total field, B_0 is the externally applied field, and B_{hfc} is nuclear hyperfine field. The *hf* mechanism is only applicable when B is dominated by B_{hfc} which corresponds to low external fields strengths of B_0 < 100-1000 mT.[190] Under these conditions the triplet substates begin to split and the spin-flip transition becomes less probable (**Figure 11**).[190] Thus, as the external magnetic field strength increases, with a greater splitting between the substates, an increase in the overall cage escape yield is expected (**Figure 12**). Once the splitting between these states becomes too large, spin-flip transitions become inaccessible allowing only the S-T_0 transition. This causes an enhancement of the cage escape yield that reaches a maximum at relatively low field strengths.

In the Δg mechanism, the spin-correlated radicals are assumed to have no nuclear magnetic interactions with different g factors, a value that defines the species magnetic moment. The spins precess at the Larmor frequency (ω) that is governed by the g factor of the radicals and the external magnetic field strength (Equation 2.12).

$$\omega_{ST_0} = \Delta g \beta \hbar^{-1} B_0 \qquad \text{Eq.2.12}$$

As the spins precess, there are intermittent configurations governed by the difference in the Larmor frequencies of the two radicals (Equation 2.12) that allow S-T_0 transitions to occur **Figure 10**. As the external magnetic field strength is increased, the frequency of S-T_0 transitions increases that in turn increases the rate of geminate charge recombination. Hence the Δg model predicts a decrease in the cage escape yield with an increased magnetic field strength saturating at high fields (B_0 < 5-7T), shown in **Figure 12b**).[189-190] Typically, both the *hf* and the Δg mechanisms are operative. When this is the case, the *hf*-mechanism is expected to dominate at smaller fields while the Δg dominates at larger fields, resulting in the behavior depicted in **Figure 12c**.

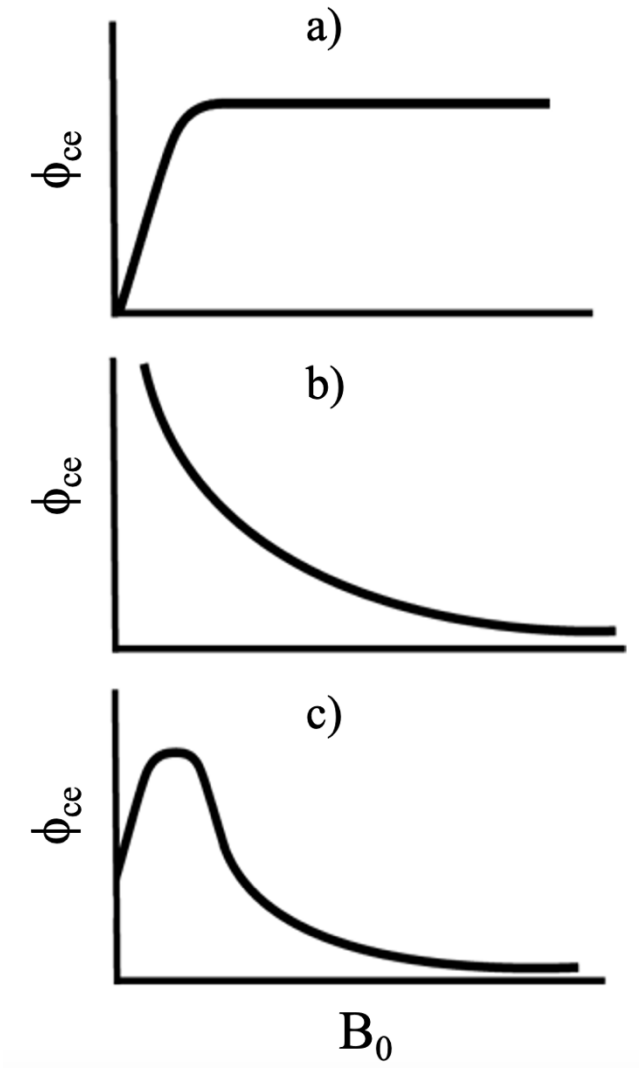

Figure 12. Depictions of the relative Cage escape yield dependence for spin-correlated triplet radical pairs as a function of applied magnetic field for a) the *hf*-mechanism, b) the Δg-mechanism, c) both the *hf*- and Δg-mechanisms.

The triplet mechanism has been invoked for cage escape with photosensitizers that bear heavy atoms and includes a triplet excited-state complex, i.e. an exciplex, that forms prior to electron transfer.[191] Within the exciplex at zero field there are three triplet substates to consider (T_x, T_y, and T_z). Spin-orbit coupling-induced intersystem crossing from the singlet excited state unevenly populates the triplet substates (T_x, T_y, and T_z) and a spin polarization results.[192] After excited-state electron transfer, the triplet exciplex can either diffuse apart to yield free radicals or return to the ground state via charge recombination through substate-selective intersystem crossing (**Figure 13**).[192]

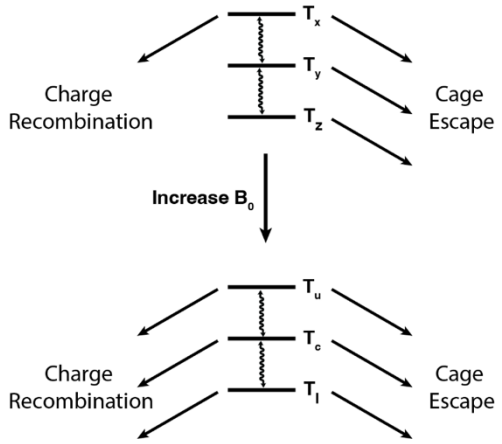

Figure 13. Effect of an external magnetic field in the triplet mechanism, where an increase in magnetic field allows charge recombination from multiple states, thus decreasing cage escape yields.

At zero field, the rate of spin-lattice relaxation between the unevenly populated triplet states dictates the cage escape yield. The effective spin-lattice relaxation rate between the substates increases with the external field strength and enhances recombination to ground state products. Additionally, the external field will mix the zero field states and allow intersystem crossing to occur from each substate with varying probabilities.[190, 192] In summary, the triplet mechanism predicts that an external field will enhance intersystem crossing rates therefore promoting charge recombination and a decrease in the cage escape yield. Like the Δg mechanism, the triplet mechanism predicts limiting cage escape yields that saturate at high field strengths.

3) Unimolecular Bond Photo-Dissociation

The first conceptual tests of the solvent cage were performed by visible light excitation of small molecules dissolved in organic solvents that populated dissociative excited states and resulted in homolytic bond cleavage. The classical example was molecular iodine, I_2, where light excitation formed two iodine atoms that were envisioned to either escape the cage and form long-lived solvated atoms that could subsequently be trapped and quantified, or to undergo geminate recombination within the cage to form I_2. The 1972 review of Lorand highlighted these studies and their extension to other molecules and ions that also have accessible dissociative excited states.[79] Here we summarize some key aspects of this early work and review several of the subsequent studies that were inspired by these foundational studies. The examples, selected from a vast body of literature, are those that focused on quantifying the bond dissociation efficiency

that provided fundamental insight into cages and cage escape that can inspire the growing community of scientist interested in this field.

3.1) The Noyes Model

Richard M. Noyes was an early pioneer in cage escape processes who developed a model to provide a quantitative means to calculate and predict cage escape yields based on experimentally measured parameters. The key features of this model are shown schematically in **Figure 14**. Noyes considered spherical radicals that could recombine within the initially formed primary pair, i.e. geminate recombination. This pair is subjected to the frictional drag of the solvent (a viscous continuum) before entering a regime where the two radicals would move randomly ultimately forming a statistical mixture of products. The initial displacements of the primary pair are critical to this model. Noyes included reversible formation of a 'secondary' pair where a single, or a few, solvent molecule(s) separated the two radicals. These solvent molecules could diffuse away to reform the initial pair. Alternatively, the secondary pair could undergo additional displacements until future motions were taken as random motion of fully solvated radicals. Therefore, the Noyes model predicted three pathways by which the photodissociated radicals could recombine: 1) (geminate) recombination within the primary pair; 2) secondary pairs that partially dissociated and returned; and 3) freely diffusing radicals in solution. Note that Noyes, and others in the older literature, referred to both 1) and 2) as being 'geminate' recombination. This description is no longer common and was not used in this review as the experimental evidence for a secondary pair is poor and the available data points to more complex solvation mechanisms. Hence, while being physically reasonable, the existence of secondary pairs in cage escape processes remains uncertain, a point that is discussed later in this review.

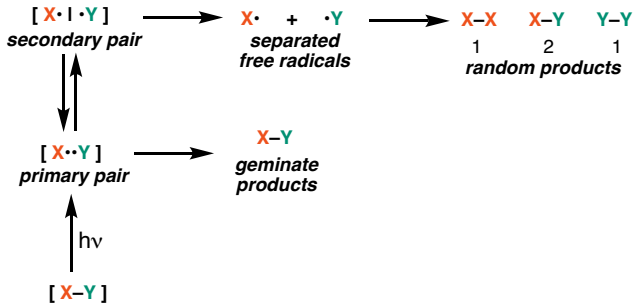

Figure 14. The Noyes model for the formation of an X–Y molecule after photoexcitation to a dissociative excited state occurring via a primary (geminate) pair, a secondary (solvent separated) pair, and from free radicals that had escaped the initial solvent cage.

Noyes considered five different statistical parameters to describe the relative reactivity of two radicals as follows:

$$\beta' = \frac{\alpha\beta}{1-\beta+\alpha\beta} \qquad \text{Eq. 3.1}$$

$$\beta_0' = \beta_0\beta' \qquad \text{Eq. 3.2}$$

- α: The probability that the two radicals will react during a collision within an encounter.
- β: The probability that two radicals that are separated from a non-reactive encounter will eventually encounter one another at least one more time.
- β_0: The probability that two radicals whose centers were initially separated by a distance r_0 will encounter one another at least one more time.
- β': The probability that two radicals separating from a non-reactive encounter will subsequently react with one another.
- β_0': The probability that two radicals whose centers were initially separated by a distance r_0 will ultimately react with each other. This is also defined as the total probability of recombination and is typically unity for persistent radicals like iodine atoms.

By virtue of the Franck-Condon principle, the initially formed radicals are present at the same internuclear distance as in the ground state. Instead, Noyes considered an initial separation distance, r_0, during the entire separation event that assumed the kinetic energy vectors present in the primary radical pair maximized the initial displacement. For iodine, this was calculated using Eq. 3.3, where *m* is the mass of the particle, *b* is the diffusion radius, ν is the frequency of the absorbed photon, E is the I–I bond dissociation energy, and η is the solvent viscosity.

$$r_0 = 2b + \frac{\sqrt{m(h\nu - E)}}{3\pi\eta b} \qquad \text{Eq. 3.3}$$

Hence, the probability that two separated iodine atoms will eventually encounter each other at least one more time can be calculated using Eq. 3.4, where the constants related to the reaction energetics have been gathered in the term A_E (Eq. 3.5).

$$\beta_0 = \frac{2b}{r_0} = \frac{1}{1+\frac{A_E}{\eta}} \qquad \text{Eq. 3.4}$$

$$A_E = \frac{\sqrt{m(h\nu - E)}}{6\pi b^2} \qquad \text{Eq. 3.5}$$

The probability that two separated radicals recombine is presumed to be unity when the distance between their centers is 2b, i.e. when they make contact.

The second displacement occurs after a subsequent encounter with kinetic energy 3/*2kt*. Hence, this probability can be written as Eq. 3.6 where r_T is the distance between their centers and where the kinetic energy is included in the term A_T (Eq. 3.7).

$$\beta = \frac{2b}{r_T} = \frac{1}{1+\frac{A_T}{\eta}} \qquad \text{Eq. 3.6}$$

$$A_T = \frac{\sqrt{\left(\frac{3}{2}\right)mkT}}{6\pi b^2} \qquad \text{Eq. 3.7}$$

Using equation 3.2, the reciprocal of the total probability of "geminate" recombination ($1/\beta_0$') can now be described as the product of the reciprocal of β_0 and β' (Eq. 3.8).

$$\frac{1}{\beta_0'} = 1 + \left(\frac{A_T+\alpha A_E}{\alpha\eta}\right)\left(\frac{1}{\eta}\right) + \left(\frac{A_T A_E}{\alpha\eta^2}\right) \qquad \text{Eq. 3.8}$$

The Noyes model was initially described for the photo-dissociation of I_2 and was later extended to the dissociation of any pair of reactive molecules/atoms, including those where other atoms or molecules separate the primary pair. Hence, an additional term for the initial separation (R_0) was introduced to account for the distance of the reactive fragment within the chemical structure. (Eq. 3.9) This would be the case for azomethane for example, as described in the seminal example of Levy and Lyon (**Figure 5**) where the nitrogen gas provides an initial separation upon photolysis.

$$\frac{1}{\beta_0'} = \frac{R_0}{2b}\left[1 + \left(\frac{A_T+\alpha A_E}{\alpha}\right)\left(\frac{1}{\eta}\right) + \left(\frac{A_T A_E}{\alpha}\right)\left(\frac{1}{\eta}\right)^2\right] \qquad \text{Eq. 3.9}$$

Hence the reciprocal of the cage efficiency minus 1 is described as the total probability for geminate recombination, F (Eq. 3.10).

$$F = \left(\frac{1}{cage\ efficiency}\right) - 1 = \left(\frac{R_0-2b}{2b}\right) + \left(\frac{R_0}{2b}\right)\left[\left(\frac{A_T+\alpha A_E}{\alpha}\right)\left(\frac{1}{\eta}\right) + \left(\frac{A_T A_E}{\alpha}\right)\left(\frac{1}{\eta}\right)^2\right] \qquad \text{Eq. 3.10}$$

This final equation reveals that the cage escape process is quantitatively dependent on the following factors: the solvent viscosity (η), the initial separation of the primary pair induced by the chemical structure (R_0), the translational energy of the separating fragments (A_E), the mass and the radius of the fragments (A_E and A_T) and the probability that two radicals will react during a collision within an encounter (α).

A critically important advance to our understanding of the solvent cage that occurred after 1972 was the development of ultrafast spectroscopic techniques that enabled the quantification of reactivity and dynamics in real time. Elementary steps like photodissociation, recombination, and cage escape were ripe for study with these techniques and afforded the possibility of state-resolved reactivity and direct characterization of transition states that led to the 1999 Nobel Prize awarded to Ahmed Zewail.[193] Furthermore, ultrafast measurements provided a means to test the Noyes model. Indeed, as is detailed below, such kinetic data supplemented with computational study have provided keen insights into our understanding of the molecular events that lead to cage escape. Perhaps not surprisingly, and likely motivated by prior measurements performed under steady-state illumination, the early studies focused on the photodissociation of molecular iodine in organic solvents as the prototypical reaction. A persistent radical product, like the iodine atom, is ideal for ultrafast study within a solvent cage and precluded complicating factors like H-atom abstraction from the solvent cage or the presence of vibrationally hot excited states.

As these ultrafast studies were extended to higher nuclearity molecules and ions, it became vividly clear that the solvent cage concept was amenable to a whole host of light-induced chemistries that included the photoejection of an electron and/or a hydrogen atom to the solvent as well as ligand loss photochemistry in transition metal complexes.[194-196] Below we review the findings most relevant to cage escape with selected examples from the pre-1972 literature that complement the more recent work and provide tests of the Noyes model. Our goal is to maintain a descriptive discussion that is understandable to most chemists. Those interested in the often-nuanced details should refer to the original citations and those interested in the older literature should consult the excellent review by Lorand.[79]

3.2) Elemental Halogens

3.2.1) Iodine

The solvent cage that surrounds molecular iodine has emerged as the most well studied and understood.[197] The early work of this prototypical cage by Noyes established the excitation wavelength and solvent viscosity dependencies of the iodine atom cage escape. Noyes and coworkers thoroughly investigated the photodissociation of I_2 which qualitatively tested the predictions of Rabinowitsch and Wood in a series of articles that appeared in the 1950-70s.[198] The quantum yields were determined under conditions of steady-state illumination with the quantification of iodine atoms that escaped the cage determined by the allyl iodide scavenging technique.[199] They noted that the quantum yield for I_2 photodissociation was greatly decreased when the viscosity of hydrocarbon solvents was increased. **Table**

2 gathers these data with the viscosities given in centiPoise (cP) and compares them with calculated quantum yields according to the Noyes model.[198] In this study, Noyes and coworkers noted that the calculated quantum yields varied significantly from the experimental values particularly in very viscous solutions, and hence developed two methods of determining β', termed Calc method 1 and Calc method 2 in **Table 2**.[198] The second method resulted in a closer match between experimental and calculated yields for very viscous solvents.

Table 2. Experimental and theoretical quantum yield for the photolysis of I_2 in solvent of various viscosity.

Solvent	Viscosity (cP)	ϕ_{ce}	Calc meth 1	Calc meth 2
Hexane	0.29	0.66 ± 0.04	0.52	0.47
CCl_4	0.92	0.14 ± 0.01	0.242	0.235
Bayol D	1.7	0.18 ± 0.025	0.145	0.155
C_4Cl_6	3.0	0.075 ± 0.009	0.086	0.107
NF 65	54	0.086 ± 0.010	0.0052	0.040
NF 95	80	0.048 ± 0.008	0.0035	0.038
USP 180	180	0.038 ± 0.004	0.0016	0.037
USP 335	380	0.036 ± 0.005	0.0007	0.036

Noyes *et al.* also investigated the impact of the excitation energy as Rabinowitsch and Wood predicted that the cage escape yield would increase as the wavelength of light decreased. The rationale was that the excess energy, beyond that needed to break the I–I bond, would be translated as kinetic energy to the iodine atom photoproducts providing a larger initial displacement and enabling them to more effectively escape the cage as indicated by Equation 3.3. Indeed. **Table 3** reveals that in hexanes the cage escape yields did increase with decreasing excitation wavelength. The more energetic blue photon increased cage escape by greater than 7-fold relative to red light. However, the yields predicted by the Noyes model did not fully account for the measured excitation wavelength dependence, and instead predicted values that were too small with blue light and too large with red light. In hexachlorobutadiene, the expected wavelength dependency was apparent, yet the Noyes model consistently predicted higher yields than were measured (**Table 3**).

Table 3. Experimental and theoretical quantum yield for the photolysis of I_2.

λ_{exc} (nm)	hν (kcal/mol)	ϕ_{ce} hexane	Noyes Model	ϕ_{ce} hexachlorobutadiene	Noyes Model
404.7	35.0	0.83	0.54		
435.8	30.0	0.66	0.52	0.075	0.087

546.1	16.6	0.46	0.46	0.036	0.070
579.0	13.9	0.36	0.44	0.018	0.065
643.0	8.9	0.14	0.40	0.023	0.055
735.0	3.3	0.11	0.31	0.020	0.040

Early ultrafast spectroscopic studies provided the first descriptions of cage escape in condensed media. Visible light excitation of I_2 yields a pre-dissociative state that underwent collisionally-induced crossing to a dissociative state that yielded the two iodine atoms. During the separation process, the solvent cage induced geminate recombination for a large fraction of the dissociated pairs to ultimately yield I_2. Hence a key conclusion was that the "caging effect" is primarily due to the initial collision of the atoms with the solvent. This recombination process yields I_2 molecules in a ground electronic state with a large excess of vibrational energy due to the formation of the bond.[43-44, 200]

The geminate recombination time for iodine atoms was first time resolved by Eisenthal and coworkers to be 140 ps in CCl_4 and 70 ps in hexadecane.[200] The transient kinetic data acquired in CCl_4 are shown in **Figure 15**. Pulsed 530 nm light promoted I_2 into the bound pre-dissociative B state or the dissociative A/A' states with relative oscillator strengths of 5.2:1.0. The kinetic data show a peak in the transmission about 20 ps after light excitation. This growth was assigned to I–I bond-breaking in the pre-dissociative excited state induced by collision with the solvent walls to yield iodine atoms. This represented a remarkable observation in its time. Indeed, early cage escape researchers were confounded by the issue of whether their steady state light excitation was quantitatively generating radical products or was instead accessing a pre-dissociative excited state that could relax to the ground state without bond rupture. At the time of the 1972 review, very few clear examples of pre-dissociative excited states were known, and the kinetic data shown is widely accepted as the first kinetic evidence for collisionally-induced dissociation of a pre-dissociative excited state occurring with an estimated rate constant of ~ 10^{11} s^{-1}.

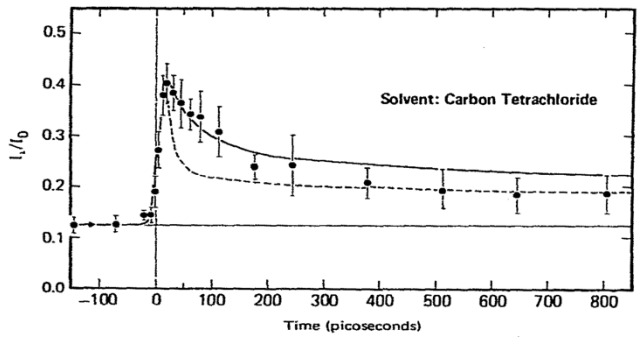

Figure 15. Transmittance change measured at 530 nm after pulsed 530 nm excitation of I_2 dissolved in CCl_4. Time-zero is indicated with a vertical line. The rise time is attributed to the reaction of a pre-dissociative B state with the solvent

walls to generate iodine atoms. The decrease over the first 500 ps is attributed to geminate recombination of the iodine atoms in the solvent cage and the nearly constant change at observation times greater than 500 ps is attributed to those iodine atoms that escape the cage. Overlaid on the data are fits to a random-walk model with emphasis on the short (solid line) and long (dashed line) time kinetic data. See text for additional details. Reproduced with permission from reference [200]. Copyright 1974 Elsevier.

At observation times greater than about 500 ps, the transmission change was nearly constant, **Figure 15**. This long-time absorption change was attributed to iodine atoms that had escaped the cage and indicated a yield of $\phi_{ce} = 0.25$. This value agreed reasonably well with prior scavenger studies $\phi_{ce} = 0.19$ and the theoretical model of Noyes that predicted $\phi_{ce} = 0.21$. The close agreement of these values further indicated that these researchers had directly quantified the impact of the solvent cage on geminate recombination and cage escape.[200]

The probability of recombination in a random walk model was considered with the form $ae^{-b/t}/t^{3/2}$ where a and b are constants related to the encounter diameter, average displacement of a displacement step and the frequency of such displacements. The authors considered modelling the early time data (solid line fits in **Figure 15**) and the long observation time data (dashed lines) and favored the long time analysis as more representative of a random walk model. The values extracted indicated a displacement size of 0.5 – 1 Å and a displacement "jump" frequency of 1-5 x 10^{12} s^{-1}. In hexadecane, the displacement distance was smaller (0.1 Å) and the frequency was somewhat larger, 2-20 x 10^{12} s^{-1}. Hence this ultrafast data provided the first quantification of the dynamics of cage escape.

In a subsequent study, the initial yield of $I^{\bullet}$ atoms and the cage escape yield were determined by picosecond spectroscopy.[201] The initial yield of atoms was independent of the bulk solvent parameters and was instead dependent on the discrete nature of the solvent, and more specifically its compressibility. In contrast, the cage escape yield was dependent upon the solution viscosity and hence the diffusion coefficient calculated from the Stokes-Einstein relation. The authors used the original description of geminate recombination presented by Noyes: primary recombination, when the original iodine atom partners had not escaped the solvent cage, and secondary recombination of those atoms that escaped the first solvent shell and recombined through diffusive-like motion. The authors' instrumentation did not have the temporal resolution required to time resolve the initial separation and instead monitored these so-called secondary recombinations. Such secondary recombination, while key to the Noyes model, have little experimental validation. Indeed, the authors concluded that there was most likely no distinction between primary and secondary recombination of iodine atoms. This conclusion was consistent with early trapping studies of the cage-escaped products by Hammond and coworkers who could not distinguish primary and secondary

recombination and concluded that there was no evidence for secondary recombination until the scavenger concentration was so high that the scavengers themselves were present in the solvent cage.[202-204]

Collectively, the picosecond data reported for iodine in weakly coordinating solvents like CCl_4, have been summarized with the potential energy surfaces shown in **Figure 16** and appear to be well established.[152] Rapid 1-2 ps dissociation or predissociation is followed by recombination on the X, A or A' states or cage escape into solution on a ~ 15 ps time scale. Hence the 15 ps predissociation time initially reported for the B state has since been revised.[155] Crossing from the A/A' to the X potential energy surface is solvent dependent and occurs on a 60 ps to few nanosecond time scale to generate vibrationally hot I_2. Vibrational relaxation on the ground potential energy surface X is also strongly solvent dependent occurring in 50-200 ps.

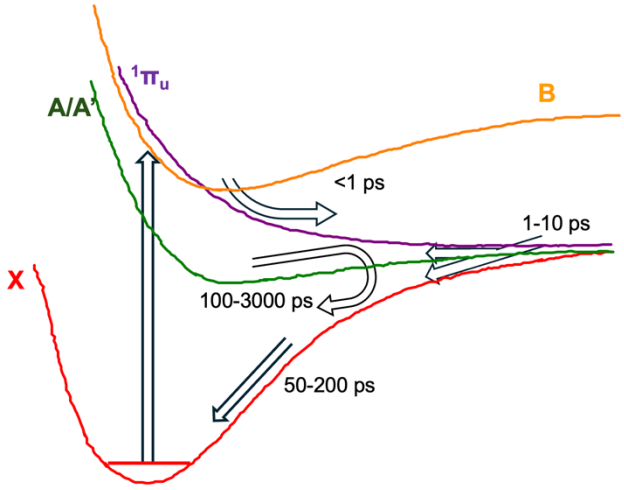

Figure 16. The potential energy surfaces relevant to the geminate recombination of iodine atoms after light excitation of I_2 in weakly coordinating solvents like CCl_4. Replotted from ref [197].

3.2.2) Bromine

The photodissociation of Br_2 in carbon tetrachloride was directly quantified by flash photolysis.[205] The authors measured a cage escape yield $\phi_{ce} = 0.22$, value that was about 100 times larger than expected based on steady state bromine exchange measurements.[206] The cage escape yield was comparable, but slightly larger than that for I_2 measured under the same conditions.

The authors used the Noyes model with a Br–Br bond dissociation energy of 45.5 kcal/mol to predict the cage escape yield. This analysis was complicated by the fact that a pulsed lamp was used to initiate the bond cleavage reaction. In other words, a well-defined excitation energy did not exist. This is important as, in the Noyes model, excitation energies greater than the bond dissociation energy provide kinetic energy to

the atoms that enable them to escape the solvent cage. Nevertheless, assuming an 'average' excitation wavelength of 440 nm and a separation distance of 4.8 Å, a cage escape yield of 0.065 was calculated, which was about a factor of three smaller than what was measured. Given the distribution of excitation wavelengths used, the agreement was satisfactory. Interestingly, the non-geminate rate constant for recombination of those Br$^{\bullet}$ atoms that escaped the cage was 1 x 10^{10} M^{-1} s^{-1}, almost a full order of magnitude smaller than that expected for a diffusion-controlled reaction leading to some speculation that there may be a barrier for Br–Br bond formation.[207]

The photodissociation of Br_2 was also quantified by photothermal grating spectroscopy (**Figure 17**).[208] Interestingly, the authors used 532 nm light excitation that was not expected to result in photodissociation. Previous authors had indicated that such relatively low energy visible light would not provide the Br atoms enough kinetic energy to escape the solvent cage.[209] Fitting transient kinetic data measured as a function of the concentration and laser irradiance, **Figure 17** provided evidence for solvated bromine atoms. Indeed, a cage escape yield of $\phi_{ce} = 0.12 \pm 0.01$ was extracted from this data. The authors reported a non-geminate recombination rate constant of 1.5 x 10^{10} $M^{-1}s^{-1}$, slightly larger than that previously reported and concluded that the results were consistent with the Noyes model.

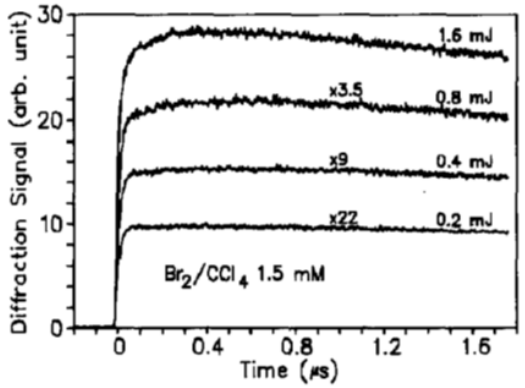

Figure 17. Diffraction signals observed at different laser energies from a CCl_4 solution containing 1.5 mM of Br_2. Reproduced with permission from ref [208]. Copyright 1991 Elsevier.

A novel time-resolved X-ray scattering technique was used to track Br$^{\bullet}$ atoms that underwent both geminate and non-geminate recombination.[210] After correcting for thermal artifacts by scaling the transient solvent response, the data revealed a cage escape yield of $\phi_{ce} = 0.12 \pm 0.01$, with geminate recombination accounting for 30% and a metastable Br_2 excited state accounting for the rest.

Interestingly, compressed gases have been shown to lower cage escape yields after pulsed-laser excitation of Br_2. Two models have appeared to rationalize the behavior. The first is a gas-phase caging effect analogous to that in fluid solution and operative for high pressure gases. The second is the formation

of gas phase "cluster complexes" envisioned to be adducts between bromine and the gaseous molecules held together by weak non-covalent van der Waals interactions.[211-214]

3.2.3) Chlorine

Ultrafast transient infrared studies were conducted to probe the impact of the solvent cage on two chlorine atoms.[215] Picosecond infrared studies after excitation of Cl_2 in hexane and per-deuterohexane were reported. Each pulse of 355 nm light excitation generated a remarkably high 0.17 M concentration of chlorine atoms. The cage escape yield was estimated ϕ_{ce} = 0.19 in good agreement with previous photoacoustic studies.[216] It appears that this estimate was based on the assumption that only the chlorine atoms that escaped the cage abstracted H atoms from the solvent. In other words, the photogenerated chlorine atoms did not react with the solvent molecules that comprised the cage. **Figure 18** shows the steady state infrared absorption spectrum of HCl (solid lines) and the transient spectra measured 400 ps after photoexcitation of Cl_2 (dashed lines). The good agreement indicates that the $Cl^{\bullet}$ atoms escaped the solvent cage and extracted a H atom in less than 400 ps. Interestingly, no kinetic isotope effect was noted for D extraction from per-deuterohexane. This study reveals some of the many challenges associated with quantifying cage escape yields when reactive radicals are formed in organic solvents.

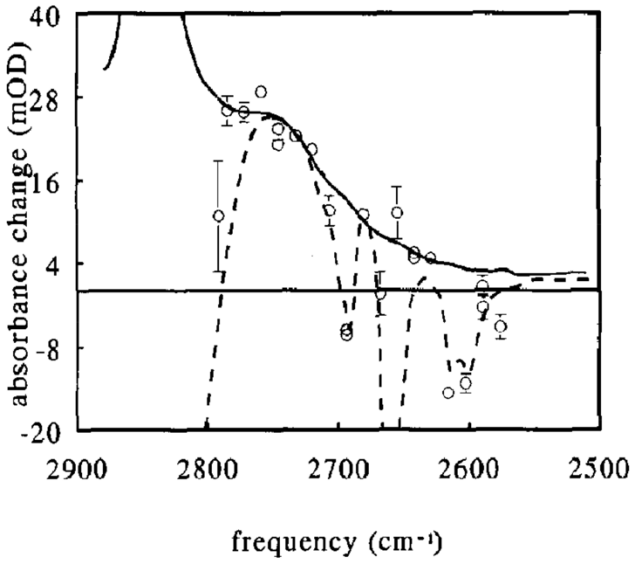

Figure 18. Transient spectrum recorded at a 400 ps delay time (open circle). Overlaid is the FTIR spectrum of HCl in C_6D_{12} (solid line). The negative absorbance spectrum of C_6H_{12} is also shown, scaled to the data at 2690 cm^{-1}, and using the HCl spectrum as the baseline. Reproduced with permission from ref [215]. Copyright 1993 Elsevier.

3.3) Tri-Atomic Species

3.3.1) Cyanogen iodide (ICN)

Ultraviolet light excitation of ICN in the energy range of 248-350 nm yields the iodine atom and the cyano radical that has been the subject of many studies. The initially formed excited state is one of three electronic states or an admixture of multiple states. The electronically excited ICN dissociates on a few hundred femtosecond time scale through two excitation wavelength dependent channels. Both channels yield a CN radical ($CN^{\bullet}$) in a rotationally hot state and an iodine atom that is either in the ground or an excited spin state as shown in Equation 3.11. The energy difference between the two channels corresponds to the spin-orbit splitting of iodine, ~ 21.7 kcal/mol.[217]

$$ICN + h\nu \rightarrow ICN^* \rightarrow CN^{\bullet} + I\ ^2P_{1/2} + I\ ^2P_{3/2} \qquad \text{Eq. 3.11}$$

Cage escape studies were complicated by interesting reactivity of the $CN^{\bullet}$ with the solvent molecules that comprised the cage. In chloroform solvents, H atom abstraction by $CN^{\bullet}$ was slower than that measured in the gas phase. The kinetic data suggested that the cyano radical must first reorient within the cage before H atom extraction occurs. A "dynamical cage effect" was proposed wherein an activationless reaction was controlled by diffusion of the cage solvent molecules that must be properly aligned in order to react with $CN^{\bullet}$. This proposal was supported by the expected temperature dependence of the reaction rate.[218] An alternative interpretation was probed by molecular dynamics simulations: a finite barrier exists in fluid solution that is absent in the gas phase.

Molecular dynamics simulations were conducted on a single ICN dispersed in 215 chloroform molecules in a truncated box that replicated the expected density.[219-223] Additional details of the simulations can be found in the original text. Consistent with experiment, the simulations revealed ballistic transport of the caged products. In other words, the mean free path was larger than the solvent cage and the products alter their motion only through collisional interactions with the solvent walls.[223-225] Interestingly, the percentage of trajectories that escaped the cage was almost identical to that observed after dissociation of the high spin triplet excited state, even though these products have about 1/3 less kinetic energy relative to the singlet state.

The distance between the primary radical pair is central to the Noyes model and was investigated recently by Winter and Do using quantum calculations with ICN as model.[226] A distance greater than 6 Å

was found to be necessary for cage escape regardless of the solvent. This distance is permitted by the strength of the solvent cage, as studied comparatively for water and ethanol. The recombination probability computed was 0.58 in ethanol and reached 0.82 in water, values that were correlated with the solvent ability to deplete energy upon collisions. Vibrational relaxation is slower in ethanol than in water, which eventually allows the ICN to maintain a longer bond distance and decreases the proportion of recombination. Interestingly, they also pointed out that aside from recombination and cage-escape, 5% of the deactivation pathways did not involve geminate recombination or cage escape and involved species in high vibrational energetic states.

3.3.2) Ozone

Excitation of ozone with 266 nm light yields two equivalents of O_2 through reactions 3.2 and 3.3.[227]

$O_3 + h\nu \rightarrow O_2 + O^{\bullet}$ Eq. 3.2

$O^{\bullet} + O^{\bullet} \rightarrow O_2$ Eq. 3.3

In the gas phase and in neat ozone, temperature independent quantum yields for O_2 formation have been reported to be 2.0 ± 0.3. This high yield indicates that the cage escape of the oxygen atom is unity, and that the escaped atoms quantitatively react with an oxygen atom to form the second equivalent of O_2. Interestingly, low temperature studies conducted in the presence of added argon gas revealed that the yields were decreased to values below 2, behavior attributed to caging of the oxygen atom by argon atoms. Variable temperature measurements from 10-30 K revealed an activation energy $E_a = 0.38 \pm 0.08$ kJ mol^{-1} attributed to collective vibrations of the ozone lattice that provided favorable orientations for escape of the oxygen atom.

3.3.3) Tri-iodide (I_3^-)

Visible or ultraviolet light excitation of I_3^- in iodide solutions results in the transient formation of $I_2^{\bullet -}$. The quantum yield has been reported to reach 2 through equations 3.4 and 3.5, indicating quantitative cage escape of the iodine atom in the initial photochemical step.

$I_3^- + h\nu \rightarrow I_2^{\bullet -} + I^{\bullet}$ Eq. 3.4

$I^{\bullet} + I^- \rightarrow I_2^{\bullet -}$ Eq. 3.5

However, studies in condensed media have shown that the yield of iodine atoms in the photochemical step can be less than unity. Pulsed ultraviolet light excitation of I_3^- yields vibrationally hot $I_2^{\bullet-}$ and the iodine atom ($I^{\bullet}$), equation 3.4, that recombine geminately by at least two processes. One leads to ground state I_3^- and the other forms a long-lived species of unknown origin that lives for about 40 ps in alcohols, acetonitrile and water at room temperature.[228] A recent temperature dependent study in ethanol revealed that the cage escape yield decreased from 0.36 ± 0.01 at 300 K to 0.02 ± 0.02 at 135 K. The more viscous ethanol present at the lower temperature precluded cage escape within experimental uncertainty.[229]

A recent nanosecond study in CH_3CN revealed that the iodine atoms that escaped the solvent cage quantitatively produced a second equivalent of $I_2^{\bullet-}$ when the iodide concentration was greater than 1 mM. When lower concentrations of iodide were present, clear evidence for a photochemical reaction was evident by a decrease in the I_3^- concentration indicating that the iodine atoms did not quantitatively recombine with $I_2^{\bullet-}$.[230]

3.4) Metal-Metal Bonded Species

Bimetallic complexes with a single M–M bond often have photodissociative excited states. Light excitation results in homolytic bond dissociation to yield a geminate radical caged pair. Systematic study of this photochemistry by Tyler and coworkers have provided keen insights into the factors that control cage escape.[231-237] The yields decreased significantly when the solvent viscosity was increased, behavior consistent with that reported for iodine atom cage escape and the Noyes model (**Figure 19**). However, as had been reported previously, the viscosity alone was not a predictor of cage escape and instead the details of the solvent, or solvent mixture, had to be considered. Importantly, the detailed nature of solvation was not needed when diffusion ordered NMR spectroscopy (DOSY) was utilized to quantify the translational diffusion coefficient *D* of a diamagnetic model complex, whose structure was similar to that of the paramagnetic radical. The reciprocal of the diffusion coefficient was termed the 'microviscosity' and was shown to be an excellent descriptor of the cage escape yield in a wide variety of polar, non-polar, aromatic and H-bonding solvents. These studies revealed that neither the solvent polarity or rotation of the radical were correlated with the cage escape yield.

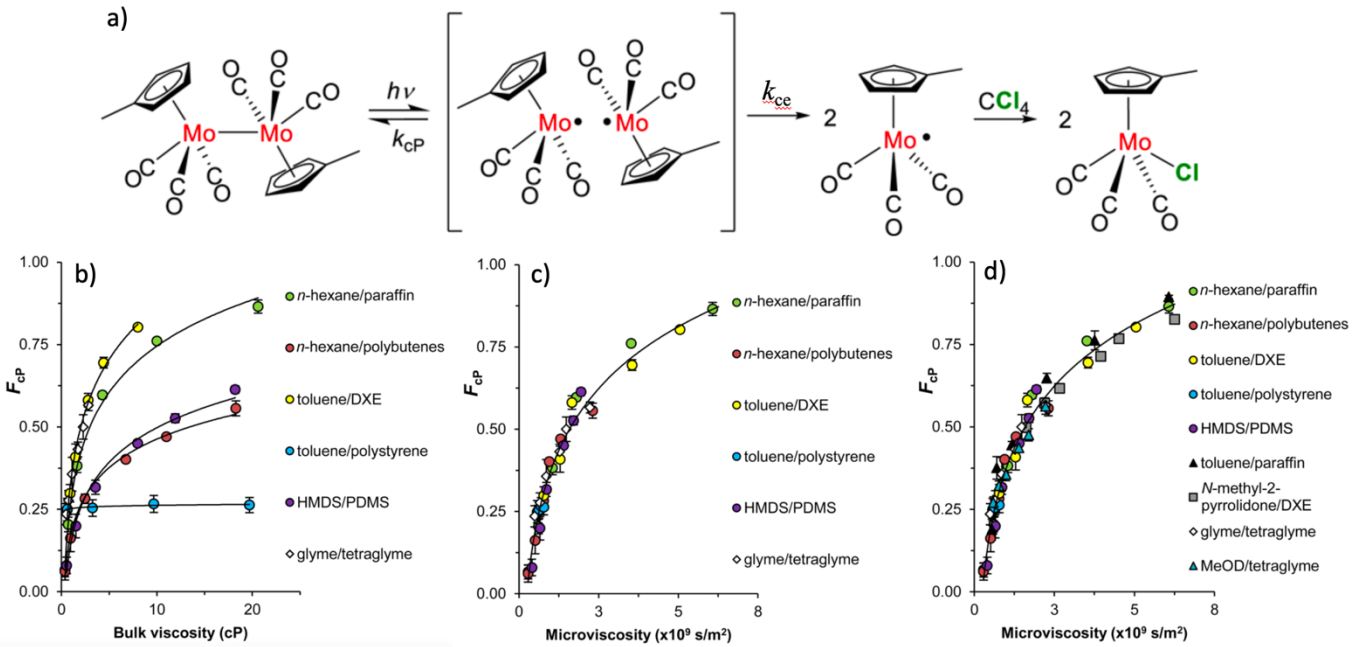

Figure 19. a) Photochemical production of caged radicals and subsequent trapping by CCl_4. Photochemical cage recombination efficiency (F_{cP}) as a function of bulk viscosity (b), or microviscosity (c and d). Each sample contains 20 wt% CCl_4 and error bars are 1σ. Curves are only a visual aid. Adapted with permission from ref [235]. Copyright 2003 American Chemical Society.

Green light excitation of the metal-metal bonded $[Mo(CH_3\text{-}Cp)(CO)_3]_2$ complex yielded the radical pair shown in brackets, **Figure 19a**. Those radicals that escape the cage with rate constant k_{ce} extract a Cl atom from carbon tetrachloride present in 20 weight percent as a radical scavenger. The concentration of the Mo–Cl species was quantified to determine the cage escape yield. Like Noyes, these authors quantified the fraction of radicals that recombined within the solvent cage, $F = 1/[1+(k_{ce}/k_{cP})]$ such that $\phi_{ce} = 1 - F$. The left-hand side of **Figure 19** shows the yields measured as a function of the solvent viscosity. In these data the viscosity of *n*-hexane, toluene, HMDS, and glyme were increased by addition of an organic species with a greater viscosity, termed a viscogen. To avoid selective solvation and significant changes to the solvent cage, viscogens with structures most similar to the solvent were selected. For example, paraffin was added to *n*-hexane and is abbreviated *n*-hexane/paraffin and is shown as the green circles. Note that the addition of the paraffin viscogen greatly increased the fraction of radicals that underwent geminate recombination. When polybutenes were added to *n*-hexane, i.e. n-hexane/polybutenes, geminate recombination also increased but to a lesser degree than when paraffin was added even when the bulk viscosity was the same. Even more dramatic effects were observed when the solvent itself was changed, such as the addition of 1-bis(3,4-dimethylphenyl)ethane (DXE) to toluene, toluene/DXE. The addition of poly(dimethylsiloxane) (Mw= 3800) PDMS to hexamethyldisiloxane (HMDS) had a negligible impact on cage escape. Note that

the solid lines connecting the solvent/viscogen data points have no physical meaning and were simply included to guide the eye.

The translational diffusion coefficient D was measured with a stable chromium surrogate [$(C_6H_6)Cr(CO)_3$] that has a mass and size similar to that of the radical Mo species formed in the cage. The fraction that recombined within the cage is plotted against the "microviscosity" equal to the reciprocal of D. These data are shown in **Figure 19d**. Note that all the experimental data now resides on the same curve. This is in sharp contrast to the disparate curves noted when the same data was plotted against the bulk solution viscosity (**Figure 19b**). Even H-bonding methanol and polar N-methyl 2-pyrrolidone solvents displayed viscosity dependent cage escape efficiencies that could be predicted by the measured diffusion coefficient. An explanation for the negligibly small impact of PDMS addition to the HMDS solvent now becomes apparent, the addition did not significantly impact the diffusion coefficient.

These experiments suggest that the direct measurement of the translational diffusion coefficients of radical surrogates will provide a metric by which the cage escape yield can be quantified. The translational diffusion coefficient for a particular radical pair enables the yield to be determined regardless of the nature of the solvent or solvent mixture. The authors noted also that the reverse should be true, if the cage escape yield is known, then the diffusion coefficient of the radicals can be determined. There was no experimental evidence supporting the notion that the relative orientation of the two radical species dictated the fraction that recombined.

Tyler and coworkers considered in more detail how viscosity impacts the solvent cage. In their work, they assessed the fact that despite having similar viscosities values, some bulk solvents show very different cage efficiencies (F_{CP}), indicating that the bulk viscosity is sometimes an incorrect metric for cage escape determination. To better describe the behaviour of the cage itself, they sought to understand why the "microviscosity", defined as the reciprocal diffusion coefficient, was such a good metric for cage escape.[235] To this end, they investigated a large variety of solvents like aromatics nonpolar (toluene/1,1-bis(3,4-dimethylphenyl)-ethane (DXE); toluene/polystyrene), aliphatics (hexane/paraffin; hexane/polybutene), a siloxane system (hexamethyldisiloxane (HMDS)/polyHMDS) and one polar system (glyme/tetraglyme). Remarkably, geminate recombination was not correlated with bulk viscosity across the different solvent mixtures with the polystyrene/toluene displaying little to no significant change in cage escape yield despite a significant change in the solution viscosity. This behaviour was attributed to a viscosity in the solvent cage that was independent of the bulk solution viscosity. In other words, since the polystyrene viscogen had

no impact on the cage escape yield, it must not be part of the solvent cage. The importance of this work is the fact that the diffusion coefficient of a diamagnetic surrogate for the photogenerated radical allowed quantitative predictions across different solvent systems that had not been previously achieved. It would be of particular interest to extend these findings to the diffusional quenching studies described in Section 4.

3.5) Transition Metal Complexes

An important application of cage escape is in ligand loss photochemistry of transition metal complexes in biology and chemistry.[195, 238-239] The classical example is carbon monoxide and dioxygen photorelease from heme complexes.[240] Cobalamin and Vitamin B_{12} photochemical cage escape also has a rich history.[241] On the other hand, some classes of ligand loss photochemistry are not amenable to cage escape study simply because the yields are too small. For example, photoinduced ligand loss through thermally activated population of d–d excited states from charge transfer excited states typically have very low yields, especially for second- and third- row metals.[242-246] In addition, the photoreductive elimination of ligands, that had been ligated through thermal oxidative addition reactions, often occur with quantum yields < 0.01.[247] Such reactivity is easily characterized by prolonged steady state illumination with quantification of the products formed as the photo-released ligands and the solvated transition metal complex are typically stable thereby facilitating characterization. Much like the early days of halogen photochemistry, it is experimentally difficult to know if the low yields are a result of geminate recombination and hence a cage effect or if instead a metastable excited state is populated that is not fully dissociative.[196, 244-246, 248-253] Future studies are likely to provide greater insights into the factors that underlie the low yields, yet at the time of this writing they remain unclear. Below we summarize the advances in cage escape yields of iron porphyrins (hemes) as well as cobalamins that have an extensive literature.[238, 240, 254-256]

In now classical experiments, Quentin Gibson and coworkers first utilized the flash photolysis technique to photorelease CO from a heme carbonyl center in myoglobin and hemoglobin in particular.[257] Importantly, the photorelease of CO in the presence of O_2 allowed the kinetics for O_2 binding to the heme to be quantified for the first time. Such ‘flash and trap’ experiments, where a thermodynamically stable complex is photoexcited and a kinetic product is subsequently trapped, represent important advances key to the improvement of the flash photolysis technique in biology. These were early days of flash photolysis that were aided by the large color changes that accompany ligand loss in hemes and intrinsically high yields of cage escape. A challenge in quantifying the exact cage escape yield in these pioneering studies was the

unknown nature of the 'solvent cage' in a complex protein environment. Indeed, a photodissociated ligand could be trapped in nearby protein pockets and subsequently undergo 'geminate recombination' over a large range of distances and time scales. Such data ultimately led to an understanding of pathways in the protein matrix by which CO and O_2 access the heme site. In addition, Gibson reported yields of unity for CO and much lower yields for O_2 release from myoglobin and hemoglobin, data that have withstood the tests of time.[258] For example, **Table 4** provides more recent data for CO and O_2 photorelease in horse and human myoglobin and O_2 release from human hemoglobin. The data are reported at 8 K, yet temperature dependent measurements revealed no variation in yields for CO. In contrast, significant geminate recombination occurred for O_2 down to temperatures of 150 K; below this temperature there was no evidence for geminate recombination lowering the cage escape yield.

Table 4. Stable photoproducts yields of Hemoglobin and Myoglobin at 8K after CW photolysis.[259] The columns represent the spectral region used to measure the yield.

Sample	Soret	760 nm	Far-IR (1950 cm^{-1})
Horse MbCO	1.0 ± 0.1	0.95 ± 0.05	0.95 ± 0.05
Human HbCO	1.0 ± 0.1	0.90 ± 0.10	N/A
Horse MbO_2	0.4 ± 0.1	0.45 ± 0.05	N/A
Human HbO_2	0.4 ± 0.1	N/A	N/A

The continued and near ubiquitous use of carbon monoxide in flash photolysis studies of heme and related complexes is due to several factors, including an ability to form meta-stable adducts, a competitive inhibitor of O_2 reduction at protein/model complex active sites, a stability toward unwanted redox reactions, and intense characteristic visible and infrared absorption bands. Shank, Rentzepis and Hochstrausser were amongst the first ultrafast spectroscopists to characterize CO and O_2 cage effects in hemoglobin.[260-262]

Ultrafast studies have also found a cage escape yield for CO release of unity at the earliest observation times. This high yield has been attributed to a spin change. The initial heme carbonyl is a low spin complex wherein all 6 d-electrons are paired. The release of CO generates a high-spin Fe(II) complex in the solvent cage and subsequent geminate recombination with CO is inhibited by the spin change and instead affords quantitative cage escape. Studies of a Cu(I) carbonyl complex where spin change and the presence of unfilled d-orbitals were precluded by the d^{10} electronic structure revealed cage escape yields of 0.30.[263] In addition, pressure dependent studies of CO coordination to ferrous hemes reveal a mechanism dominated by activation rather than diffusional contributions.[264-265]

Ultrafast kinetic studies revealed that the release of O_2 from oxyhemoglobin was due to both ultrafast relaxation to non-reactive sites and to geminate recombination. About 40% of the photodissociated O_2 was found to geminately recombine in a 200 ± 70 ps time scale corresponding to a cage escape yield of about 0.60. Ultrafast studied revealed an even smaller yield for oxymyoglobin, ϕ_{ce} = 0.30.[266-267] The coordination of O_2 to hemes generates a species that is best formulated as a ferric superoxide complex. Hence in this formalism, photorelease and rebinding of dioxygen are electron transfer reactions, likely occurring by inner-sphere mechanisms, i.e. $PFe^{III}–O_2^- + hv \rightarrow [PFe^{II}, O_2] \rightarrow PFe^{III}–O_2^-$. The transient data have hence been evaluated based on orbital correlations among the electronic states of the heme center. Further insights have been gained through the study of synthetic oxy-hemes that have been shown to photorelease O_2 with quantum yields very close to the value known for oxy-myoglobin and oxy-hemoglobin.[268] At a minimum, this indicates that the protein matrix and structure of the heme pocket are not strict requirements for modeling the photorelease of O_2 from heme proteins.

Heme-copper oxidases, such as cytochrome c oxidase, CcO, catalyze the four-electron reduction of dioxygen to water which is coupled to membrane proton translocation utilized by ATP synthase.[269-270] As a result there has been and continues to be tremendous interest in dioxygen activation at the heme-copper ($heme_{a3}/Cu_B$) center (**Figure 20**).[271-272]

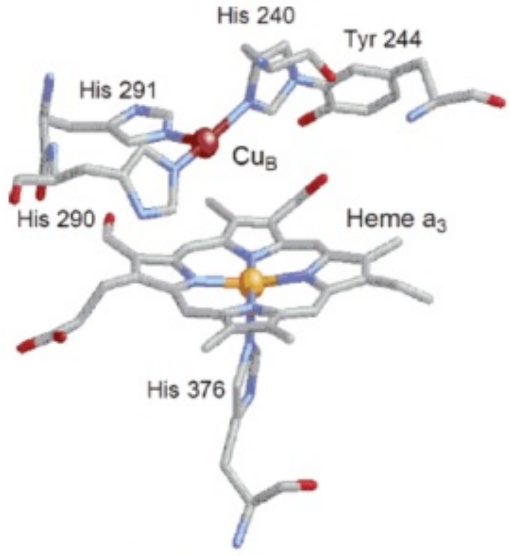

Figure 20. Structure of the fully reduced ($heme_{a3}$/CuB) active site of bovine cytochrome c oxidase, Fe•••Cu = 5.19Å. Reproduced with permission from ref [272]. Copyright 2005 American Chemical Society.

Gibson pioneered the use of flash photolysis to characterize CO and O_2 coordination to CcO[273-274] that has been further investigated by others,[275-283] and Alben provided early evidence that CO can migrate between

the heme and Cu centers.[284] Time-resolved infrared (TRIR) and visible absorption measurements were made to investigate CO and O_2 binding in a synthetic heme-CO/copper complex, $[(^6L)Fe^{II}(CO)\bullet\bullet\bullet Cu^I]^+$ (**Figure 21**), in CH_3CN and in acetone at room temperature. In both solvents, photodissociation of CO from the heme occurred with a quantum yield of unity. Interestingly, a significant fraction of the photodissociated CO molecules were shown to transiently bind to copper (2091 cm^{-1}) yielding $[(^6L)Fe^{II}\bullet\bullet\bullet Cu^I(CO)]^+$, followed by direct transfer of CO from copper back to the heme (1975 cm^{-1}) with a measured rate constant of 1600 s^{-1}. Eyring analysis yielded $\Delta H^{\ddagger}$ = 43.9 kJ mol^{-1} for CO transfer from Cu to Fe that was similar to that for CO dissociation from a copper model complex, $[Cu^I(tmpa)(CO)]^+$, $\Delta H^{\ddagger}$ = 43.6 kJ mol^{-1}, providing evidence that CO dissociation from copper regulates the binding of small molecules to the heme.

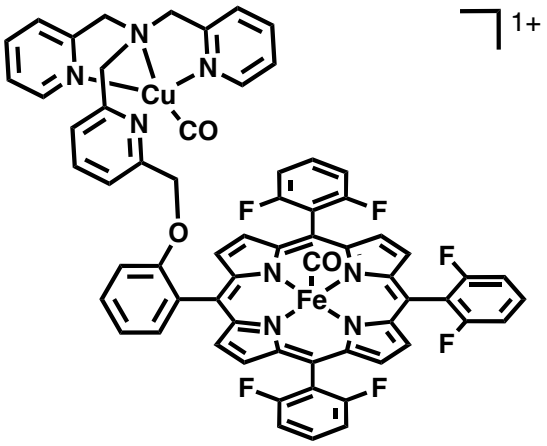

Figure 21. Structure of the heme-CO/copper complex

Reversible photodissociation of O_2 from hemes and bimetallic Cu/heme and non-heme Fe/heme compounds have also been reported in low temperature THF solutions to understand the impact of the second metal center on O_2 cage escape and rebinding.[268] Light excitation of $(^6L)Fe^{III}(O_2^-)$ yielded O_2 with a yield of 0.22. Interestingly, the presence of the non-heme Fe center had only a minimal impact on the yield while the presence of Cu^I resulted in a significant increase in the yield (**Table 5**). The data suggest that Cu also regulates O_2 binding to the heme, however unlike the case for CO migration, there was no direct evidence for O_2 coordination to Cu.

Table 5. Quantum yields for O_2 Cage Escape and O_2-rebinding rate constants

Photosensitizers	k_{O2} ($M^{-1}s^{-1}$)	ϕ_{ce}
$(F_8TPP)Fe^{III}(O_2^-)$	5.7 x 10^5	0.60 ± 0.02
$(^6L)Fe^{III}(O_2^-)$	6.4 x 10^5	0.22 ± 0.03

$[(^6L)Fe^{III}(O_2^-)Cu^I]^+$	6.8×10^5	0.34 ± 0.04
$[(^6L)Fe^{III}(O_2^-)Fe^{II}(Cl)]^+$	9.0×10^5	0.18 ± 0.02

[a]All experiments performed in THF at 198 K with 532.5 nm excitation (2-5 mJ/pulse, fwhm 8-10 ns).

The 'flash and trap' technique has also been applied to synthetic copper complexes that are of relevance to CcO. For example, the photorelease of CO from $[Cu^I(tmpa)(CO)]^+$ occurs with a yield of 0.30 in THF at 188 K. In the presence of O_2, a copper superoxide species was trapped $[Cu^{II}(tmpa)(O_2^{-})]^+$. Temperature dependent measurements with extrapolation to room temperature indicated that this simple Cu complex binds O_2 more rapidly than do hemes, $k_{O2} = 1.3 \times 10^9$ $M^{-1}s^{-1}$.[285] This and related Cu-superoxo complexes display intense superoxide-to-Cu^{II} ligand-to-metal charge-transfer (LMCT) absorption bands in the visible region, $\lambda_{max} = 425$ nm. It was later shown that under some conditions, LMCT excitation results in photo-ejection of O_2.[286-287] Interestingly, a marked wavelength dependence of the yield for O_2 release was noted that was 0.029 with 436 nm blue light and decreased to 0.078 with red 683 nm light excitation. It would be of interest to compare this excitation wavelength dependent data to the Noyes model.

Vitamin B_{12} has a rich history in photochemistry with a notable impact of sunlight being recognized decades ago.[288] A review article has recently appeared.[241] Common to Vitamin B_{12} and all its cobalamin analogues is a tetrapyrrole macrocyclic structure that chelates a Co metal center with an intramolecular axial base (**Figure 22**). A unique aspect of the Co center is that the coordination number often depends on the formal oxidation state of the metal; Co(III) is low spin six-coordinate, Co(II) is five coordinate and Co(I) is four coordinate. The classical crystal structure first reported by Dorothy Hodgkin is in fact of cyanocobalamin, which is generally referred to as Vitamin B_{12}.[289] The photochemical studies of most relevance to cage escape were performed on 5'-deoxy-adenosylcobalamin (also called coenzyme B_{12} or AdoCbl) and methyl cobalamin (MeCbl) where the cobalt center is in the formal oxidation state of three. Vitamin B_{12} is in fact the only organometallic complex with a metal-carbon bond found in nature.

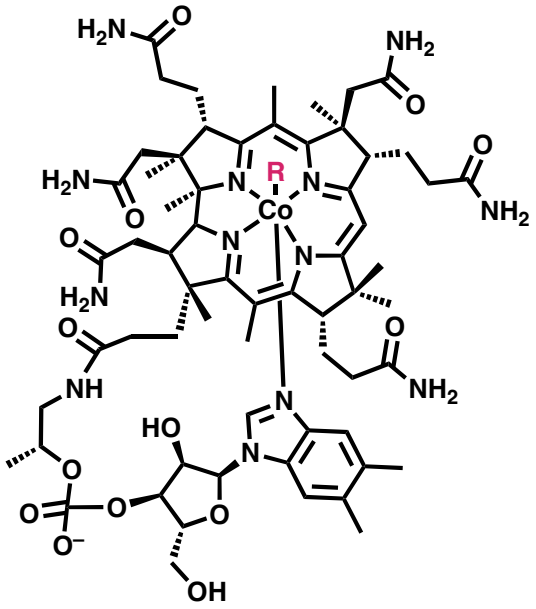

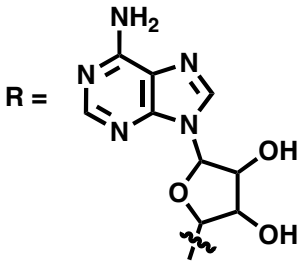

Figure 22. Structure of Vitamin B_{12} derivatives with variable upper and axial ligands.

Within 400 ps of light excitation, AdoCbl undergoes nearly quantitative Co–C bond cleavage.[290] This photochemistry is nearly insensitive to the excitation wavelength. While the initial quantum yield is near unity, there is a consensus in this field that the cage effect lowers the effective yield of radicals to 0.20 ± 0.02.[291-292] Studies in viscous ethylene glycol revealed a lower yield of 0.08, indicating that diffusion out of the solvent cage impacts the yield.[293-295] Protonation of the axial base also has a significant impact on the yield,[296] behavior that has been attributed to the spin state of the products.[297-299]

In sharp contrast to the cage effect for AdoCbl, there is a notable excitation wavelength dependence on the yield of long-lived radicals for methyl (and other alkyl) cobalamins.[291, 300-301] For example, the cage escape yield for blue light excitation (~0.3) is almost double that of green light (~0.15). In addition, and unlike AdoCbl, the Co–C bond breaks heterolytically generating a Co(II) product in the radical pair.[302-303] Like heme carbonyl complexes, the higher yield measured with blue light excitation may result from a spin

effect. The initial Co(III) methylcobalamin is low spin d^6 and light excitation yields a high spin d^7 Co(II) whose spin state is expected to inhibit recombination within the solvent cage. Indeed, magnetic studies suggest the presence of both triplet and singlet radical pair states, the former having the higher cage escape yield.[241, 297-298]

4) Cage Escape From Diffusional Excited States

Section 4 is focused on the cage escape process following diffusional bimolecular excited-state electron transfer using organic (section 4.1) and inorganic (section 4.2) photosensitizers. Each of these sections is further divided by the type of photosensitizer that was utilized. Seminal literature contributions that have reported specific cage escape yields are included and provide a fruitful discussion of the parameters that impact the yields. Studies that investigated bimolecular excited-state electron transfer but did not report cage escape yields were not included. Similarly, studies where the cage escape yields were determined for only one quencher, with no specific discussion, are not presented herein unless they provided key insight in context with the larger body of literature. Nevertheless, all cage-escape yields found in the available literature, whether discussed in detail in this section or not, are tabulated for clarity in the appendices (section 6) at the end of this review.

4.1) Organic Light Absorbers

In the following section, cage-escape yields employing organic photosensitizers, such as anthracene, other (polycyclic) aromatic hydrocarbons, pyrylium, thiopyrylium, xanthene, thiazine and ketone-containing photosensitizers are reported. The structures of these photosensitizers are represented in **Figure 23.**

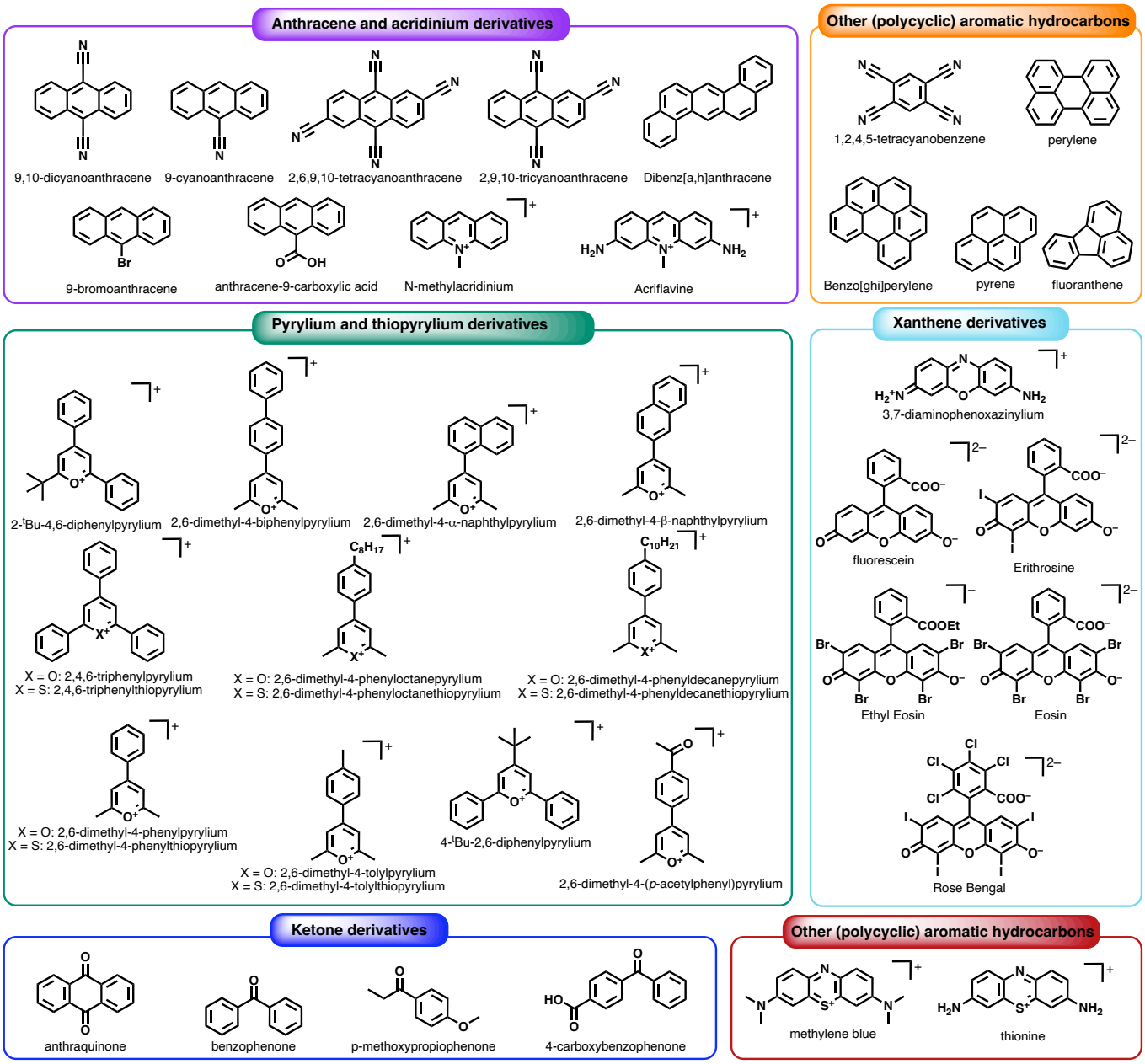

Figure 23. Structures of organic photosensitizers utilized for cage escape yield determination and described in this section.

4.1.1) Anthracene and acridinium derivatives

As an aromatic molecule with a well-defined singlet and triplet state, anthracene continues to be of interest to photosensitize redox reactions and as a molecular probe.[304] The ground state absorption spectra shows well defined vibronic structure that is perfectly mirrored in the fluorescence spectra providing a textbook example of vibration structure in the excited singlet and ground state.[29] The triplet excited state is non-phosphorescent at room temperature with a well-defined visible absorption spectrum that was widely

studied in the early days of flash photolysis. The singlet and triplet energies, as well as the intersystem crossing yields, have been tuned through introduction of substituents on the aromatic rings, much of this data is included in the early review by Birks and in a more recent review.[305-306] Anthracene also has well defined electrochemical behavior and early studies showed that photoexcitation of the one electron reduced species provided a means to create a 'super reductant' capable of generating solvated electrons in fluid solution.[307] With these desirable photophysical and redox properties it is perhaps unsurprising that anthracene and its many derivatives have emerged as an exceptional probe of spin, Coulombic, sterics, and driving force effects on cage escape yields. These particular advances are described below.

4.1.1.1) Spin

Anthracene derivates have been used as photosensitizers to quantify the impact of spin on cage escape yields. Indeed, anthracene has been used as an energy transfer shuttle to enhance the cage escape yield in the classical [$Ru(bpy)_3^{2+}$, MV^{2+}] assembly described in Section 4.2.1. While anthracene has well-defined singlet and triplet states, intersystem crossing is inefficient and the use of derivatives with larger triplet yields have been used. For example, Kikuchi et. al. utilized acriflavine, a nitrogen containing anthracene derivative, and demonstrated reductive excited-state quenching from aniline and *para*-halogenated anilines.[308] It was shown that the cage escape yield after electron transfer from the acriflavine triplet excited state decreased from 0.82 with aniline to 0.49 with *para*-iodoaniline. This was attributed to an increased rate constant for charge recombination within the solvent cage due to the enhanced spin-orbit coupling induced by the heavy halogen *para*- substituent.

In a related study, a series of *para*-halogenated anisole, aniline, and *N*,*N*-dimethylaniline derivates were utilized to reductively quench the triplet excited state of 9,10-dicyanoanthracene.[309] Cage escape after electron transfer decreased when heavy atoms were introduced onto the anisole donors, similarly to the previously described example. However, the aniline and dimethylaniline quenchers did not show a clear trend when heavy atoms were introduced, behavior attributed to the presence of an exciplex formed within the solvent cage.

Acridinium photosensitizers were recently utilized to perform light-initiated C–N coupling reactions.[310] In this study, various benzene derivatives were photo-oxidized in the presence of a cyclic amine. Time-resolved studies revealed very small (0.05) cage escape yield of the benzene radical cation that underlie the need for prolonged irradiation times to achieve high product conversion. The small cage

escape yields were rationalized with the singlet nature of the geminate radical pair, leading to rapid spin-allowed recombination to yield the ground state reactants.

4.1.1.2) Coulombic Interactions

Conjugated aromatic hydrocarbons form π-π adducts with other aromatic compounds and were the subject of a series of studies by Gould, Farid, and coworkers.[96, 311-321] Tetra- and dicyanoanthracene were utilized as excited-state acceptors with a series of aromatic donors. For 2,6,9,10-tetracyanoanthracene (TCA), the π-π donor-acceptor interactions resulted in the appearance of a new charge transfer absorption band at lower energy, ~ 460 nm, where the free TCA did not absorb light, **Figure 24**. The authors found that light excitation into this band resulted in different photophysical and cage escape properties than did direct excitation of the anthracene with higher energy light. The change in absorption upon forming the π-π adduct provided a convenient means to selectively form contact radical ion pairs (CRIPs) through a static quenching mechanism while higher energy excitation of the cyanoanthracenes generated solvent separated radical ion pairs (SSRIP). Through a wavelength dependent excitation, it was found that the CRIPs consistently displayed lower cage escape yields $(\phi_{ce})_{cp}$ than did the SSRIPs $(\phi_{ce})_{ss}$, **Table 6**. Interestingly, the magnitude of the difference was acutely sensitive to the nature of the donor. For 1,2,4-trimethylbenzene as the donor, the solvent separated cage escape yield was only about 15% lower than that for the contact pair, while over an order of magnitude was reported for hexamethylbenzene. The yields for both pairs decreased with decreasing driving force for charge recombination as estimated by the difference in the reduction potentials, $E^{o'}(TCA^{0/-}) - E^{o'}(D^{+/0})$. The smaller cage escape yields measured after light excitation of the CRIPs were attributed to strong electronic coupling and a smaller solvent reorganization energy than that present in the SSRIP. Marcus theory predicts that both these factors will increase the charge recombination rate constant and hence lower the cage escape yield. The lower yields measured after excitation of low energy charge transfer were consistently found for other π-π adducts.[313, 316, 318] This data provides perhaps the best evidence for the presence of both a primary and secondary radical pair proposed in the Noyes cage escape model.

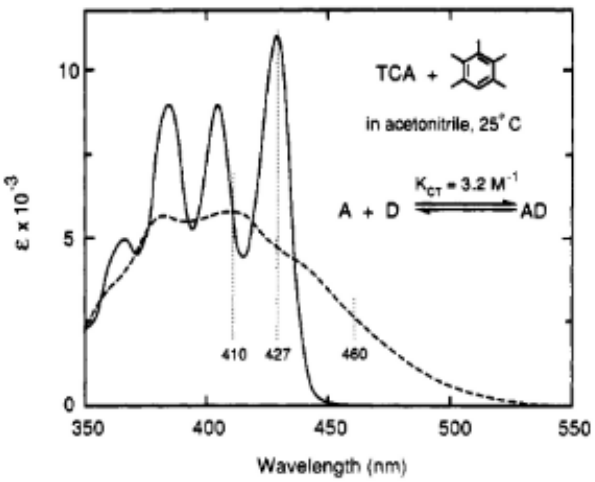

Figure 24. Absorption spectra of 2,6,9,10-tetracyanoanthracene (solid line) and the adduct formed between 2,6,9,10-tetracyanoanthracene (TCA) and pentamethylbenzene in CH_3CN. Variable concentration studies provided an equilibrium constant of 3.2 M^{-1}. Reproduced with permission from reference [318]. Copyright 1991 American Chemical Society.

Table 6. Cage escape yield from solvent-separated radical ion pairs (SSRIPs) and contact radical ion pairs (CRIPs) of tetracyanoanthracene radical anion and substituted benzene radical cations in acetonitrile at 25°C. Subscripts ss and cp refer to data of the solvent-separated and contact pairs, respectively.

Electron Donor	$E^{o'}(TCA^{0/-}) - E^{o'}(D^{+/0})$	$(\phi_{ce})_{ss}$	$(\phi_{ce})_{cp}$
	2.36	0.058	0.052
	2.28	0.042	0.020
	2.27	0.041	0.018
	2.22	0.041	0.016
	2.15	0.035	0.0063
	2.03	0.031	0.0028

When naphthalene was used in place of alkylbenzene as an electron donor, the same excited-state cyanoanthracene acceptors were found to yield 1:2 anthracene:naphthalene π-π adducts. It was shown that the cage escape yield decreased at larger concentrations of donor upon which the equilibrium favors formation of the 1:2 adduct. These adducts similarly to ones previously described will increase the rate constant for charge recombination and decrease the ability for products to escape the solvent cage.[96] This

low yield was attributed to the same Marcus parameters invoked to rationalize the lower yield of CRIPs relative to SSRIPs. Due to this, a concentration dependence was borne out where at larger concentrations of donor, the cage escape yield decreased with the formation of 1:2 adducts.

In these examples, the ground state adducts were formed by non-covalent intermolecular π-π interactions. After excited-state electron transfer, the radical ion pairs also experienced an electrostatic (Coulombic) attraction that impacts the so-called work terms for electron transfer that could in turn influence cage escape yields. To better understand the possible role(s) of electrostatic interactions, this same research group utilized monocationic *N*-methylacridinum in place of the neutral cyanoanthracenes. With *N*-methylacridinum the cationic charge is "shifted" to the alkylbenzene donor. Such "charge shift reactions" are often utilized to understand the role of electrostatics.[315] In comparisons with the cyanoanthracenes at the same driving force for excited-state electron transfer, the ratio of the charge recombination rate to the cage escape rate was reported to be smaller for the charge shift reaction, resulting in a larger cage escape yield for the charge shift than the charge separation reaction. The difference between the ratio of rates for each reaction was dependent on the driving force for charge recombination, whereas the driving force increased the difference too increased. To the extent that the structure of the π-π adducts for *N*-methylacridinum and cyanoanthracene can be equated, the data suggest that a higher cage escape yield is expected for electron transfer reactions that yield products with less coulombic attraction.

4.1.1.3) Distance/Sterics

As previously described, ground state intermolecular 1:1 π-π adducts of 2,6,9,10-tetracyanoanthracene and alkylbenzenes have been shown to give rise to unique long wavelength charge transfer absorption features; charge transfer excitation gives rise to what has been termed contact radical ion pairs (CRIPs) whereas direct light excitation yields solvent-separated radical ion pairs (SSRIPs). The electron transfer distances were approximated to be 3.5 Å in the CRIP and 6-8 Å in the SSRIP, and hence a much larger electronic coupling and smaller outer-sphere reorganization energy were expected in the CRIPs.[318] This distance effect further emphasizes the observed cage escape yields for ground state π-π adducts of cyanoanthracene derivatives and alkylbenzenes discussed in Section 4.1.1.2. As another means to probe the distance/steric dependence on cage escape yields, a series of hindered alkylated benzenes donors were used to quench the excited state of 9,10-dicyanoanthrancene (DCA) and 2,6,9,10-tetracyanoanthracene (TCA).[319]

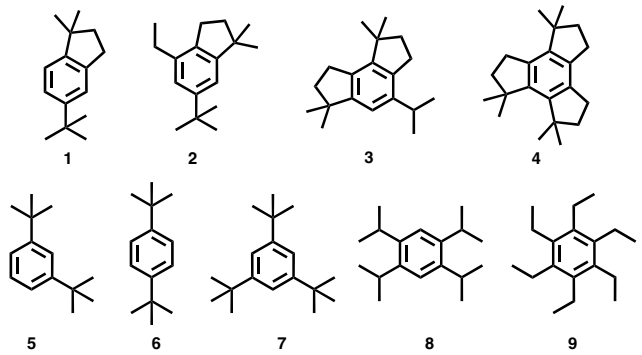

Figure 25. Structure of alkylated benzene electron donors

The alkylated benzenes donors were categorized into two groups as shown in **Figure 25**. Donors 1-4 contained at least one 5-member ring with hydrogen atoms in the alpha position to the benzene ring that provided hyperconjugation to stabilize the radical cation formed after electron transfer. The second group 5-9 did not have this same hyperconjugation. To account for variations in the thermodynamic driving force for electron transfer that were introduced by these substituents, comparisons were made to previously published values of non-hindered alkylbenzenes that had nearly the same driving force as determined by the reduction potential of the benzene donor, **Table 7**.

Table 7. Cage escape yield for sterically hindered (sh) substituted benzene donors with cyanoanthracene acceptors. Cage escape yields are compared to literature values of non-hindered (nh) alkylbenzenes that had nearly the same driving force.

PS	Donor	$E^{o'}_{\square}(D+/0)$ (V vs SCE)	$(\phi_{ce})_{sh}$	$(\phi_{ce})_{nh}$
DCA	**1**	1.90	0.582	0.344
	2	1.82	0.403	0.245
	3	1.68	0.307	0.135
	4	1.63	0.208	0.111
	8	1.77	0.549	0.205
	9	1.64	0.397	0.112
TCA	**1**	1.90	0.113	0.0517
	2	1.82	0.0861	0.0408
	3	1.68	0.0665	0.0302
	4	1.63	0.0625	0.0282
	5	2.13	0.364	0.125
	6	2.03	0.266	0.0830

7	2.01	0.325	0.0769
8	1.77	0.109	0.0369
9	1.64	0.0736	0.0283

DCA = 9,10-dicyanoanthracene, TCA = 2,6,9,10-tetracyanoanthracene.

Table 7 shows that the cage escape yield from the hindered donors was consistently larger than that of the non-hindered donors, $(\phi_{ce})_{sh} > (\phi_{ce})_{nh.}$ The degree to which the electronic coupling and reorganization energy contributed to the enhanced yields measured for the sterically hindered donors was difficult to disentangle.[319] Nevertheless, the data presented point towards the use of sterics to control cage escape yields. These steric dependencies previously discussed have also been demonstrated by other groups using similar photosensitizers and quenchers.[322] However, Braun and coworkers interestingly noted that the magnitude of the steric effect was solvent dependent. In polar solvents, the recombination rate will decrease with steric bulk and the rate of escape will increase, overall increasing the yield. In non-polar solvents however, the observed steric dependence is caused by an increase in the initial separation distance of the PS and Q.[322] This is anticipated to be smaller due to an enhancement of attractive Coulombic forces and as such decrease the cage escape yield in non-polar solvents.

Interestingly, and of some relevance to these sterically hindered benzene studies, are the reductive quenching studies of DCA* and TCA* by *cis*- and *trans*-stilbene derivatives.[317] It was consistently found with each substituted stilbene that the cage escape yields were larger for the *trans*- isomer than for the *cis*-isomer. The authors hypothesized that the electron density is delocalized in the planar *trans*- isomer and was localized in the non-planar *cis*- isomer. For this reason, the average charge recombination distance was larger for the *trans*- and the cage escape yield was larger. Similar delocalization discussions have been invoked for the quenching of di- and tetracyanoanthracene by biphenyl and phenanthrene derivatives.[316]

4.1.1.4) Driving Force

Reductive quenching of 9,10-dicyanoanthracene and 2,6,9,10-tetracyanoanthracene by a series of substituted benzene donors as well as biphenyl, naphthalene, and fluorene donors were investigated to understand the impact of driving force on cage escape yields.[311, 315-316, 319-321] As the caged radical products were not directly observed, the rate constant for charge recombination k_{cr} was calculated from the measured cage escape yield and using an estimate of the rate constant for diffusion out of the cage, $k_{ce.}$. With this analysis, it was found that k_{cr} decreases with increasing driving force, consistent with electron transfer occurring in the Marcus kinetic inverted region, **Figure 26a**. Interestingly, driving force was not the only

important parameter as the nature and radius of the donor were also found to play a role, presumably due to differences in the reorganization energy and electronic coupling for electron transfer.[314] The extracted charge recombination rate constants were fit to the semiclassical Marcus expression that provided estimates of the total reorganization energy (λ) and the electronic coupling matrix element H_{DA}. The coupling was small in all cases with $H_{DA} < 12$ cm^{-1}, consistent with non-adiabatic electron transfer and appropriate for the theory used. The authors determined an inner sphere reorganization energy of 0.25 eV for all donors used from which they reported that the outer sphere reorganization energy decreased from 1.63 eV to 1.48 eV to 1.40 eV as the number of aromatic rings was increased from 1 to 2 to 3. An important subtlety in the use of 9,10-dicyanoanthracene and 2,6,9,10-tetracyanoanthracene as photosensitizers and benzene derivatives as donors is the formation of stable 1:1 π-π adducts formed in the ground state (Section 4.1.1.2).[313]

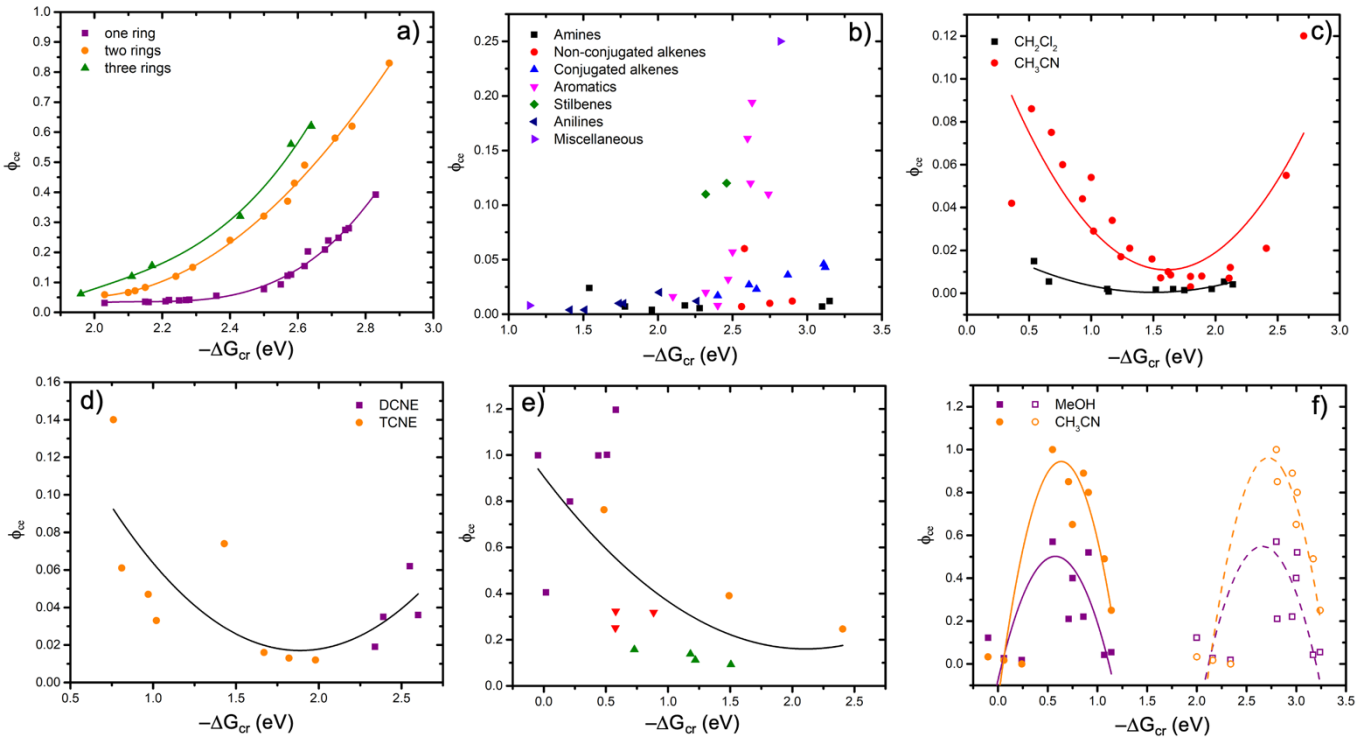

Figure 26. Selected plots from the literature investigating the impact of the Gibbs free energy change for geminate charge recombination, $-\Delta G_{GCR}$, on the cage-escape yield. a) Cage-escape yields vs $-\Delta G_{GCR}$ for radical-ion pairs of 9,10-dicyanoanthracene and 2,6,9,10-tetracyanoanthracene radical anions with one-ring, two-ring and three-ring donor radical cations. Replotted from data available in reference [316] b) Cage-escape yields vs $-\Delta G_{GCR}$ for stilbenes (green diamonds), aromatics (pink triangles), conjugated alkenes (blue triangles), non-conjugated alkenes (red circles), amines (black squares), anilines (blue triangles) and miscellaneous (purple triangle) donors. Replotted from data available in reference [323] c) Cage-escape yields vs $-\Delta G_{GCR}$ for the reaction between cyanoanthracene derivatives and amino- and methoxybenzene derivatives in dichloromethane (black squares) and acetonitrile (red circles). Replotted from data available in reference [324]. d) Cage-escape yields vs $-\Delta G_{GCR}$ for the reaction between different photosensitizers and TCNE

(orange circles) and DCNE (purple squares). Replotted from data available in reference [325] e) Cage-escape yields vs $-\Delta G_{GCR}$ for several pyrene-quencher combination in acetonitrile. The quenchers are classified into four categories: amines (purple squares), nitriles (orange circle), esters (red triangles), and anhydrides (green triangles). Replotted from data available in reference [326] f) Cage-escape yields vs $-\Delta G_{GCR}$ for the quenching of pyrene and dibenz[a,h]anthracene by cyanobenzenes in methanol (purple squares) and in acetonitrile (orange circles). Geminate recombination is calculated assuming recombination to the triplet state (solid line and filled symbols) or towards the singlet ground state (dashed lines and open symbols). Lines and parabolas are used to guide the eye. Replotted from data available in reference [327].

Jaques and coworkers conducted a thorough study of 9,10-dicyanoanthracene quenching by a series of 42 electron donors, including amines, alkenes, and aromatics.[323] A plot of the cage escape yield versus the driving force for geminate recombination was "Marcus-like," particularly for stilbene and aromatic donors, with a decrease in yield as the driving force became highly favorable, **Figure 26b**. For other families of electron donors, a weaker driving force dependance was observed . With a variety of possible contributions to the weak dependence, the internal reorganization energy (λ) and the specific vibrational acceptor mode (ν) were posited as the most critical. Qualitatively, the magnitude of the dependence was attributed to the degree of charge delocalization within the radical pair, with greater delocalization translating to a broader $-\log(\phi_{ce})$ vs $-\Delta G$ plot.

Miyashi and coworkers studied the quenching of anthracene derivatives quenched by substituted pyridines donors in CH_2Cl_2[324] to compare to previous work done by their group and others in CH_3CN, **Figure 26c**.[96, 311-320, 328-330] They assumed that electron transfer occurred over the same distance for these two solvents. The authors calculated the cage escape rate constant utilizing a model proposed by Tachiya,[331] and calculated k_{cr} with Eqn 1.1. From the calculated k_{ce} and the measured cage escape they extracted k_{cr} and plotted it as a function of driving force. The free energy dependent k_{cr} data were fit to the Marcus equation, providing a λ = 1eV and H_{DA} = 18 cm^{-1} in CH_2Cl_2. Importantly, included in their analysis was a solvent dependent reaction radius that was most relevant in low polarity solvents at low driving forces, where low polarity solvents reduced the reaction radius and resulted in decreased cage escape yields. Note that Gould and coworkers also reported lower cage escape yields in CH_2Cl_2 than in CH_3CN.[96, 318]

The presence of competitive quenching mechanisms has complicated study of the free energy dependence on cage escape yield. A case in point is the work of Kikuchi and coworkers who quantified the quenching of a series of fluorophores, including fluoranthene, 9,10-dicyanoanthracene, 2,9,10-tricyanoanthracene, and 2,6,9,10-tetracyanoanthracene, quenched by tetracyanoethylene and fumaronitrile (**Figure 26d**).[324-325, 330] Evidence for exciplexes were found in some cases and not in others leading to a complicated plot of the charge recombination rate constant versus the driving force. Following a method by

Mataga and coworkers,[332] they were able to measure the biexponential excited-state decay and assigned the faster component as relaxation via exciplex and the slower component to $k_{cr.}$ This kinetic data when overlaid with the k_{cr} values determined indirectly provided more compelling evidence for charge recombination occurring in the Marcus normal, activationless, and inverted regions.

4.1.3) Other (Polycyclic) Aromatic Hydrocarbons

Mataga and coworkers studied the quenching of pyrene by 21 quenchers, that included aromatic amines, nitriles, esters, and anhydrides, in acetonitrile and acetone.[326] The goal of this study was to understand the free energy dependence of the measured cage escape yields. A plot of the relative yield versus the driving force was most consistent with electron transfer in the Marcus normal region, **Figure 26e**. This was true even for driving forces that were much larger than the expected reorganization energy and hence where inverted behavior was anticipated. The authors attributed the lack of inverted behavior to result from additional pathways for charge recombination that included population of the pyrene triplet state rather than the ground state.[333-335]

Zanini et. al. quantified the quenching of pyrene with substituted benzenes in both methanol and acetonitrile.[327] The Eigen equation was utilized to determine k_{cr} values from measured cage escape yields. When plotted against ΔG, they too found that the data were most consistent with normal electron transfer rather than the expected Marcus kinetic inverted region when recombination produced ground state products. These authors then replotted the data assuming that triplet pyrene, and not ground state pyrene, was a product of the charge recombination reaction (**Figure 26f**). This resulted in a good fit to the Marcus expression with normal electron transfer occurring with driving forces that were smaller than the expected reorganization energy.

The data in **Figure 26f** imply a small change in the outer sphere reorganization energy in changing the solvent from methanol to acetonitrile, while the cyanoanthracene data indicated a more significant impact in going from CH_3CN to CH_2Cl_2. Hence, solvent appeared to impact kinetics of geminate charge recombination and cage escape, but the magnitude to which it does so is less clear. In 1975, Masuhara and co-workers classified the solvent effects on cage escape into two groups: 1) those that impact the nature of the dissociative states (which translates to the nature of the excited state, singlet/triplet); and 2) those that impact the rate of charge recombination and cage escape yield. The first classification refers to excited-state dynamics that can be highly solvent dependent as was recently emphasized by Orr-Ewing and

Venkatraman.[336] The second classification is implicit in Marcus theory and the expectation that a polar solvent will help stabilize the charge-separated products. To provide a more rigorous quantification for cage escape, tetracyanobenzene-toluene and pyrene-donor systems were investigated. For both systems, the cage escape yields were enhanced in solvents with a larger dielectric constant. The authors associated this behavior with the dissociative excited state. A linear relationship was proposed for $\log(1/\phi_{ce} - 1)$ and $1/\varepsilon$.[334] Four years later, the same research group investigated oxidative quenching of photoexcited pyrene and suggested that other solvent dependent paths were competing with cage escape.[337]

It hence appears that solvent polarity, as quantified by the dielectric constant, plays an important role in the cage escape yields. For example, in benzene, concerted electron and proton transfer from photoexcited acenaphthene to tetrachloro-1,4-benzoquinone (chloranil) was observed while no proton transfer occurred in dichloroethane.[338] In dichloroethane, the primary ion pair products were considered to be spatially separated in the solvent cage, weakening the coulombic attraction between the two partners and resulting in very low activation energies for ionic dissociation and back electron transfer. In contrast when benzene was the solvent, a strongly associated triplet primary pair was formed with strong coulombic interactions that prevented cage escape.

Coulombic interactions were also found to be important for cage escape associated with light-induced symmetry breaking (self-quenching) of perylene that yields a geminate radical ion pair comprised on an oxidized and a reduced perylene.[339] In nonpolar solvents, such as toluene, chloroform and THF, there was no evidence of cage escape. In solvents of increasing polarity, such as acetone, acetonitrile and DMSO, cage escape yields between 0.003 and 0.16 were determined. These yields were shown to increase with the solvent dielectric constant. In ionic liquids, i.e. extremely polar solvents, the cage escape yields increased dramatically to values between 0.46 and 0.55. The trend in cage escape yields was explained by Coulombic attraction within the radical ion pair that was very large in nonpolar solvents, leading to no escaped products. Charge screening by more polar or ionic solvent molecules lead to larger cage escape yields. It is interesting that the yields were most optimal in the high viscosity ionic liquids that would not have been predicted by the Noyes model. The strong solvent dependency also suggest that solvent-separated radical ion pairs are important to the cage escape process.

Gould *et al.* studied the quenching of 1,2,4,5-tetracyanobenzene by substituted benzene donors.[320-321, 329] Much like cyanoanthracenes, 1:1 adducts were formed with low energy charge transfer bands. Log plots of k_{cr} values, extracted from an evaluation of the emission rate constant and luminescence lifetimes,

as a function of $-\Delta G_{GCR}$ were linear. Hence, like the cyanoanthracene studies, the extracted charge recombination rate constants decreased with increased driving force but not in the parabolic form expected based on Marcus's semiclassical expression, **Figure 27**.

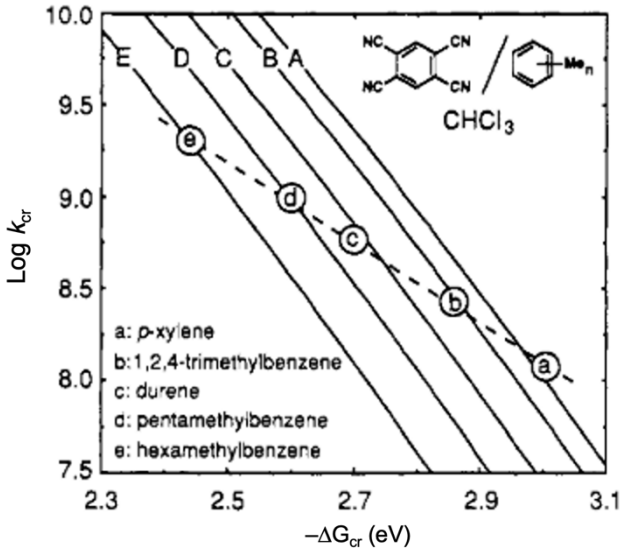

Figure 27. Plot of log measured geminate charge recombination rate constant (k_{cr}) vs the driving force ($-\Delta G_{cr}$) for contact radical-ion pairs of 1,2,4,5-tetracyanobenzene and methylbenzenes. The solid lines represent the calculated driving force dependencies for the reorganization parameters characteristic of each radical-ion par (the slopes of the approximate straight lines are $-4.6\ eV^{-1}$). The dashed line represents the apparent driving force dependence of the data (slope of the approximate straight line is $-2.2\ eV^{-1}$) if the variation of the reorganization parameters with the structure of the radical-ion pair is not taken into account. Reproduced with permission from ref [320]. Copyright 1993 Elsevier.

A number of groups studied the ionic dissociation of di- and tetra-cyanobenzene (TCNB) exciplexes with methyl-substituted benzenes, most commonly toluene. A representative example by Masuhara *et al.* studied the cage escape yield for ionic dissociation of TCNB and toluene as a function of solvent dielectric as controlled by a 1:2 mixture of toluene to solvent.[334] They discovered that cage escape yields increased from ϕ_{ce} <0.01 in 1,2-dichloroethane (ε = 10.4) to ϕ_{ce} = 0.1 in acetonitrile (ε = 37.5). The authors also studied how the addition of toluene to a dichloromethane solution of TCNB affected the cage escape yield. They observed that cage escape yield increased as the bulk solvent dielectric increases. These results were confirmed by other groups.[337, 340-342] Other studies observed a number of photo-induced substitutions that can occur between TCNB and such aromatic quenchers, but those reactions are not of interest in the scope of this review, so interested readers should refer to the original source.[342]

4.1.4) Pyrylium

The internal heavy atom effect on cage escape yields has been studied using the singlet excited states of pyrylium and thiopyrylium photosensitizers quenched by electron transfer from a series of benzene, toluene, and anisole donors.[343-344] In acetonitrile, the pyrylium photosensitizers consistently gave larger cage escape yields than did the heavy atom containing thiopyrylium, behavior attributed to spin-orbit coupling induced charge recombination to ground state reactants. In addition, a series of halogenated benzene, toluene, and anisole derivatives were also used to test whether an internal heavy atom impacted the cage escape yield. For example, when halogenated benzene derivatives were added to pyrylium solutions, the cage escape yield decreased from benzene (ϕ_{ce} = 0.75) to chloro- (ϕ_{ce} = 0.56), to bromo- (ϕ_{ce} = 0.33), and to iodo- (ϕ_{ce} = 0.10) benzene. The entire family of halogens (Cl, Br, I) were not rigorously quantified for the toluene and anisole derivatives however the expected heavy atom effect was present with these quenchers as well.[343] With the thiopyrylium photosensitizer, the same trend in cage escape yield was observed when heavy atoms were introduced into the quencher solutions, however the effect was much smaller in magnitude.[344] Additionally, using the pyrylium photosensitizer, the cage escape yields were measured in acetonitrile and chloroform. The cage escape yields were markedly different in each solvent and those measured in chloroform were consistently 1.5-2 times less than the values in acetonitrile. The difference between these solvents was attributed to a generally larger separation between the radicals formed after charge separation in acetonitrile due to a greater degree of solvation.[343]

Apart from the spin effect on cage escape yield, a driving force dependence on calculated charge recombination rate constant was presented. Using the pyrylium photosensitizer with the quenchers mentioned previously, Marcus inverted behavior was observed where the charge recombination rate constant decreased with increasing driving force.[344] Assuming a constant rate of cage escape for the different quenchers, this would imply that the cage escape yield will increase with increasing driving force, placing the charge recombination rate constant in the “inverted” region.

4.1.5) Xanthene

A series of common xanthene dyes (fluorescein, ethyl eosin, erythrosine, and rose bengal) conveniently contain different halogen atoms present in various positions on the molecules.[345] For this reason, these organic compounds have been used to study the internal and external heavy atom effect as well as the magnetic field effects on cage escape yields. Under the application of a magnetic field, an increase in the cage escape yield at low magnetic field strengths (0 - 0.1 T) was observed. This study found that the cage escape yield increased sharply and at a field strength of ~50 mT reached a maximum

enhancement of ϕ_{ce} = 1.0 for fluorescein and ϕ_{ce} = 0.5 for the other dyes.[345] The saturation of the magnification of the cage escape yields at relatively low field strengths is evidence for the *hf* radical pair mechanism and while data were not presented to suggest this, the authors note that the Δg mechanism becomes operative at high field strengths ($B_0 >> 0.1$ T). In addition to seeing an enhancement in the cage escape yield in the presence of a magnetic field, an internal and external heavy atom effect was considered. After excited-state electron transfer from the xanthene dyes to *p*-cresol as the acceptor, the cage escape yields decreased when halogen atoms with larger atomic numbers were present on the xanthene dye.[345] However, the influence of an external heavy atom, in this case iodomethane, was less clear. In general, the effect of the external heavy atom was dye and viscosity dependent. It was found that at the extreme viscosities studied (less than 0.0295 cP or greater than 0.236 cP), there was no noticeable impact of an external heavy atom. For the dyes fluorescein and erithrosine, there was a slight dampening of the magnetic field enhancement upon addition of external heavy atom at moderate viscosities. It was hypothesized that the presence of the heavy atom decreased the magnetic field enhancement due to an increase in spin-orbit coupling and charge recombination in the solvent cage. Interestingly, the dyes, ethyl eosine and rose bengal, showed a slight increase in the magnetic field enhancement at moderate viscosities. This was explained as being due to "*some special cases [where] there can be compensation of spin orbit coupling under the interaction of two species each containing a heavy atom*".[345] Another study that considered the effect of spin state on cage escape yields looked at the quenching of xanthenium and thioxanthenium excited states by various aromatic donors.[170] Here the cage escape yield after electron transfer from biphenyl to excited 9-arylxanthenium was measured to be ϕ_{ce} = 0.04. While cage escape yields using the heavy atom substituted thioxanthenium were not measured, the authors noted that much more effective cage escape was achieved with the triplet states relative to singlet states and thus the inclusion of the heavy atom was anticipated to decrease cage escape yields with these singlet excited states.

The xanthene dyes, rose bengal and eosin Y, contain charged substituents that have been used to understand the effect of ground-state adduct formation on cage escape. In particular, electron transfer reactions from anionic xanthene excited states to the cationic methyl viologen electron acceptor have been studied.[346] Ground state adducts were formed due to a Coulombic attraction between the anionic xanthene and the cationic methyl viologen that ultimately resulted in very low cage escape yields. The small yields were attributed to the close proximity and increased electronic coupling of the donor and acceptor leading to rapid recombination. In contrast, the same study examined xanthene dyes quenched by zwitterionic viologens, 2,2'- and 4,4'-bipyridinium-N,N'-di(propylsulphonate) and reported less ground-state adduct

formation with these compounds. The cage escape yields increased slightly with the use of these neutral viologens providing some evidence that ground state adduct formation does indeed result in smaller cage escape yields.[346] To further probe this behavior, an ionic strength dependence on the cage escape yield of the rose bengal/methyl viologen adduct was studied. At high ionic strength, using potassium nitrate as an ionic moderator, no significant dependence on the cage escape yield was observed, though a fairly small range of ionic strengths were studied. However, it was shown that the association constant for ground-state adduct formation decreased with increasing ionic strength, as one would expect. While the authors provided no further hypotheses for the observed behavior, the data suggest that coulombic interactions within the solvent cage are important even when absent in the ground state.

Eosin Y has also been used as a photosensitizer to probe the steric effect on cage escape yields.[347] In one study, the triplet excited state of eosin Y underwent oxidative quenching by a series of phenol donors with varying steric bulk. The authors note that this series of phenols were particularly useful for isolating the impact of steric effects on cage escape yields as their reduction potentials, and hence the driving force for charge recombination, were nearly the same. The least sterically hindered phenol, *o*-cresol, escaped the solvent cage with ϕ_{ce} = 0.028 once reduced. The cage escape yield increased to ϕ_{ce} = 0.07 for 2,4,6-trimethylphenol, ϕ_{ce} = 0.17 for 2,6-di-*tert*-butyl-4-methylphenol, and ϕ_{ce} = 0.14 for 2,4,6-tri-*tert*-butylphenol. While the slight decrease in yield with addition of a third tertiary butyl group was unexpected, the other quenchers trend with anticipated steric bulk. The results for the other phenols were explained by an increase in the electron transfer distance and a decrease in the electronic coupling due to the steric bulk.[347]

Iwa et. al. studied the quenching of oxonine by 24 aromatic amines and methoxy-benzenes in methanol with particular attention paid to the driving force for the electron transfer**, Figure 28**.[348] Plots of the cage escape yield vs. –ΔG showed an increase in cage escape yields as the charge recombination reaction was made more favorable, consistent with electron transfer in the normal region. Ohno et. al. investigated the cage-escape process following the excited-state electron transfer from tetraiodofluorescein (2,4,5,7-Erythrosin) to benzo-, dimethyl-, naphthyl-, tetramethyl-, and anthraquinones in methanol.[349] They reported behavior consistent with Marcus normal region.

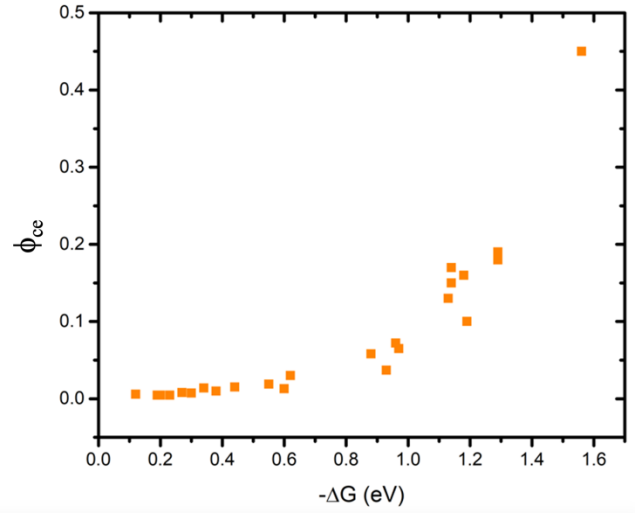

Figure 28. Cage-escape yield as a function of the driving force for charge separation for the reaction between oxonine and aromatic amines and methoxy-benzene derivatives in methanol.

4.1.6) Thiazine

The triplet excited state of thionine, a thiazine derivative, was quenched by various halogenated aniline derivatives. The impact of a magnetic field on the cage escape yields was quantified along with the heavy atom effect in methanol. In the low field regime (B_0 < 1T), a steep increase in the cage escape efficiency was observed in line with expectation based on the *hf* mechanism.[191] Studies in the high field regime revealed a gradual decrease in cage escape efficiency leveling off around 5 T, which they attributed to the triplet mechanism.[350] In contrast, the thiazine derivative, methylene blue, quenched with *p*-iodoaniline displayed cage escape yields that decreased as the field strength was increased.[351] Overall, a decrease in the cage escape yield as a function of the applied field was observed.[351] Excited state electron transfer studies from ferrocene to methylene blue yielded similar behavior with ferrocene acting as a heavy atom that inherently decreased the cage escape yield as well.[352]

The viscosity dependence on the magnetic field effect for cage escape yields was studied with methylene blue and *p*-iodoanisole photosensitizers.[351] Ethylene glycol was added in controlled amounts to increase the viscosity of a methanol solution. The decrease observed under the presence of an external magnetic field was largest in the most viscous solvents where the cage escape yields were the smallest. This is consistent with the anticipated effect of solvent viscosity where the most viscous solvents slow down the rate of cage escape and lower overall yield.

Several publications have reported quenching of the triplet state of thionine with halogenated aniline derivatives as a means to observe the heavy atom effect on cage escape yields.[191, 350-351, 353] While in many studies heavy atom effects were noted when changing the mass of the halogen substituent, Steiner and Winter published a full comparative study where the halogen atom identity on the aniline ring was changed from fluorine to iodine. In addition, the position of the halogen on the aniline quencher (*ortho*-, *meta*-, and *para*-) was varied. As an internal control, the cage escape yield of triplet thionine with unsubstituted aniline was determined to be $\phi_{ce} = 0.91$. Within experimental error, fluorine substituents on each position of the aniline ring had no impact on the cage escape yield. The substitution of chlorine saw a slight decrease from the control while bromine and iodine substituents resulted in significant decreases in the cage escape yields (**Table 8**). Hence the impact of spin-orbit coupling on mixing more singlet state character into the triplet radical pair was evident with these quenchers. Interestingly with each halogen substituent, the *para*-substitution resulted in the lowest cage escape yields that increased in the *ortho*- and *meta*- positions, respectively. It was found that this trend correlated with the π-electron spin density on the carbon adjacent to the halogen substituent for the oxidized aniline compound.

Table 8. Standard reduction potentials (V vs SCE) and observed cage escape yields for the quenching of triplet thionine with various halogenated aniline derivatives.

Quencher	ϕ_{ce}	$E^{o'}$
aniline	0.91	0.87
o-fluoro-aniline	0.91	
m-fluoro-aniline	0.91	
p-fluoro-aniline	0.90	0.85
o-chloro-aniline	0.88	
m-chloro-aniline	0.91	
p-chloro-aniline	0.86	0.90
o-bromo-aniline	0.63	
m-bromo-aniline	0.75	
p-bromo-aniline	0.48	0.89
o-iodo-aniline	0.21	
m-iodo-aniline	0.46	
p-iodo-aniline	0.11	0.88

Substitution of cationic and anionic groups onto the nitrogen atom of a phenothiazine photosensitizer has also been employed to investigate Coulombic effects on cage escape yields. In one study, a relationship between the cage escape yield and the work terms for the electron transfer products and reactants was discovered.[354] The coulombic work term (ΔG_w) describes the free energy difference associated with electrostatic interactions between the reactants and products throughout the electron transfer reaction. A positive ΔG_w value indicates that the products have more electrostatic interaction than the reactants, while a negative value indicates the reactants have more electrostatic interaction than the products. The cage escape yields were found to decrease as the ΔG_w values increased from negative to positive values. In other words, the photosensitizers and quenchers that had stronger Coulombic interactions in the reactants relative to the products displayed larger cage escape yields.

4.1.7) Ketones

One of the earliest studies examining the impact of external magnetic fields on cage escape yields dates back to 1979 when Periasamy and Linschitz studied the quenching of fluorenone by 1,4-diazabicyclo[2.2.2]octane (DABCO).[355] In this study, the triplet fluorenone accepted an electron from the DABCO donor to form a spin-correlated triplet radical pair. The cage escape yield increased with the field strength from 50-270 mT at which the yield reached a plateau and remained constant up to 900 mT. This study also quantified the cage escape yield with and without an external field of 270 mT at a range of temperatures (–60 °C to 70 °C). The yield enhancement under a magnetic field decreased with increasing temperature, likely due to an increase in the spin-rephasing rate. Similar behavior has also been observed using ruthenium tris(diamine) complexes as well (Section 4.2.1.2).The data were interpreted in accordance with the *hf* mechanism as detailed in Section 2.3 of this review.[189-190, 355] Another study examined the triplet excited states of benzophenones quenched by anilines and phenols without an external field and with a single field strength of 450 mT. An increase in the cage escape yield was observed with the applied field and the same *hf* mechanism was proposed.[356]

Several studies have reported heavy atom effects on cage escape yields using ketone-based photosensitizers.[338, 356-359] In one example, Levin and Kuzmin reported cage escape yields after the quenching of triplet benzophenone and 4-bromobenzophenone by 4-phenylphenol and 4-phenylaniline.[356] The cage escape yields were consistently smaller for the halo-substituted benzophenone, both with and without a magnetic field, attributed to an increase in spin-orbit coupling that enhanced charge recombination within the encounter complex.

Khydyakov, Levin, and Kuzmin also reported magnetic field effects on the photoreduction of the triplet excited state of 1,4-benzoquinone.[360] In this study, the triplet benzoquinone can accept a hydrogen atom from hydrogen-donating solvent, in this case glycerol. The application of a moderate magnetic field decreased the rate of geminate recombination and therefore increased the cage escape yield as the dissociation into free radicals would not be impacted by an external magnetic field. It was also shown that an increase in the overall temperature decreased the viscosity of the solvent and in turn increased the cage escape yields.

Kobashi and coauthors used tetrachloro-1,4-benzoquinone (chloranil) as the photosensitizer and naphthalene derivatives as quenchers that form 1:2 chloranil:naphthalene adducts in the ground state.[338, 357] As discussed throughout this review, the formation of ground-state adducts can have a considerable effect on the cage escape yields. However, in this system the authors noted that the barrier for dissociation from the adduct was relatively small. With unsubstituted naphthalene, $\phi_{ce} = 0.54$ and decreased slightly to $\phi_{ce} = 0.52$ and $\phi_{ce} = 0.46$ upon chlorine substitution in the 1 and 2 positions respectively. Substitution of bromine in the same positions decreased the cage escape yield more dramatically to $\phi_{ce} = 0.08$ and $\phi_{ce} = 0.16$ respectively, in line with other studies of heavy atom effects.

Benzophenone as a photosensitizer was studied with a much wider range of substituted quenchers, primarily phenol derivatives, some of which include heavy atom substituents.[359] Similar to other studies, a decrease in the cage escape yield was observed when a heavy halogen atom was present in the *para*- position of the phenol quencher. This same study employed *p*-methoxypropiophenone as a quencher and reported larger cage escape yields than benzophenone with *p*-bromophenol and *p*-iodophenol. Sul'timova et.al. studied halo-substituted phenols as quenchers with 4-carboxybenzophenone as the photosensitizer. The decrease in cage escape yield with increasing halogen atomic number was observed.[358] The decrease in cage escape with the heavy atom was quite dramatic and was near unity for the unsubstituted phenol and decreased to $\phi_{ce} = 0.18$ for iodo-substituted phenol.

Dielectric constant and solvent polarity have been found to impact the reaction mechanism and cage escape yield. For benzophenone with N,N-diethylaniline quenchers, a clear solvent dependent reaction mechanism was evident.[337] In acetonitrile, cage escape was evident by appearance of the radical ions products whose formation was coincident with the decay of the benzophenone triplet. In sharp contrast, in benzene a ketyl radical was observed after the triplet had fully decayed. In acetone and pyridine with a dielectric constant between CH_3CN and benzene, both phenomena were observed and the sum of the

respective yields were around unity, indicating that hydrogen abstraction competes with cage escape in these solvents. In this case, only two paths were identified that could be controlled with solvent. Similar observations were made in other nitrile solvents with dielectric constant ranging from 17.4 to 37.5 for hexane-, butyro-, propio- and acetonitrile where solvents with lower dielectric constants favour the formation of the ketyl radical.[361]

Another example of solvent control was reported by Jones *et al.*, where the efficiency of quadricyclene to norbornadiene isomerization was quantified in solvents with different dielectric constants. The solvents (ε; relative polarity) ranged from cyclohexane (2; 0.006), dioxane (2; 0.164), acetonitrile (37.5; 0.46) to 80% acetonitrile/water (46; 0.568) and the isomerization efficiencies dropped from 0.71 to 0.15 when going from cyclohexane to dioxane, and lowered to 0.049 in CH_3CN/H_2O mixture. They described a "short-circuit decay" in polar solvents, where electron transfer occurs over a longer distance resulting in spin-correlated ion pairs that are solvent separated. The long distance prevents the collision of the donor and acceptor leading to a predominant recombination process. In non-polar solvents, a closer encounter with the photosensitizer results in more efficient isomerization.[341] For electron transfer quenching of β-lapachone by β-amino alcohols, the products obtained were different in polar solvents relative to nonpolar solvents. In benzene, charge recombination was dominant relative to cage escape while in polar solvents a higher cage escape yield was evident.[362]

4.2) Inorganic Light Absorbers

In the following section, cage-escape yields measured with inorganic photosensitizers based on transition metals Ru(II), Ir(III), Rh(III), Os(II), Cu(I), Cr(III), Fe(III), Pt(II), and Re(I) are reported. The cage-escape yields are discussed in the following sections and are tabulated for clarity in the appendices (section 6) at the end of this manuscript.

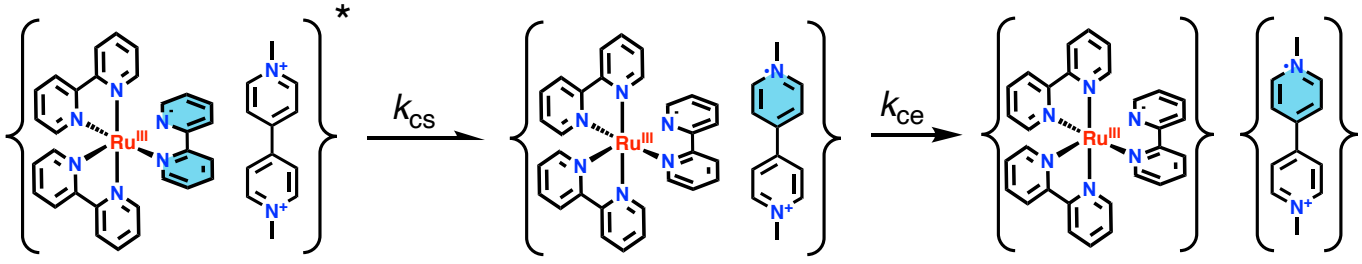

Figure 29. Excited-state reaction between excited $[Ru(bpy)_3]^{2+}$* and methyl viologen (MV^{2+})

Special attention is called to the oxidative quenching of the metal-to-ligand charge transfer (MLCT) excited state of $[Ru(bpy)_3]^{2+*}$ by dicationic methyl viologen, **Figure 29**. This reaction is certainly the most well characterized dynamic (diffusional) electron transfer reaction from a cage escape point of view. T.J. Meyer, D. Whitten and coworkers at UNC Chapel Hill first reported time resolved absorption studies that provided unambiguous evidence for oxidative excited-state electron transfer.[363] An important aspect of the reaction is that the Gibbs free energy stored in the charge separated products is sufficient to drive the water splitting reaction. Indeed, with elemental Pt catalysts, the reduced viologen will generate hydrogen gas and the $[Ru(bpy)_3]^{3+}$ will mediate oxygen gas evolution with the appropriate catalyst.[364] It was soon discovered that excited-state quenching was essentially quantitative in water, but a cage escape yield of $\phi_{ce} \sim 0.4$ severely limited the retention of useful products. These findings motivated studies to understand the factors that impacted cage escape, for both oxidative and reductive quenching, and the use of alternative transition metal complexes with higher intrinsic cage escape yields and lower costs.

4.2.1) Ruthenium

Ruthenium(II) photosensitizers represent the most prominent class of transition metal photosensitizers that have been used to study cage-escape processes. Indeed, more than 80% of the literature dealing with transition metal complexes for cage-escape yields uses $[Ru(bpy)_3]^{2+}$ or derivatives thereof. As such, some of these photosensitizers that are discussed in the following sections are gathered in **Figure 30**.

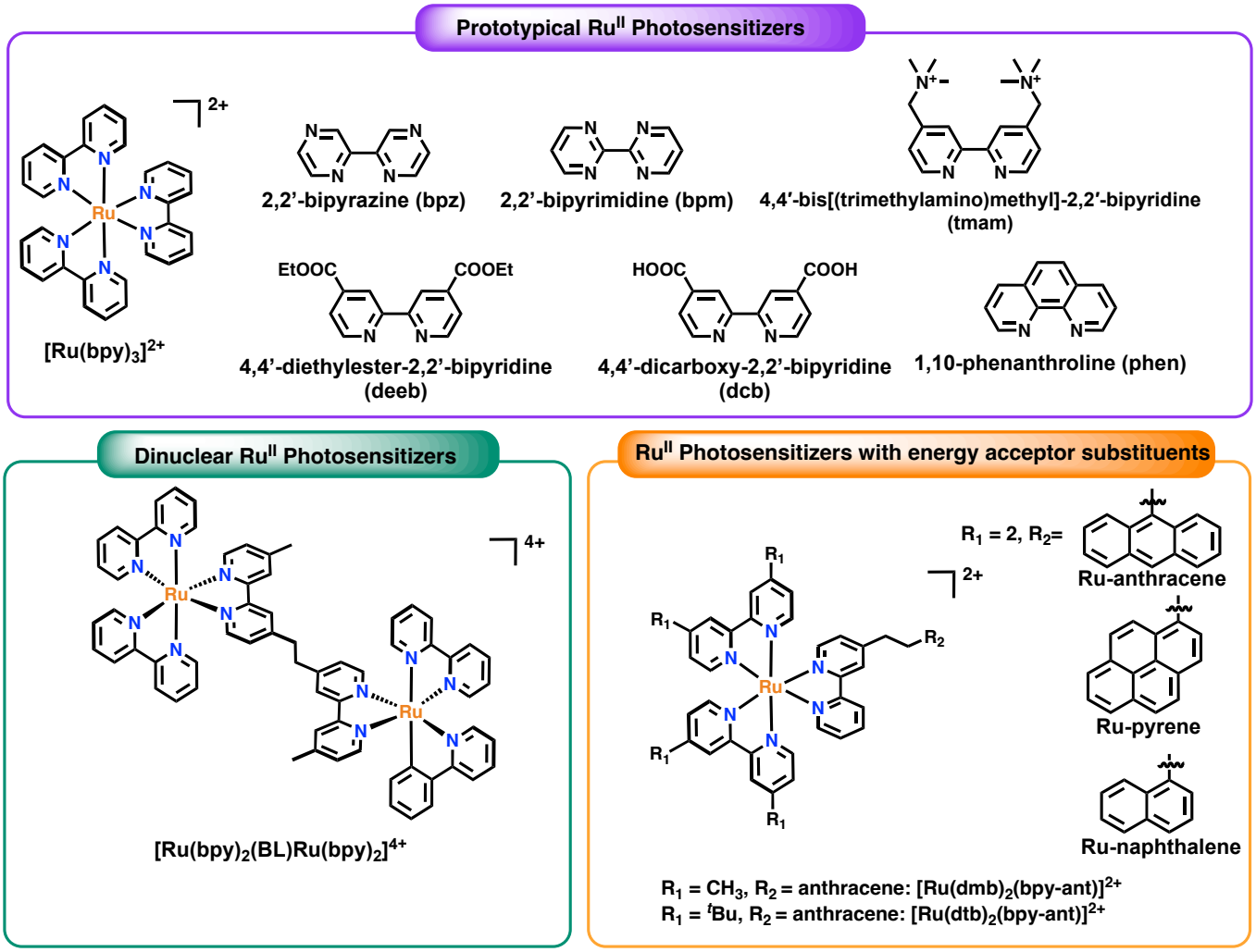

Figure 30. Structure of Ru(II) photosensitizers and useful ligands discussed in the present section.

4.2.1.1) Spin

The low cage escape yields for oxidative quenching of $[Ru(bpy)_3]^{2+*}$ have been attributed to spin-orbit coupling (SOC) by the heavy Ru center that imparts both triplet and singlet character to the excited state. Indeed, it is now well documented that the metal-center enhanced spin-orbit coupling leads to poor cage escape yields (ϕ_{ce} = 0.2-0.4) for the famed $[Ru(bpy)_3]^{2+}/MV^{2+}$ system.[82, 365-374] Molecular approaches to control and better understand the impact of spin with ruthenium polypyridyl complexes are described below.

In the quest for more efficient cage escape, organic compounds with well-defined spin states have been employed as energy transfer shuttles.[82, 171, 366, 375] Both covalently bound[171, 366] and diffusive energy transfer shuttles have been reported.[82, 375] In one study with covalently linked shuttles, a control

$[Ru(bpy)_3]^{2+}/MV^{2+}$ system displayed a cage escape yield of $\phi_{ce} = 0.27$ that decreased slightly to $\phi_{ce} = 0.22$ when naphthalene was covalently linked to a 2,2'-bipyridine ligand through an ethylene spacer. With the same ethylene spacer, the cage escape yield increased for pyrene to $\phi_{ce} = 0.88$ and to almost unity for anthracene, $\phi_{ce} = 0.96$.[366] These behaviors were rationalized by the relative energy of the lowest energy ^{3}MLCT and ^{3}arene excited states. For the Ru-naphthalene complex that showed cage escape efficiencies comparable to $[Ru(bpy)_3]^{2+}$, intramolecular energy transfer from the ^{3}MLCT to ^{3}napthalene did not occur because the triplet state of naphthalene was too high in energy. In contrast, intramolecular energy transfer for the Ru-pyrene and Ru-anthracene complexes was energetically favored and yielded a triplet arene excited state that was not impacted by spin-orbit coupling from the remote Ru center. As described previously with organic photosensitizers, the spin selection rule inhibits charge recombination for triplet charge separated states generated in a solvent cage; mixing singlet character through the external heavy atom effect lowers the yield significantly.

In 1987, Olmsted and Meyer reported quenching of $[Ru(bpy)_3]^{2+*}$ by MV^{2+} using two anthracene derivatives as energy shuttles to probe the impact on cage escape.[82] The ^{3}MLCT excited state was shown to quantitatively transfer energy to the anthracene shuttles, the ^{3}An subsequently transferred an electron to MV^{2+}(**Figure 31**). Both 9-methyl and 9-bromoanthracene were utilized to probe the internal heavy atom effect. The cage escape yield for the 9-methyl anthracene shuttle was $\phi_{ce} = 1.00$, relative to $\phi_{ce} = 0.23$ in the absence of the energy transfer shuttle (**Table 9**). With 9-bromoanthracene the yield was $\phi_{ce} = 0.74$, behavior that was reasonably attributed to an internal heavy atom effect.[82] The presence of iodomethane in the acetonitrile electrolyte impacted the cage escape yield though the external heavy atom effect, while the presence of dichloromethane had no measurable impact. In the presence of iodomethane, the ϕ_{ce} values decreased from 1 to 0.7 in the case of 9-methylanthracene and from ϕ_{ce} =0.74 to $\phi_{ce} = 0.3$ in the case of 9-bromoanthracene. A clear effect was thus observed upon the addition of an external heavy atom implying that these additives were present in, or very proximate to, the solvent cage.

Table 9. Cage escape yields for methylviologen (MV^{2+})-anthracene charge-transfer pairs[a]

Shuttle Compound	**Solvent additives[b]**	**Relative ϕ_{ce}[c]**
9-methylanthracene	CH_2Cl_2	1.0
9-methylanthracene	CH_3I	0.70
9-bromoanthracene	CH_2Cl_2	0.74
9-bromoanthracene	CH_3I	0.30

[a] $[Ru(bpy)_3]^{2+}$ as photosensitizer. [b] Solvent was 8:5 (v/v) 0.1M $TEAClO_4/CH_3CN$ to halocarbon. [c] Relative to $\phi_{ce} = 0.23$ for $[Ru(bpy)_3]^{2+}$-MV^{2+}.

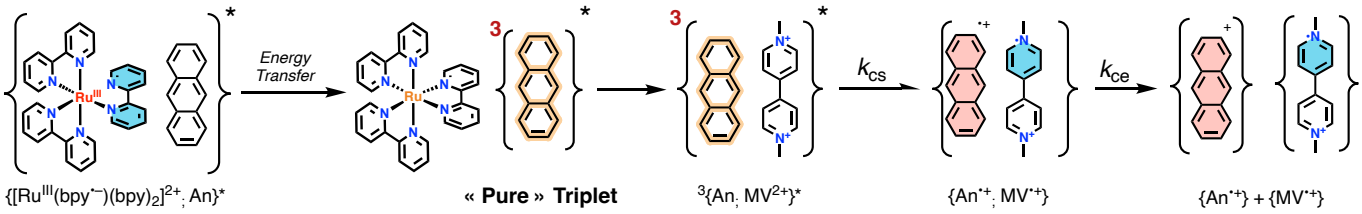

Figure 31. Approach used by Olmsted and Meyer to increase the cage-escape yields by population of a "pure" triplet anthracene excited state by energy transfer from $[Ru(bpy)_3]^{2+}$*.[82]

Interestingly, the reductive quenching of $[Ru(deeb)_3]^{2+}$, where deeb is 4,4'-$(CO_2Et)_2$-2,2'-bipyridine, by aniline occurred with a cage escape yield of unity.[372] This high yield stands in sharp contrast to the oxidative quenching by methyl viologen with cage escape yields that are typically less than half this value. The authors attributed the high yield to the molecular orbitals involved in the reductive quenching process. In the MLCT excited state an electron transfer is formally from aniline to the oxidized metal center. As a result, charge recombination occurs from the reduced bipyridyl ligand to the oxidized aniline. While one might reasonably conclude that the electronic coupling between the reduced ligand and the oxidized aniline would be significant and enhance geminate recombination, this was not the case. The authors concluded that spin-orbit coupling by the metal center on the reduced ligand was negligibly small providing a pure triplet state that enhanced the cage escape yield. Further evidence for this interpretation was evident from studies of anilines substituted with a chlorine, bromine, or iodine atom.[372] The cage escape yield decreased as the atomic number of the halogen atom increased. It was also shown that the position of the halogen substituent on the aniline ring impacted the cage escape yield. For example, the cage escape yield with 4-iodoaniline ($\phi_{ce} = 0.14$) was significantly smaller than 2-iodoaniline ($\phi_{ce} = 0.23$), behavior attributed to the effective spin density on the carbon atom adjacent to the halogen substituent. We note that reductive quenching studies by other electron donors (described further below) also indicated cage escape yields of unity under some conditions while oxidative quenching yields are consistently far less than unity. Taken together, this data indicates that the spin state of a reduced bipyridine ligand coordinated directly to a heavy metal is sufficiently pure to afford quantitative charge separation.

In contrast to this model, a related reductive quenching study utilized anthracene linked to $[Ru(bpy)_3]^{2+}$ through *p*-xylene spacers with ascorbate as the electron donor. Low cage escape yields were reported that increased to only $\phi_{ce} = 0.58$ with the anthracene shuttle. It is likely that Coulombic effects by the anionic ascorbate and/or the sacrificial nature of this donor underlie the poor cage escape yields that

were reported.[171] Another interesting study using covalent energy shuttles looked at a series of $[Ru(bpy)_3]^{2+}$ derivatives with an anthracene moiety covalently bound to one of the 2,2'-bipyridine ligands through an alkyl chain (**Figure 30**).[376]

In covalently linked $[Ru(bpy)_2(bpy\text{-anthracene})]^{2+}$ complexes, the MLCT excited state is expected to transfer energy to anthracene and the triplet state of anthracene is then oxidatively quenched by methyl viologen. These types of intramolecular energy shuttles have been used as a means to negate the spin-orbit coupling contributions from the metal center and decrease S-T spin flip transitions to the ground state analogous to the intermolecular energy transfer studied by Meyer and Olmsted.[82] With the 4,4'-dimethyl-2,2'-bipyridine-substituted complex shown in **Figure 30**, the non-rigid alkyl chain allows the triplet anthracene to approach the Ru metal center and the enhanced spin-orbit coupling that results was proposed to decrease the cage escape yield to $\phi_{ce} = 0.26$. Substitution on the ancillary bipyridine ligands with di-*tert*-butyl groups, resulted in $\phi_{ce} = 0.55$ that was attributed to a larger separation distance between the Ru and triplet anthracene within the encounter complex with methyl viologen.

Finally, Sutin and co-workers quantified the oxidative quenching of $[Ru(bpy)_3]^{2+}$* by $[Rh(bpy)_3]^{3+}$ and reported a quenching rate constant $k_q = 3.9 \times 10^8$ $M^{-1}s^{-1}$.[377] Transient absorption spectroscopy confirmed that oxidative electron transfer occurred with the formation of $[Ru(bpy)_3]^{3+}$ and $[Rh(bpy)_3]^{2+}$ with a corresponding cage escape yield of $\phi_{ce} = 0.13 \pm 0.03$. The cage escape yields for this reaction are likely small due to the heavy ruthenium and rhodium metal centers. The low cage-escape yield was proposed to limit the overall efficiency for hydrogen production.

4.2.1.2) Magnetic Field

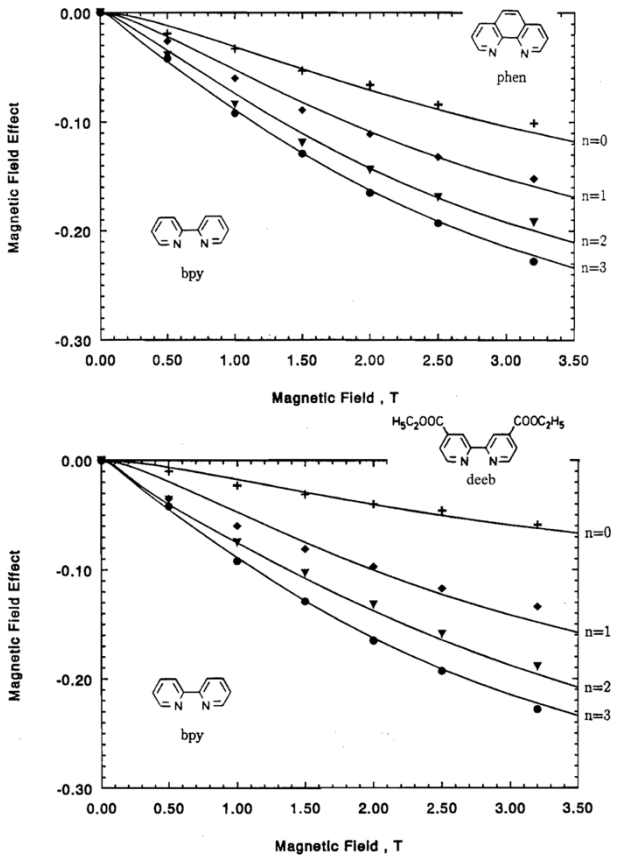

Figure 32. Relative magnetic field effect on the cage escape efficiency measured with the series $[Ru(bpy)_n(phen)_{3-n}]^{2+*}$ and $[Ru(bpy)_n(deeb)_{3-n}]^{2+*}$ (n = 3 (circle), n = 2 (triangle), n = 1 (diamond) and n = 0 (+)) after oxidative quenching by MV^{2+}. The solid lines are results of theoretical calculations. Reproduced with permission from reference [370]. Copyright 1993 de Gruyter.

The magnetic field effect of excited state reactions involving metal complexes has primarily focused on $[Ru(bpy)_3]^{2+}$ derivatives oxidatively quenched by methyl viologen or propyl viologen sulfonate,[365, 367-374, 378] and reductively quenched by halogenated anilines.[191, 308-309, 350-351, 353, 372] As spin-orbit coupling is known to be important, a significant difference in g factors is anticipated with the $[Ru(bpy)_3]^{2+}/MV^{2+}$ radical pair. This provides some indication that magnetic field effects may be dominated by the Δg mechanism. This was indeed confirmed by the work of Steiner and others, however a hybrid of the Δg and triplet mechanisms is often invoked.[371-373] With these two dominant mechanisms, one would predict that magnetic field effects on cage escape of $[Ru(bpy)_3]^{2+}$ sensitized redox reaction will be negative. In other words, an externally applied magnetic field will lower the yields. This is indeed what has been disseminated in several reports.[365, 367-368, 370-374] The magnetic field effect for $\{[Ru(bpy)_3]^{3+}; MV^{\bullet+}\}$ cage escape saturates to a value of –0.20 to –0.30 at relatively high field strengths in line with the Δg and triplet mechanisms.[365,

[368] The sensitivity to ligand substitution has been studied extensively. The examples presented in **Figure 32** shows this trend effectively. Substitution of the 2,2'-bipyridine ligands in $[Ru(bpy)_3]^{2+}$ with 1,10-phenanthroline (phen) (**Figure 32 top**) or with 4,4'-$(CO_2Et)_2$-2,2'-bipyridine (deeb) (**Figure 32 bottom**) ligands decreased the magnitude of the magnetic field effect quite dramatically.[369] This behavior has been attributed to a change in the spin relaxation lifetime of the photosensitizer due to ligand substitution.[370] As the spin relaxation lifetime decreases so too does the magnitude of the negative field effect on cage escape yields. In a related study, a 4,4'-dicyano-2,2'-bipyridine was shown to yield similar effects, suggesting that the electronic coupling for the recombination reaction might also increase with the presence of cyano groups.[367]

The temperature and viscosity dependence of the magnetic field effect have also been investigated for the $[Ru(bpy)_3]^{2+}/MV^{2+}$ system. Recall that the Noyes model predicts a larger cage escape yield at higher temperatures and in less viscous media. This was borne out in all studies of $[Ru(bpy)_3]^{2+}/MV^{2+}$. The negative magnitude of an external magnetic field was smaller at high temperatures than it was at room temperature.[355, 374] The viscosity dependence was quantified by adding controlled amounts of ethylene glycol to the solvent system. As the viscosity increases at low magnetic field strengths ($B_0 < 1$ T) the (negative) magnitude of the field effect first increases and then decreases at high viscosities.[345, 365, 372] At high field strengths, the field effect simply decreases with an increase in viscosity. This behavior was attributed to the impact of solvent dielectric relaxation on the rate of geminate charge recombination.

4.2.1.3) Ionic Strength

Several studies have investigated the impact of ionic strength on the cage escape yield in the $[Ru(bpy)_3]^{2+}/MV^{2+}$ system. [83-84, 111, 373, 379-383] These studies consistently reported a decrease in the cage escape yield as the ionic strength was increased. An example is shown in **Figure 33**. The decreased yield was attributed to screening of the coulombic repulsion of the positively charged primary pair, $\{[Ru(bpy)_3]^{3+}; MV^{\bullet+}\}$.[83, 111, 373, 379-380, 383] Decreased coulombic repulsion in the solvent cage was proposed to result in more favorable charge recombination relative to cage escape. Such data indicate that both solvent and ions are present in the "solvent cage". This interpretation was consistent with the work of Scandola and coworkers in their evaluation of the ionic strength dependence for caged products of like charge.[111]

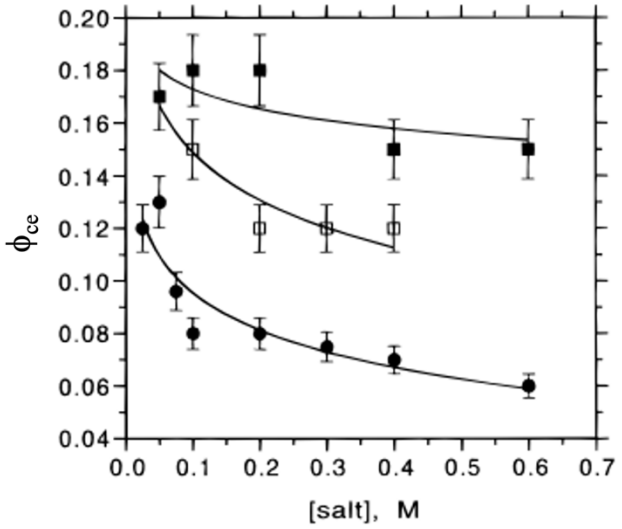

Figure 33. The cage escape yield dependence on ionic strength of a few additive inert salts ($NaClO_4$ (filled squares), NaCl (open squares), NaH_2PO_4 (filled circles)). Reproduced with permission from reference [84]. Copyright 1996 American Chemical Society.

In addition to the ionic strength dependence, a counterion dependence became evident in the $[Ru(bpy)_3]^{2+}/MV^{2+}$ system. Clark and Hoffman performed a detailed study of the counterion dependence of cage escape in aqueous solutions with Na^+ salts of the following anions: F^-, Cl^-, Br^-, I^-, $H_2PO_4^-$, HPO_4^{2-}, SO_4^{2-}, ClO_4^-, $CH_3CO_2^-$ at a constant ionic strength.[84] For the oxyanions, the cage escape yield decreased in the order $ClO_4^- >> SO_4^{2-} \sim HPO_4^{2-} > H_2PO_4^- \sim CH_3CO_2^-$ and for the halide anions in the order $I^- > Br^- > Cl^- > F^-$. These trends were explained by specific ions being present in the encounter complex and impacting the outer sphere reorganization energy for charge recombination. The anions with a larger reorganization energy slow charge recombination and increased cage escape yields. Similar trends have been shown in other studies, however in these, ionic strength was not constant making comparative analysis more difficult.[379, 382]

Interestingly, a related study examined the impact of the cation identity on cage escape in the $[Ru(bpy)_3]^{2+}/ MV^{2+}$ system. A very weak cation dependence was noted relative to that reported for anions. At constant ionic strength, cation chloride salts slightly impacted the cage escape yield in the following order $La^{3+} > Ca^{2+} \sim Li^+ > Na^+ > Cs^+$.[381] For example, the cage escape yields spanned a narrow range (0.10-0.15) when 0.2 M of cation chloride salts were used. The small cation dependence was attributed to a change in the solution viscosity or dielectric properties. Since both the $[Ru(bpy)_3]^{2+}$ and MV^{2+} are dicationic, the nature of the anion is expected to impact cage escape yields more dramatically than a cation that would be

coulombically repelled from the cage. This data suggests that electrolyte anions of opposite charge to the reactants in the solvent cage will have the largest impact.

A reductive quenching study of $[Ru(bpy)_3]^{2+}$* by tetra-anionic tungsten (IV) octacyanide donors reported a very slight increase in the cage escape yield of 10-11% as the solution ionic strength was increased from 0.12 M to 1.32 M. However, ionic strength had no measurable impact on the cage escape yields with tetra-anionic iron (II) hexacyanide, suggesting that the structure of the cage is also an important parameter.[384] The ionic strengths used in these studies were large and Chiorboli et. al. have shown that cage escape yields begin to plateau at these concentrations.[111] A mechanistic understanding of the small or immeasurable impact of ionic strength on primary pairs with opposite ionic charge have not been thoroughly investigated.[346, 384] More detailed studies looking at a wider range of ionic strengths could prove useful to the overall understanding of the field.

A comparative study of oxidative quenching of $[Ru(bpy)_3]^{2+}$ by MV^{2+} in acetonitrile and an ionic liquid, (1-butyl-3-methylimidazolium hexafluorophosphate), reported a decrease in the cage escape yield in the ionic liquid, especially at high temperature, and this was likely due to the high viscosity of the ionic liquid.[385]

4.2.1.5) Ground-State Adducts

Non-covalent interactions have been used to position quenchers in specific locations relative to a photosensitizer in the ground state providing new opportunities to study the impact of the solvent cage on cage escape.[384] In one example, a series of $[Ru(bpy)_3]^{2+}$ photosensitizers were synthesized to control the overall ionic charge during reductive quenching by anionic hexa- (Os and Fe) and octacyanometallates (W and Mo). Four photosensitizers bearing carboxylate groups in the 4,4' positions of the 2,2'-bipyridine ligand, a neutral photosensitizer bearing two carboxylate ions on one of the 2,2'-bipyridine ligands, the $[Ru(bpy)_3]^{2+}$ dication, and a Ru(bpy)-dimer with an overall 4+ charge were investigated (**Figure 30**). Evidence for ground state adducts between the cationic and neutral ruthenium complexes with the anionic cyanometallates were obtained from non-linear Stern-Volmer plots, an indication that static quenching may be operative. The measured cage escape yields for both the hexa- and octacyanometallates were the smallest when the photosensitizer bore an overall 4+ charge, behavior that was expected based on the optimal Coulombic attraction. The cage escape yields for the hexacyanometallates also followed an expected trend wherein increased electrostatic attraction lowered the yield. The octacyanometallates however, did not show

an obvious trend with ionic charge and in general had much larger cage escape yields than did the hexacyanometallates.

Other non-covalent interactions may also be relevant to cage escape as revealed in a comparative study of the reductive quenching of $[Ru(bpy)_3]^{2+*}$ and $[Ru(bpy)_2(deeb)]^{2+*}$, where deeb is 4,4'-$(CO_2Et)_2$-bpy, by iodide in dichloromethane solutions. Ground state adduct formation between iodide and these photosensitizers was evident through UV-Vis titration experiments, from which an equilibrium constant of $K_{eq} \sim 60{,}000\ M^{-1}$ was obtained for $[Ru(bpy)_2(deeb)]^{2+}$, which was much larger than that for $[Ru(bpy)_3]^{2+}$. Cage escape yields of the iodine atom and the reduced photosensitizer were largest for the parent $[Ru(bpy)_3]^{2+}$ ($\phi_{ce} = 0.50$) compared to $[Ru(bpy)_2(deeb)]^{2+}$ ($\phi_{ce} = 0.25$), providing another example where a large equilibrium constant for ground state adduct formation resulted in a small cage escape yield.[386] It should be emphasized however that the generation of an iodine atom removed the Coulombic incentive for association in the primary pair suggesting that other non-covalent interactions were operative with highly polarizable iodine.

Dicationic trimethylammonium substituents on a bipyridine ligand have also been employed for association of anions to photosensitizers.[118, 387-393] An example relevant to cage escape is the association of salicylate anions with cationic Ru(II) photosensitizers that undergo excited state proton-coupled electron transfer (PCET) reactivity when illuminated with visible light.[392] In this study $[Ru(bpy')_2(tmam)]^{4+}$ photosensitizers, where bpy' is bpy, a 4,4'-disubstituted 2,2'-bipyridine, or 2,2'-bipyrazine and tmam is [4,4′-bis[(trimethylamino)methyl]-2,2′-bipyridine]$^{2+}$, were quenched by a family of substituted salicylate ions in acetonitrile solutions. Visible absorption and ^{1}H NMR spectroscopies provided clear evidence for ground state adduct formation from which equilibrium constants in the range $K_{eq} = 0.5 – 2.4 \times 10^5\ M^{-1}$ were extracted. Excited-state PCET quenching yielded the reduced Ru photosensitizer and the oxidized salicylate. The cage escape yields were notably large in the range of $\phi_{ce} =$ 0.60 - 0.70. This was attributed to both the neutral charge of the salicylate product and the mechanistic details of the geminate recombination that required both proton and an electron transfer.

4.2.1.8) Solvent

In 1995, Previtali reported the quenching of $[Ru(bpy)_3]^{2+}$ by aromatic amines and nitrobenzenes in different solvents to investigate how the solvent dielectric impacted reactivity.[394] Methanol and acetonitrile were selected as they have similar macroscopic dielectric properties ($\varepsilon = 32.6_{MeOH}$ and 35.9_{MeCN}; $\eta_{MeOH} = 1.331$ and $\eta_{MeCN} = 1.342$). The quenching rate constants were systematically greater in MeOH than in MeCN

and, in addition, the cage escape yields were 50-60% larger in methanol than in acetonitrile where ϕ_{ce} < 0.10. In accordance with Marcus theory, several parameters were considered that could account for this behavior: i) solvent stabilization of the primary radical pair that impacts the driving force for electron transfer; ii) a change in the outer sphere reorganization energy (λ_{out}) associated with the solvent static and optical dielectric constants; and iii) the relevant nuclear frequency that may be solvent dependent. In methanol, hydrogen bonding was proposed to fix the photosensitizer and quencher in an ordered structure that was absent in an aprotic solvent like acetonitrile.

The influence of viscosity on cage-escape yields was studied by Wolff *et al.* through the oxidative quenching of $[Ru(bpy)_3]^{2+}$* by methylviologen in H_2O/CH_3CN mixtures with increased amounts of ethylene glycol at a constant ionic strength of 0.2M NaCl.[365, 372] The solvent viscosity, assessed via a Höppler viscosimeter, was tuned between values of 0.834 cP and 13.40 cP which led to cage-escape yields that gradually decreased from ϕ_{ce} = 0.19 in neat H_2O/CH_3CN to ϕ_{ce} = 0.06 when the solution contained 80% ethylene glycol (**Figure 34**). The cage-escape yield only marginally decreased when 95% ethylene glycol was used with 5% of water. The change in ethylene glycol proportion also led to a change in solvent dielectric constant which changed from 57.8 in H_2O/CH_3CN to 38.3 when 95% of ethylene glycol was used.

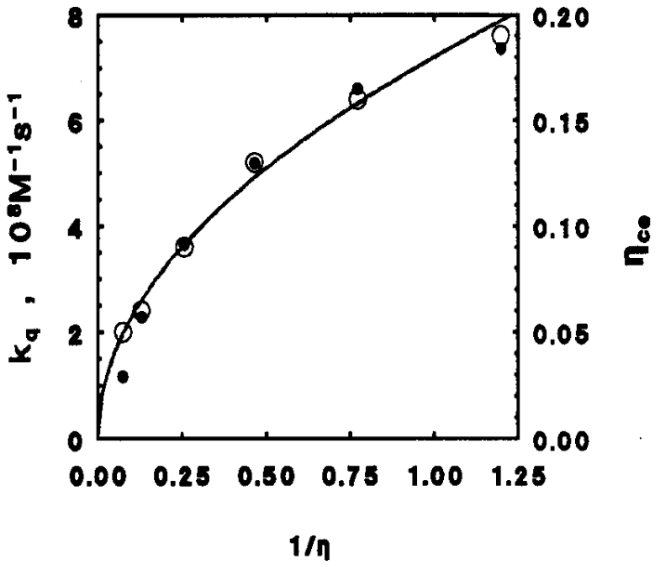

Figure 34. Viscosity dependence of k_q (filled circles) and cage-escape yields (open circles). Reproduced with permission from ref [365]. Copyright 1995 de Grutyer.

The rate of cage escape yields as well as the rate of charge recombination were calculated through Eq. 1.1 and 1.2 and were both shown to decrease as the solvent viscosity was increased. The rate for cage escape yields was decreased by a factor of 35 and the rate of charge recombination was decreased by a

factor of 17. Quenching rate constant, cage escape yields and secondary recombination were shown to be viscosity dependent and approximately proportional to $\eta^{-0.5}$. The viscosity dependence of ϕ_{ce} was approximately linear with $1/\eta$ and calculated k_{cr} values followed an approximate square root dependence ($\eta^{-0.65}$). However, it should be emphasized that in both cases, the data without any ethylene glycol was located significantly above the correlation line.

The effect of solvent polarity on ΔG_{cr} was further estimated using the Born equation where ε_1 and ε_2 are the static dielectric constant of the solvent without and with ethylene glycol, respectively, and r_{12} is the reaction distance, which was estimated at 10Å in the present case, Eq. 4.1. The authors determined that the geminate charge recombination driving force was 0.012 eV more favored in mixtures containing ethylene glycol.

$$\Delta G_{cr}^{0}(\varepsilon_2) - \Delta G_{cr}^{0}(\varepsilon_1) \approx \frac{e_0^2}{r_{12}}\left(\frac{1}{\varepsilon_1} - \frac{1}{\varepsilon_2}\right) \qquad \text{Eq. 4.1}$$

Even though the author suggested that the solvent mixture was directly impacting geminate charge recombination through the dielectric solvent relaxation, they could not unambiguously identify the factors that impacted cage escape yields. They concluded that a more rigorous treatment of spin, electron transfer through nuclear tunneling, and dielectric solvent relaxation should be further developed.

Further information about the influence of viscosity was provided by Sun in a comparative study of cage-escape yields in water, acetonitrile and propylene carbonate.[395] The reductive quenching of a series of homoleptic and heteroleptic Ru(II) photosensitizers bearing 2,2'-bipyridine, 2,2'-bipyrimidine and 2,2'-bipyrazine ancillary ligands by MV^{2+} was investigated in solutions that contained a large 0.6 M concentration of triethanolamine (TEOA) as a sacrificial electron donor. The sequence of events depicted in **Figure 35** following light excitation were proposed where reductive quenching by TEOA yielded the monoreduced photosensitizer and an oxidized TEOA. Both products are known to reduce methyl viologen, either directly, like in the case of monoreduced $[Ru(bpy)_3]^+$, or following an irreversible degradation pathway for the oxidized TEOA. The kinetics associated with the growth of the reduced methyl viologen were then used to determine the cage escape yields for the reductive quenching of $[Ru(NN)_3]^{2+}$* by TEOA, where NN are diamine ligands shown in **Figure 30**.

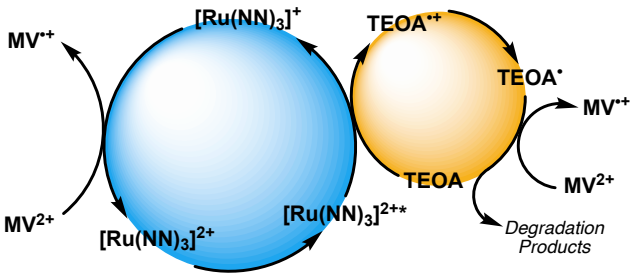

Figure 35. Reaction scheme for the $[Ru(NN)_3]^{2+}$/TEOA/MV^{2+} reaction.

In water with a viscosity of 0.89 cP at 25°C, the cage escape yields were ϕ_{ce} ~ 0.5-0.6, and increased slightly with increasing driving force (**Figure 36**). When solvent with lower viscosity were used, like acetonitrile with a viscosity of 0.3334 cP at 25°C, ϕ_{ce} ~ 0.8 were determined. Finally, propylene carbonate, with its viscosity of 2.45 cP at 25°C, led to cage escape yields that were ϕ_{ce} ~ 0.4 throughout the series of ruthenium photosensitizers. Overall, the data showed a weak trend with ΔG^0_{cr} in water, but not in propylene carbonate and acetonitrile, which prevented general conclusion to be reached. Qualitatively, the cage escape yields do reflect variation of solution medium parameters, especially the viscosity.

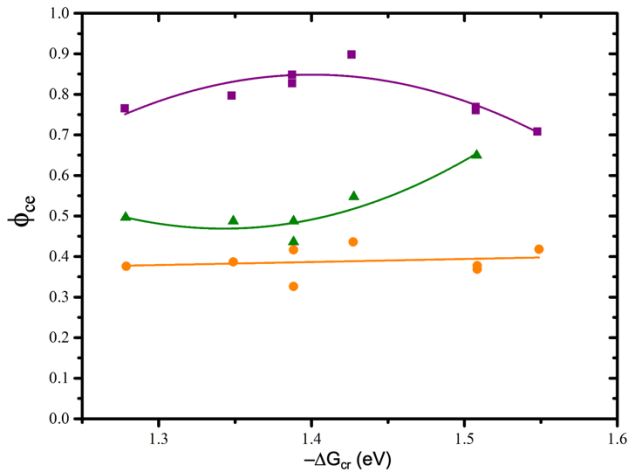

Figure 36. Plots of cage-escape yields versus the driving force for geminate charge recombination in water (green triangles), acetonitrile (purple squares) and propylene carbonate (orange circles). Data replotted from reference [395].

Finally, the reductive quenching of $[Ru(bpy)_3]^{2+}$* by 2,4-dichlorophenolate, 2,5-dichlorophenolate and 2,6-dichlorophenolate anions was studied in deareated methanol and methanol/water mixtures at 30°C.[396] The cage escape yields were determined by transient absorption spectroscopy using the comparative actinometry method with the formation of the triplet state of zinc tetraphenylporphyrin as an actinometer.[396] The cage escape yields followed the expected trend with solvent viscosity, i.e. the cage escape yields increased from ϕ_{ce} = 0.1-0.2 in aqueous solutions containing 25% methanol (1.24 cP) to ϕ_{ce} = 0.5-0.6 in neat methanol (0.511 cP). The Eigen equation was used to estimate the rate constant for cage

escape (k_{ce}) that was larger in methanol than in methanol/water mixtures. The geminate charge recombination rates, calculated from the measured cage escape yields were found to vary only slightly across this series of solvents. The authors conclude that solvent viscosity led to an increase in k_{ce} while less polar solvent led to weaker cage which in turn produced a decrease in k_{cr}.

4.2.1.9) Micelles

Charge separation in micelles, microemulsions, vesicles and liposomes have been investigated to understand how these structures might inhibit charge recombination and thus increase the cage escape yields. Historically, several early studies focused on organic light absorbers, such as ketone derivatives, 1,2-diphenyl-2-methyl-1-propanone or other alkyl-substituted derivatives.[397-401] Oftentimes, the micelle was found to be beneficial to the cage escape process relative to that measured in the absence of the micelle. For example, Turro *et al.* showed that the yield of benzaldehyde and α-methylstyrene after light excitation of 1,2-diphenyl-2-methyl-1-propanone was enhanced by a factor of 10 when the reaction was performed in micellar environment compared to homogeneous organic solvents.[398] In addition, Atik *et al.* investigated excited-state electron transfer between photoexcited pyrene derivatives and dimethylaniline or dibutylaniline quenchers in organized assemblies.[402] It was found that an increase in micelle (or microemulsion) size and/or rigidity led to decreased cage escape yields. The cage escape yields increased when polar derivatives of pyrene were utilized, an observation consistent with localization of the pyrene chromophores in the polar regions within the organized assemblies.

Micelles or lipid bilayer have been chemically engineered to tune the cage escape yields by introduction of ionic charges, micelles or lipid bilayers that attract or repel redox active species.[7, 403-410] In these assemblies, charge separation was modulated and facilitated by pre-association of the photosensitizers and the redox active quenchers at the micelle interface. After excited state electron transfer, the cage escape process was impacted by the hydrophobicity and ionic charges of the radical products that differed from those of the ground state.

One of the most comprehensive micellar examples that emphasized the above-mentioned considerations comes from the works of Adams and Schmehl who studied ruthenium polypyridyl photosensitizers integrated into micelles. This was achieved with a series of $[Ru(bpy)_2(LL)]^{2+}$ complexes, where LL is 2,2'-bipyridine or a 4-R-4'-methyl-2,2'-bipyridine where R was pentyl, terdecyl, heptadecyl, and 4,4'-di(heptadecyl)-bpy. Reductive quenching of these photosensitizers by a $[Ru(NH_3)_6]^{2+}$ donor was thermodynamically favored. In fluid aqueous solution, the cage escape yields were $\phi_{ce} \sim 0.1$.[411] Upon the

addition of a surfactant, cetyltrimethylammonium bromide (CTAB), micelles were formed and the cationic ruthenium polypyridyl photosensitizers with the ancillary alkyl chain were envisioned to organize within the micelle structure. Interestingly, the cage escape yields in these micelles increased to ϕ_{ce} = 0.40 for the terdecyl, and ϕ_{ce} = 0.70 for heptadecyl, photosensitizer. The significantly increased cage escape yields were attributed to the positively charged micelle surface that coulombically repulses the cationic quencher after charge separation thereby decreasing the charge recombination rate constant.

In a related study, electron transfer between excited $[Ru(bpy)_3]^{2+*}$ and methyl viologen was studied in aqueous solutions and in the presence of sodium dodecyl sulfate (SDS) and sodium laurate (SL) micelles.[412] In aqueous solutions, the cage escape yields varied from ϕ_{ce} = 0.2-0.4 and were dependent on the ionic strength and the pH. The behavior was quite different in the micelles where the cage escape yields plummet to zero in SDS and to ϕ_{ce} = 0.08 in SL micelles. SDS is an anionic micelle, thus the cationic reagents were expected to be electrostatically attracted to the micelle surface and thus recombine with a larger rate. Despite SL also being anionic, some cage escape products were observed. The authors noted that SL micelles hydrolyze fairly readily in water and proposed that protonation of the anionic carboxylate group decreased the effective charge on the micelle surface that enabled the cationic reagents to escape more readily. In addition, ^{23}Na NMR experiments demonstrated that the sodium ions associated with the surfactants penetrated the surface of the SL micelle more significantly than in SDS. It was suggested that the sodium ions present could repel the cationic reagents, favoring escape. Under the application of an external magnetic field, the cage escape yield was enhanced by about 25% from 0-0.2 T and remained constant upon increase the external field strength to 0.5 T. This enhancement is in agreement with the *hf* mechanism and the expect enhancement and saturation at relatively low magnetic field strengths.[412]

4.2.1.10) Driving Force

The stability of ruthenium polypyridyl complexes in adjacent oxidation states and the ability to tune reduction potentials with electron withdrawing or donating functional groups is particularly amenable to fundamental electron transfer studies as a function of the driving force. To this end, the Hoffman group reported the reductive quenching of $[Ru(bpy)_3]^{2+*}$ by nine different aromatic amines in 1:1 H_2O/CH_3CN.[413] The cage escape yields and quenching rate constants were measured as a function of temperature over a 50°C range in 1:1 H_2O/CH_3CN.[413] With the exception of the para-anisole donor, the cage escape yields ranged from ϕ_{ce} = 0.25-0.53 at 10°C and increased to ϕ_{ce} = 0.40-0.75 at 60°C. The Debye-Smoluchowski

and Eigen expressions were utilized to extract the electron transfer rate constants, k_{cr}. Evidence for Marcus 'inverted' kinetics within the solvent cage were presented, with a total reorganization energy that was dependent on the number of aromatic rings present on the amine donor.

Ohno et. al. also studied the reductive quenching of $[Ru(bpz)_3]^{2+}$, bpz is 2,2'-bipyrazine, by methoxybenzenes and aromatic amines in 1:1 H_2O/CH_3CN solutions.[414] The quenchers included 1,3,5-trimethoxybenzene, 1,2-dimethoxybenzene, 1,4-dimethoxybenzene, 1,2,4-trimethoxybenzene, diphenylamine, 1,4-anisidine, phenothiazine, 3,3'-dimethylbenzidine, diphenyl-1,4-phenylenediamine, and tetramethyl-1,4-phenylenediamine. The cage escape yields varied between ϕ_{ce} = 0.55 – 0.88. This study was later extended to the reductive quenching of $[Ru(LL)_3]^{2+*}$ photosensitizers (where LL is 2,2'-bipyridine, 1,10-phenanthroline and 4,7'-$(C_6H_5)_2$-1,10-phenantroline (dpphen) by aromatic amines in the same solvent mixture (**Figure 37**).[415] The cage escape yields showed a marked dependence on the photosensitizers that increased in the order $[Ru(dpphen)_3]^{2+}$ < $[Ru(phen)_3]^{2+}$ < $[Ru(bpy)_3]^{2+}$. The cage escape yields for $[Ru(bpy)_3]^{2+}$ varied between ϕ_{ce} = 0.56 – 0.91. Plots of the cage escape yields versus the driving force for geminate recombination showed some evidence for a parabolic dependence suggesting that recombination occurs in the Marcus 'normal', 'activationless', and 'inverted' kinetic regions.

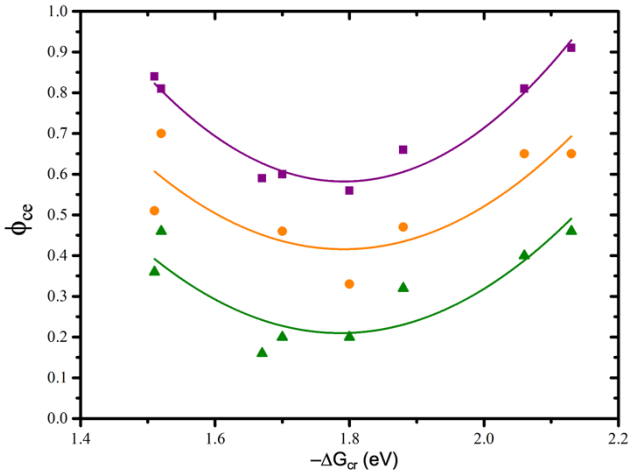

Figure 37. A plot of ϕ_{ce} versus the free energy change for geminate recombination of $[Ru(bpy)_3]^+$ (purple squares), $[Ru(phen)_3]^+$ (orange circles) and $[Ru(dpphen)_3]^+$ (green triangles) with oxidized aromatic amines. The lines are drawn to guide the eye. Date replotted from reference [415].

Ohno and Hoffman reported the quenching and cage escape of nine different ruthenium complexes with MV^{2+} in 4:1 H_2O/CH_3CN.[383] A complex dependence of ϕ_{ce} on ΔG was discussed that seemed to be more dependent on the identity of the photosensitizers. Very similar conclusions were drawn by Mallouk and coworkers for oxidative quenching by MV^{2+} and related pyridiniums where no clear dependence on

ΔG was observed, suggesting that details of the encounter complex structure were instead responsible for cage escape.[416-417]

Creutz, Sutin and coworkers assembled a number of studies in order to compare cage escape yields across different inorganic systems.[418] These studies were extended to the oxidative quenching of $[Ru(LL)_3]^{2+}$ photosensitizers by caged Co(III) amine complexes.[419] The cobalt cages rendered the metal center less susceptible to ligand loss chemistry with decreased electronic coupling within the encounter complex. The quenching data were complicated by the presence of a competitive energy transfer pathway, however the electron transfer products were identified by transient absorption spectroscopy and appeared with cage escape yields that varied from $\phi_{ce} = 0.3 – 1.0$. The cage escape yield decreased as the free energy stored in the charge separated state increased, data consistent with charge recombination in the Marcus normal region.

Sutin and coworkers also reported the oxidative quenching of $[Ru(LL)_3]^{2+*}$ photosensitizers by Cu(II) ions in 0.5 M sulfuric acid.[382] An electron transfer mechanism was established and was important as the Cu(II) aquo species was colored and energy transfer quenching was possible. Dependent on the identity of the photosensitizer, the cage escape yields for the oxidized photosensitizers and the Cu(I) aquo complex varied from $\phi_{ce} = 0.3 – 1.0$. To our knowledge this work provides the highest cage escape yield reported for oxidative quenching of a $[Ru(bpy)_3]^{2+*}$ excited state. The cage escape yields decreased as the free energy change for geminate recombination increased (**Figure 38**). This behavior was consistent with that measured for the cobalt cage quenchers but occurred at a much smaller $|–\Delta G|$. The possible origins of the driving force dependence were discussed and may be a result of the significant inner-sphere reorganization energies that are inherent to Cu(II/I) redox chemistry.

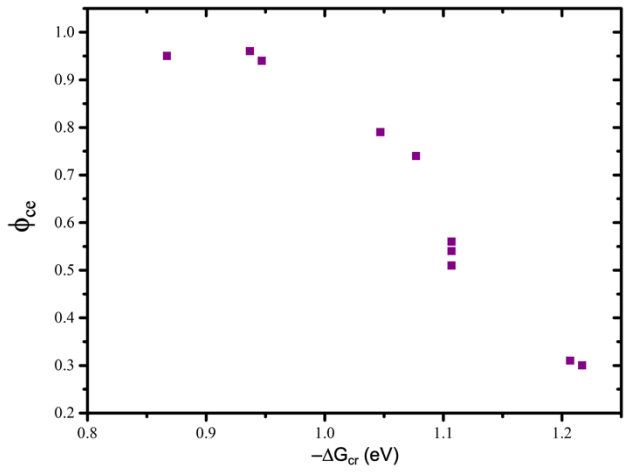

Figure 38. A plot of ϕ_{ce} vs $–\Delta G_{cr}$ for the quenching of $[Ru(LL)_3]^{2+*}$ by Cu(II) ions in 0.5 M sulfuric acid.

Several cage escape studies have appeared that utilize sacrificial donors, such as triethanolamine (TEOA), ascorbate, oxalate, and ethylenediaminetetraacetic acid (EDTA). Because these reagents are sacrificial and undergo irreversible chemistry, the use of pulsed lasers and transient absorption to characterize yields is complicated. Furthermore, in some cases such as triethanolamine oxidation, a second equivalent of $MV^{\bullet+}$ was generated through thermal reactions that artificially increased the theoretical yield of $MV^{\bullet+}$ to 2.[395, 418, 420-423] Interpretation of such data often requires assumptions about the sequence of electron transfer events and their respective yields. For these reasons, this important work is not reviewed in further details here and interested readers are directed towards the primary references.[395, 418, 420-423]

4.2.1.11) Distance/Sterics

Few studies have systematically investigated the impact of steric bulk on cage escape yields using ruthenium polypyridyl photosensitizers. Nevertheless, several studies have pointed to distance and sterics as explanations for some observed behavior. One example was reported by Mallouk and coworkers that was discussed in detail in Section 4.2.1.5 in the reductive quenching of a series of variably charged Ru polypyridyl complexes by hexa- and octacyanometallates.[384] It was found that the cage escape yields were significantly higher for larger octacyanometallates than for the smaller hexacyanometallates, behavior consistent with a size dependent changes in the electronic coupling and/or reorganization energy.[384] Other studies have qualitatively found relationships between cage escape yields and the size of photosensitizers and quenchers.[419, 424]

4.2.2) Iridium

Ir(III) photosensitizers are considered as widely utilized in fields such as photoredox catalysis and photochemotherapy.[45, 52, 425-428] In photoredox catalysis, these photosensitizers have likely surpassed the Ru(II) photosensitizers due to their increased photostability and wider range of accessible excited-state reduction potentials. Nevertheless, cage-escape yield determinations are rare, likely because of their excited state absorption spectra that are often broad and structureless and the reduced or oxidized spectra often exhibit moderate molar extinction coefficients, which makes detection more difficult, especially when the cage escape yields are small. Yet, the various fields using iridium photosensitizers would gain immensely from cage escape yield determinations, as these have also been proposed to influence product yields[51, 429] or product distributions.[430] In this section, we briefly summarize cage escape yields employing the Ir(III) photosensitizers represented in **Figure 39**.

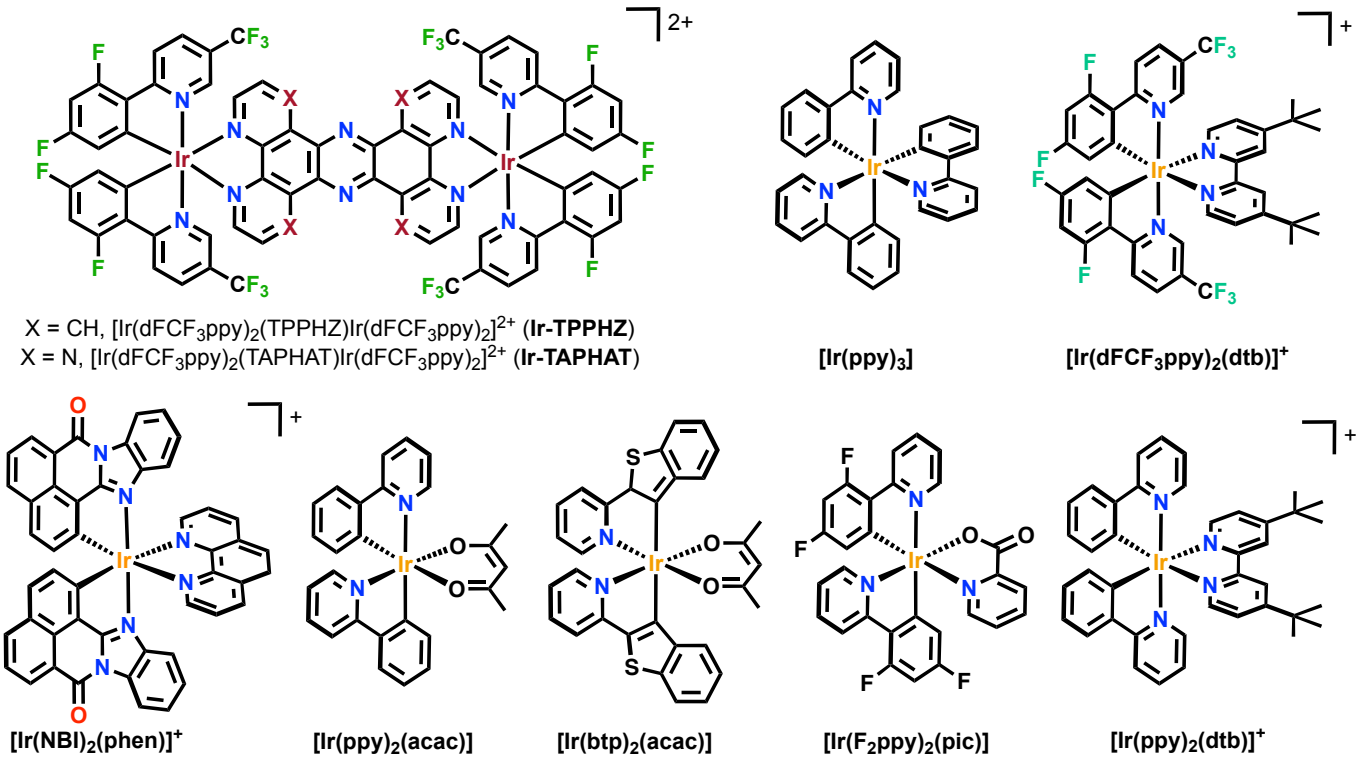

Figure 39. Ir(III) photosensitizers described in the present section.

In a comparative study, Ripak *et al.* investigated the cage escape yields of three iridium photosensitizers, i.e. $[Ir((dFCF_3)ppy)_2(dtb)]^+$, $[Ir(ppy)_2(dtb)]^+$ and $[Ir(ppy)_3]$ with a series or aryldiazonium electron acceptors.[94] The three Ir(III) photosensitizers were all competent for excited-state oxidative electron transfer to the 4-methoxy, 4-bromo, 4-carboxyethyl ester and 4-nitro benzene diazonium tetrafluoroborate derivatives. For $[Ir((dFCF_3)ppy)_2(dtb)]^+$ and $[Ir(ppy)_2(dtb)]^+$, the cage escape yields were almost unitary in all cases, with the exception of 4-methoxybenzene diazonium where cage escape yields of $\phi_{ce} = 0.43\text{-}0.44$ were determined. This cage escape yield increased to $\phi_{ce} = 0.61$ when $[Ir(ppy)_3]$ was used. The cage escape yields with this photosensitizer and 4-carboxyethyl ester and 4-nitro benzenediazonium tetrafluoroborate derivatives could not be measured as irreversible ground-state electron transfer occurred that was attributed to thermal reduction of the diazonium derivative. As the reduction of diazonium liberates N_2, the oxidized photosensitizer accumulated in solution. Similar observations were made with two iron photosensitizers that exhibited similar reduction potentials.[94] In all cases, the approach of using aryl diazonium derivatives that liberate N_2 after electron transfer and cage escape was successful.

Large cage-escape yields of $\phi_{ce} = 0.78$ were also obtained by Castellano and co-workers in the reductive quenching of $[Ir(NBI)_2(phen)]^{+*}$ by N,N-dimethyltoluidine (DMT). Such cage escape yields are

larger than the ϕ_{ce} = 0.52 determined with $[Ru(bpy)_3]^{2+}$ analogues. This increased yield could stem from the significant triplet ligand-centered (^{3}LC) character of the lowest excited state of $[Ir(NBI)_2(phen)]^+$ compared to the increased singlet character in the MLCT excited state of Ru photosensitizers. The authors further emphasized that, due to the smaller contribution of the d-orbitals in Ir(III) photosensitizer compare to Ru(II) analogues, the excited state has less spin−orbit coupling than the MLCT state of the Ru photosensitizers that resulted in radical ion pairs with more triplet character and thus a higher cage escape efficiency. An alternative explanation, similar to the one of Hoffman and co-workers, is related to the different geometries of the encounter complex and the orbitals involved in the forward and reverse electron transfer that could prevent recombination and increase cage escape yields. Overall, these large cage-escape yields also led to enhanced performances for H_2 solar fuel production.

Also within the context of solar fuel formation, De Kreijger et. al. investigated the excited-state reductive quenching of two Ir(III) dinuclear complexes, Ir-TAPHAT and Ir-TPPHZ, by chloride, bromide and iodide in acetonitrile/water mixtures.[431] Evidence for excited-state electron transfer from the three halides to both iridium photosensitizers was obtained by transient absorption spectroscopy as the reduced form of these photosensitizer exhibits intense absorption in the visible range which facilitate the cage escape yields measurements. Whether in acetonitrile or acetonitrile/water, 50/50, ϕ_{ce} followed the periodic trend I > Br > Cl (**Figure 40**). In acetonitrile, the yields were always large, with values upwards of ϕ_{ce} = 0.5 (**Table 10**). Those yields dropped significantly when 50% water was added but remained larger for Ir-TAPHAT than for Ir-TPPHZ. It should also be emphasized that, in acetonitrile, the data for Ir-TPPHZ evolved linearly with the percentage of excited-state quenching with ϕ_{ce} values determined from the slope while for Ir-TAPHAT the data was only linear until approximately one equivalent of halide was added. The initial slope was hence used by the authors to estimate the cage escape yields reported in **Table 10**. The authors hypothesized that since the change of slope occurred around 1 equivalent of added halide, an underlying static quenching mechanism may be operative.[118, 432-434] At any rate, this result highlights the importance of determining the cage escape yields at multiple data points and not relying on single concentration measurements. This would indeed help in providing a better description and understanding of cage escape process that are ionic strength dependent.

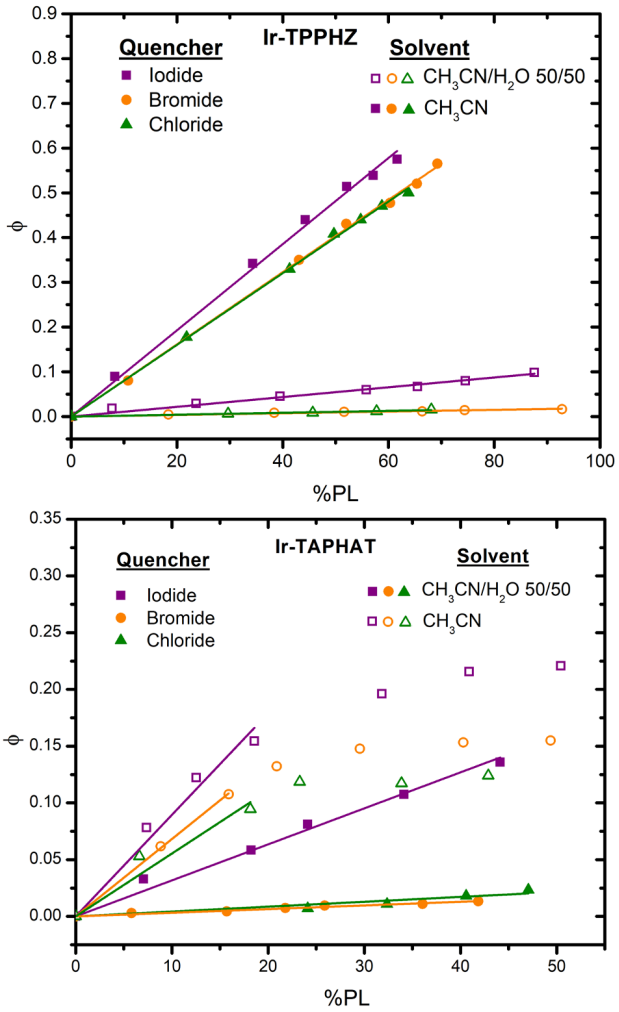

Figure 40. Cage-escape yields recorded using Ir-TPPHZ (top) and Ir-TAPHAT (bottom) in argon-purged CH_3CN (open symbols) and CH_3CN/H_2O 50/50 (closed symbols) in the presence of iodide (purple), bromide (orange) and chloride (green). Reproduced with permission from ref [431]. Copyright 2023 American Chemical Society.

Table 10. Cage-escape yields (ϕ_{ce}) recorded in argon-purged CH_3CN and CH_3CN/H_2O

	ϕ_{ce} Ir-TAPHAT		ϕ_{ce} Ir-TPPHZ	
	CH_3CN	CH_3CN/H_2O	CH_3CN	CH_3CN/H_2O
I^-	0.90	0.32	0.96	0.11
Br^-	0.70	0.03	0.81	0.02
Cl^-	0.55	0.04	0.80	0.02

Bernhard and co-workers highlighted the importance of cage-escape yields in one of their highly parallelized studies looking at the activity of 1440 photosensitizers.[435] Relative cage escape yields were determined with respect to a single photocatalyst as true cage escape yields would have required knowledge

of the photon flux. They proposed that the excited state electron transfer in the encounter complex occurred in the Marcus 'normal' region and hypothesized that geminate recombination occurred in the Marcus 'inverted' region and was faster than irreversible amine oxidation. Within the series that they investigated for cage escape yields, photosensitizers presenting a 1,10-phenanthroline ligand exhibited small cage escape yields. The authors proposed that this ligand offered minimal reorganization energy relative to the torsional bond rotation within a 2,2'-bipyridine ligand that was deemed important for cage escape. The trends observed among the set of photosensitizers suggested that nuclear reorganization strongly influenced cage escape yields.

Finally, Tobita and co-coworkers studied the cage escape yields following oxidative electron transfer quenching from $[Ir(ppy)_2(acac)]$, $[Ir(btp)_2(acac)]$ and $[Ir(F_2ppy)_2(pic)]$ to 1,4-dinitrobenzene. The cage escape yields were overall small and ranged from $\phi_{ce} = 0.1$ to 0.17, as determined by nanosecond transient absorption spectroscopy. The authors suggested that charge recombination was fast and facilitated by triplet to singlet spin conversion within the primary radical ion pair.[436]

4.2.3) Rhodium

Ohno et. al. studied the reductive quenching of $[Rh(dpphen)_3]^{3+*}$, where dpphen 4,7-diphenyl-1,10-phenanthroline, in 1:1 H_2O/CH_3CN solutions by a series of 11 electron donors that included methoxy-substituted benzenes, i.e. methoxybenzene, 1,3,5-trimethoxybenzene, 1,2-dimethoxybenzene, 1,4-dimethoxybenzene, 1,2,4-trimethoxybenzene and functionalized aniline derivatives, i.e. diphenylamine, 3,3'-dimethylbenzidine, 1,2-phenylenediamine, 1,4-phenylenediamine, N,N,N',N'-tetramethylbenzidine and N,N,N',N'-tetramethyl-1,4-phenylenediamine.[349] The methoxybenzene derivatives efficiently quenched the excited-state of $[Rh(dpphen)_3]^{3+*}$ with quenching rate constant of (0.25-7.4) $x10^9$ $M^{-1}s^{-1}$. The radical cation of the quenchers and mono-reduced $[Rh(dpphen)_3]^{2+}$ were observed by transient absorption spectroscopy. Similar results were obtained with the aniline derivatives, with quenching rate constant of (6.1-9.7) $x10^9$ $M^{-1}s^{-1}$.[437] The concentration of oxidized quenchers after excited-state electron transfer was quantified spectroscopically. The cage escape yields varied from $\phi_{ce} = 0.38 - 0.88$ and depended on the electron donor. When aniline derivatives were used, the cage escape increased and the driving force for geminate charge recombination decreased. When methoxybenzene derivatives were used, the cage escape yields were all around $\phi_{ce} = 0.51 \pm 0.07$ and no clear trend with driving force could be obtained. (**Figure 41**).

Additional cage escape yields were measured with $[Rh(dpphen)_2Cl_2]^+$, $[Rh(phen)_3]^{3+}$ and $[Rh(phen)_2Cl_2]^+$ in CH_3CN/H_2O 1:1 mixtures with 1,3,5-trimethoxybenzene, 1,4-dimethoxybenzene and 1,2,4-trimethoxybenzene electron donors.[437] The cage escape yields ranged from ϕ_{ce} = 0.065 for $[Rh(phen)_2Cl_2]^+$ with 1,2,4-trimethoxybenzene to ϕ_{ce} = 0.48 for $[Rh(dpphen)_2Cl_2]^+$ with 1,4-dimethoxybenzene. Taken altogether, the cage-escape yields followed the trend $[Rh(dpphen)_3]^{3+}$ > $[Rh(dpphen)_2Cl_2]^+ \geq [Rh(phen)_3]^{3+} > [Rh(phen)_2Cl_2]^+$.

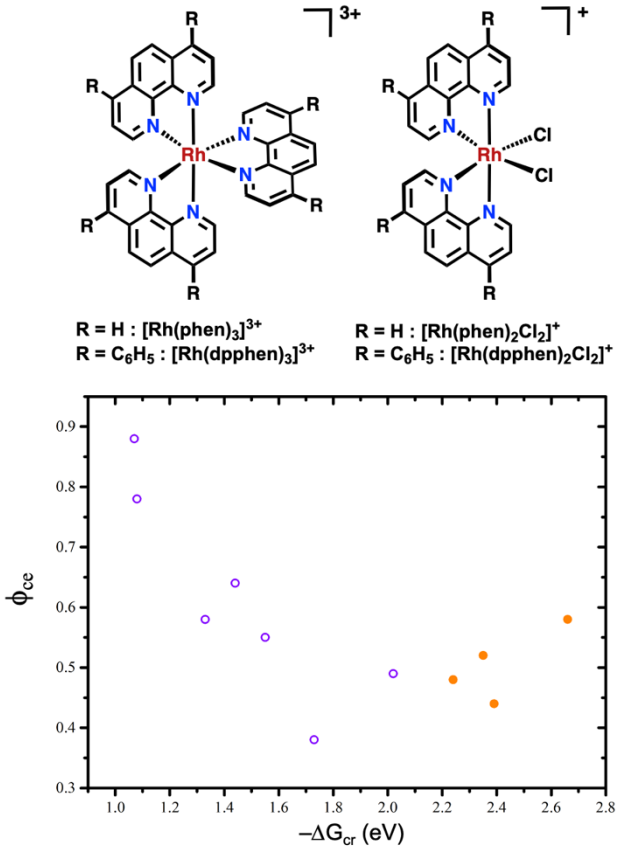

Figure 41. Structure of the Rh(III) photosensitizers discussed in the present study alongside the efficiency of cage escape versus the Gibbs free energy change for geminate charge recombination measured after reductive quenching of $Rh(dpphen)_3^{3+*}$ by amine- and methoxy- benzene derivatives. The yields drop off steeply with driving force (open purple circles) and then then appear to saturate (closed orange circles). Data replotted from reference [437]

4.2.4) Osmium

Cage escape yields after oxidative quenching of osmium photosensitizers have been reported. T.J. Meyer and co-workers quantified the cage-escape yields of three osmium photosensitizers, $[Os(bpy)_2(das)]^{2+}$, $[Os(phen)_2(dppm)]^{2+}$ and $[Os(phen)_2(dmpp)_2]^{2+}$ (**Figure 42**) that were oxidatively quenched by methyl viologen in a solvent mixture composed of 0.1 M tetraethylammonium perchlorate in

acetonitrile to dichloromethane in 8:5 v/v proportions. The cage escape yields were reported relative to 9-methylanthracene that was taken to be unity. Cage-escape yields of ϕ_{ce} = 0.21, 0.18 and 0.14 were determined for $[Os(bpy)_2(das)]^{2+}$, $[Os(phen)_2(dppm)]^{2+}$ and $[Os(phen)_2(dmpp)_2]^{2+}$, respectively. Similar yields were also obtained for ruthenium analogues, and it was concluded that, despite variation of sensitizer, quencher and solvent, the geminate charge recombination within the solvent cage occurred about 4 times faster than the rate of charge separation. The difference in yields observed between Os(II) photosensitizers and "pure" triplet photosensitizers such as 9-methylanthracene have been detailed previously. However, if electron spin were the only factor, the large ~3000 cm^{-1} spin-orbit coupling for the third row Os should have given lower yields than the second row Ru. Therefore, other factors such as the driving force for forward and reverse electron transfer must also play a role. This was also proposed by Ripak *et al.* that reported the oxidative quenching of $[Os(bpy)_3]^{2+*}$ by 4-methoxy, 4-bromo, 4-carboxyethyl ester and 4-nitro benzene diazonium tetrafluoroborate derivatives. The cage escape yields were shown to linearly increase with the driving force for excited-state electron transfer with ϕ_{ce} = 0.18, 0.61, 0.89 and 0.97 for 4-methoxy, 4-bromo, 4-carboxyethyl ester and 4-nitro benzene diazonium, respectively.

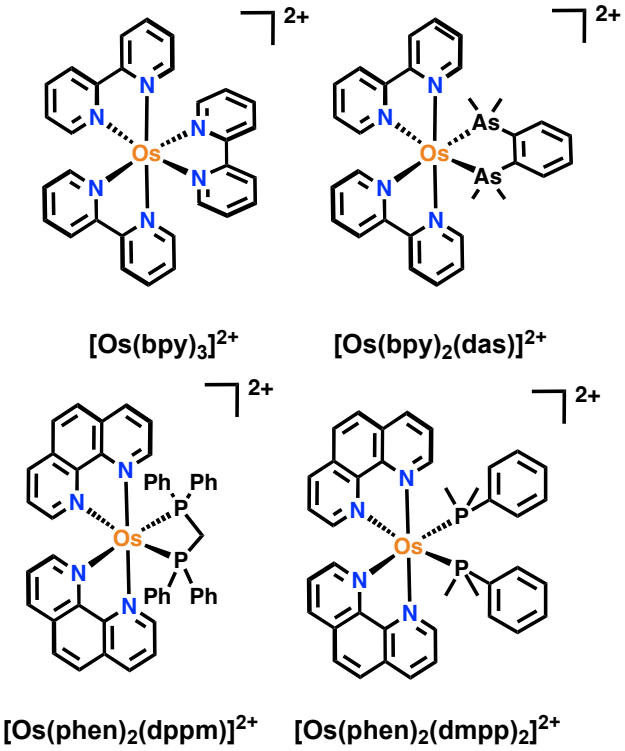

Figure 42. Os(II) Photosensitizers discussed in the present section.

4.2.5) Copper

The oxidative quenching of a $[Cu(dpp)_2]^{+*}$ photosensitizer (**Figure 43**) by methyl (MV^{2+}) and benzyl (BV^{2+}) viologen were reported in CH_3CN solution, where dpp is 2,9-$(C_6H_5)_2$-1,10-phenanthroline. The cage escape yields measured after MV^{2+} quenching were near unity $\phi_{ce} = 0.95 \pm 0.05$ and were $\phi_{ce} = 0.57 \pm 0.05$ for BV^{2+} quenching. The authors attributed the higher cage escape yields than those measured for $[Ru(bpy)_3]^{2+}$ to a smaller spin orbit coupling and more pure triplet state for copper.[378] In addition, the large inner-sphere reorganization change that accompanies the reduction of the d^9 Cu(II) from a flattened geometry to the d^{10} Cu(I) tetrahedral geometry was also considered. Such structural changes within the encounter complex may increase the cage escape yield and also be operative when Cu(II) is used as an electron acceptor.[382]

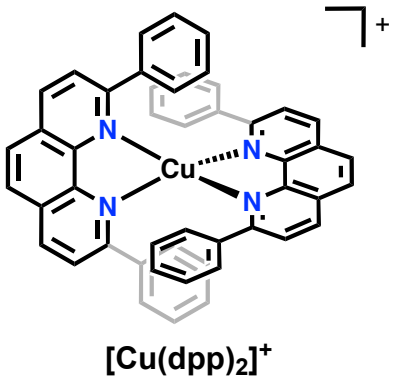

$[Cu(dpp)_2]^+$

Figure 43. Structure of $[Cu(dpp)_2]^+$

4.2.6) Chromium

Ohno and coworkers reported reductive quenching of the ligand field excited states of $[Cr(bpy)_3]^{3+}$ and $[Cr(dpphen)_3]^{3+}$ in acetonitrile using a series of organic donors that included methoxy-substituted benzenes, i.e. 1,3,5-trimethoxybenzene, 1,4-dimethoxybenzene, 1,2,4-trimethoxybenzene and functionalized aniline derivatives, i.e. triphenylamine, diphenylamine, N,N-dimethylaniline, 1,4-anisidine, 2-aminonaphthalene, 3,3'-dimethylbenzidine, 1,2-phenylenediamine, 1,4-phenylenediamine, N,N,N',N'-tetramethylbenzidine, N,N'-diphenyl-1,4-phenylenediamine, N,N,N',N'-tetramethyl-1,4-phenylenediamine as well as phenothiazine.[349] The cage escape yields ranged from $\phi_{ce} = 0.019$ to 0.80 over a driving force for charge recombination of –2.0 eV to –0.67 eV. The cage-escape yields were shown to decrease as the driving force for charge recombination increased from –0.67 to ~ –1.4 eV before reaching a plateau of negligible cage escape yields at the most favorable driving forces (**Figure 44**). Very low cage

escape yields of $\phi_{ce} = 0.01$ were also obtained by Pizzocaro *et al.* for the reductive quenching of $[Cr(bpy)_3]^{3+}$ by acrylamide, although thermodynamic considerations for the geminate charge recombination were not provided.[438]

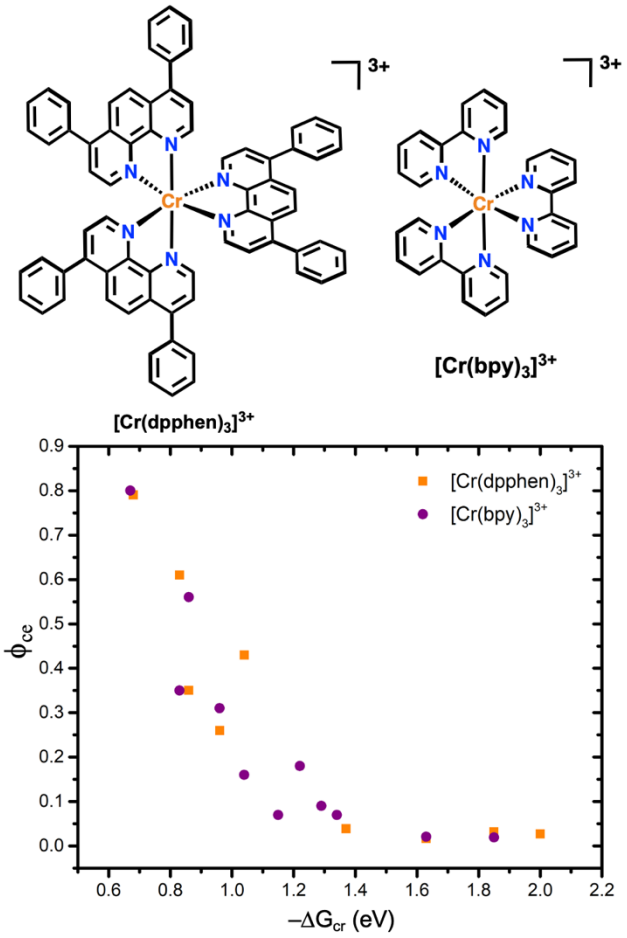

Figure 44. Structure of some Cr(III) photosensitizers described in the present section alongside a plot of the cage escape as a function of driving force after reductive quenching of $[Cr(bpy)_3]^{3+}$(purple circles) and $[Cr(dpphen)_3]^{3+}$ (orange squares).

Wenger and co-workers reported the reductive quenching of the $^2E/^2T_1$ excited $[Cr(dpq)_2]^{3+}$* by a series of electron donors (**Figure 45**). The cage escape yields were only determined for the aromatic tri-(*p*-anisyl)amine (TAA) electron donor in dry argon-purged acetonitrile at 20°C.[439] The cage-escape yields were moderate, $\phi_{ce} = 0.13$, which is smaller than values obtained with prototypical Ru(II) photosensitizers but greater than values obtained with the doublet excited state of iron photosensitizers in acetonitrile (*vide infra*). This moderate cage escape likely stems from the doublet character of $[Cr(dpq)_2]^{3+}$* rendering the charge recombination to the ground state spin allowed.

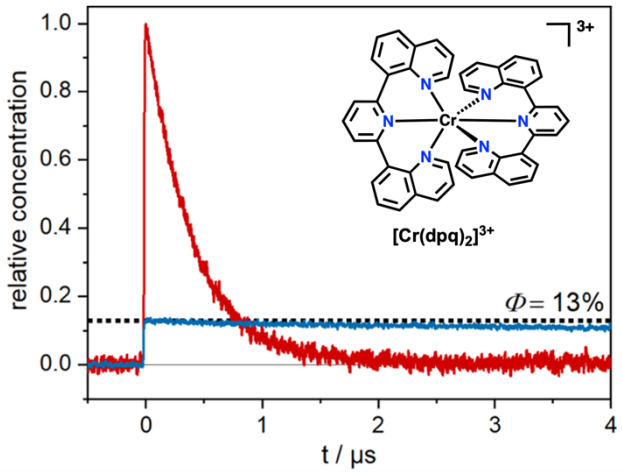

Figure 45. Structure of $[Cr(dpq)_2]^{3+}$ described in the present section a well as the cage-escape yield measurement of a solution containing 35 µM of $[Cr(dpq)_2]^{3+}$ in the presence of 10 mM of tri-(*p*-anisyl)amine (TTA) in aerated dry acetonitrile at 20°C. The blue trace corresponds to the $TTA^{\bullet+}$ concentration whereas the red trace corresponds to the $[Ru(bpy)_3]^{2+}$ actinometer at 455 nm from which $\phi_{ce} = 0.13$ was determined. Reproduced with permission from ref [439]. Copyright 2022 American Chemical Society.

In a follow-up study, Wenger and co-workers determined the cage-escape yields after reductive quenching of the $[Cr(dpq)_2]^{3+*}$ $^2E/^2T_1$ excited by a series of 12 electron donors and compared them with analogous reactions carried out with $[Ru(bpz)_3]^{2+*}$.[440] The electron donors encompassed tri-*p*-arylamine derivatives, anilines as well as aliphatic amines. The cage escape yields were significantly lower with the $[Cr(dpq)_2]^{3+}$ photosensitizer (ϕ_{ce} = 0.07-0.19) relative to $[Ru(bpz)_3]^{2+}$ (ϕ_{ce} = 0.35-0.87). Although an explanation based on spin might have satisfactorily explained this difference, an additional analysis in the broader context of Marcus theory revealed that the driving force for charge recombination was more favored for $[Ru(bpz)_3]^{2+}$ resulting in Marcus inverted kinetic behavior that favored cage escape relative to charge recombination. In contrast, charge recombination was closer to the normal region for the Cr photosensitizer and charge recombination was dominant. The results suggest that by tuning the ground and excited state reduction potentials it may be possible to enhance cage escape yields with earth abundant Cr photosensitizers.

Heinze and co-workers reported visible-light induced fixation of SO_2 to yield sulfones and sulfonamides with a $[Cr(tpe)_2]^{3+}$ photosensitizer, where tpe in 1,1,1-tris(pyrid-2-yl)ethane.[441] A three-component reaction between alkylfluoroborates, SO_2 and alkenes was characterized, alongside the visible-light mediated aminosulfonylation of diaryliodonium salts. In both cases, a single-electron transfer intermediate was proposed, i.e. cyclohexyltrifluoroborate or 4-aminomorpholine, respectively. Large cage escape yields of 0.73 were determined when 4-aminomorpholine was used as quencher. These yields

dropped to 0.27 when cyclohexyltrifluoroborate was employed. Other reaction partners, such as DABSO and DABCO led to cage escape yields that were smaller than 0.08. The cage escape yields were shown to be important for these photoredox catalytic transformations. Interestingly, it appears that in this case the cage escape yields did not track with the driving force for geminate charge recombination. However, this conclusion may be challenged as some of the quenchers were sacrificial reagents where subsequent reactivity within the cage may impact the cage escape yields.

4.2.7) Iron

Iron photosensitizers have been scarcely reported in the literature for bimolecular reactivity.[442-443] This stems from very short excited-state lifetimes that inhibit diffusional electron transfer. Nevertheless, there have been some recent reports that forecast great opportunities for applications of these photosensitizers in the future.[51, 429] For example, Wärnmark and co-workers recently reported $[Fe(phtmeimb)_2]^+$ (phtmeimb = phenyl[tris(3-methyl-imidzaolin-2-ylidene)] borate), an Fe(III) photosensitizer with a doublet Ligand-to-Metal Charge Transfer (LMCT) excited state with a ~2 ns lifetime in several solvents (**Figure 46**).[51, 444-450] This relatively long excited-state lifetime was sufficient for bimolecular excited-state reactivity with highly soluble quenchers. Oxidative and reductive excited-state electron transfer with methyl viologen and diphenylaniline were quantified in acetonitrile, respectively.[444] The cage escape yields were quite small, ϕ_{ce} ~0.05. The photocycle of charge separation and recombination was investigated further down to ultrafast timescales[451] that highlighted donor-dependent charge separation rates of up to 1.25 ps^{-1} that exceed the rates found for typical Ru^{II}-based systems and are instead more similar to those reported for organic sensitizers. [452-453] It hence appears that the low cage escape yields in acetonitrile were due to rapid subpicosecond charge recombination.

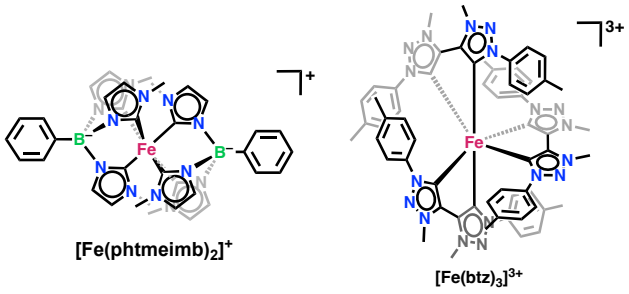

Figure 46. Structure of the Fe(III) photosensitizers discussed in the present section

Troian-Gautier and co-workers recently used the same Fe(III) photosensitizer for dehalogenation reactions and cage escape yield studies.[51, 429] Visible light excitation of $[Fe(phtmeimb)_2]^{2+}$ led to efficient diffusional quenching with a series of electron donors in acetonitrile, DMF, acetone, butyronitrile and dichloromethane. The corresponding dehalogenation yields were much larger in dichloromethane than in any other solvent. Hence, the cage escape yields were quantified in acetonitrile, dichloromethane, and dimethylformamide using three electron donors, i.e. N,N-dimethyl-*p*-toluidine (DMT), N,N-dimethylaniline (DMA) and tri-*p*-tolylamine (TTA). The cage escape yields in the polar CH_3CN and DMF were small ϕ_{ce} = 0.01 – 0.07 and were significantly larger in dichloromethane, ϕ_{ce} = 0.36 – 0.63. These solvent dependent cage escape yields paralleled the isolated product yields obtained during the photoredox catalysis.

The authors proposed several hypotheses to explain the solvent-dependent cage escape yields. The electrostatic repulsion was expected to be larger in low dielectric dichloromethane than in acetonitrile or DMF. This hypothesis was further supported by experiments that showed that ϕ_{ce} decreased by ~70% in CH_2Cl_2 (from ϕ_{ce} = 0.60 to ϕ_{ce} = 0.17) when the ionic strength was increased by the addition of 1.0 M tetrabutylammonium hexafluorophosphate ($TBAPF_6$). Note however that decrease in cage escape yields with ionic strength have been reported already, albeit to a smaller extent.[381, 422]

Another plausible hypothesis was that electron spin underlies the solvent dependent cage escape yields. Geminate charge recombination is expected to be a spin-allowed transition due to the doublet nature of the iron excited state. However, the external heavy Cl atoms in CH_2Cl_2 may induce more quartet character thereby introducing some spin forbiddenness to the charge recombination reaction (**Figure 47**). This hypothesis was further substantiated by additional experiments in CH_2Br_2 and in acetonitrile:iodomethane mixtures, that may enhance excited-state intersystem crossing.[82, 454-457] The cage escape yields determined in CH_2Br_2 and CH_2Cl_2 were equal within experimental error. The addition of iodomethane into a solution of acetonitrile led to a ~5 fold increase in cage escape yields from ϕ_{ce} = 0.02 to 0.09. Noteworthy is the fact that the cage escape yields in these CH_3CN/iodomethane mixtures never reached values as high as those reported in CH_2Br_2 and CH_2Cl_2, suggesting that state-mixing might not be the sole contributor to these large cage escape yields.

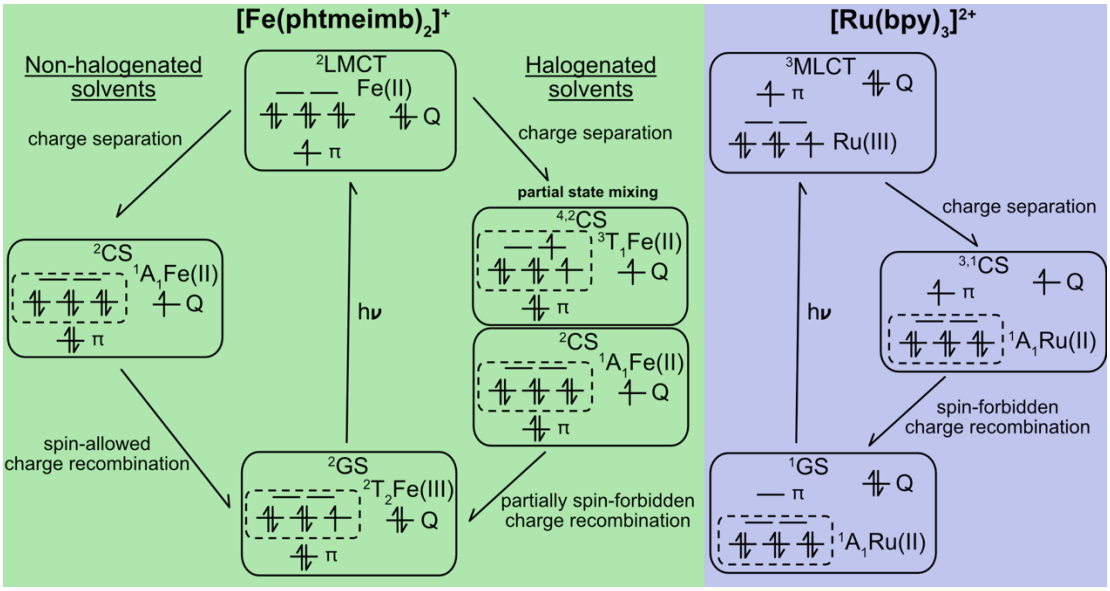

Figure 47. Schematic representation of the light-induced electronic transition involving iron(III) based LMCT photosensitizers (left), and ruthenium(II) based MLCT photosensitizers (right), together with an electron donor quencher (Q). Reproduced with permission from reference [51]. Copyright 2021 American Chemical Society.

$[Fe(phtmeimb)_2]^+$ was also recently used as photosensitizer for hydrogen photo-production in the presence of Pt-colloids or $[Co(dmgH)_2(py)Cl]$ as proton reduction catalysts, $[HNEt_3][BF_4]$ as a proton donor, and triethanolamine or triethylamine as sacrificial electron donors.[458] Turnover numbers greater than 1000 without significant photosensitizer degradation were obtained. The cage escape yields in acetonitrile were however very small (ϕ_{ce} = 0.02 - 0.03) and it was suggested that hydrogen production could be further improved by increasing the cage escape yields. Unfortunately, using solvent such as dichloromethane, previously shown to increase cage escape yields, did not lead to increased yields in hydrogen photoproduction.

Photoinduced symmetry-breaking charge separation was also observed using $[Fe(phtmeimb)_2]^+$ as a photosensitizer. This rare process involves the formation of an excited state capable of undergoing electron transfer with a ground-state photosensitizer to generate the corresponding pair of mono-oxidized and monoreduced photosensitizer ($PS^* + PS \rightarrow PS^+ + PS^-$).[459-460] This symmetry-breaking charge separation to generate the corresponding $[Fe^{II}(phtmeimb)_2]$ and $[Fe^{IV}(phtmeimb)_2]^{2+}$ in equimolar concentration was reported to proceed with a cage escape yield ϕ_{ce} =0.04.

Finally, the cage escape yields were quantified in an atom transfer radical addition (ATRA) reaction using $[Fe(btz)_3]^{3+}$ as photosensitizer with green light irradiation.[461] The reaction proceeded via the excited-state quenching of the ^{2}LMCT excited state to generate the corresponding $[Fe(btz)_3]^{2+}$. The Fe(II) product

has an MLCT excited state that is a stronger reductant than the ^{2}LMCT of $[Fe(btz)_3]^{3+}$ and as such, consecutive ^{2}LMCT-^{3}MLCT excitation of $[Fe(btz)_3]^{3+}$ to activate challenging substrates was developed. Reductive excited-state electron transfer with triethylamine to generate $[Fe(btz)_3]^{2+}$ was confirmed by transient absorption spectroscopy with cage escape yields $\phi_{ce} > 0.20$ in 4:3 acetonitrile:methanol mixtures, greatly exceeding those previously determined in acetonitrile.[51, 429, 444]

4.2.8) Rhenium

Rhenium photosensitizers with three carbonyl ligands in a facial geometry are well-studied photocatalysts for carbon dioxide reduction.[462-463] These photosensitizers exhibit an MLCT excited state with nanosecond lifetimes that can be used for diffusional intermolecular reactivity. Lucia *et al.* studied the cage escape yields associated with the reductive quenching of a series of $[Re(LL)(CO)_3(BP)]^+$ photosensitizers by diaza[2.2.2]octane (DABCO) in degassed acetonitrile, where LL included 2,2'-bipyridine (bpy), 4,4'-$(CH_3)_2$-2,2'-bipyridine (dmb), or 2,2'-bipyrazine (bpz) and BP is 4-benzylpyridine (**Figure 48)**.[464] The variation in bidentate diimine ligand allowed tuning of the corresponding reduction potential, and hence the driving force for reductive electron transfer and geminate charge recombination. It should be noted that, since the structural variations among the series of photosensitizers were comparatively small, the cage-escape rate constant (k_{ce}) was considered constant across the series. Hence, the measured cage escape yields reported on the dependence of k_{cr} on ΔG_{cr}. Cage escape yields that range from $\phi_{ce} = 0.85$ for $[Re(dmb)(CO)_3(BP)]^+$, to $\phi_{ce} = 0.54$ for $[Re(bpz)(CO)_3(BP)]^+$. Interestingly, the cage escape yields increased as the driving force for geminate charge recombination increased (**Figure 48**).

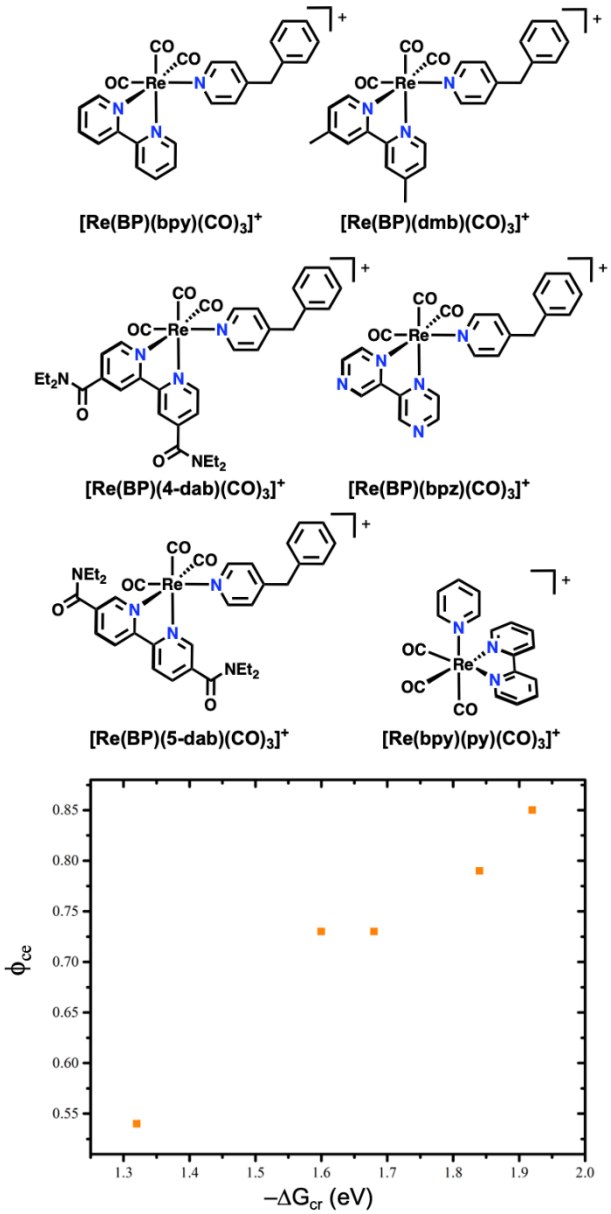

Figure 48. A plot of ϕ_{ce} vs $-\Delta G_{cr}$ for $[(LL)Re^{I}(CO)_3X]^+$ photosensitizers quenched by DABCO in acetonitrile.

Taking **Equation 1.1** into consideration, this result also highlights that k_{cr} decreases as $-\Delta G_{GCR}$ increases, in agreement with expectations based on the semi-classical Marcus theory of highly exothermic electron transfer processes.[32] In addition, comparison with other intramolecular Re-donor dyads indicate that the rate determining step for the decay of the charge-separated state is triplet-singlet intersystem crossing.

Lucia *et al.* also studied the quenching of $[Re(LL)(CO)_3(BP)]^+$ derivatives with a $[Co(CO)_4]^-$ counter-ion.[465] The $[Re(LL)(CO)_3(BP)][Co(CO)_4]$ ion pair exhibited a low-intensity ion-pair charge transfer

(IPCT) absorption band in nonpolar solvents. This absorption band decreased in energy with the LUMO energy of the diamine ligand. In addition, the classical MLCT transitions were also observed for this ion-paired complex. Reductive excited-state quenching was observed from $[Co(CO)_4]^-$, irrespective of whether the IPCT or the MLCT band was excited. Interestingly however, the cage escape yields of $\{Re(LL^{\bullet-})(CO)_3(BP);Co(CO)_4\bullet\}$ were different whether this species was generated via irradiation in the IPCT or MLCT band. Indeed, irradiation of $[Re(LL)(CO)_3(BP)][Co(CO)_4]$ in THF at 355 nm (MLCT) led to cage-escape yields $\phi_{ce} = 0.66$ whereas irradiation at 532 nm (IPCT) led to cage escape yields of $\phi_{ce} = 0.04$. Since the same geminate pair was produced in both cases, it was hypothesized that the cage escape rate constants were identical which implies that the charge recombination rate constant is significantly smaller for MLCT excitation. The smaller charge recombination rate constant was attributed to the spin state of the geminate radical pair. MLCT excitation provides a triplet state that is carried within the geminate radical pair, formally decreasing geminate recombination due to spin forbindenness, whereas IPCT excitation leads to a singlet state, with a spin-allowed transition back to the ground state products. Another hypothesis is that the geometry of the encounter complex between diffusing species and ion-paired species is different and would lead to different cage-escape yields after charge separation.

Rhenium photosensitizers have recently been used in combination with [tris-(2-carboxyethyl)-phosphine] (TCEP), hydroquinone electron relay derivatives and a cobalt catalyst for hydrogen photoproduction applications.[466] The reductive quenching of $[Re(bpy)(py)(CO)_3]^{*+}$ by 1,4-dihydroxybenzene, 1,2-dihydroxybenzene and 2,5-dihydroxybenzoic acid was studied in D_2O by transient IR and visible absorption spectroscopies. TCEP was shown to be an inefficient quencher whose sole purpose was to regenerate the oxidized quinone derivatives to the corresponding hydroquinones.[467] In all cases, the cage escape yields were shown to be $\phi_{ce} = 0.35 \pm 0.02$. Interestingly, hydrogen photoproduction was a factor of 5-10 larger when 1,4-dihydroxybenzene was used compared to the other two electron relays. This highlights that, in agreement with what was previously described for iron(III) photosensitizer for hydrogen photoproduction, cage escape yields are not the sole contributors to the overall reaction efficiency. In related studies, the cage escape yields for the reductive quenching of $[Re(bpy)(py)(CO)_3]^+$ by triethanolamine and sodium ascorbate in D_2O were determined as $\phi_{ce} = 0.75$ and $\phi_{ce} = 0.60$, respectively.[468] A cage escape yield of $\phi_{ce} = 0.75$ was also determined for the reductive quenching of $[Re(phen)(py)(CO)_3]^+$ by triethanolamine in D_2O.[469]

Finally, it should be mentioned that cage escape yields and geminate charge recombination process in the reductive quenching of Re(I) photosensitizers were also studied on insulating mesoporous ZrO_2 thin

films.[470] Cage escape yield of ϕ_{ce} = 0.42 with phenothiazine as electron donor were determined when the Re photosensitizer was surface anchored relative to ϕ_{ce} = 0.15-0.26 when the photosensitizer was free in solution. Encounter complex formation and cage escape are quite different for the surface anchored photosensitizer and deserve further study in the future.

4.2.9) Platinum

Kisch *et al.* investigated the excited-state behavior of 1:1 ion pairs of 2,2'- or 4,4'-bipyridinium derivatives, i.e. 1-Ethyl-1'-(3-sulfonatepropyl)-3,3'-dimethyl-4,4'-bipyridinium ($EPSDMP^+$), N,N'-(1,3-propenyl)-2,2'-bipyridinium (PQ^{2+}) and 1-ethyl-1'-(3-sulfonatepropyl)-4,4'-bipyridinium ($EPSP^+$) with $[Pt(mnt)_2]^{2-}$, where mnt^{2-} is maleonitriledithiolate (**Figure 49**).[471] Experiments were carried out in DMSO and it was shown that the cage escape yields were very sensitive to the charge of the bipyridinium derivatives, with unitary cage escape yields for singly charged derivatives ($EPSDMP^+$ and $EPSP^+$) and ϕ_{ce} = 0.11 for doubly charged analogues (PQ^{2+}). This drastic difference in cage escape yields was explained in terms of coulombic repulsion. For the singly charged derivatives, oxidative excited-state electron transfer leads to a neutral quencher and a mono-anionic $[Pt(mnt)_2]^-$, whereas in the case of doubly charged quenchers, oxidative excited-state electron transfer leads to a mono-cationic quencher and mono-anionic $[Pt(mnt)_2]^-$ which would experience electrostatic attraction and lead to a decreased cage escape yield. Additional experiments with neutral bipyridinium quenchers, such as 2,2'- or 4,4'-bipyridinium-N,N'-di(propylsulphonate), would have provided additional information on the impact of electrostatic repulsion in these platinum complexes.

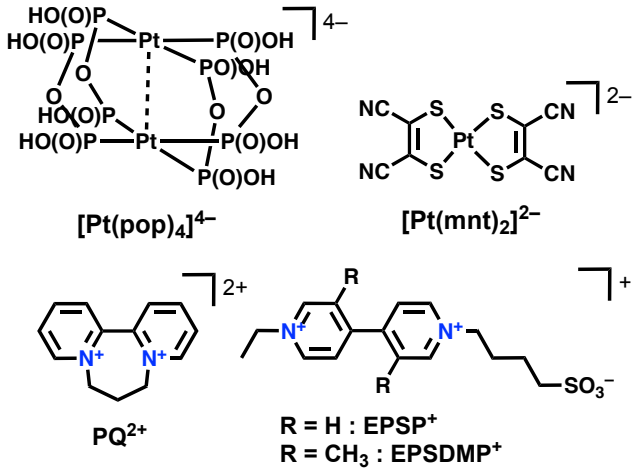

Figure 49. Structure of the platinum photosensitizers and some quenchers discussed in the present section.

The reductive quenching of the triplet state of tetrakis(μ-pyrophosphito-PP')diplatinate(II), $[Pt_2(pop)_4]^{4-}$, by $[Ni(cyclam)]^{2+}$ was studied in 0.01M $HClO_4$ containing 0.1M Na_2SO_4 as electrolyte.[472] The cage escape yields were determined to be ϕ_{ce} = 0.054 and 0.028 in air-saturated and in nitrogen-saturated solution, respectively. The larger cage escape yields for the formation of Ni(III) obtained under air point towards a scavenging of the reduced Pt complex ($[Pt_2(pop)_4]^{5-}$) from the solvent cage by oxygen. Nevertheless, these small cage escape yields point towards a very efficient geminate charge recombination, presumably a consequence of the strong coulombic attraction within the pair {($[Pt_2(pop)_4]^{5-}$;$[Ni(cyclam)]^{3+}$}.

4.3) Porphyrins

Utilizing porphyrin and metalloporphyrin photosensitizers and quinone acceptors, Holten, Gouterman and Harriman were amongst the first to propose that triplet states gave rise to high cage escape yields while singlets were negligibly small.[166-167] Harriman and coworkers showed that the cage escape yields after oxidative quenching of metalloporphyrins by benzoquinone acceptors decreased when closed shell heavy metal atoms such as Cd, Ru, and Pd were coordinated to the porphyins.[168] The authors attributed this to increased spin-orbit coupling that enhanced the geminate recombination rate constant. No cage escaped products were observed when paramagnetic metals were present in the porphyrin pocket.

The impact of external heavy atoms on cage escape yields after oxidative quenching of the singlet and triplet excited states of bacteriochlorophyll by *p*-benzoquinone were investigated with iodomethane.[166] In the presence of 8 M iodomethane, the lifetimes of both the singlet and triplet states decreased. The researchers concluded that the cage escape was undetectable from the singlet excited state but occurred with a considerable yield of ϕ_{ce} = 0.63 from the triplet state.[166-167]

Harriman and coworkers reported the quenching of metalloporphyrins of the form M(TPP), where TPP = meso-5,10,15,20-tetraphenylporphin and M = Mg, Cd, Ru, Zn, Pd, Cu, Cr, Al, and H_2 (freebase porphyrin), by benzoquinone in ethanol.[168] The cage escape yields for these porphyrins were significant ranging ϕ_{ce} = 0.05-0.25, with the exception of Cu and Cr, where the cage escape yields were negligible. A plot of cage escape vs -ΔG revealed a weak dependence. Ohno and coworkers reported oxidative quenching of octaethyl Zn(II) porphyrin, Zn(OEP), by quinones (benzo-, dimethyl-, naphthyl-, tetramethyl-, and anthra- quinones) in hexanol .[349] A significant cage escape yield from the porphyrin triplet state was

measured that decreased from ϕ_{ce} = 0.27 to 0.13 as the free energy stored in the charge separated state was increased from 1.15 eV to 1.62 eV.

In 1979, Harriman and co-workers reported that polar solvents stabilise the formation of the encounter complex between zinc tetraphenylporphyrin (ZnTPP) and benzo-1,4-quinone (BQ).[473] The authors also pointed out that ZnTPP can react either from a singlet or triplet excited state, and that the latter was more sensitive to polarity changes (10 fold) than the singlet excited state. Moreover, singlet states did not produce high yields of separated ions while triplet states exhibit large cage escape yields. These observations were consistent with classifications proposed by Masuhara a few years earlier. For the solvents tested in their work, solvents with $\varepsilon < 7$ (ethyl acetate), no cage escape was measured from the triplet state whereas for solvents with $9 < \varepsilon < 18$ (hexan-1-ol, butan1-ol, propan-1-ol), an approximately linear relationship between ε and the cage escape yields was established, with a maximum yield for $\varepsilon = 24$ (ethanol).

Oxidative quenching of a tetracationic Zn porphyrin photosensitizer by dicationic methyl viologen was characterized as a function of the ionic strength. The cage escape yields from the porphyrin triplet state increased as the ionic strength increased from 0.02 M to 0.1 M. However, increasing the ionic strength past 0.1 M lowered the cage escape yield to a plateau value around 1.0 M ionic strength. This behavior is similar to what was observed with other systems where the PS and Q bear charge of similar sign,[474] such as in ruthenium complexes quenched by methyl viologen (Section 4.2.1.3). At low ionic strengths, the cationic charges assist cage escape while at high ionic strength the charges are screened by ions present in the solvent cage and the repulsion is tempered.[111] The ionic strength dependence of porphyrin quenching in micellar solutions have also been studied. Though, it must be noted that the extent of ionic strength has been proven somewhat difficult to determine with the localized charge on their surface of the micelles.[475] However, in each study, no significant ionic strength dependence on the cage escape yield was observed in micellar systems.

One of the earliest reports of coulombic interactions on cage escape yields is the oxidative quenching of zinc porphyrins with methyl viologen.[474] A series of five Zn porphyrins were synthesized with overall charges of 4+ to 4–. The cage escape yields were as large as 0.75 for the 4+ porphyrin and those for the tetraanionic porphyrins were virtually undetectable. This data indicates that coulombic attraction within the solvent cage lowers the cage escape yield significantly, while coulombic repulsion in the solvent cage gave rise to the largest cage escape yields.

It was theorized that micelles with charged surfaces could lead to enhanced cage escape yields,[418] but it took some time for experimental evidence to arise.[475-476] Two complimentary studies using anionic Zn porphyrins and dicationic methyl viologen were utilized to study the effect on cage escape yields when changing the micelle surface charge from negative[475] to positive.[476] In fluid solution, oxidative quenching of the tetraanionic porphyrin by MV^{2+} lead to fairly small cage escape yields ($\phi_{ce} < 0.2$) due to coulombic attraction between the charge separated products. However, in the presence of micelles composed of dihexadecylphosphate that have a negative surface charge, a significant cage escape yield was measured, $\phi_{ce} < 0.8$.[475] This is due to the cationic methyl viologen associating with the negatively charged surface, thus after charge separation the anionic Zn porphyrin is repulsed from the surface enhancing cage escape yields. The addition of a positive charged liposomes formed with 1,2-dimyristoyl-sn-glycero-3-ethylphosphocholine chloride (eDMPCCl) was also shown to have a significant increase on the cage escape yields ($\phi_{ce} = 0.57$) for similar reasons except in this case the anionic Zn porphyrin is associated to the liposome surface.[476]

5) Conclusions

It has been 90 years since the concept of a solvent cage was first introduced. The late Nicholas Turro referred to the solvent cage as the first example of supramolecular chemistry in the rich history of photochemistry.[477] This review provides new insights into fascinating organization of solvents and ions that surround a radical pair. Three mechanisms were described for the generation of the radical pair: 1) light excitation of a stable molecule or ion to a dissociative or pre-dissociative excited state; 2) light-initiated electron transfer in a non-covalent donor-acceptor complex and 3) diffusional encounters of a photoexcited sensitizer with a redox active quencher. Ultrafast spectroscopic techniques have enabled a glimpse of the solvent cage for only the first two of these processes and have revealed some of the most rapid reactions known in all of chemistry. The encounter complex formed by diffusional encounters of a photosensitizer and a quencher are more elusive and have not yet been directly detected but are arguably the most important for emerging applications in solar energy conversion and photoredox catalysis. The breadth of photochemistry is remarkable, encompassing organic, main group, and transition metal complexes.

In this section, an attempt is made to provide our state-of-the-art knowledge on solvent cages and cage escape that unite these three photochemical generation mechanisms. Some might argue that such attempts are in vain as cage escape is indeed nuanced and oftentimes very specific to a reaction type. Such arguments have merit. The age-old challenge in scientific research of fixing all parameters and varying only one is

exceedingly difficult, particularly for elusive solvent cages. Yet by bringing together seven factors that have been identified to impact cage escape, a researcher can select which are most appropriate for their own applications. In doing so the researcher is advised that often times these factors of electron spin, magnetic fields, non-covalent interactions, temperature, distance, free energy, and solvent are inherently coupled and should not be treated as individual contributions that can be simply added to predict cage escape behavior.

Critical analysis of what is truly known about these factors, and perhaps more importantly what is unknown, in this important research area may guide research toward a molecular understanding of solvent cages. Indeed, it is our hope that such analysis will inspire future researchers to develop the supramolecular chemistry of solvent cages so as to enable quantitative release of desired products through the specifically designed "windows" alluded to in the Introduction of this review. Such next generation solvent cages will likely require more complexity than solvent molecules alone can provide, with ionizable groups and hydrophobic/hydrophilic regions like those found in biology. Hence it seems appropriate to drop the word 'solvent' and simply refer to cages for many applications in photochemistry. We conclude this section with specific examples that provide new opportunities for advancing our understanding of cage escape.

5.1) Spin

The early work on oxidative quenching of porphyrins provided compelling evidence that spin matters: triplet states provide nearly quantitative cage escape, singlets negligibly small.[166-168, 478] The quantitative cage escape of CO after light excitation of carboxy hemes is also likely a result of a spin change at the iron center.[258, 273-274] Hence the well-known spin selection rule in spectroscopy is clearly relevant to the charge recombination reaction and hence the cage escape yield.

Unfortunately, spin is a poor quantum number for many classes of photosensitizers and quenchers. In particular, the presence of a heavy atom induces significant spin-orbit coupling that effectively mixes spin states. For a photosensitizer with a singlet excited state, such quantum mechanical mixing may enhance the cage escape yield while for triplet photosensitizers the yields become smaller. This provides opportunities for photosensitizer design where the introduction of pure triplet acceptor states physically remote from heavy atoms can enhance cage escape yields, such as ligands that contain an anthracene group. Quenchers can also be custom designed at the molecular level to enhance cage escape from singlet excited states where the presence and the position of a heavy atom quencher has been shown to have a significant impact.

The impact of spin-orbit coupling can be subtle and there are aspects that deserve additional study. For example, in the well-studied family of photosensitizers based on $[Ru(bpy)_3]^{2+}$, this review found only two special example where oxidative quenching gave rise to a cage escape yield of unity. These 'special cases'

involved a Cu(II) donor that is expected to have large structural changes associated with reduction and 4-nitrobenzene diazonium that is expected to release N_2 upon reduction. In contrast, several examples of quantitative cage escape after reductive quenching have been reported. If spin-orbit coupling mixes the singlet and triplet states and this is the main determinant in cage escape yields, why would reductive quenching give rise to higher yields than oxidative quenching? Some authors have attributed this to the molecular orbitals involved in the charge recombination reaction.[372] Oxidative quenching formally yields a Ru(III) acceptor, while reductive quenching yields a reduced bipyridine radical anion that is distant from the metal center. The reduced bipyridine ligand (specifically $[Ru(deeb)_2(deeb^{-})]^{+}$) was proposed to be less susceptible to spin-orbit coupling and hence present as a purer triplet state that allows quantitative cage escape. This points to quantitative cage escapes after reductive quenching of heavy metal photosensitizers, if this observation is generalizable to other metal-ligand photosensitizers. This interpretation indicates that the excited state itself does not determine the spin state of the primary pair and raises questions about when the spin state of the primary pair is determined. In addition, how much coupling between a heavy metal and a redox active ligand/quencher is required to invoke significant spin orbit coupling? The answers to these questions are relevant to our understanding of spin effects in cage escape and to the design of next generation photosensitizers with enhanced cage escape yields after both oxidative and reductive quenching.

Studies of the external heavy atom effect, where heavy atoms that are not oxidized or reduced impact the cage escape yield, continue to be of interest. The external heavy atom effect is well known in photochemistry and has long been used to enhance phosphorescence from triplet states of organic molecules. The published data demonstrate quite convincingly that heavy atom additives become part of the solvent cage and thereby impact the yield.[51, 82, 429] Solution properties such as the viscosity and dielectric constants inherent to the original Noyes model need to be taken into account in addition to spin orbit coupling, especially when the heavy atoms are present in high concentrations and selectively solvate the reactants or products.

5.2) Magnetic Fields

The fact that the internal magnetic field impacts cage escape yields suggested early on that an external field would also have an impact. This has been borne out through experiment. Three different mechanisms have been identified by which an external field can impact cage escape, only one of which enhances the yield. The enhancement of cage escape yields occurs with small magnetic fields that can be introduced with an inexpensive permanent magnet for practical applications, although according to reported data, the impact has been small. Perhaps the most significant impact of magnetic field studies is in

enhancing our fundamental understanding of cage escape for specific photosensitizer-quencher systems. For example, the role an external heavy atom has on cage escape is better understood when yields are measured in the presence and absence of an external field. The observation of nuclear polarization in diamagnetic products from the primary radical pair (CIDNP) has been realized and could be further developed to provide quantitative information on cage escape.[172, 189]

5.3) Non-Covalent Interactions

There is compelling evidence that non-covalent forces in the primary radical pair impact cage escape yields. In particular, photosensitizers that ion-pair with quenchers in the ground state with favorable electrostatic interactions in the charge separated state usually give rise to very low cage escape yields.[88, 386, 392] These yields may be enhanced when one of the partners in the charge-separated state is neutral. In the well-studied oxidative quenching of $[Ru(bpy)_3]^{2+}$ by MV^{2+}, specific anion and ionic strength dependencies have been documented.[83-84, 395, 413, 422, 479-480] The +1 charge on each partner in the charge separated state provides a Coulombic incentive for cage escape. At high ionic strengths the cage escape yields decrease, behavior attributed to screening of these charges by ions in the solvent cage. Studies where the cation identity was fixed and the anion was varied, and vice-versa, have revealed that it is indeed the anion that was responsible for the decreased yields by imposing larger reorganization energies and slowing charge recombination rates.

The π–π interactions in 1:1 aromatic photosensitizer:quencher pairs are clearly relevant to cage escape. In some cases, these interactions are so strong that new intermolecular electronic transitions appear; light excitation in resonance with these transitions generate contact radical ion pairs that have significantly lower cage escape yields than does direct light excitation of the photosensitizer. Further, the introduction of functional groups that decrease the magnitude of the π–π interactions result in more efficient cage escape.[96, 311-321, 328-329]

Other non-covalent interactions such as H-bonding, halogen bonding, and van der Waals forces are also likely to be important for cage escape. Photosensitizers with H-bonding groups designed to associate with specific quenchers have been reported, however Coulombic forces are also operative, and it has been difficult to disentangle the two non-covalent interactions.[118] A recent thermochemical analysis has indicated that non-covalent forces other than Coulombic must be operative. Future study in this direction provides opportunities to tailor cages for enhanced escape.

5.4) Temperature

Relatively few studies have reported the temperature dependence of cage escape, those that have noticed a significant increase in yield with temperature. In principle, temperature could impact both the geminate recombination rate constant and diffusion from the cage. The available literature for diffusional quenching of excited states as well as for population of dissociative excited states, indicate that diffusion out of the cage is enhanced and is the primary determinant in the larger cage escape yields measured at high temperatures.[381, 422] Such behavior can be understood as temperature impacting the viscosity of the solution as defined in the early Noyes model. Indeed, early studies of photodissociative excited states attempts were made to extract the ratio of activation energies for diffusion and charge recombination by accounting for the temperature dependent viscosity. It is unclear how successful this approach was. As thermal effects are difficult to avoid and are certainly present in any spectroscopic measurement, further analysis of the temperature dependence of cage escape seems warranted.

5.5) Distance

The Noyes model specifically invoked the radical pair distance as a key to predicting cage escape yields. Marcus theory indicates that both the reorganization energy and the electronic coupling favor charge recombination at short distances. Hence one would predict that an obvious way to enhance cage escape yields would be to increase the distance. In early studies of dissociative excited states this was accomplished by release of a stable small molecule between the photogenerated radical pairs, like in the cross-over studies described of diazomethane and perdeutero diazomethane where N_2 was released. Higher cage escape yields have been realized through the introduction of steric groups in π–π interactions of aromatic charge-separated states that have been reasonably attributed to decreased electronic coupling relative to control studies with aromatic molecules that did not contain the bulky substituents.

There is also data that indicates distance is important in diffusional charge separation. Bulky pyridinium electron acceptors generally gave rise to larger cage escape yields after oxidative quenching.[416, 481] Likewise, eight-coordinate metal cyano quenchers gave larger cage escape yields for reductive quenching of excited states than did six-coordinate cyano complexes.[384] As the Gibbs free energy change was also impacted in these comparative studies, it is not possible to assign these differences completely to the distance between the radical pairs. Nevertheless, all existing theoretical models predict higher cage escape yields at larger separations and future research in this area is hence likely to be fruitful.

5.6) Free Energy

Many cage escape studies have attempted to quantify the Gibbs free energy dependence of geminate charge recombination. The most compelling data is for the π–π interactions in 1:1 aromatic

photosensitizer:quencher pairs.[314] Across three types of π quenchers over an appreciable change in the driving force, good agreement with the semiclassical Marcus expression was obtained with geminate charge recombination occurring in the Marcus kinetic inverted region.[316, 332] The Marcus analysis provided estimates of both the electronic coupling and the reorganization energy for geminate recombination. It is noteworthy that in several cases, the π–π adducts were sufficiently stable that the recombination reaction could be directly quantified by ultrafast absorption spectroscopy.

For diffusional excited-state quenching, the transiently formed encounter complex has not been directly observed through spectroscopic measurements. Instead, the charge recombination rate constant has been extracted from the measured cage escape yield. This is typically done by calculation of the rate constant for diffusion out of the solvent cage, k_{ce}, usually with the Eigen expression. For a homologous series of quenchers, a single value of k_{ce} was often assumed. Plots of k_{cr} obtained in this fashion versus –ΔG have given mixed results, some showing little free energy dependence while other showing evidence for normal electron transfer with rate constants that saturate at large driving forces or even show a hint of Marcus kinetic inverted behavior. In principle, this approach is attractive as geminate recombination is not subject to the diffusional contributions described in the first section of this review. In practice however, the unknown structure of the encounter complex and the likelihood for charge recombination occurring over a range of distances and orientations, especially when the free energy change is large, make this data difficult to interpret. For this reason, this review emphasized analysis of the measured cage escape yields as a function of the driving force, rather than charge recombination rate constants that were extracted from the yield measurements. Clearly an improved understanding of the encounter complex structure would enable greater insights into the free energy dependence of charge recombination.

5.7) Solvent

Both Marcus theory and the Noyes model predict that cage escape yields should be highly solvent dependent. This is indeed the case. However, understanding why a specific solvent impacts a particular cage escape yield is exceedingly difficult. Indeed, comparative studies where the photosensitizer and quencher are held constant and the solvent is changed are often difficult to understand or quantitatively model. A change in solvent may impact all three Marcus parameters in a manner that are often times impossible to disentangle. Two solvent parameters have emerged as being the most relevant to cage escape, the dielectric constant and the viscosity. Below the impact of these two quantities on cage escape are summarized.

Recall that the dielectric constant ε, or relative permittivity, is the factor by which the electric field between two points charges in the material is decreased relative to vacuum. The dielectric constant is also

related qualitatively to the solvent polarity, as it is directly proportional to the electric susceptibility χ_E, the degree of polarization in response to an applied electric field. Solvents with a high ε tend to stabilize more polar transition states.[482] This stabilization has been correlated with the solvent "caging effect",[226] where nonpolar solvents like chloroform are proposed to form a "weaker cage" than a highly polar solvent like water.[219, 221] Perhaps more intuitively, the dielectric constant is a measure of the solvent ability to stabilize the charge-separated radical pair that directly impacts cage escape. A low dielectric constant like dichloromethane does not stabilize the classical [$Ru(bpy)_3^{3+}$; $MV^{\bullet+}$] as effectively as does water, thereby favoring cage escape over charge recombination.[361-362] In contrast, a charge separated pair comprised of an anion and a cation would be held together more tightly in a low dielectric solvent thereby favoring charge recombination. Hence when considering the impact of the solvent dielectric constant on cage escape yields, many of the same factors described above for noncovalent interactions arise.

The viscous drag associated with radicals leaving the solvent cage is central to the early Noyes model for cage escape that were in turn inspired by the original Franck and Rabinowitch publication. Indeed, early studies of iodine photodissociation clearly showed that the yield of iodine atoms decreased when a viscogen was present in the solvent that increased the solution viscocity. These researchers were cognizant of the fact that the added viscogen might preferentially solvate the primary pair of radicals and selected them carefully to have chemical structures similar to that of the solvent. There is now little doubt that increased solution viscosity lowers the cage escape yield. However, this knowledge did not have predictive power. In other words, knowledge of the cage escape yield for a solvent/viscogen mixture with a measured viscosity in cP did not allow one to predict the cage escape yield in another solvent/mixture.

A breakthrough was realized when the diffusion coefficients were measured directly in the solvent/viscogen mixture using NMR spectroscopy.[233-237] The reciprocal of the measured diffusion coefficient was shown to scale directly with the cage escape yield and enabled predictions of cage escape yield to be made in alternative solutions provided that the diffusion coefficient was known. This advance was realized for measured cage escape yields after light excitation of bimetallic complexes to dissociative excited states. The diffusion coefficients of the radicals themselves were not measured, but rather a diamagnetic surrogate with similar structure, size and charge. Extension of this work to diffusional quenching of excited states would certainly be of interest. Further, electrochemical techniques exist that oftentimes allow the diffusion coefficient of the radical itself to be measured.[483] Hence electrochemical and NMR studies are expected to provide insights into cage escape yields and provide a means to improve our understanding of diffusion in practically useful solutions.

5.8) Dissociative Excited States

Light excitation of molecules to dissociative or pre-dissociative excited states represented the first tests of the cage effect that were summarized in Section 3 of this review. There is good reason to believe that a renaissance will occur in this research area and there is little doubt that continued study will afford insights into the processes that occur within cages from which new applications will emerge. Unlike the solvent cages formed by diffusional encounters of excited states and quenchers that have precluded our detection, the cage surrounding primary radical pairs generated by ground state excitation have been directly probed. This breakthrough was first demonstrated after pulsed light excitation of iodine some 50 years ago.[200] The application of ultrafast kinetic measurements with state-of-the-art spectroscopic tools should continue to provide critically important details of the kinetics for bond rupture and formation within cages. Such data would allow rigorous testing of the Noyes model[199] as well as its extension to more modern theories such as that of Marcus described herein[33-34, 484] as well as those that explicitly account for the bond dissociation energy.[485-486]

Dissociative excited states often generate radical species that drive subsequent redox reactions relevant to organic synthesis, health care, and environmental remediation. Some brief examples of each are given here that emphasize the importance of advancing our fundamental understanding of cages for these applications. The photogeneration of chlorine atoms provides a means to activate C-H bond bonds.[23-24, 44, 442] A discovery that would enable quantitative transfer of a caged chlorine atom to a specific C-H bond on a compound of interest would be of high impact and enable new chemistry. The recent Covid epidemic revealed the need for alternative chemistries competent of killing dangerous pathogens where the photochemistry of dissociative excited states that generate potent oxidants holds considerable promise. Of relevance to environmental chemistry is the critical need to remove plastics and other manmade organic pollutants from our waterways. Here too photochemistry and the cage effect will play an important role. The rupture of strong C-C or C-X, where X = Cl or F, bonds requires high energy photons that have historically been limited to ultraviolet light.[23-24] Recent advances in photon up-conversion suggest that this photochemistry may one day soon be accessed by visible photons.[487-491]

The dissociative excited states of hemes, cobalamins, and other transition metals in biology continue to provide opportunities to probe the pathways that natural evolution has provided for small molecule exchange and activation.[254-257] A more detailed understanding of dissociative excited states in synthetic transition metal complexes is also needed as ligand loss photochemistry has important applications in synthetic chemistry and in medicine.[207,208] In addition, knowledge of how best to optimize such

photochemistry will likely provide insights into avoiding ligand loss that represent unwanted reactivity for the development of first-row transition metal photosensitizers competent of diffusional quenching.[59, 450, 492-496] Hence, a more detailed knowledge of dissociative excited states in synthetic and naturally occurring transition metal complexes may one day allow the rationale design windows that enable quantitative release of ligands from dissociative excited states and caged redox equivalents from long-lived excited states.

5.9) Opportunities for Future Study of Solvent Cages and Cage Escape Processes

The examples reported in this review reveal the intense interest in bimolecular excited-state electron transfer, yet does not provide a comprehensive model that would enable one to predict cage escape yields. This is unfortunate and future research should be directed towards this goal. Many literature studies focused on cage escape yields measured as a function of the thermodynamic driving force for geminate charge recombination. Some reported a free energy dependence while others did not. It is not clear why. Clearly, other important factors exist. Inorganic photosensitizers have been investigated in considerable detail, but more than 80% of this literature focused on $[Ru(bpy)_3]^{2+}$, which raises questions about the generality of the findings. Remarkably few studies have utilized synthetic chemistry to tune the photosensitizer structure as a means to control cage escape yields which provides new opportunities for future studies. This and other avenues of future research are given in **Figure 50** and are discussed briefly below.

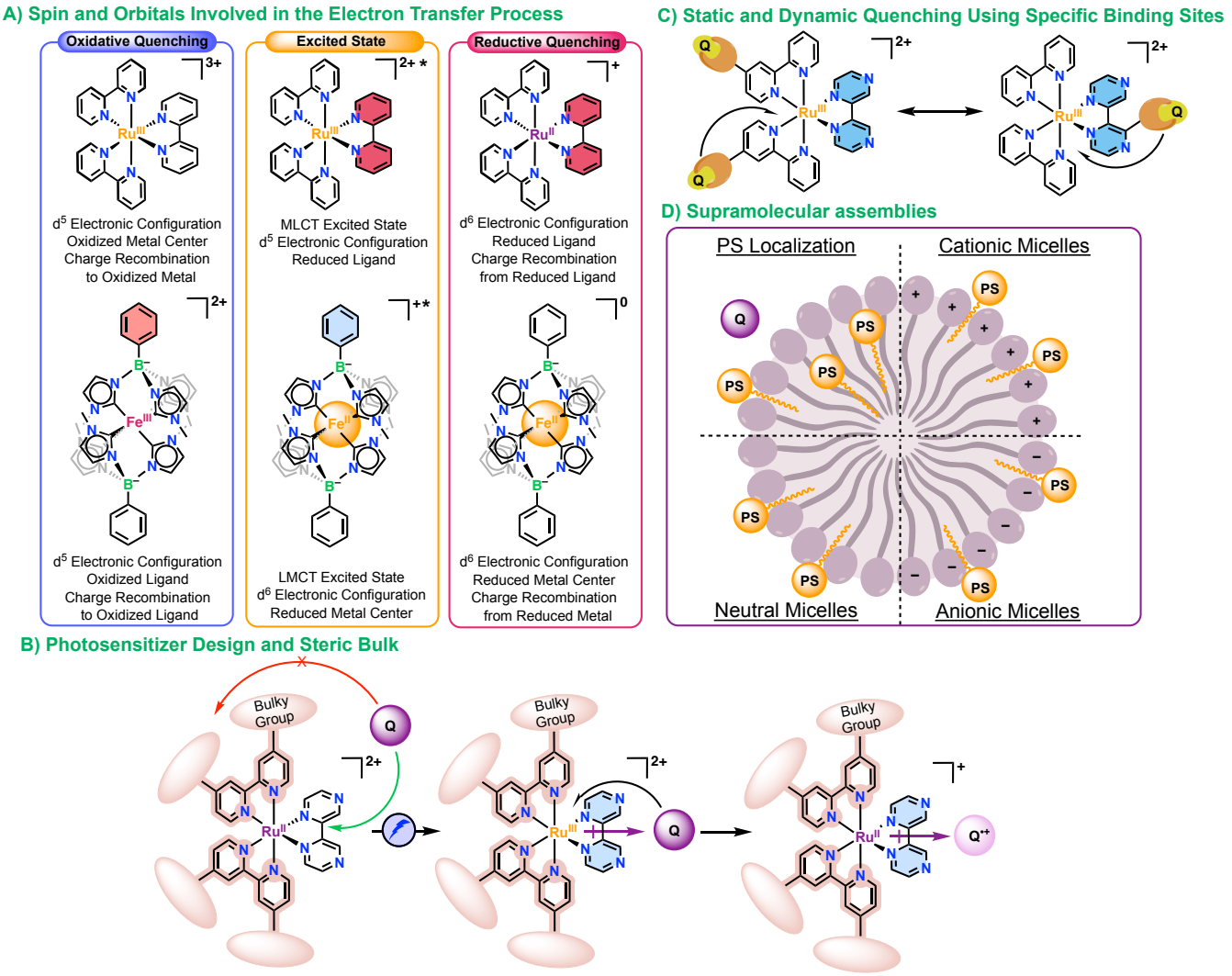

Figure 50. Opportunities for future research in solvent cages and cage escape. A) Spin and molecular orbitals involved in the electron transfer process where both the excited state spin as well as the molecular orbital can impact cage-escape yields. B) Photosensitizer design where the excited-state structure is controlled with sterically bulky groups to control the geometry of the encounter complex cage. C) The impact of static and dynamic quenching on cage escape yields where a specific binding group (orange color) is used to trap the quencher (purple sphere) close to (right) or far from (left) the recombination center. D) Supramolecular assemblies using micelles to control electrostatic repulsion/attraction and impact cage escape.

Spectroscopic techniques and theoretical calculations. Advances in spectroscopic techniques are needed to directly probe the cage(s) formed after diffusional interactions of an excited photosensitizer with a quencher. Electron transfer within these cages, unlike those present after visible light excitation of I_2, have not yet been directly measured. Important questions exist about the electronic coupling and reorganization energy for electron transfer and how they are related to the solvent cage structure(s). The development of new spectroscopic and computational tools that enable visualization of these solvent cages are hence

expected to be of high impact.[194, 497-502] It would be of particular interest to understand why some geminate recombination processes are dependent on the free energy change for electron transfer while others are not.

Spin and orbitals involved in the electron transfer processes. Electron spin has been shown to be a key contributor to cage escape yields.[82, 172, 174, 189, 233, 349-350, 355-356, 365, 368, 372, 439, 503] Triplet states undergo efficient cage-escape while singlet and doublet states do not. The role of spin is more complicated when second- and third-row transition metal inorganic sensitizers are utilized as spin becomes a poor quantum number due to spin orbit coupling by the heavy metal center.

Consider for example the oxidative and reductive quenching of MLCT and LMCT excited states shown in **Figure 50A**. For MLCT excited states, reductive excited-state electron transfer results in larger cage-escape yields than does oxidative quenching regardless of the thermodynamic driving force. At first glance, this seems counterintuitive. Oxidative quenching yields a Ru(III) center in a d^5 electronic configuration whereas reductive electron transfer yields a Ru(II) center with an odd electron on a ligand. Hence geminate recombination after oxidative quenching requires electron tunneling through the diimine ligand(s). On the other hand, after reductive quenching, geminate recombination occurs with the reduced ligand that would reasonably be expected to have stronger coupling and a smaller reorganization barrier for electron transfer; yet the cage escape yield is typically much larger than that measured after oxidative quenching. As detailed in the last section, our present understanding of this behavior is qualitative and attributed to the degree of spin-orbit coupling in the geminate pair. Recombination to the heavy metal center after oxidative quenching has more singlet character than does recombination after reductive quenching where the reduced ligand is involved. The direct quantification of the spin state of the geminate pair would be impactful as would be the value of the singlet-triplet (S-T) energy gap. Computational study of the S-T splitting and spin orbit coupling for the geminate radical pair would thus provide new insight into the cage escape process. The available literature also suggests that photosensitizers with a pendant organic donor that facilitates intramolecular D-B-M_{ox} → D^+-B-M_{red} electron transfer after oxidative quenching would result in higher cage escape yields; studies of this type would also address questions concerning the optimal distance for quantitative cage escape from inorganic photosensitizers.

Based on the known behavior of MLCT excited-state quenching, one would anticipate larger cage escape yields after oxidative quenching of an LMCT excited state relative to reductive quenching. This expectation has not been probed experimentally, in part because long lived LMCT excited states remain relatively rare. In one study of Fe(III) LMCT photosensitizers, high cage escape yields were measured after reductive quenching that increased when the solvent was changed from acetonitrile to dichloromethane.[51,

[429] The origin(s) of this solvent dependency, as well as that after oxidative quenching, remain unclear and may emanate from the spin state, the frontier orbitals, or both. We emphasize again that new spin flip Cr(III) photosenstizers, as well as those based on high spin ligand field states of iron, provide new opportunities to probe the roles of spin that go beyond the traditional singlets and triplets.

Photosensitizer design. Surprisingly, there has been little effort to structurally modify the photosensitizer to enhance cage escape. Sterically bulky groups on two of the diimine ligands of an inorganic photosensitizer could be used to direct the quencher towards the third ligand as is shown generically in **Figure 50B**, for example. For an MLCT excited state with an electron localized on the unhindered ligand, the excited-state dipole could be directed towards the quencher and the impact on cage escape yields could thus be investigated. With the 2,2'-bipyrazine ligand shown and transition metal ion quenchers, the possibility exists for an inner-sphere electron transfer mechanism that may enhance charge separation relative to charge recombination. Careful mechanistic study of a series of photosensitizers with known steric and electronic structures would provide insights into the molecular details of the caged structure.

Static Quenching Processes. Several examples were described in this review wherein static electron transfer in stable ground state photosensitizer-quencher adducts resulted in lower cage escape yields than those formed by diffusional (dynamic) interactions.[96, 311-321, 431] It is not clear that this should always be the case. For example, one could envision an enhanced cage escape with an anionic donor that forms an adduct with the 2,2'-bipyrazine ligand shown in **Figure 50C**. After excited-state electron transfer, the dipole and charge provide an incentive for cage escape. The ability to tune the ground state adduct geometry and the physical location of the quencher can be directly measured by steady state techniques such as NMR spectroscopy. This would have immediate implications in the field of photoredox catalysis, for example, based on the pre-association of the photosensitizer and the quencher.

Supramolecular assemblies and local environment. As covalent chemistry and photosensitizer design can be used to tune the structure of the encounter complex, so too can non-covalent interactions. Control of the local photosensitizer-quencher environment could provide valuable insight into the cage escape process and some of the unusual solvent dependencies that have been reported. Functional groups present on the photosensitizer that are competent of hydrogen bonding, π-stacking, and/or a cationic/anionic charge may tune cage escape yields in a rational manner. An avenue that deserves further investigation is the supramolecular assembly of photosensitizers within micelles or liposomes, **Figure 50D**.[7, 404-405, 411] Such supramolecular assemblies provide unique opportunities for vectoral electron transfer that provides the

physical separation of the redox products and hence enhanced cage escape. In addition, local charges on the micelles or liposomes prove useful platforms for the study of coulombic attraction/repulsion on cage escape processes.

Author Information

Corresponding Author

E-mail: Ludovic.Troian@uclouvain.be

E-mail: gjmeyer@email.unc.edu

Orcid

Matthew J. Goodwin: 0000-0002-4790-3501

John C. Dickenson: 0000-0002-7788-6810

Alexia Ripak : 0000-0002-1532-5129

Alexander M. Deetz: 0000-0003-4324-0584

Jackson S. McCarthy: 0000-0002-2908-1823

G. J. Meyer: 0000-0002-4227-6393

L. Troian-Gautier: 0000-0002-7690-1361

Notes

The authors declare no competing financial interest.

Biographies

Matthew J. Goodwin received his B.S. (2021) from the College of William and Mary where he researched the amplification of energy transfer processes using organic fluorophores and conjugated polymer nanoparticles under the supervision and guidance of Dr. Elizabeth Harbron. He then began and is currently working on his doctoral research at the University of North Carolina at Chapel Hill studying halide photoredox chemistry and the optimization of cage escape yields under the supervision and guidance of Dr. Gerald Meyer.

John C. Dickenson received his B.S. (2020) from the Virginia Military Institute where he studied the electrochemical properties of homoleptic terpyridine complexes of cobalt and other first-row transition metals in relation to the carbon dioxide reduction reaction, under the supervision and mentorship of Dr. Daniel Harrison. He then began work on his PhD at the University of North Carolina at Chapel Hill under

Dr. Gerald J. Meyer, pursuing renewable energy research through the study of halide oxidation and nanosecond charge-carrier dynamics at silicon-based hybrid photoelectrodes.

Alexia Ripak received her B.S. (2019) and M.S. (2021) in chemistry from the Université Catholique de Louvain (UCLouvain – Belgium). She then secured a FRIA grant from the Belgian National Funds for Scientific Research (F.R.S.-FNRS) to pursue her PhD at UCLouvain under the supervision of Prof. B. Elias and Prof. L. Troian-Gautier. She is dedicating her research to the development of photoactive iron(III) complexes and the study of key factors influencing cage-escape yields using transition metal-based and organic photosensitizers.

Alexander M. Deetz received his B.A. (2015) from Carleton College where he studied metal–ligand cooperativity for small molecule activation under Dr. Matt Whited. Zander then began his graduate studies at Harvard University in the laboratory of Dr. Dan Nocera where he examined systems for HX splitting using photocrystallography. After receiving his Masters, Zander traded Ivy for grapevines and moved to Napa Valley to work in the wine industry. In 2018, he returned to chemistry at the University of North Carolina at Chapel Hill to join the lab of Dr. Gerald Meyer where he received his PhD in 2023 studying light-initiated halide oxidation. Zander is now a Scientist at Procter & Gamble studying the interactions of biodegradable polymers and sustainably-produced surfactants for next generation beauty care products.

Jackson S. McCarthy received his B.S. (2020) from Furman University where he studied organometallic synthesis of titanocene based photosensitizers under the supervision of Dr. Paul Wagenknecht. After graduating, he worked briefly in the custom chemical manufacturing industry at Ortec INC, before returning to Furman University, where he studied the effects of molecular and matrix rigidity on the luminescence efficiency and chromaticity in platinum-based phosphors. Jackson joined the Meyer Lab in December of 2022 and is currently studying the conditions that impact cage escape yields in photoredox reactions involving ruthenium polypyridyl complexes.

Gerald J. Meyer received his B.S. in chemistry and mathematics from SUNY-Albany and a Ph.D. from the University of Wisconsin at Madison. After 20 years as a Professor of Chemistry and Materials Science and Engineering at Johns Hopkins University, he is currently a Professor of Chemistry at UNC and Director of the Center for Hybrid Approaches in Solar Energy to Liquid Fuels (CHASE). His interests include photocatalysis and photoelectrochemistry of inorganic coordination complexes and inorganic materials.

Ludovic Troian-Gautier received his B.S. (2008), M.S (2010) and Ph.D. in chemistry (2014) from the Université libre de Bruxelles (ULB – Belgium) under the supervision of Pr. C. Moucheron and guidance of Pr. A. Kirsch-De Mesmaeker. He undertook post-doctoral research at X4C, a new start-up, under the

supervision of Pr. I. Jabin and Dr. A. Mattiuzzi where he worked on surface modification using calix[4]arene derivatives. Between 2015 and 2019, he performed research within the Alliance for Molecular PhotoElectrode Design for Solar Fuels directed by Prof. G. J. Meyer at UNC-Chapel Hill. In May 2019, he started a Chargé de Recherches position (F.R.S.-FNRS) at ULB and, in October 2022, he was promoted to Chercheur Qualifié F.R.S.-FNRS at UCLouvain where he pursues his research endeavors on mechanistic photoredox catalysis and energy related challenges.

Acknowledgments

M.J.G., J.S.M., A.M.D., and G.J.M. acknowledge support from the National Science Foundation for support of this work, NSF 2247589. L.T.-G. is a Chercheur Qualifié of the Fonds de la Recherche Scientifique – FNRS. L.T.-G. acknowledges the support from the "Action de Recherche Concertée" through the project "UNCAGED" under grant no. 23/28-135. A. R. thanks the Belgian National Funds for Scientific Research (F.R.S.-FNRS) for their Fund for Research Training in Industry and Agriculture (FRIA) PhD grant. A.R. and L.T.-G. gratefully acknowledge the UCLouvain for financial support. J.C.D. acknowledges the support of the Department of Defense (DoD) through the from the National Defense Science & Engineering Graduate (NDSEG) Fellowship Program.

6) Appendices - Tables

6.1) Tabulated values for the cage-escape yields of anthracene and acridinium derivatives

Table 11 gathers the cage-escape yields of anthracene and acridinium derivatives with several quenchers and solvents. Electron transfer quenching sensitized by anthracene and acridinium derivatives occur primarily from singlet and triplet states. For a specific excited state description, see relevant reference(s).

Table 11. Cage-escape yields (ϕ_{ce}) of anthracene and acridinium derivatives.

Entry	Photosensitizer	Quencher	Solvent	ϕ_{ce}	Ref
1	2,6,9,10-tetracyanoanthracene	1,2,3-trimethoxybenzene	CH_2Cl_2	0.0014	[324]
2	2,6,9,10-tetracyanoanthracene	1,2,3,4-tetramethylbenzene	CH_3CN	0.042	[316]
3	2,6,9,10-tetracyanoanthracene	1,2,3,5-tetramethylbenzene	CH_3CN	0.041	[316]
4	2,6,9,10-tetracyanoanthracene	1,2,4-trimethoxybenzene	CH_2Cl_2	0.0017	[324]

5	2,6,9,10-tetracyanoanthracene	1,2,4-trimethylbenzene	CH_3CN	0.055	316
6	2,6,9,10-tetracyanoanthracene	1,4-bis(1-pyrrolidinyl)benzene	CH_3CN	0.042	330
7	2,6,9,10-tetracyanoanthracene	1,4-phenylendiamine	CH_2Cl_2	0.0055	324
8	2,6,9,10-tetracyanoanthracene	1,4-phenylendiamine	CH_3CN	0.075	324
9	2,6,9,10-tetracyanoanthracene	2-methylnaphthalene	CH_3CN	0.072	316
10	2,6,9,10-tetracyanoanthracene	2-methylphenanthrene	CH_3CN	0.120	316
11	2,6,9,10-tetracyanoanthracene	2,6-dimethylnaphthalene	CH_3CN	0.059	316
12	2,6,9,10-tetracyanoanthracene	3,3'-dimethylbiphenyl	CH_3CN	0.15	316
13	2,6,9,10-tetracyanoanthracene	3,6-dimethylphenanthrene	CH_3CN	0.062	316
14	2,6,9,10-tetracyanoanthracene	4-cyanoaniline	CH_2Cl_2	0.0019	324
15	2,6,9,10-tetracyanoanthracene	4-cyanoaniline	CH_3CN	0.0061	330
16	2,6,9,10-tetracyanoanthracene	4-cyanoaniline	CH_3CN	0.0085	324
17	2,6,9,10-tetracyanoanthracene	4,4'-dimethylbiphenyl	CH_3CN	0.066	316
18	2,6,9,10-tetracyanoanthracene	5,8-dimethyltetrahydronaphthalene	CH_3CN	0.04	316
19	2,6,9,10-tetracyanoanthracene	aniline	CH_3CN	0.0093	330
20	2,6,9,10-tetracyanoanthracene	aniline	CH_3CN	0.021	324
21	2,6,9,10-tetracyanoanthracene	anisidine	CH_2Cl_2	0.0020	324
22	2,6,9,10-tetracyanoanthracene	anisidine	CH_3CN	0.054	324
23	2,6,9,10-tetracyanoanthracene	biphenyl	CH_3CN	0.24	316
24	2,6,9,10-tetracyanoanthracene	BPB	CH_3CN	0.042	324
25	2,6,9,10-tetracyanoanthracene	*cis*-4-chlorostilbene	CH_3CN	0.029	317
26	2,6,9,10-tetracyanoanthracene	*cis*-4-cyanostilbene	CH_3CN	0.054	317
27	2,6,9,10-tetracyanoanthracene	*cis*-4-methoxy-stilbene	CH_3CN	0.023	317
28	2,6,9,10-tetracyanoanthracene	*cis*-4-methylstilbene	CH_3CN	0.019	317
29	2,6,9,10-tetracyanoanthracene	*cis*-4,4'-dimethylstilbene	CH_3CN	0.022	317
30	2,6,9,10-tetracyanoanthracene	*cis*-stilbene	CH_3CN	0.027	317
31	2,6,9,10-tetracyanoanthracene	durene	CH_3CN	0.041	316
32	2,6,9,10-tetracyanoanthracene	fluorene	CH_3CN	0.083	316
33	2,6,9,10-tetracyanoanthracene	hexamethylbenzene	CH_2Cl_2	0.0041	324
34	2,6,9,10-tetracyanoanthracene	hexamethylbenzene	CH_3CN	0.031	316
35	2,6,9,10-tetracyanoanthracene	*m*-xylene	CH_3CN	0.126	316
36	2,6,9,10-tetracyanoanthracene	mesitylene	CH_3CN	0.093	316
37	2,6,9,10-tetracyanoanthracene	N,N,N',N'-tetramethyl-1,4-phenylenediamine	CH_2Cl_2	0.015	324
38	2,6,9,10-tetracyanoanthracene	N,N,N',N'-tetramethyl-1,4-phenylenediamine	CH_3CN	0.082	330
39	2,6,9,10-tetracyanoanthracene	N,N,N',N'-tetramethyl-1,4-phenylenediamine	CH_3CN	0.086	324
40	2,6,9,10-tetracyanoanthracene	naphthalene	CH_3CN	0.12	316
41	2,6,9,10-tetracyanoanthracene	*o*-xylene	CH_3CN	0.122	316
42	2,6,9,10-tetracyanoanthracene	octahydroanthracene	CH_3CN	0.034	316
43	2,6,9,10-tetracyanoanthracene	octahydrophenanthrene	CH_3CN	0.037	316
44	2,6,9,10-tetracyanoanthracene	*p*-xylene	CH_3CN	0.077	316
45	2,6,9,10-tetracyanoanthracene	pentamethylbenzene	CH_3CN	0.035	316
46	2,6,9,10-tetracyanoanthracene	phenanthrene	CH_3CN	0.156	316
47	2,6,9,10-tetracyanoanthracene	tetracyanoethylene	CH_3CN	0.012	325

48	2,6,9,10-tetracyanoanthracene	*trans*-4-chlorostilbene	CH_3CN	0.057	317
49	2,6,9,10-tetracyanoanthracene	*trans*-4-cyanostilbene	CH_3CN	0.11	317
50	2,6,9,10-tetracyanoanthracene	*trans*-4-methoxy-stilbene	CH_3CN	0.029	317
51	2,6,9,10-tetracyanoanthracene	*trans*-4-methylstilbene	CH_3CN	0.048	317
52	2,6,9,10-tetracyanoanthracene	*trans*-4,4'-dimethylstilbene	CH_3CN	0.043	317
53	2,6,9,10-tetracyanoanthracene	*trans*-stilbene	CH_3CN	0.053	317
54	2,9,10-tricyanoanthracene	1,4-phenylenediamine	CH_3CN	0.044	324
55	2,9,10-tricyanoanthracene	4-cyanoaniline	CH_3CN	0.008	330
56	2,9,10-tricyanoanthracene	4-cyanoaniline	CH_3CN	0.008	324
57	2,9,10-tricyanoanthracene	aniline	CH_3CN	0.0069	330
58	2,9,10-tricyanoanthracene	aniline	CH_3CN	0.0072	324
59	2,9,10-tricyanoanthracene	anisidine	CH_3CN	0.017	324
60	2,9,10-tricyanoanthracene	N,N,N',N'-tetramethyl-1,4-phenylenediamine	CH_3CN	0.06	330
61	2,9,10-tricyanoanthracene	N,N,N',N'-tetramethyl-1,4-phenylenediamine	CH_3CN	0.06	324
62	2,9,10-tricyanoanthracene	tetracyanoethylene	CH_3CN	0.013	325
63	3,9-dicyanophenanthrene	benzyl viologen	CH_3OH	0.500	504
64	3,9-dicyanophenanthrene	methyl viologen	CH_3OH	0.320	504
65	3AcrCOO)*	4-bromophenol	0.1M $NaHCO_3$(aq)	0.32	505
66	3AcrCOO)*	4-chlorophenol	0.1M $NaHCO_3$(aq)	0.76	505
67	3AcrCOO)*	4-hydroxybenzoic acid	0.1M $NaHCO_3$(aq)	0.82	505
68	9-Br-anthracene	methyl viologen	0.1M $TEAClO_4$ $(CH_3CN)/CH_2Cl_2$ 8/5	0.74	82
69	9-Br-anthracene	methyl viologen	0.1M $TEAClO_4$ $(CH_3CN)/CH_3I$ 8/5	0.3	82
70	9-cyanoanthracene	1,4-diazabicyclo[2.2.2]octane (DABCO)	CH_3CN	<0.08	163
71	9-cyanoanthracene	1,4-phenylendiamine	CH_3CN	0.0078	324
72	9-cyanoanthracene	4-cyanoaniline	CH_3CN	0.032	330
73	9-cyanoanthracene	4-cyanoaniline	CH_3CN	0.12	324
74	9-cyanoanthracene	aniline	CH_3CN	0.12	330
75	9-cyanoanthracene	aniline	CH_3CN	0.021	324
76	9-cyanoanthracene	anisidine	CH_3CN	0.007	324
77	9-cyanoanthracene	benzyl viologen	CH_3OH	0.042	504
78	9-cyanoanthracene	methyl viologen	CH_3OH	0.071	504
79	9-cyanoanthracene	N,N-dimethylaniline	CH_3CN	<0.08	163
80	9-cyanoanthracene	N,N,N',N'-tetramethyl-1,4-phenylenediamine	CH_3CN	<0.01	330
81	9-cyanoanthracene	N,N,N',N'-tetramethyl-1,4-phenylenediamine	CH_3CN	0.02	324
82	9-cyanoanthrance	*trans*-stilbene	CH_3CN	0.71	317
83	9-Me-anthracene	methyl viologen	0.1M $TEAClO_4$ $(CH_3CN)/CH_2Cl_2$ 8/5	1	82
84	9-Me-anthracene	methyl viologen	0.1M $TEAClO_4$ $(CH_3CN)/CH_3I$ 8/5	0.7	82

85	9,10-dicyanoanthracene	(2*E*,4*E*)-2,4-hexadiene	CH_3CN	0.027	[323]
86	9,10-dicyanoanthracene	1-azabicyclo[2.2.2]octane (ABCO)	CH_3CN	<0.007	[323]
87	9,10-dicyanoanthracene	1-methylcyclohexene	CH_3CN	0.01	[323]
88	9,10-dicyanoanthracene	1,2,3-trimethoxybenzene	CH_3CN	0.008	[323]
89	9,10-dicyanoanthracene	1,2,3,4-tetramethylenzene	CH_3CN	0.28	[316]
90	9,10-dicyanoanthracene	1,2,3,5-tetramethylbenzene	CH_3CN	0.274	[316]
91	9,10-dicyanoanthracene	1,2,4-trimethoxybenzene	CH_2Cl_2	0.0020	[324]
92	9,10-dicyanoanthracene	1,2,4-trimethoxybenzene	CH_3CN	0.016	[323]
93	9,10-dicyanoanthracene	1,2,4-trimethylbenzene	CH_3CN	0.392	[316]
94	9,10-dicyanoanthracene	1,2,4,5-tetra-*iso*-propylbenzene	1,2-dichlorobenzene	0.026	[322]
95	9,10-dicyanoanthracene	1,2,4,5-tetra-*iso*-propylbenzene	Butyronitrile	0.69	[322]
96	9,10-dicyanoanthracene	1,2,4,5-tetra-*iso*-propylbenzene	CH_2Cl_2	0.23	[322]
97	9,10-dicyanoanthracene	1,2,4,5-tetra-*iso*-propylbenzene	CH_3CN	0.51	[322]
98	9,10-dicyanoanthracene	1,2,4,5-tetra-*iso*-propylbenzene	THF	0.046	[322]
99	9,10-dicyanoanthracene	1,3,5-trimethoxybenzene	CH_3CN	0.032	[323]
100	9,10-dicyanoanthracene	1,4-diazabicyclo[2.2.2]octane (DABCO)	CH_3CN	<0.05	[163]
101	9,10-dicyanoanthracene	1,4-diazabicyclo[2.2.2]octane (DABCO)	CH_3CN	0.024	[323]
102	9,10-dicyanoanthracene	1,4-dimethoxybenzene	CH_3CN	0.02	[323]
103	9,10-dicyanoanthracene	1,4-diphenylbutadiyne	CH_3CN	0.25	[323]
104	9,10-dicyanoanthracene	1,4-phenylendiamine	CH_2Cl_2	0.0008	[324]
105	9,10-dicyanoanthracene	1,4-phenylendiamine	CH_3CN	0.034	[324]
106	9,10-dicyanoanthracene	2-butylamine	CH_3CN	<0.012	[323]
107	9,10-dicyanoanthracene	2-methoxyethylamine	CH_3CN	<0.01	[323]
108	9,10-dicyanoanthracene	2-methoxynaphthalene	CH_3CN	0.057	[323]
109	9,10-dicyanoanthracene	2-methylbut-2-ene	CH_3CN	0.012	[323]
110	9,10-dicyanoanthracene	2-methylbuta-1,3-diene	CH_3CN	0.043	[323]
111	9,10-dicyanoanthracene	2-methylnaphthalene	CH_3CN	0.37	[316]
112	9,10-dicyanoanthracene	2-methylphenanthrene	CH_3CN	0.56	[316]
113	9,10-dicyanoanthracene	2,3-dimethylbut-2-ene	CH_3CN	<0.007	[323]
114	9,10-dicyanoanthracene	2,3-dimethylbuta-1,3-diene	CH_3CN	0.046	[323]
115	9,10-dicyanoanthracene	2,4-dimethoxy-N,N-dimethylaniline	CH_3CN	0.004	[323]
116	9,10-dicyanoanthracene	2,5-dimethylhexa-2,4-diene	CH_3CN	0.017	[323]
117	9,10-dicyanoanthracene	2,6-dimethylnaphthalene	CH_3CN	0.32	[316]
118	9,10-dicyanoanthracene	3,3'-dimethylbiphenyl	CH_3CN	0.062	[316]
119	9,10-dicyanoanthracene	3,4-dimethoxy-N,N-dimethylaniline	CH_3CN	0.004	[323]
120	9,10-dicyanoanthracene	3,6-dimethylphenanthrene	CH_3CN	0.32	[316]
121	9,10-dicyanoanthracene	4-bromo-N,N-dimethylaniline	CH_3CN	0.01	[309]
122	9,10-dicyanoanthracene	4-bromoaniline	CH_3CN	0.005	[309]
123	9,10-dicyanoanthracene	4-bromonisole	CH_3CN	0.016	[309]
124	9,10-dicyanoanthracene	4-chloro-N,N-dimethylaniline	CH_3CN	0.011	[309]
125	9,10-dicyanoanthracene	4-chloroaniline	CH_3CN	0.004	[309]
126	9,10-dicyanoanthracene	4-chloroanisole	CH_3CN	0.071	[309]

127	9,10-dicyanoanthracene	4-cyanoaniline	CH_2Cl_2	0.0054	324
128	9,10-dicyanoanthracene	4-cyanoaniline	CH_3CN	0.012	330
129	9,10-dicyanoanthracene	4-cyanoaniline	CH_3CN	0.012	324
130	9,10-dicyanoanthracene	4-iodo-N,N-dimethylaniline	CH_3CN	0.018	309
131	9,10-dicyanoanthracene	4-iodoaniline	CH_3CN	0.006	309
132	9,10-dicyanoanthracene	4-iodoanisole	CH_3CN	0.006	309
133	9,10-dicyanoanthracene	4-methylpenta-1,3-diene	CH_3CN	0.023	323
134	9,10-dicyanoanthracene	4,4'-dimethylbiphenyl	CH_3CN	0.37	316
135	9,10-dicyanoanthracene	5,8-dimethyltetrahydronaphthalene	CH_3CN	0.248	316
136	9,10-dicyanoanthracene	aniline	CH_3CN	0.003	330
137	9,10-dicyanoanthracene	aniline	CH_3CN	0.003	324
138	9,10-dicyanoanthracene	aniline	CH_3CN	0.003	309
139	9,10-dicyanoanthracene	aniline	CH_3CN	0.012	323
140	9,10-dicyanoanthracene	anisidine	CH_3CN	0.016	324
141	9,10-dicyanoanthracene	anisole	CH_3CN	0.055	324
142	9,10-dicyanoanthracene	anisole	CH_3CN	0.055	309
143	9,10-dicyanoanthracene	anisole	CH_3CN	0.11	323
144	9,10-dicyanoanthracene	benzyl viologen	CH_3OH	0.071	504
145	9,10-dicyanoanthracene	benzylamine	CH_3CN	0.008	323
146	9,10-dicyanoanthracene	biphenyl	CH_3CN	0.83	316
147	9,10-dicyanoanthracene	biphenyl	CH_3CN	0.41	323
148	9,10-dicyanoanthracene	*cis*-4-chlorostilbene	CH_3CN	0.019	317
149	9,10-dicyanoanthracene	*cis*-4-cyanostilbene	CH_3CN	0.39	317
150	9,10-dicyanoanthracene	*cis*-4-methoxy-stilbene	CH_3CN	0.032	317
151	9,10-dicyanoanthracene	*cis*-4-methylstilbene	CH_3CN	0.077	317
152	9,10-dicyanoanthracene	*cis*-4,4'-dimethylstilbene	CH_3CN	0.048	317
153	9,10-dicyanoanthracene	*cis*-stilbene	CH_3CN	0.14	317
154	9,10-dicyanoanthracene	cyclohexa-1,4-diene	CH_3CN	0.06	323
155	9,10-dicyanoanthracene	cycloocta-1,3-diene	CH_3CN	0.036	323
156	9,10-dicyanoanthracene	diethylamine	CH_3CN	0.0055	323
157	9,10-dicyanoanthracene	durene	1,2-dichlorobenzene	0.0014	322
158	9,10-dicyanoanthracene	durene	Butyronitrile	0.22	322
159	9,10-dicyanoanthracene	durene	CH_2Cl_2	0.0043	322
160	9,10-dicyanoanthracene	durene	CH_3CN	0.239	316
161	9,10-dicyanoanthracene	durene	CH_3CN	0.16	323
162	9,10-dicyanoanthracene	durene	CH_3CN	0.19	322
163	9,10-dicyanoanthracene	durene	THF	0.0034	322
164	9,10-dicyanoanthracene	fluorene	CH_3CN	0.49	316
165	9,10-dicyanoanthracene	fluorene	CH_3CN	0.194	323
166	9,10-dicyanoanthracene	hexaethylbenzene	1,2-dichlorobenzene	0.083	322
167	9,10-dicyanoanthracene	hexaethylbenzene	Butyronitrile	0.34	322
168	9,10-dicyanoanthracene	hexaethylbenzene	CH_2Cl_2	0.14	322

169	9,10-dicyanoanthracene	hexaethylbenzene	CH_3CN	0.33	322
170	9,10-dicyanoanthracene	hexaethylbenzene	THF	0.063	322
171	9,10-dicyanoanthracene	hexamethylbenzene	1,2-dichlorobenzene	0.0022	322
172	9,10-dicyanoanthracene	hexamethylbenzene	Butyronitrile	0.072	322
173	9,10-dicyanoanthracene	hexamethylbenzene	CH_2Cl_2	0.0048	322
174	9,10-dicyanoanthracene	hexamethylbenzene	CH_3CN	0.078	316
175	9,10-dicyanoanthracene	hexamethylbenzene	CH_3CN	0.079	322
176	9,10-dicyanoanthracene	hexamethylbenzene	THF	0.011	322
177	9,10-dicyanoanthracene	mesitylene	CH_3CN	0.21	323
178	9,10-dicyanoanthracene	methyl viologen	CH_3OH	0.079	504
179	9,10-dicyanoanthracene	*n*-butylamine	CH_3CN	0.012	323
180	9,10-dicyanoanthracene	N-methylaniline	CH_3CN	0.02	323
181	9,10-dicyanoanthracene	N,N-dimethylaniline	CH_3CN	0.01	324
182	9,10-dicyanoanthracene	N,N-dimethylaniline	CH_3CN	<0.05	163
183	9,10-dicyanoanthracene	N,N-dimethylaniline	CH_3CN	0.01	309
184	9,10-dicyanoanthracene	N,N-dimethylaniline	CH_3CN	0.01	323
185	9,10-dicyanoanthracene	N,N-dimethylaniline	CH_3CN	0.01	323
186	9,10-dicyanoanthracene	N,N,N',N'-tetramethyl-1,4-phenylenediamine	CH_3CN	0.026	330
187	9,10-dicyanoanthracene	N,N,N',N'-tetramethyl-1,4-phenylenediamine	CH_3CN	0.029	324
188	9,10-dicyanoanthracene	N,N,N',N'-tetramethyl-1,4-phenylenediamine	CH_3CN	0.008	323
189	9,10-dicyanoanthracene	naphthalene	CH_3CN	0.58	316
190	9,10-dicyanoanthracene	naphthalene	CH_3CN	0.12	323
191	9,10-dicyanoanthracene	octahydroanthracene	CH_3CN	0.203	316
192	9,10-dicyanoanthracene	octahydrophenanthrene	CH_3CN	0.209	316
193	9,10-dicyanoanthracene	*p*-terphenyl	CH_3CN	>0.22	323
194	9,10-dicyanoanthracene	*p*-xylene	CH_3CN	0.33	323
195	9,10-dicyanoanthracene	pentamethylbenzene	CH_3CN	0.154	316
196	9,10-dicyanoanthracene	phenanthrene	CH_3CN	0.62	316
197	9,10-dicyanoanthracene	pyridine	CH_3CN	<0.007	323
198	9,10-dicyanoanthracene	tetracyanoethylene	CH_3CN	0.016	325
199	9,10-dicyanoanthracene	*trans*-4-chlorostilbene	CH_3CN	0.27	317
200	9,10-dicyanoanthracene	*trans*-4-cyanostilbene	CH_3CN	0.53	317
201	9,10-dicyanoanthracene	*trans*-4-methoxy-stilbene	CH_3CN	0.052	317
202	9,10-dicyanoanthracene	*trans*-4-methylstilbene	CH_3CN	0.14	317
203	9,10-dicyanoanthracene	*trans*-4-trifluoromethylstilbene	CH_3CN	0.48	317
204	9,10-dicyanoanthracene	*trans*-4,4'-dimethylstilbene	CH_3CN	0.095	317
205	9,10-dicyanoanthracene	*trans*-α-methylstilbene	CH_3CN	0.11	323
206	9,10-dicyanoanthracene	*trans*-stilbene	CH_3CN	0.26	317
207	9,10-dicyanoanthracene	*trans*-stilbene	CH_3CN	0.12	323
208	9,10-dicyanoanthracene	triethylamine	CH_3CN	0.004	323
209	9,10-dimethoxyanthracene	benzyl viologen	CH_3OH	0.160	504
210	9,10-dimethoxyanthracene	methyl viologen	CH_3OH	0.280	504

211	9,10-dimethylanthracene	benzyl viologen	CH_3OH	0.096	[504]
212	9,10-dimethylanthracene	methyl viologen	CH_3OH	0.220	[504]
213	9,10-diphenylanthracene	benzyl viologen	CH_3OH	0.060	[504]
214	9,10-diphenylanthracene	methyl viologen	CH_3OH	0.140	[504]
215	9,10-diphenylanthracene	tetracyanoethylene	CH_3CN	0.062	[325]
216	9,10-diphenylanthracene	*trans*-1,2-dicyanoethylene	CH_3CN	0.047	[325]
217	a,h-dibenzanthracene	*m*-dicyanobenzene	CH_3CN	0.65	[327]
218	a,h-dibenzanthracene	*m*-dinitrobenzene	CH_3CN	0.05	[394]
219	a,h-dibenzanthracene	*m*-dinitrobenzene	MeOH	0.5	[394]
220	a,h-dibenzanthracene	*m*-nitrobenzene	CH_3CN	0.05	[394]
221	a,h-dibenzanthracene	*m*-nitrobenzene	MeOH	0.5	[394]
222	a,h-dibenzanthracene	*p*-chloronitrobenzene	CH_3CN	0.1	[394]
223	a,h-dibenzanthracene	*p*-chloronitrobenzene	MeOH	0.6	[394]
224	a,h-dibenzanthracene	*p*-dicyanobenzene	CH_3CN	1	[327]
225	a,h-dibenzanthracene	*p*-nitrobenzaldehyde	CH_3CN	0.1	[394]
226	a,h-dibenzanthracene	*p*-nitrobenzaldehyde	MeOH	0.6	[394]
227	Acriflavine	4-bromoaniline	CH_3CN	0.7	[308]
228	Acriflavine	4-chloroaniline	CH_3CN	0.78	[308]
229	Acriflavine	4-iodoaniline	CH_3CN	0.49	[308]
230	Acriflavine	aniline	CH_3CN	0.82	[308]
231	N-methylacridinium	1-bromo-2,3-dimethylbenzene	CH_3CN	0.19	[504]
232	N-methylacridinium	1,2-dimethoxybenzene	CH_3CN	0.0062	[504]
233	N-methylacridinium	1,2,3,4-tetramethylbenzene	CH_3CN	0.054	[315]
234	N-methylacridinium	1,2,3,5-tetramethylbenzene	CH_3CN	0.049	[315]
235	N-methylacridinium	1,2,4-trimethoxybenzene	CH_3CN	0.013	[504]
236	N-methylacridinium	1,2,4-trimethylbenzene	CH_3CN	0.084	[315]
237	N-methylacridinium	1,3,5-trimethylbenzene	CH_3CN	0.19	[504]
238	N-methylacridinium	1,4-dimethoxybenzene	CH_3CN	0.0096	[504]
239	N-methylacridinium	1,4-dimethyltetrahydronaphthalene	CH_3CN	0.051	[315]
240	N-methylacridinium	1,4-phenylenediamine	CH_3CN	0.45	[504]
241	N-methylacridinium	4-bromo-N,N-dimethylaniline	CH_3CN	0.070	[504]
242	N-methylacridinium	4-bromoanisole	CH_3CN	0.035	[504]
243	N-methylacridinium	4-bromobiphenyl	CH_3CN	0.20	[504]
244	N-methylacridinium	4-bromotoluene	CH_3CN	0.22	[504]
245	N-methylacridinium	4-cyanoaniline	CH_3CN	0.010	[504]
246	N-methylacridinium	aniline	CH_3CN	0.013	[504]
247	N-methylacridinium	anisidine	CH_3CN	0.065	[504]
248	N-methylacridinium	anisole	CH_3CN	0.035	[504]
249	N-methylacridinium	biphenyl	CH_3CN	0.10	[504]
250	N-methylacridinium	*cis*-stilbene	CH_3CN	0.023	[317]
251	N-methylacridinium	diphenylamine	CH_3CN	0.058	[504]
252	N-methylacridinium	durene	CH_3CN	0.042	[315]
253	N-methylacridinium	hexamethylbenzene	CH_3CN	0.031	[315]

254	N-methylacridinium	hexamethylbenzene	CH_3CN	0.021	[504]
255	N-methylacridinium	*m*-xylene	CH_3CN	0.27	[315]
256	N-methylacridinium	mesitylene	CH_3CN	0.19	[315]
257	N-methylacridinium	N,N-dimethylaniline	CH_3CN	0.038	[504]
258	N-methylacridinium	N,N,N',N'-tetramethyl-1,4-phenylenediamine	CH_3CN	0.24	[504]
259	N-methylacridinium	*o*-xylene	CH_3CN	0.27	[315]
260	N-methylacridinium	*o*-xylene	CH_3CN	0.27	[504]
261	N-methylacridinium	octahydroanthracene	CH_3CN	0.039	[315]
262	N-methylacridinium	octahydrophenanthrene	CH_3CN	0.044	[315]
263	N-methylacridinium	*p*-xylene	CH_3CN	0.16	[315]
264	N-methylacridinium	*p*-xylene	CH_3CN	0.094	[504]
265	N-methylacridinium	pentamethylbenzene	CH_3CN	0.037	[315]
266	N-methylacridinium	*trans*-stilbene	CH_3CN	0.054	[317]
267	perylene	benzyl viologen	CH_3OH	0.12	[504]

6.2) Tabulated values for the cage-escape yields of 1,2,4,5-tetracyanobenzene

Table 12 gathers the cage-escape yields of 1,2,4,5-tetracyanobenzene with several quenchers and solvents. Electron transfer quenching sensitized by 1,2,4,5-tetracyanobenzene occur primarily from triplet states. For a specific excited state description, see relevant reference(s).

Table 12. Cage-escape yields (ϕ_{ce}) of 1,2,4,5-tetracyanobenzene.

Entry	Photosensitizer	Quencher	Solvent	ϕ_{ce}	Ref
1	1,2,4,5-tetracyanobenzene	benzene	1-methylethylalcohol	0.014	[334]
2	1,2,4,5-tetracyanobenzene	benzene	1,2-dichloroethane	0.003	[334]
3	1,2,4,5-tetracyanobenzene	benzene	benzene/ CH_3CN 30/70	0.92	[340]
4	1,2,4,5-tetracyanobenzene	benzene	benzene/ CH_3CN 40/60	0.86	[340]
5	1,2,4,5-tetracyanobenzene	benzene	benzene/ CH_3CN 50/50	0.6	[340]
6	1,2,4,5-tetracyanobenzene	benzene	benzene/ CH_3CN 60/40	0.51	[340]
7	1,2,4,5-tetracyanobenzene	benzene	benzene/ CH_3CN 70/30	0.19	[340]
8	1,2,4,5-tetracyanobenzene	benzene	benzene/ CH_3CN 80/20	0.07	[340]
9	1,2,4,5-tetracyanobenzene	benzene	benzene/CH_3CN 100/0	0	[340]
10	1,2,4,5-tetracyanobenzene	benzene	CH_3CN	0.1	[334]
11	1,2,4,5-tetracyanobenzene	naphthalene	1,2-dichloroethane	0.024	[334]
12	1,2,4,5-tetracyanobenzene	naphthalene	butyronitrile	0.031	[334]
13	1,2,4,5-tetracyanobenzene	naphthalene	CH_3CN	0.053	[334]
14	1,2,4,5-tetracyanobenzene	naphthalene	diethylether	0.001	[334]
15	1,2,4,5-tetracyanobenzene	toluene	1,1,2,2-tetrachloroethane	0.05	[334]
16	1,2,4,5-tetracyanobenzene	toluene	1,2-dichloroethane	0.11	[334]
17	1,2,4,5-tetracyanobenzene	toluene	1,2-dichloroethane	0.003	[334]
18	1,2,4,5-tetracyanobenzene	toluene	acetone	0.26	[334]

19	1,2,4,5-tetracyanobenzene	toluene	acetone	0.019	[334]
20	1,2,4,5-tetracyanobenzene	toluene	CH_2Cl_2	0.07	[334]
21	1,2,4,5-tetracyanobenzene	toluene	CH_2Cl_2 + 5% toluene	0.07	[334]
22	1,2,4,5-tetracyanobenzene	toluene	CH_2Cl_2 + 10% toluene	0.04	[334]
23	1,2,4,5-tetracyanobenzene	toluene	CH_2Cl_2 + 15% toluene	0.03	[334]
24	1,2,4,5-tetracyanobenzene	toluene	CH_2Cl_2 + 20% toluene	0.02	[334]
25	1,2,4,5-tetracyanobenzene	toluene	CH_2Cl_2 + 25% toluene	0.02	[334]
26	1,2,4,5-tetracyanobenzene	toluene	CH_2Cl_2 + 30% toluene	0.01	[334]
27	1,2,4,5-tetracyanobenzene	toluene	CH_2Cl_2 + 50% toluene	0.01	[334]
28	1,2,4,5-tetracyanobenzene	toluene	CH_3CN	0.1	[334]
29	1,2,4,5-tetracyanobenzene	toluene	ethylacetate	0.03	[334]
30	1,2,4,5-tetracyanobenzene	toluene	methyl ethyl ketone	0.23	[334]
31	1,2,4,5-tetracyanobenzene	toluene	methylacetate	0.04	[334]

6.3) Tabulated values for the cage-escape yields of polycyclic aromatic hydrocarbons

Table 13 gathers the cage-escape yields of polycyclic aromatic hydrocarbons with several quenchers and solvents. Electron transfer quenching sensitized by polycyclic aromatic hydrocarbons derivatives occur primarily from singlet and triplet states. For a specific excited state description, see relevant reference(s).

Table 13. Cage-escape yields (ϕ_{ce}) of polycyclic aromatic hydrocarbons.

Entry	Photosensitizer	Quencher	Solvent	ϕ_{ce}	Ref
1	1,12-Benzoperylene	tetracyanoethylene	CH_3CN	0.035	[325]
2	1,12-Benzoperylene	*trans*-1,2-dicyanoethylene	CH_3CN	0.061	[325]
3	Fluoranthene	1,2-dicyanoethylene	CH_3CN	0.074	[325]
4	Perylene	tetracyanoethylene	CH_3CN	0.019	[325]
5	Perylene	*trans*-1,2-dicyanoethylene	CH_3CN	0.14	[325]
6	Perylene	Perylene	Acetone	0.003	[339]
7	Perylene	Perylene	Acetonitrile	0.11	[339]
8	Perylene	Perylene	DMSO	0.16	[339]
9	Perylene	Perylene	EMIDCA (ionic liquid)	0.55	[339]
10	Perylene	Perylene	BMIM (ionic liquid)	0.46	[339]
11	Pyrene	1,2,4,5-tetracyanobenzene	Acetone	0.68	[337]
12	Pyrene	3-cyanopyridine	CH_3CN	0.49	[327]
13	Pyrene	diethyl isophthalate	Acetone	0.43	[337]
14	Pyrene	diethyl phthalate	Acetone	0.33	[337]
15	Pyrene	diethyl tetraphthalate	Acetone	0.41	[337]
16	Pyrene	indole	butyronitrile	0.24	[506]
17	Pyrene	indole	CH_3CN	0.37	[506]
18	Pyrene	indole	EtOH	0.11	[506]
19	Pyrene	indole	MeOH	0.22	[506]

20	Pyrene	*m*-dicyanobenzene	Acetone	0.65	[337]
21	Pyrene	*m*-dicyanobenzene	CH_3CN	0.8	[327]
22	Pyrene	*m*-nitrobenzaldehyde	CH_3CN	0.017	[327]
23	Pyrene	maleic anhydride	Acetone	0.15	[337]
24	Pyrene	N,N-dimethylaniline	1,2-dichloroethane	0.04	[334]
25	Pyrene	N,N-dimethylaniline	Acetone	0.344	[334]
26	Pyrene	N,N-dimethylaniline	CH_2Cl_2	0.03	[334]
27	Pyrene	N,N-dimethylaniline	CH_3CN	0.5	[334]
28	Pyrene	N,N-dimethylaniline	pyridine	0.08	[334]
29	Pyrene	*o*-dicyanobenzene	Acetone	0.94	[337]
30	Pyrene	*o*-dicyanobenzene	CH_3CN	0.89	[327]
31	Pyrene	*o*-nitroanisole	CH_3CN	0	[327]
32	Pyrene	*p*-benzoquinone	Acetone	0.63	[337]
33	Pyrene	*p*-chlorobenzonitrile	CH_3CN	0.25	[327]
34	Pyrene	*p*-dicyanobenzene	Acetone	1	[337]
35	Pyrene	*p*-dicyanobenzene	CH_3CN	0.85	[327]
36	Pyrene	*p*-nitrobenzaldehyde	CH_3CN	0.033	[327]
37	Pyrene	phthalic anhydride	Acetone	0.2	[337]
38	Pyrene	pyromellitic dianhydride	Acetone	0.12	[337]
39	Pyrene	tetrachlorophthalic anhydride	Acetone	0.17	[337]
40	Pyrene	tetracyanoethylene	CH_3CN	0.036	[325]
41	Pyrene	*trans*-1,2-dicyanoethylene	CH_3CN	0.033	[325]

6.4) Tabulated values for the cage-escape yields of pyrylium and thiopyrilium derivatives

Table 14 gathers the cage-escape yields of pyrilium and thiopyrylium derivatives with several quenchers and solvents. Electron transfer quenching sensitized by pyrylium and thiopyrylium derivatives occur primarily from singlet and triplet states. For a specific excited state description, see relevant reference(s).

Table 14. Cage-escape yields (ϕ_{ce}) of pyrylium and thiopyrilium derivatives.

Entry	Photosensitizer	Quencher	Solvent	ϕ_{ce}	Ref
1	2-^{t}Bu-4,6-diphenylpyrilium	THF	THF	0.047	[507]
2	2,4,6-triphenylpyrilium	benzene	CH_3CN	0.75	[343]
3	2,4,6-triphenylpyrilium	benzene	$CHCl_3$	0.51	[343]
4	2,4,6-triphenylpyrilium	bromobenzene	CH_3CN	0.33	[343]
5	2,4,6-triphenylpyrilium	bromobenzene	$CHCl_3$	0.18	[343]
6	2,4,6-triphenylpyrilium	chlorobenzene	CH_3CN	0.56	[343]
7	2,4,6-triphenylpyrilium	chlorobenzene	$CHCl_3$	0.31	[343]
8	2,4,6-triphenylpyrilium	iodobenzene	CH_3CN	0.1	[343]
9	2,4,6-triphenylpyrilium	iodobenzene	$CHCl_3$	0.047	[343]
10	2,4,6-triphenylpyrilium	*o*-bromoanisole	CH_3CN	0.04	[343]

11	2,4,6-triphenylpyrilium	*o*-bromoanisole	$CHCl_3$	0.024	[343]
12	2,4,6-triphenylpyrilium	*p*-bromotoluene	CH_3CN	0.1	[343]
13	2,4,6-triphenylpyrilium	*p*-bromotoluene	$CHCl_3$	0.051	[343]
14	2,4,6-triphenylpyrilium	*p*-chlorotoluene	CH_3CN	0.21	[343]
15	2,4,6-triphenylpyrilium	*p*-chlorotoluene	$CHCl_3$	0.123	[343]
16	2,4,6-triphenylpyrilium	*p*-iodoanisole	CH_3CN	0.08	[343]
17	2,4,6-triphenylpyrilium	*p*-iodoanisole	$CHCl_3$	0.044	[343]
18	2,4,6-triphenylpyrilium	THF	THF	0.21	[507]
19	2,4,6-triphenylpyrilium	toluene	CH_3CN	0.25	[343]
20	2,4,6-triphenylpyrilium	toluene	$CHCl_3$	0.135	[343]
21	2,4,6-triphenylthiopyrylium	benzene	CH_3CN	0.08	[344]
22	2,4,6-triphenylthiopyrylium	bromobenzene	CH_3CN	0.02	[344]
23	2,4,6-triphenylthiopyrylium	chlorobenzene	CH_3CN	0.07	[344]
24	2,4,6-triphenylthiopyrylium	cyclohexanone	CH_3CN	0.09	[344]
25	2,4,6-triphenylthiopyrylium	cyclopentanone	CH_3CN	0.09	[344]
26	2,4,6-triphenylthiopyrylium	fluorobenzene	CH_3CN	0.08	[344]
27	2,4,6-triphenylthiopyrylium	*p*-bromotoluene	CH_3CN	0.03	[344]
28	2,4,6-triphenylthiopyrylium	*p*-chlorotoluene	CH_3CN	0.03	[344]
29	2,4,6-triphenylthiopyrylium	THF	THF	0.53	[507]
30	2,4,6-triphenylthiopyrylium	toluene	CH_3CN	0.06	[344]
31	2,6-dimethyl-4-(*p*-acetylphenyl)pyrilium	biphenyl	CH_2Cl_2	0.71	[508]
32	2,6-dimethyl-4-a-naphthylpyrilium	biphenyl	CH_2Cl_2	0.3	[508]
33	2,6-dimethyl-4-b-naphthylpyrilium	biphenyl	CH_2Cl_2	0.26	[508]
34	2,6-dimethyl-4-biphenylpyrilium	biphenyl	CH_2Cl_2	0.36	[508]
35	2,6-dimethyl-4-phenyldecanepyrilium	biphenyl	CH_3CN	0.19	[509]
36	2,6-dimethyl-4-phenyldecanethiopyrilium	biphenyl	CH_3CN	0.35	[509]
37	2,6-dimethyl-4-phenyloctanepyrilium	biphenyl	CH_3CN	0.17	[509]
38	2,6-dimethyl-4-phenyloctanethiopyrilium	biphenyl	CH_3CN	0.35	[509]
39	2,6-dimethyl-4-phenylpyrilium	biphenyl	CH_3CN	0.42	[509]
40	2,6-dimethyl-4-phenylthiopyrilium	biphenyl	CH_3CN	0.51	[509]
41	2,6-dimethyl-4-tolylpyrilium	biphenyl	CH_3CN	0.2	[509]
42	2,6-dimethyl-4-tolylthiopyrilium	biphenyl	CH_3CN	0.38	[509]
43	4-^{t}Bu-2,6-diphenylpyrilium	THF	THF	0.23	[507]

6.5) Tabulated values for the cage-escape yields of xanthene derivatives

Table 15 gathers the cage-escape yields of xanthene derivatives with several quenchers and solvents. Electron transfer quenching sensitized by xanthene derivatives occur primarily from singlet and triplet states. For a specific excited state description, see relevant reference(s).

Table 15. Cage-escape yields (ϕ_{ce}) of xanthene derivatives.

Entry	Photosensitizer	Quencher	Solvent	ϕ_{ce}	Ref
1	3,7-diaminophenoxazinylium chloride	1-methoxynaphthalene	CH_3OH	0.014	[348]
2	3,7-diaminophenoxazinylium chloride	1,2-dimethoxybenzene	CH_3OH	0.008	[348]
3	3,7-diaminophenoxazinylium chloride	1,2,3-trimethoxybenzene	CH_3OH	0.0073	[348]
4	3,7-diaminophenoxazinylium chloride	1,2,4-trimethoxybenzene	CH_3OH	0.013	[348]
5	3,7-diaminophenoxazinylium chloride	1,3,5-trimethoxybenzene	CH_3OH	0.0046	[348]
6	3,7-diaminophenoxazinylium chloride	1,4-dimethoxybenzene	CH_3OH	0.0098	[348]
7	3,7-diaminophenoxazinylium chloride	1,4-dimethoxynaphthalene	CH_3OH	0.03	[348]
8	3,7-diaminophenoxazinylium chloride	1,5-bis(dimethylamino)naphthalene	CH_3OH	0.15	[348]
9	3,7-diaminophenoxazinylium chloride	1,5-dimethoxynaphthalene	CH_3OH	0.015	[348]
10	3,7-diaminophenoxazinylium chloride	1,8-dimethoxynaphthalene	CH_3OH	0.019	[348]
11	3,7-diaminophenoxazinylium chloride	2-methoxynaphthalene	CH_3OH	0.0046	[348]
12	3,7-diaminophenoxazinylium chloride	2,4-dimethoxy-N,N-dimethylaniline	CH_3OH	0.1	[348]
13	3,7-diaminophenoxazinylium chloride	3,3'-bis(methoxy)biphenyl	CH_3OH	0.0058	[348]
14	3,7-diaminophenoxazinylium chloride	3,4-dimethoxy-N,N-dimethylaniline	CH_3OH	0.19	[348]
15	3,7-diaminophenoxazinylium chloride	4-methoxybiphenyl	CH_3OH	0.0046	[348]
16	3,7-diaminophenoxazinylium chloride	diphenylmethylamine	CH_3OH	0.058	[348]
17	3,7-diaminophenoxazinylium chloride	*m*-methoxy-N,N-dimethylaniline	CH_3OH	0.065	[348]
18	3,7-diaminophenoxazinylium chloride	N,N-diethylaniline	CH_3OH	0.072	[348]
19	3,7-diaminophenoxazinylium chloride	N,N-dimethylaniline	CH_3OH	0.037	[348]
20	3,7-diaminophenoxazinylium chloride	N,N,N',N'-tetramethyl-1,2-phenylenediamine	CH_3OH	0.16	[348]
21	3,7-diaminophenoxazinylium chloride	N,N,N',N'-tetramethyl-1,3-phenylenediamine	CH_3OH	0.17	[348]
22	3,7-diaminophenoxazinylium chloride	N,N,N',N'-tetramethyl-1,4-phenylenediamine	CH_3OH	0.45	[348]
23	3,7-diaminophenoxazinylium chloride	N,N,N',N'-tetramethylbenzidine	CH_3OH	0.18	[348]
24	3,7-diaminophenoxazinylium chloride	*p*-methoxy-N,N-dimethylaniline	CH_3OH	0.13	[348]
25	Rose bengal	2,2'-bipyridinium-N,N'-di(propylsulphonate)	H_2O μ = 0.2 M	0.07	[346]
26	Rose bengal	4,4'-bipyridinium-N,N'-di(propylsulphonate)	H_2O μ = 0.2 M	0.033	[346]
27	Rose bengal	Methyl Viologen	H_2O μ = 0.04 M	0.018	[346]
28	Rose bengal	Methyl Viologen	H_2O μ = 0.075 M	0.026	[346]
29	Rose bengal	Methyl Viologen	H_2O μ = 0.075 M	0.022	[346]
30	Rose bengal	Methyl Viologen	H_2O μ = 0.15 M	0.02	[346]
31	Rose bengal	Methyl Viologen	H_2O μ = 0.45 M	0.018	[346]
32	Tetraiodofluorescein	1,4-benzoquinone	CH_3OH	0.53	[349]
33	Tetraiodofluorescein	2,5-dimethyl-1,4-benzoquinone	CH_3OH	0.5	[349]
34	Tetraiodofluorescein	1,4-naphthoquinone	CH_3OH	0.35	[349]
35	Tetraiodofluorescein	tretramethyl-1,4-benzoquinone	CH_3OH	0.35	[349]
36	Tetraiodofluorescein	9,10-anthraquinone	CH_3OH	0.24	[349]

6.6) Tabulated values for the cage-escape yields of thiazine derivatives

Table 16 gathers the cage-escape yields of thiazine derivatives with several quenchers and solvents. Electron transfer quenching sensitized by thiazine derivatives occur primarily from triplet states. For a specific excited state description, see relevant reference(s).

Table 16. Cage-escape yields (ϕ_{ce}) of Thiazine derivatives.

Entry	Photosensitizer	Quencher	Solvent	ϕ_{ce}	Ref
1	Methylene blue	4-iodo-anisole	CH_3CN /Ethylene glycol 100:0	0.1	[351]
2	Methylene blue	4-iodo-anisole	CH_3CN /Ethylene glycol 60:40	0.042	[351]
3	Methylene blue	4-iodo-anisole	CH_3CN /Ethylene glycol 80:20	0.066	[351]
4	Methylene blue	4-iodo-anisole	CH_3CN /Ethylene glycol 90:10	0.085	[351]
5	Thionine	2-bromoaniline	Cetyldimethylbenzylammonium chloride micelles	0.13	[191]
6	Thionine	2-bromoaniline	CH_3OH	0.7	[191]
7	Thionine	3-bromoaniline	Cetyldimethylbenzylammonium chloride micelles	0.21	[191]
8	Thionine	3-bromoaniline	CH_3OH	0.9	[191]
9	Thionine	4-bromoaniline	Cetyldimethylbenzylammonium chloride micelles	0.1	[191]
10	Thionine	4-bromoaniline	CH_3OH	0.51	[191]
11	Thionine	4-chloroaniline	Cetyldimethylbenzylammonium chloride micelles	0.27	[191]
12	Thionine	4-chloroaniline	CH_3OH	0.97	[191]
13	Thionine	4-iodoaniline	Cetyldimethylbenzylammonium chloride micelles	0.06	[191]
14	Thionine	4-iodoaniline	CH_3OH	0.13	[191]
15	Thionine	aniline	Cetyldimethylbenzylammonium chloride micelles	0.29	[191]
16	Thionine	aniline	CH_3OH	1	[191]
17	Thionine	aniline	CH_3OH + 0.015M phenylacetic acid, 0.005M CH_3ONa	0.91	[353]
18	Thionine	*m*-bromoaniline	CH_3OH + 0.015M phenylacetic acid, 0.005M CH_3ONa	0.75	[353]
19	Thionine	*m*-chloroaniline	CH_3OH + 0.015M phenylacetic acid, 0.005M CH_3ONa	0.91	[353]
20	Thionine	*m*-fluoroaniline	CH_3OH + 0.015M phenylacetic acid, 0.005M CH_3ONa	0.91	[353]
21	Thionine	*m*-iodoaniline	CH_3OH + 0.015M phenylacetic acid, 0.005M CH_3ONa	0.46	[353]
22	Thionine	*o*-bromoaniline	CH_3OH + 0.015M phenylacetic acid, 0.005M CH_3ONa	0.63	[353]
23	Thionine	*o*-chloroaniline	CH_3OH + 0.015M phenylacetic acid, 0.005M CH_3ONa	0.88	[353]
24	Thionine	*o*-fluoroaniline	CH_3OH + 0.015M phenylacetic acid, 0.005M CH_3ONa	0.91	[353]
25	Thionine	*o*-iodoaniline	CH_3OH + 0.015M phenylacetic acid, 0.005M CH_3ONa	0.21	[353]
26	Thionine	*p*-bromoaniline	CH_3OH + 0.015M phenylacetic acid, 0.005M CH_3ONa	0.48	[353]
27	Thionine	*p*-choroaniline	CH_3OH + 0.015M phenylacetic acid, 0.005M CH_3ONa	0.86	[353]
28	Thionine	*p*-fluoroaniline	CH_3OH + 0.015M phenylacetic acid, 0.005M CH_3ONa	0.9	[353]
29	Thionine	*p*-iodoaniline	CH_3OH + 0.015M phenylacetic acid, 0.005M CH_3ONa	0.11	[353]

6.7) Tabulated values for the cage-escape yields of ketones derivatives

Table 17 gathers the cage-escape yields of ketones derivatives with several quenchers and solvents. Electron transfer quenching sensitized by ketones derivatives occur primarily from triplet states. For a specific excited state description, see relevant reference(s).

Table 17. Cage-escape yields (ϕ_{ce}) of ketones derivatives.

Entry	Photosensitizer	Quencher	Solvent	ϕ_{ce}	Ref
1	4-carboxybenzophenone	phenol	D_2O pH 7,2	0.85	[358]
2	4-carboxybenzophenone	phenol	H_2O pH 13	1.1	[358]
3	4-carboxybenzophenone	*p*-methoxyphenol	H_2O pH 13	1.1	[358]
4	4-carboxybenzophenone	*p*-chlorophenol	H_2O pH 13	1.1	[358]
5	4-carboxybenzophenone	*p*-bromophenol	H_2O pH 13	0.55	[358]
6	4-carboxybenzophenone	*p*-iodophenol	H_2O pH 13	0.13	[358]
7	4-carboxybenzophenone	phenol	H_2O pH 5.4	0.75	[358]
8	4-carboxybenzophenone	phenol	H_2O pH 5.9	0.98	[358]
9	4-carboxybenzophenone	phenol	H_2O pH 7.2	1	[358]
10	4-carboxybenzophenone	*p*-methoxyphenol	H_2O pH 7.2	0.81	[358]
11	4-carboxybenzophenone	*p*-chlorophenol	H_2O pH 7.2	0.73	[358]
12	4-carboxybenzophenone	*p*-bromophenol	H_2O pH 7.2	0.41	[358]
13	4-carboxybenzophenone	*p*-iodophenol	H_2O pH 7.2	0.18	[358]
14	4-carboxybenzophenone	phenol	H_2O pH 8.0	0.78	[358]
15	Anthraquinone	N,N-dimethylaniline	CH_3CN	0.88	[163]
16	Anthraquinone	1,4-diazabicyclo[2.2.2]octane (DABCO)	CH_3CN	0.88	[163]
17	Benzophenone	phenol	C_6H_6	0.84	[359]
18	Benzophenone	*p*-methoxyphenol	C_6H_6	0.79	[359]
19	Benzophenone	*p*-cresol	C_6H_6	0.83	[359]
20	Benzophenone	*p*-fluorophenol	C_6H_6	0.91	[359]
21	Benzophenone	*p*-chlorophenol	C_6H_6	0.75	[359]
22	Benzophenone	*p*-bromophenol	C_6H_6	0.71	[359]
23	Benzophenone	*p*-iodophenol	C_6H_6	0.61	[359]
24	Benzophenone	*p*-cyanophenol	C_6H_6	0.88	[359]
25	Benzophenone	N,N-dimethylaniline	CH_3CN	ND	[163]
26	Benzophenone	1,4-diazabicyclo[2.2.2]octane (DABCO)	CH_3CN	0.95	[163]
27	Benzophenone	1,4-hydroquinone	C_6H_6	0.84	[359]
28	*p*-methoxypropiophenone	*p*-bromophenol	C_6H_6	0.55	[359]
29	*p*-methoxypropiophenone	*p*-iodophenol	C_6H_6	0.21	[359]
30	*p*-methoxypropiophenone	*p*-cyanophenol	C_6H_6	0.56	[359]

6.8) Tabulated values for the cage-escape yields of Ru(II) photosensitizers

Table 18 gathers the cage-escape yields of Ru(II) photosensitizers with several quenchers and solvents. Electron transfer quenching sensitized by ruthenium derivatives occur primarily from triplet states. For a specific excited state description, see relevant reference(s).

Table 18. *Cage-escape yields (ϕ_{ce}) of Ru(II) photosensitizers*

Entry	PS	Quencher	Solvent	ϕ_{ce}	Ref
1	$[(CN)(bpy)_2RuCNPt(dien)]^{2+}$	methyl viologen	0.3M Na_2SO_4	0.17	[510]
2	$[(dien)PtNC[Ru(bpy)_2]CNPt(dien)]^{4+}$	methyl viologen	0.3M Na_2SO_4	0.29	[510]
3	$[Ru(3,4,7,8\text{-}(CH_3)_4\text{-}phen)_3]^{2+}$	$CuSO_4$	0.5M H_2SO_4	0.95	[382]
4	$[Ru(3,4,7,8\text{-}(CH_3)_4\text{-}phen)_3]^{2+}$	methyl viologen	CH_3CN/H_2O 1:9, μ = 0.3M KCl	0.22	[383]
5	$[Ru(3,4,7,8\text{-}(CH_3)_4\text{-}phen)_3]^{2+}$	methyl viologen	CH_3CN/H_2O 1:4	0.15	[383]
6	$[Ru(4,4'\text{-}(CH_3)_2\text{-}bpy)_3]^{2+}$	$CuSO_4$	0.5M H_2SO_4	0.94	[382]
7	$[Ru(4,4'\text{-}(CH_3)_2\text{-}bpy)_3]^{2+}$	methyl viologen	CH_3CN/H_2O 1:9, μ = 0.3M KCl	0.11	[383]
8	$[Ru(4,4'\text{-}(CH_3)_2\text{-}bpy)_3]^{2+}$	methyl viologen	H_2O/CH_3CN 4:1	0.21	[383]
9	$[Ru(4,7\text{-}(CH_3)_2\text{-}phen)_3]^{2+}$	$[Co(diamsar)]^{2+}$	H_2O + 0.2M LiCl, 0.05M N-ethylmorpholine, pH 8.3	0.9	[419]
10	$[Ru(4,7\text{-}(CH_3)_2\text{-}phen)_3]^{2+}$	$[Co(sep)]^{2+}$	H_2O + 0.2M LiCl	0.64	[419]
11	$[Ru(4,7\text{-}(CH_3)_2\text{-}phen)_3]^{2+}$	$CuSO_4$	0.5M H_2SO_4	0.96	[382]
12	$[Ru(5\text{-}Br\text{-}phen)_3]^{2+}$	$CuSO_4$	0.5M H_2SO_4	0.3	[382]
13	$[Ru(5\text{-}C_6H_5\text{-}phen)_3]^{2+}$	$CuSO_4$	0.5M H_2SO_4	0.51	[382]
14	$[Ru(5\text{-}CH_3\text{-}phen)_3]^{2+}$	$CuSO_4$	0.5M H_2SO_4	0.74	[382]
15	$[Ru(5\text{-}Cl\text{-}phen)_3]^{2+}$	$[Co(diamsar)]^{2+}$	H_2O + 0.2M LiCl, 0.05M N-ethylmorpholine, pH 8.1	0.3	[419]
16	$[Ru(5\text{-}Cl\text{-}phen)_3]^{2+}$	$[Co(sep)]^{2+}$	H_2O + 0.2M LiCl	0.35	[419]
17	$[Ru(5\text{-}Cl\text{-}phen)_3]^{2+}$	$CuSO_4$	0.5M H_2SO_4	0.31	[382]
18	$[Ru(5\text{-}Cl\text{-}phen)_3]^{2+}$	tri-*p*-tolylamine	CH_3CN	1	[511]
19	$[Ru(5\text{-}Cl\text{-}phen)_3]^{2+}$	tri-*p*-tolylamine	CH_3CN	1	[511]
20	$[Ru(5,6\text{-}(CH_3)_2\text{-}phen)_3]^{2+}$	$CuSO_4$	0.5M H_2SO_4	0.79	[382]
21	$[Ru(bpm)(bpz)(bpy)]^{2+}$	triethanolamine	Propylene carbonate	0.44	[421]
22	$[Ru(bpm)(bpz)(bpy)]^{2+}$	triethanolamine	CH_3CN	0.90	[421]
23	$[Ru(bpm)(bpz)(bpy)]^{2+}$	triethanolamine	H_2O	0.55	[395]
24	$[Ru(bpm)_2(bpy)]^{2+}$	triethanolamine	Propylene carbonate	0.42	[421]
25	$[Ru(bpm)_2(bpy)]^{2+}$	triethanolamine	CH_3CN	0.71	[421]
26	$[Ru(bpm)_2(bpz)]^{2+}$	EDTA	H_2O, pH = 8.5, μ = 1.0M (Na_2SO_4)	0.51	[420]
27	$[Ru(bpm)_2(bpz)]^{2+}$	triethanolamine	Propylene carbonate	0.33	[421]
28	$[Ru(bpm)_2(bpz)]^{2+}$	triethanolamine	CH_3CN	0.84	[421]
29	$[Ru(bpm)_2(bpz)]^{2+}$	triethanolamine	H_2O	0.44	[395]
30	$[Ru(bpm)_2(bpz)]^{2+}$	triethanolamine	H_2O, pH = 10.0, μ = 1.0M (Na_2SO_4)	0.51	[420]
31	$[Ru(bpm)_2(bpz)]^{2+}$	triethanolamine + methyl viologen	H_2O, pH 10	0.51	[420]
32	$[Ru(bpm)_2(bpz)]^{2+}$	triethanolamine + methyl viologen	H_2O, pH 8.5	0.51	[420]
33	$[Ru(bpm)_3]^{2+}$	EDTA	H_2O, pH = 8.5, μ = 1.0M (Na_2SO_4)	0.73	[420]

34	$[Ru(bpm)_3]^{2+}$	triethanolamine	Propylene carbonate	0.380	[421]
35	$[Ru(bpm)_3]^{2+}$	triethanolamine	CH_3CN	0.77	[421]
36	$[Ru(bpm)_3]^{2+}$	triethanolamine	H_2O	0.65	[395]
37	$[Ru(bpm)_3]^{2+}$	triethanolamine + methyl viologen	H_2O, pH 10	0.66	[420]
38	$[Ru(bpm)_3]^{2+}$	triethanolamine + methyl viologen	H_2O, pH 8.5	0.73	[420]
39	$[Ru(bpy)(bpz)(bpm)]^{2+}$	EDTA	H_2O, pH = 8.5, μ = 1.0M (Na_2SO_4)	0.64	[420]
40	$[Ru(bpy)(bpz)(bpm)]^{2+}$	Triethanolamine	H_2O, pH = 10.0, μ = 1.0M (Na_2SO_4)	0.58	[420]
41	$[Ru(bpy)(bpz)(bpm)]^{2+}$	triethanolamine + methyl viologen	H_2O, pH 10	0.58	[420]
42	$[Ru(bpy)(bpz)(bpm)]^{2+}$	triethanolamine + methyl viologen	H_2O, pH 8.5	0.64	[420]
43	$[Ru(bpy)(CN)_4]^{2-}$	methyl viologen	H_2O	0.24	[512]
44	$[Ru(bpy)(dmbpy)_2]^{2+}$	methyl viologen	H_2O	0.23	[513]
45	$[Ru(bpy)(dpp)_2]^{2+}$	methyl viologen	H_2O	0.095	[513]
46	$[Ru(bpy)(pyq)_2]^{2+}$	methyl viologen	H_2O	0.18	[513]
47	$[Ru(bpy)_2(BL)Ru(bpy)_2]^{4+}$	$[Fe(CN)_6]^{4-}$	H_2O	0.02	[384]
48	$[Ru(bpy)_2(BL)Ru(bpy)_2]^{4+}$	$[Mo(CN)_6]^{4-}$	0.1M K_2HPO_4	0.52	[384]
49	$[Ru(bpy)_2(BL)Ru(bpy)_2]^{4+}$	$[Os(CN)_6]^{4-}$	0.1M K_2HPO_4	0.04	[384]
50	$[Ru(bpy)_2(BL)Ru(bpy)_2]^{4+}$	$[W(CN)_8]^{4-}$	0.1M K_2HPO_4	0.41	[384]
51	$[Ru(bpy)_2(bpy\text{-}anthracene)]^{2+}$	methyl viologen	H_2O	0.03	[366]
52	$[Ru(bpy)_2(bpy\text{-}anthracene)]^{2+}$	methyl viologen	CH_3OH	0.95	[366]
53	$[Ru(bpy)_2(bpy\text{-}naphthalene)]^{2+}$	methyl viologen	Acetate buffer	0.06	[366]
54	$[Ru(bpy)_2(bpy\text{-}naphthalene)]^{2+}$	methyl viologen	H_2O	0.07	[366]
55	$[Ru(bpy)_2(bpy\text{-}naphthalene)]^{2+}$	methyl viologen	CH_3OH	0.07	[366]
56	$[Ru(bpy)_2(bpy\text{-}pyrene)]^{2+}$	methyl viologen	Acetate buffer	0.06	[366]
57	$[Ru(bpy)_2(bpy\text{-}pyrene)]^{2+}$	methyl viologen	H_2O	0.06	[366]
58	$[Ru(bpy)_2(bpy\text{-}pyrene)]^{2+}$	methyl viologen	CH_3OH	0.7	[366]
59	$[Ru(bpy)_2(bpz)]^{2+}$	triethanolamine	Propylene carbonate	0.37	[421]
60	$[Ru(bpy)_2(bpz)]^{2+}$	triethanolamine	CH_3CN	0.76	[421]
61	$[Ru(bpy)_2(dcb)]$	$[Fe(CN)_6]^{4-}$	H_2O	0.11	[384]
62	$[Ru(bpy)_2(dcb)]$	$[Mo(CN)_6]^{4-}$	0.1M K_2HPO_4	0.48	[384]
63	$[Ru(bpy)_2(dcb)]$	$[Os(CN)_6]^{4-}$	0.1M K_2HPO_4	0.06	[384]
64	$[Ru(bpy)_2(dcb)]$	$[W(CN)_8]^{4-}$	0.1M K_2HPO_4	0.8	[384]
65	$[Ru(bpy)_2(deeb)]^{2+}$	methyl viologen	CH_3CN/H_2O 1:1, μ = 0.2M NaCl	0.12	[369]
66	$[Ru(bpy)_2(deeb)]^{2+}$	methyl viologen	H_2O/CH_3CN 4:1	0.11	[383]
67	$[Ru(bpy)_2(deeb)]^{2+}$	tetra-*n*-butylammonium iodide	CH_2Cl_2	0.25	[386]
68	$[Ru(bpy)_3]^{2+}$	$[Co(sep)]^{2+}$	H_2O + 0.2M LiCl	0.51	[419]
69	$[Ru(bpy)_3]^{2+}$	$[Cr(bpy)_3]^{3+}$	0.5M H_2SO_4	>0	[418]
70	$[Ru(bpy)_3]^{2+}$	$[Fe(CN)_6]^{4-}$	H_2O	0.03	[384]
71	$[Ru(bpy)_3]^{2+}$	$[Mo(CN)_6]^{4-}$	0.1M K_2HPO_4	0.87	[384]
72	$[Ru(bpy)_3]^{2+}$	$[Os(CN)_6]^{4-}$	0.1M K_2HPO_4	0.05	[384]
73	$[Ru(bpy)_3]^{2+}$	$[Rh(bpy)_3]^{3+}$	H_2O	0.15	[418]
74	$[Ru(bpy)_3]^{2+}$	$[W(CN)_8]^{4-}$	0.1M K_2HPO_4	0.86	[384]

75	$[Ru(bpy)_3]^{2+}$	1,4-anisdine	CH_3CN/H_2O 1:1	0.81	415
76	$[Ru(bpy)_3]^{2+}$	1,4-phenylenediamine	CH_3CN/H_2O 1:1	0.81	415
77	$[Ru(bpy)_3]^{2+}$	1,4-toluidine	CH_3CN/H_2O 1:1	0.91	415
78	$[Ru(bpy)_3]^{2+}$	2,4-dichlorophenol	CH_3OH/H_2O 25/75	0.19	396
79	$[Ru(bpy)_3]^{2+}$	2,4-dichlorophenol	CH_3OH/H_2O 50/50	0.25	396
80	$[Ru(bpy)_3]^{2+}$	2,4-dichlorophenol	CH_3OH/H_2O 75/25	0.33	396
81	$[Ru(bpy)_3]^{2+}$	2,4-dichlorophenol	CH_3OH/H_2O 100/0	0.52	396
82	$[Ru(bpy)_3]^{2+}$	2,4-dichlorophenol	CH_3OH/H_2O 25/75		396
83	$[Ru(bpy)_3]^{2+}$	2,4-dichlorophenol	CH_3OH/H_2O 50/50	0.17	396
84	$[Ru(bpy)_3]^{2+}$	2,4-dichlorophenol	CH_3OH/H_2O 75/25	0.34	396
85	$[Ru(bpy)_3]^{2+}$	2,4-dichlorophenol	CH_3OH/H_2O 100/0	0.62	396
86	$[Ru(bpy)_3]^{2+}$	2,4-dichlorophenol	CH_3OH/H_2O 25/75	0.14	396
87	$[Ru(bpy)_3]^{2+}$	2,4-dichlorophenol	CH_3OH/H_2O 50/50	0.26	396
88	$[Ru(bpy)_3]^{2+}$	2,4-dichlorophenol	CH_3OH/H_2O 75/25	0.42	396
89	$[Ru(bpy)_3]^{2+}$	2,4-dichlorophenol	CH_3OH/H_2O 100/0	0.51	396
90	$[Ru(bpy)_3]^{2+}$	3,3'-dimethylbenzidine	DMF	1.06	514
91	$[Ru(bpy)_3]^{2+}$	3,3'-dimethylbenzidine	CH_3OH	1.04	514
92	$[Ru(bpy)_3]^{2+}$	3,3'-dimethylbenzidine	CH_3CN/H_2O 1:1	0.56	415
93	$[Ru(bpy)_3]^{2+}$	4-ethylbenzene diazonium	CH_3CN	0.45	94
94	$[Ru(bpy)_3]^{2+}$	4-ethylesterbenzene diazonium	CH_3CN	0.74	94
95	$[Ru(bpy)_3]^{2+}$	4-methoxybenzene diazonium	CH_3CN	0.38	94
96	$[Ru(bpy)_3]^{2+}$	4-methoxybenzene diazonium	CH_3CN + 0.1 M $TBABF_4$	0.39	94
97	$[Ru(bpy)_3]^{2+}$	4-nitrobenzene diazonium	CH_3CN	0.98	94
98	$[Ru(bpy)_3]^{2+}$	4,4'-bipyridinium-N,N'-di(propylsulphonate)	H_2O	0.14	379
99	$[Ru(bpy)_3]^{2+}$	4,4'-bipyridinium-N,N'-di(propylsulphonate)	H_2SO_4 0.5M	0.23	379
100	$[Ru(bpy)_3]^{2+}$	anthraquinone-2,6-sulphonate	H_2O + 7 mM phosphate buffer, μ = 0.04M	<0.01	515
101	$[Ru(bpy)_3]^{2+}$	ascorbate	H_2O pH4	0.55	516
102	$[Ru(bpy)_3]^{2+}$	ascorbate	H_2O + Acetate buffer pH 2.74	0.99	517
103	$[Ru(bpy)_3]^{2+}$	ascorbate	H_2O + Acetate buffer pH 7.85	0.94	517
104	$[Ru(bpy)_3]^{2+}$	ascorbate	H_2O + Acetate buffer pH 6.86	0.99	517
105	$[Ru(bpy)_3]^{2+}$	ascorbate	H_2O + Acetate buffer pH 5.93	0.92	517
106	$[Ru(bpy)_3]^{2+}$	ascorbate	H_2O + 0.5M H_2SO_4	0.5	418
107	$[Ru(bpy)_3]^{2+}$	ascorbate	H_2O + Acetate buffer pH 3.44	0.99	517
108	$[Ru(bpy)_3]^{2+}$	ascorbate	H_2O + Acetate buffer pH 4.04	0.77	517
109	$[Ru(bpy)_3]^{2+}$	ascorbate	H_2O + Acetate buffer pH 4.48	0.95	517
110	$[Ru(bpy)_3]^{2+}$	ascorbate	H_2O + Acetate buffer pH 5.16	0.86	517
111	$[Ru(bpy)_3]^{2+}$	benzylviologen	8 :5 (v/v) 0.1M $TEAClO_4/CH_3CN$ to CH_2Cl_2	0.18	82
112	$[Ru(bpy)_3]^{2+}$	$CuSO_4$	0.5M H_2SO_4	0.56	418
113	$[Ru(bpy)_3]^{2+}$	$CuSO_4$	0.5M $HClO_4$	0.68	382
114	$[Ru(bpy)_3]^{2+}$	$CuSO_4$	2.4M $HClO_4$	0.76	382
115	$[Ru(bpy)_3]^{2+}$	$CuSO_4$	1M $HClO_4$, 0.3M $Ca(ClO_4)$)	1	382

116	$[Ru(bpy)_3]^{2+}$	diphenyl-1,4-phenylenediamine	DMF	1.11	514
117	$[Ru(bpy)_3]^{2+}$	diphenyl-1,4-phenylenediamine	CH_3CN/H_2O 1:1	0.6	415
118	$[Ru(bpy)_3]^{2+}$	diphenylamine	CH_3CN/H_2O 1:1		415
119	$[Ru(bpy)_3]^{2+}$	Eu^{2+}	H_2O	1	418
120	$[Ru(bpy)_3]^{2+}$	Eu^{3+}	H_2O	>0	418
121	$[Ru(bpy)_3]^{2+}$	Fe^{3+}	H_2O	1	418
122	$[Ru(bpy)_3]^{2+}$	Hg(II)	0.5M H_2SO_4	0.32	379
123	$[Ru(bpy)_3]^{2+}$	Hg(II)	3.0M HCl	<0.01	379
124	$[Ru(bpy)_3]^{2+}$	methyl viologen	CH_3OH	0.27	82
125	$[Ru(bpy)_3]^{2+}$	methyl viologen	H_2O + 95% ethylene glycol	0.05	82
126	$[Ru(bpy)_3]^{2+}$	methyl viologen	H_2O	0.25	418
127	$[Ru(bpy)_3]^{2+}$	methyl viologen	H_2O, μ = 0.80 M NaCl	0.24	111
128	$[Ru(bpy)_3]^{2+}$	methyl viologen	H_2O	0.51	514
129	$[Ru(bpy)_3]^{2+}$	methyl viologen	CH_3OHl	0.42	514
130	$[Ru(bpy)_3]^{2+}$	methyl viologen	H_2O, [MV] = 1 mM	0.18	380, 480
131	$[Ru(bpy)_3]^{2+}$	methyl viologen	H_2O, [MV] = 2 mM	0.22	380, 480
132	$[Ru(bpy)_3]^{2+}$	methyl viologen	H_2O, [MV] = 4 mM	0.22	380, 480
133	$[Ru(bpy)_3]^{2+}$	methyl viologen	H_2O, [MV] = 10 mM	0.25	380, 480
134	$[Ru(bpy)_3]^{2+}$	methyl viologen	H_2O, [MV] = 20 mM	0.21	380, 480
135	$[Ru(bpy)_3]^{2+}$	methyl viologen	H_2O, [MV] = 1 mM, $[C_2O_4(^{2-})]$ = 0.80 M	0.09	380, 480
136	$[Ru(bpy)_3]^{2+}$	methyl viologen	H_2O, [MV] = 2 mM, $[C_2O_4(^{2-})]$ = 0.70 M	0.10	380, 480
137	$[Ru(bpy)_3]^{2+}$	methyl viologen	H_2O, [MV] = 2 mM, $[C_2O_4(^{2-})]$ = 1 M	0.09	380, 480
138	$[Ru(bpy)_3]^{2+}$	methyl viologen	0.025M $NaClO_4$	0.12	84
139	$[Ru(bpy)_3]^{2+}$	methyl viologen	0.075M $NaClO_4$	0.096	84
140	$[Ru(bpy)_3]^{2+}$	methyl viologen	CH_3CN + 5% H_2O	0.35	379
141	$[Ru(bpy)_3]^{2+}$	methyl viologen	H_2O	0.25	379
142	$[Ru(bpy)_3]^{2+}$	methyl viologen	1M NaCl	0.2	379
143	$[Ru(bpy)_3]^{2+}$	methyl viologen	2M NaCl	0.19	379
144	$[Ru(bpy)_3]^{2+}$	methyl viologen	1M $NaNO_3$	0.18	379
145	$[Ru(bpy)_3]^{2+}$	methyl viologen	1M Na_2SO_4	0.16	379
146	$[Ru(bpy)_3]^{2+}$	methyl viologen	8 :5 (v/v) 0.1M $TEAClO_4/CH_3CN$ to CH_2Cl_2	0.23	82
147	$[Ru(bpy)_3]^{2+}$	methyl viologen	H_2O, μ = 0.01 M NaCl	0.38	111
148	$[Ru(bpy)_3]^{2+}$	methyl viologen	0.1M Na_2SO_4, [MV] = 1 mM	0.15	380, 480
149	$[Ru(bpy)_3]^{2+}$	methyl viologen	0.1M Na_2SO_4, [MV] = 2 mM	0.17	380, 480
150	$[Ru(bpy)_3]^{2+}$	methyl viologen	0.1M Na_2SO_4, [MV] = 10 mM	0.17	380, 480
151	$[Ru(bpy)_3]^{2+}$	methyl viologen	H_2O, [MV] = 0.5 mM, $[C_2O_4(^{2-})]$ = 0.1 M	0.13	380, 480
152	$[Ru(bpy)_3]^{2+}$	methyl viologen	H_2O, [MV] = 1 mM, $[C_2O_4(^{2-})]$ = 0.1 M	0.15	380, 480
153	$[Ru(bpy)_3]^{2+}$	methyl viologen	H_2O, [MV] = 2 mM, $[C_2O_4(^{2-})]$ = 0.1 M	0.17	380, 480
154	$[Ru(bpy)_3]^{2+}$	methyl viologen	H_2O, [MV] = 10 mM, $[C_2O_4(^{2-})]$ = 0.1 M	0.18	380, 480
155	$[Ru(bpy)_3]^{2+}$	methyl viologen	H_2O, pH 4.7, [MV] = 10 mM, [EDTA] = 0.01 M	0.19	380, 480
156	$[Ru(bpy)_3]^{2+}$	methyl viologen	0.21 M Na_2SO_4, pH 4.7, [MV] = 20 mM, [EDTA] = 0.1 M	0.10	380, 480

157	$[Ru(bpy)_3]^{2+}$	methyl viologen	0.30 M Na_2SO_4, pH 4.7, [MV] = 20 mM, [EDTA] = 0.01 M	0.09	380, 480
158	$[Ru(bpy)_3]^{2+}$	methyl viologen	0.30 M Na_2SO_4, pH 4.7, [MV] = 2 mM, [EDTA] = 0.01 M	0.15	380, 480
159	$[Ru(bpy)_3]^{2+}$	methyl viologen	0.25 M Na_2SO_4, pH 4.7, [MV] = 2 mM, [EDTA] = 0.1 M	0.16	380, 480
160	$[Ru(bpy)_3]^{2+}$	methyl viologen	0.11 M Na_2SO_4, pH 8.7, [MV] = 20 mM, [EDTA] = 0.1 M	0.09	380, 480
161	$[Ru(bpy)_3]^{2+}$	methyl viologen	0.29 M Na_2SO_4, pH 8.7, [MV] = 20 mM, [EDTA] = 0.01 M	0.10	380, 480
162	$[Ru(bpy)_3]^{2+}$	methyl viologen	H_2O + pH 11, [MV] = 20 mM, [EDTA] = 0.1 M	0.10	380, 480
163	$[Ru(bpy)_3]^{2+}$	methyl viologen	0.28 M Na_2SO_4, pH 11, [MV] = 20 mM, [EDTA] = 0.01 M	0.09	380, 480
164	$[Ru(bpy)_3]^{2+}$	methyl viologen	0.1 M NaCl	0.15	84
165	$[Ru(bpy)_3]^{2+}$	methyl viologen	0.1M $NaClO_4$	0.081	84
166	$[Ru(bpy)_3]^{2+}$	methyl viologen	0.1M NaH_2PO_4	0.181	84
167	$[Ru(bpy)_3]^{2+}$	methyl viologen	$C_{H3}CN$ + 0.1M $TBAClO_4$	0.42	379
168	$[Ru(bpy)_3]^{2+}$	methyl viologen	H_2O pH 4.7, acetate buffer 0.1M	0.25	379
169	$[Ru(bpy)_3]^{2+}$	methyl viologen	0.1M $NaClO_4$	0.2	379
170	$[Ru(bpy)_3]^{2+}$	methyl viologen	1M Na_2SO_4 + 0.1M Acetate buffer	0.1	379
171	$[Ru(bpy)_3]^{2+}$	methyl viologen	H_2O:CH_3CN 1:1 + 0.2M NaCl	0.19	82
172	$[Ru(bpy)_3]^{2+}$	methyl viologen	H_2O:CH_3CN 1:1 + 0.2M NaCl + 20% ethylene glycol	0.16	82
173	$[Ru(bpy)_3]^{2+}$	methyl viologen	H_2O:CH_3CN 1:1 + 0.2M NaCl + 40% ethylene glycol	0.13	82
174	$[Ru(bpy)_3]^{2+}$	methyl viologen	H_2O:CH_3CN 1:1 + 0.2M NaCl + 60% ethylene glycol	0.09	82
175	$[Ru(bpy)_3]^{2+}$	methyl viologen	H_2O:CH_3CN 1:1 + 0.2M NaCl + 80% ethylene glycol	0.06	82
176	$[Ru(bpy)_3]^{2+}$	methyl viologen	H_2O, μ = 0.02 M NaCl	0.35	111
177	$[Ru(bpy)_3]^{2+}$	methyl viologen	0.30 M Na_2SO_4, pH 4.7, [MV] = 2 mM, [EDTA] = 0.02 M	0.13	380, 480
178	$[Ru(bpy)_3]^{2+}$	methyl viologen	0.2 M NaCl	0.12	84
179	$[Ru(bpy)_3]^{2+}$	methyl viologen	0.2M $NaClO_4$	0.081	84
180	$[Ru(bpy)_3]^{2+}$	methyl viologen	0.2M NaH_2PO_4	0.181	84
181	$[Ru(bpy)_3]^{2+}$	methyl viologen	0.2M Na_2SO_4	0.24	379
182	$[Ru(bpy)_3]^{2+}$	methyl viologen	H_2O/CH_3CN 9:1, μ = 0.3M KCl	0.16	383
183	$[Ru(bpy)_3]^{2+}$	methyl viologen	0.3 M NaCl	0.12	84
184	$[Ru(bpy)_3]^{2+}$	methyl viologen	0.3M $NaClO_4$	0.075	84
185	$[Ru(bpy)_3]^{2+}$	methyl viologen	H_2O + 8 mM phosphate buffer, μ = 0.04M	0.4	515
186	$[Ru(bpy)_3]^{2+}$	methyl viologen	0.4 M NaCl	0.12	84
187	$[Ru(bpy)_3]^{2+}$	methyl viologen	0.4M $NaClO_4$	0.072	84
188	$[Ru(bpy)_3]^{2+}$	methyl viologen	0.4M NaH_2PO_4	0.152	84
189	$[Ru(bpy)_3]^{2+}$	methyl viologen	H_2O, [MV] = 0.5 mM	0.16	380, 480
190	$[Ru(bpy)_3]^{2+}$	methyl viologen	0.1M Na_2SO_4, [MV] = 0.5 mM	0.14	380, 480
191	$[Ru(bpy)_3]^{2+}$	methyl viologen	H_2O, [MV] = 0.5 mM, $[C_2O_4(^{2-})]$ = 0.85 M	0.10	380, 480
192	$[Ru(bpy)_3]^{2+}$	methyl viologen	0.50M Na_2SO_4, [MV] = 2 mM, $[C_2O_4(^{2-})]$ = 0.5 M	0.07	380, 480
193	$[Ru(bpy)_3]^{2+}$	methyl viologen	H_2O, pH 4.7, [MV] = 0.5 mM, [EDTA] = 0.095 M	0.11	380, 480
194	$[Ru(bpy)_3]^{2+}$	methyl viologen	0.30 M Na_2SO_4, pH 4.7, [MV] = 2 mM, [EDTA] = 0.05 M	0.13	380, 480
195	$[Ru(bpy)_3]^{2+}$	methyl viologen	0.18 M Na_2SO_4, pH 8.7, [MV] = 0.5 mM, [EDTA] = 0.010 M	0.19	380, 480

196	$[Ru(bpy)_3]^{2+}$	methyl viologen	0.20 M Na_2SO_4, pH 8.7, [MV] = 0,5 mM, [EDTA] = 0.0011 M	0.15	380, 480
197	$[Ru(bpy)_3]^{2+}$	methyl viologen	0.30 M Na_2SO_4, pH 11, [MV] = 0,5 mM, [EDTA] = 0.010 M	0.20	380, 480
198	$[Ru(bpy)_3]^{2+}$	methyl viologen	0.33 M Na_2SO_4, pH 11, [MV] = 0.5 mM, [EDTA] = 0.001 M	0.10	380, 480
199	$[Ru(bpy)_3]^{2+}$	methyl viologen	0.05 M NaCl	0.17	84
200	$[Ru(bpy)_3]^{2+}$	methyl viologen	0.05M $NaClO_4$	0.13	84
201	$[Ru(bpy)_3]^{2+}$	methyl viologen	0.05M NaH_2PO_4	0.171	84
202	$[Ru(bpy)_3]^{2+}$	methyl viologen	0.5M NaCl	0.24	379
203	$[Ru(bpy)_3]^{2+}$	methyl viologen	0.5M H_2SO_4	0.24	379
204	$[Ru(bpy)_3]^{2+}$	methyl viologen	0.5M $NaNO_3$	0.2	379
205	$[Ru(bpy)_3]^{2+}$	methyl viologen	0.5M Na_2SO_5	0.22	379
206	$[Ru(bpy)_3]^{2+}$	methyl viologen	0.6M $NaClO_4$	0.062	84
207	$[Ru(bpy)_3]^{2+}$	methyl viologen	0.6M NaH_2PO_4	0.152	84
208	$[Ru(bpy)_3]^{2+}$	methyl viologen	H_2O, μ = 0.08 M NaCl	0.34	111
209	$[Ru(bpy)_3]^{2+}$	methyl viologen	0.8M Na_2SO_4, [MV] = 20 mM	0.10	380, 480
210	$[Ru(bpy)_3]^{2+}$	methyl viologen	H_2O, [MV] = 10 mM, $[C_2O_4(^{2-})]$ = 0.8 M	0.09	380, 480
211	$[Ru(bpy)_3]^{2+}$	methyl viologen	H_2O, pH 4.7, [MV] = 10 mM, [EDTA] = 0.08 M	0.15	380, 480
212	$[Ru(bpy)_3]^{2+}$	methyl viologen	0.23M Na_2SO_4, [MV] = 1 mM, $[C_2O_4(^{2-})]$ = 0.10 M	0.12	380, 480
213	$[Ru(bpy)_3]^{2+}$	methyl viologen	0.23M Na_2SO_4, [MV] = 2 mM, $[C_2O_4(^{2-})]$ = 0.10 M	0.14	380, 480
214	$[Ru(bpy)_3]^{2+}$	methyl viologen	0.90M Na_2SO_4, [MV] = 2 mM, $[C_2O_4(^{2-})]$ = 0.10 M	0.08	380, 480
215	$[Ru(bpy)_3]^{2+}$	methyl viologen	H_2O, μ = 0.16 M NaCl	0.32	111
216	$[Ru(bpy)_3]^{2+}$	methyl viologen	0.30 M Na_2SO_4, pH 11, [MV] = 1 mM, [EDTA] = 0.010 M	0.18	380, 480
217	$[Ru(bpy)_3]^{2+}$	methyl viologen	0.30 M Na_2SO_4, pH 11, [MV] = 2 mM, [EDTA] = 0.010 M	0.16	380, 480
218	$[Ru(bpy)_3]^{2+}$	methyl viologen	0.31 M Na_2SO_4, pH 11, [MV] = 2 mM, [EDTA] = 0.001 M	0.13	380, 480
219	$[Ru(bpy)_3]^{2+}$	methyl viologen	0.33 M Na_2SO_4, pH 11, [MV] = 1 mM, [EDTA] = 0.001 M	0.11	380, 480
220	$[Ru(bpy)_3]^{2+}$	methyl viologen	0.33 M Na_2SO_4, pH 11, [MV] = 2 mM, [EDTA] = 0.001 M	0.12	380, 480
221	$[Ru(bpy)_3]^{2+}$	methyl viologen	H_2O, μ = 0.35 M NaCl	0.29	111
222	$[Ru(bpy)_3]^{2+}$	methyl viologen	H_2O, μ = 0.52 M NaCl	0.25	111
223	$[Ru(bpy)_3]^{2+}$	methyl viologen	CH_3CN/H_2O 1:1	0.19	365
224	$[Ru(bpy)_3]^{2+}$	methyl viologen	$H_2O:CH_3CN$ 1:1 + 20% ethylene glycol	0.16	365
225	$[Ru(bpy)_3]^{2+}$	methyl viologen	$H_2O:CH_3CN$ 1:1 + 40% ethylene glycol	0.13	365
226	$[Ru(bpy)_3]^{2+}$	methyl viologen	$H_2O:CH_3CN$ 1:1 + 60% ethylene glycol	0.09	365
227	$[Ru(bpy)_3]^{2+}$	methyl viologen	$H_2O:CH_3CN$ 1:1 + 80% ethylene glycol	0.06	365
228	$[Ru(bpy)_3]^{2+}$	methyl viologen	$H_2O:CH_3CN$ 1:1 + 95% ethylene glycol	0.05	365
229	$[Ru(bpy)_3]^{2+}$	methyl viologen	H_2O, μ = 1.6 M NaCl	0.22	111
230	$[Ru(bpy)_3]^{2+}$	methyl viologen	CH_3CN/H_2O 1:4	0.2	383
231	$[Ru(bpy)_3]^{2+}$	methyl viologen	H_2O, pH 4.7, [MV] = 1 mM, [EDTA] = 0.080 M	0.12	380, 480
232	$[Ru(bpy)_3]^{2+}$	methyl viologen	H_2O, pH 4.7, [MV] = 2 mM, [EDTA] = 0.070 M	0.14	380, 480
233	$[Ru(bpy)_3]^{2+}$	methyl viologen	H_2O, pH 4.7, [MV] = 2 mM, [EDTA] = 0.010 M	0.17	380, 480
234	$[Ru(bpy)_3]^{2+}$	methyl viologen	H_2O, pH 4.7, [MV] = 10 mM, [EDTA] = 0.001 M	0.20	380, 480

235	$[Ru(bpy)_3]^{2+}$	methyl viologen	0.31 M Na_2SO_4, pH 4.7, [MV] = 20 mM, [EDTA] = 0.001 M	0.12	380, 480
236	$[Ru(bpy)_3]^{2+}$	methyl viologen	0.33 M Na_2SO_4, pH 4.7, [MV] = 2 mM, [EDTA] = 0.001 M	0.13	380, 480
237	$[Ru(bpy)_3]^{2+}$	methyl viologen	0.33 M Na_2SO_4, pH 4.7, [MV] = 2 mM, [EDTA] = 0.005 M	0.13	380, 480
238	$[Ru(bpy)_3]^{2+}$	methyl viologen	0.18 M Na_2SO_4, pH 8.7, [MV] = 1 mM, [EDTA] = 0.010 M	0.17	380, 480
239	$[Ru(bpy)_3]^{2+}$	methyl viologen	0.18 M Na_2SO_4, pH 8.7, [MV] = 2 mM, [EDTA] = 0.010 M	0.17	380, 480
240	$[Ru(bpy)_3]^{2+}$	methyl viologen	0.20 M Na_2SO_4, pH 8.7, [MV] = 1 mM, [EDTA] = 0.001 M	0.14	380, 480
241	$[Ru(bpy)_3]^{2+}$	methyl viologen	0.20 M Na_2SO_4, pH 8.7, [MV] = 2 mM, [EDTA] = 0.001 M	0.14	380, 480
242	$[Ru(bpy)_3]^{2+}$	methyl viologen	0.31 M Na_2SO_4, pH 8.7, [MV] = 20 mM, [EDTA] = 0.001 M	0.13	380, 480
243	$[Ru(bpy)_3]^{2+}$	N,N,N',N'-tetramethyl-1,4-phenylenediamine	DMF	1.08	514
244	$[Ru(bpy)_3]^{2+}$	N,N,N',N'-tetramethyl-1,4-phenylenediamine	CH_3CN/H_2O 1:1	0.84	415
245	$[Ru(bpy)_3]^{2+}$	N,N,N',N'-tetramethyl-1,6-pyrenediamine	DMF	1	514
246	$[Ru(bpy)_3]^{2+}$	N,N,N',N'-tetramethylbenzidine	DMF	1.11	514
247	$[Ru(bpy)_3]^{2+}$	N,N,N',N'-tetramethylbenzidine	CH_3CN/H_2O 1:1	0.59	415
248	$[Ru(bpy)_3]^{2+}$	$Na_2S_2O_8$	H_2O	0.75	518
249	$[Ru(bpy)_3]^{2+}$	*p*-benzoquinone	5 mM phosphate buffer, μ = 0.04M	0.08	515
250	$[Ru(bpy)_3]^{2+}$	phenothiazine	DMF	1.12	514
251	$[Ru(bpy)_3]^{2+}$	phenothiazine	CH_3CN/H_2O 1:1	0.66	415
252	$[Ru(bpy)_3]^{2+}$	tetra- *n* -butylammonium iodide	CH_2Cl_2	0.5	386
253	$[Ru(bpy)_3]^{2+}$	Tl(III)	HCl 3M	0.14	379
254	$[Ru(bpy)_3]^{2+}$	Tl(III)	H_2SO_4 0.5M	2	379
255	$[Ru(bpy)_3]^{2+}$	tri-*p*-tolylamine	CH_3CN	1	511
256	$[Ru(bpy)_3]^{2+}$	tri-*p*-tolylamine	CH_3CN	1	511
257	$[Ru(bpy)_3]^{2+}$	triethylamine	CH_2Cl_2	0.15	429
258	$[Ru(bpy)_3]^{2+}$	triethylamine	CH_3CN	0.39	429
259	$[Ru(bpy)_3]^{2+}$	triethylamine	DMF	0.58	429
260	$[Ru(bpy)_3]^{2+}$	trimethyl-*p*-benzoquinone	6 mM phosphate buffer, μ = 0.04M	<0.01	515
261	$[Ru(bpy)_3]^{2+}$	β-naphthylamine	DMF	1.07	514
262	$[Ru(bpz)(dpq)_2]^{2+}$	Methyl Viologen	H_2O	1.07	513
263	$[Ru(bpz)_2(bpm)]^{2+}$	EDTA	H_2O, pH = 8.5, μ = 1.0M (Na_2SO_4)	0.62	420
264	$[Ru(bpz)_2(bpm)]^{2+}$	triethanolamine	Propylene carbonate	0.39	421
265	$[Ru(bpz)_2(bpm)]^{2+}$	triethanolamine	CH_3CN	0.80	421
266	$[Ru(bpz)_2(bpm)]^{2+}$	triethanolamine	H_2O	0.493	395
267	$[Ru(bpz)_2(bpm)]^{2+}$	triethanolamine	H_2O, pH = 10.0, μ = 1.0M (Na_2SO_4)	0.52	420
268	$[Ru(bpz)_2(bpm)]^{2+}$	triethanolamine + methyl viologen	H_2O, pH 10	0.52	420
269	$[Ru(bpz)_2(bpm)]^{2+}$	triethanolamine + methyl viologen	H_2O, pH 8.5	0.62	420
270	$[Ru(bpz)_2(bpy)]^{2+}$	EDTA	H_2O, pH = 8.5, μ = 1.0M (Na_2SO_4)	0.55	420
271	$[Ru(bpz)_2(bpy)]^{2+}$	triethanolamine	Propylene carbonate	0.42	421
272	$[Ru(bpz)_2(bpy)]^{2+}$	triethanolamine	CH_3CN	0.85	421
273	$[Ru(bpz)_2(bpy)]^{2+}$	triethanolamine	H_2O	0.489	395

274	$[Ru(bpz)_2(bpy)]^{2+}$	triethanolamine	H_2O, pH = 10.0, μ = 1.0M (Na_2SO_4)	0.49	420
275	$[Ru(bpz)_2(bpy)]^{2+}$	triethanolamine + methyl viologen	H_2O, pH 10	0.49	420
276	$[Ru(bpz)_2(bpy)]^{2+}$	triethanolamine + methyl viologen	H_2O, pH 8.5	0.55	420
277	$[Ru(bpz)_2(CN)_2]$	methyl viologen	0.3M Na_2SO_4	0.11	510
278	$[Ru(bpz)_2(deeb)]^{2+}$	tetra-*n*-butylammonium iodide	CH_2Cl_2	0.042	230
279	$[Ru(bpz)_2(tmam)]^{4+}$	acetyl-salicylate	CH_3CN	0.6-0.7	392
280	$[Ru(bpz)_2(tmam)]^{4+}$	Cl-salicylate	CH_3CN	0.6-0.7	392
281	$[Ru(bpz)_2(tmam)]^{4+}$	F-salicylate	CH_3CN	0.6-0.7	392
282	$[Ru(bpz)_2(tmam)]^{4+}$	H-salicylate	CH_3CN	0.6-0.7	392
283	$[Ru(bpz)_2(tmam)]^{4+}$	Me-salicylate	CH_3CN	0.6-0.7	392
284	$[Ru(bpz)_2(tmam)]^{4+}$	OH-salicylate	CH_3CN	0.6-0.7	392
285	$[Ru(bpz)_2(tmam)]^{4+}$	OMe-salicylate	CH_3CN	0.6-0.7	392
286	$[Ru(bpz)_3]^{2+}$	1,2-dimethoxybenzene	CH_3CN/H_2O 1:1	0.78	414
287	$[Ru(bpz)_3]^{2+}$	1,2,4-trimethoxybenzene	CH_3CN/H_2O 1:1	0.71	414
288	$[Ru(bpz)_3]^{2+}$	1,3,5-trimethoxybenzene	CH_3CN/H_2O 1:1	0.86	414
289	$[Ru(bpz)_3]^{2+}$	1,4-anisidine	CH_3CN/H_2O 1:1	0.64	414
290	$[Ru(bpz)_3]^{2+}$	1,4-dimethoxybenzene	CH_3CN/H_2O 1:1	0.64	414
291	$[Ru(bpz)_3]^{2+}$	3,3'-dimethylbenzidine	CH_3CN/H_2O 1:1	0.57	414
292	$[Ru(bpz)_3]^{2+}$	4,4'-bipyridinium-N,N'-di(propylsulphonate)	CH_3CN/H_2O 1:1, μ = 0.2M NaCl	0.09	369
293	$[Ru(bpz)_3]^{2+}$	diphenyl-1,4-phenylenediamine	CH_3CN/H_2O 1:1	0.71	414
294	$[Ru(bpz)_3]^{2+}$	diphenylamine	CH_3CN/H_2O 1:1	0.55	414
295	$[Ru(bpz)_3]^{2+}$	EDTA	H_2O, pH = 8.5, μ = 1.0M (Na_2SO_4)	0.70	420
296	$[Ru(bpz)_3]^{2+}$	methyl viologen	CH_3CN/H_2O 1:1, μ = 0.2M NaCl	0.19	369
297	$[Ru(bpz)_3]^{2+}$	N,N,N',N'-tetramethyl-1,4-phenylenediamine	CH_3CN/H_2O 1:1	0.88	414
298	$[Ru(bpz)_3]^{2+}$	phenothiazine	CH_3CN/H_2O 1:1	0.61	414
299	$[Ru(bpz)_3]^{2+}$	triethanolamine	Propylene carbonate	0.38	421
300	$[Ru(bpz)_3]^{2+}$	triethanolamine	CH_3CN	0.77	421
301	$[Ru(bpz)_3]^{2+}$	triethanolamine	H_2O	0.501	395
302	$[Ru(bpz)_3]^{2+}$	triethanolamine	H_2O, pH = 10.0, μ = 1.0M (Na_2SO_4)	0.49	420
303	$[Ru(bpz)_3]^{2+}$	triethanolamine	H_2O, pH = 10.0, μ = 1.0M (Na_2SO_4)	0.66	420
304	$[Ru(bpz)_3]^{2+}$	triethanolamine + methyl viologen	H_2O, pH 10	0.49	420
305	$[Ru(bpz)_3]^{2+}$	triethanolamine + methyl viologen	H_2O, pH 8.5	0.7	420
306	$[Ru(bpz)_3]^{2+}$	tri-*p*-anisylamine	CH_3CN	0.58	440
307	$[Ru(bpz)_3]^{2+}$	tri-*p*-PEG_3-arylamine	CH_3CN	0.62	440
308	$[Ru(bpz)_3]^{2+}$	tri-*p*-PEG_7-arylamine	CH_3CN	0.78	440
309	$[Ru(bpz)_3]^{2+}$	Tris(4-chlorophenyl)amine	CH_3CN	0.65	440
310	$[Ru(bpz)_3]^{2+}$	Tris(4-bromophenyl)amine	CH_3CN	0.87	440
311	$[Ru(bpz)_3]^{2+}$	Tris(4-iodophenyl)amine	CH_3CN	0.60	440
312	$[Ru(bpz)_3]^{2+}$	N,N-dimethylaniline	CH_3CN	0.73	440
313	$[Ru(bpz)_3]^{2+}$	N,N-dimethyltoluidine	CH_3CN	0.85	440

314	$[Ru(bpz)_3]^{2+}$	4-methoxy-N,N'-dimethylaniline	CH_3CN	0.69	440
315	$[Ru(bpz)_3]^{2+}$	THIQ	CH_3CN	0.35	440
316	$[Ru(bpz)_3]^{2+}$	triethylamine	CH_3CN	0.37	440
317	$[Ru(bpz)_3]^{2+}$	diisopropylethylamine	CH_3CN	0.44	440
318	$[Ru(dbpy)_2(im)_2]^{2+}$	methyl viologen	CH_3CN/H_2O 1:4	0.16	383
319	$[Ru(dcb)_3]^{4-}$	$[Fe(CN)_6]^{4-}$	H_2O	0.27	384
320	$[Ru(dcb)_3]^{4-}$	$[Mo(CN)_6]^{4-}$	0.1M K_2HPO_4	0.74	384
321	$[Ru(dcb)_3]^{4-}$	$[Os(CN)_6]^{4-}$	0.1M K_2HPO_4	0.06	384
322	$[Ru(dcb)_3]^{4-}$	$[W(CN)_8]^{4-}$	0.1M K_2HPO_4	0.67	384
323	$[Ru(deeb)_2(bpy)]^{2+}$	methyl viologen	CH_3CN/H_2O 1:1, μ = 0.2M NaCl	0.18	369
324	$[Ru(deeb)_3]^{2+}$	methyl viologen	CH_3CN/H_2O 1:1, μ = 0.3M NaCl	0.31	369
325	$[Ru(deeb)_3]^{2+}$	methyl viologen	CH_3CN/H_2O 1:9, μ = 0.3M KCl	0.15	383
326	$[Ru(deeb)_3]^{2+}$	methyl viologen	H_2O/CH_3CN 4:1	0.23	383
327	$[Ru(dmbpy)(CN)_4]^{2-}$	methyl Viologen	H_2O	0.25	512
328	$[Ru(dmph)_3]^{2+}$	methyl viologen	8 :5 (v/v) 0.1M $TEAClO_4/CH_3CN$ to CH_2Cl_2	0.27	82
329	$[Ru(dpp)_3]^{2+}$	tri-*p*-tolylamine	CH_3CN	0.93	511
330	$[Ru(dpphen)_3]^{2+}$	1,4-anisdine	CH_3CN/H_2O 1:1	0.4	415
331	$[Ru(dpphen)_3]^{2+}$	1,4-phenylenediamine	CH_3CN/H_2O 1:1	0.46	415
332	$[Ru(dpphen)_3]^{2+}$	1,4-toluidine	CH_3CN/H_2O 1:1	0.46	415
333	$[Ru(dpphen)_3]^{2+}$	3,3'-dimethylbenzidine	CH_3CN/H_2O 1:1	0.2	415
334	$[Ru(dpphen)_3]^{2+}$	diphenyl-1,4-phenylenediamine	CH_3CN/H_2O 1:1	0.2	415
335	$[Ru(dpphen)_3]^{2+}$	diphenylamine	CH_3CN/H_2O 1:1		415
336	$[Ru(dpphen)_3]^{2+}$	methyl viologen	CH_3CN/H_2O 1:4	0.07	383
337	$[Ru(dpphen)_3]^{2+}$	N,N,N',N'-tetramethyl-1,4-phenylenediamine	CH_3CN/H_2O 1:1	0.36	415
338	$[Ru(dpphen)_3]^{2+}$	N,N,N',N'-tetramethylbenzidine	CH_3CN/H_2O 1:1	0.16	415
339	$[Ru(dpphen)_3]^{2+}$	phenothiazine	CH_3CN/H_2O 1:1	0.32	415
340	$[Ru(dpphen)_3]^{2+}$	tri-*p*-tolylamine	CH_3CN	0.93	511
341	$[Ru(dtb)_2(dea)]^{2+}$	tetra- *n* -butylammonium iodide	CH_2Cl_2	0.35	88
342	$[Ru(HAT)_3]^{2+}$	adenosine-5'-monophosphate	H_2O + 0.1 M Phosphate buffer pH7	0.2	519
343	$[Ru(HAT)_3]^{2+}$	guanosine-5'-monophosphate	H_2O	0.23	519
344	$[Ru(phen)_2(mim)_2]^{2+}$	methyl viologen	H_2O/CH_3CN 4:1	0.18	383
345	$[Ru(phen)_3]^{2+}$	$[Co(diamsar)]^{2+}$	H_2O + 0.2M LiCl, 0.05M N-ethylmorpholine, pH 8.3	0.65	419
346	$[Ru(phen)_3]^{2+}$	$[Co(diamsarH_2)]^{4+}$	H_2O + 0.1M HCl + 0+1M LiCl	1	419
347	$[Ru(phen)_3]^{2+}$	$[Co(sep)]^{2+}$	H_2O + 0.2M LiCl	0.53	419
348	$[Ru(phen)_3]^{2+}$	$CuSO_4$	0.5M H_2SO_4	0.54	382
349	$[Ru(phen)_3]^{2+}$	1,4-anisdine	CH_3CN/H_2O 1:1	0.65	415
350	$[Ru(phen)_3]^{2+}$	1,4-phenylenediamine	CH_3CN/H_2O 1:1	0.7	415
351	$[Ru(phen)_3]^{2+}$	1,4-toluidine	CH_3CN/H_2O 1:1		415
352	$[Ru(phen)_3]^{2+}$	3,3'-dimethylbenzidine	CH_3CN/H_2O 1:1	0.33	415
353	$[Ru(phen)_3]^{2+}$	diphenyl-1,4-phenylenediamine	CH_3CN/H_2O 1:1	0.46	415
354	$[Ru(phen)_3]^{2+}$	diphenylamine	CH_3CN/H_2O 1:1	0.65	415

355	$[Ru(phen)_3]^{2+}$	methyl viologen	H_2O/CH_3CN 9:1, μ = 0.3M KCl	0.12	[383]
356	$[Ru(phen)_3]^{2+}$	methyl viologen	CH_3CN/H_2O 1:4	0.2	[383]
357	$[Ru(phen)_3]^{2+}$	N,N,N',N'-tetramethyl-1,4-phenylenediamine	CH_3CN/H_2O 1:1	0.51	[415]
358	$[Ru(phen)_3]^{2+}$	N,N,N',N'-tetramethylbenzidine	CH_3CN/H_2O 1:1		[415]
359	$[Ru(phen)_3]^{2+}$	phenothiazine	CH_3CN/H_2O 1:1	0.47	[415]
360	$[Ru(TAP)_2(HAT)]^{2+}$	adenosine-5'-monophosphate	H_2O + 0.1 M Phosphate buffer pH7	0.32	[519]
361	$[Ru(TAP)_2(HAT)]^{2+}$	guanosine-5'-monophosphate	H_2O	0.35	[519]
362	$[Ru(TAP)_3]^{2+}$	adenosine-5'-monophosphate	H_2O + 0.1 M Phosphate buffer pH7	0.28	[519]
363	$[Ru(TAP)_3]^{2+}$	guanosine-5'-monophosphate	H_2O	0.3	[519]

6.9) Tabulated values for the cage-escape yields of $[Ru(bpy)_3]^{2+}$ in different electrolytes and at different temperatures

Table 19 gathers the cage-escape yields of $[Ru(bpy)_3]^{2+}$ with several quenchers in different electrolytes and at different temperatures. Electron transfer quenching sensitized by ruthenium derivatives occur primarily from triplet states. For a specific excited state description, see relevant reference(s).

Table 19. Cage-escape yields *(ϕ_{ce})* for $[Ru(bpy)_3]^{2+}$ in different electrolytes and at different temperatures.

Entry	Quencher	Solvent	ϕ_{ce}	T (°C)	Ref
1	1,4-phenylenediamine	CH_3CN/H_2O	0.44	10	[423]
2	1,4-phenylenediamine	CH_3CN/H_2O	0.49	20	[423]
3	1,4-phenylenediamine	CH_3CN/H_2O	0.5	30	[423]
4	1,4-phenylenediamine	CH_3CN/H_2O	0.49	40	[423]
5	1,4-phenylenediamine	CH_3CN/H_2O	0.51	50	[423]
6	1,4-phenylenediamine	CH_3CN/H_2O	0.5	60	[423]
7	3,3'-dimethylbenzidine	CH_3CN/H_2O	0.25	10	[423]
8	3,3'-dimethylbenzidine	CH_3CN/H_2O	0.36	20	[423]
9	3,3'-dimethylbenzidine	CH_3CN/H_2O	0.35	30	[423]
10	3,3'-dimethylbenzidine	CH_3CN/H_2O	0.37	40	[423]
11	3,3'-dimethylbenzidine	CH_3CN/H_2O	0.41	50	[423]
12	3,3'-dimethylbenzidine	CH_3CN/H_2O	0.45	60	[423]
13	3,3',5,5'-tetramethylbenzidine	CH_3CN/H_2O	0.23	10	[423]
14	3,3',5,5'-tetramethylbenzidine	CH_3CN/H_2O	0.33	20	[423]
15	3,3',5,5'-tetramethylbenzidine	CH_3CN/H_2O	0.32	30	[423]
16	3,3',5,5'-tetramethylbenzidine	CH_3CN/H_2O	0.39	40	[423]
17	3,3',5,5'-tetramethylbenzidine	CH_3CN/H_2O	0.41	50	[423]
18	3,3',5,5'-tetramethylbenzidine	CH_3CN/H_2O	0.4	60	[423]
19	diphenylamine	CH_3CN/H_2O	0.4	10	[423]
20	diphenylamine	CH_3CN/H_2O	0.65	20	[423]
21	diphenylamine	CH_3CN/H_2O	0.53	30	[423]

22	diphenylamine	CH_3CN/H_2O	0.58	40	[423]
23	diphenylamine	CH_3CN/H_2O	0.49	50	[423]
24	diphenylamine	CH_3CN/H_2O	0.59	60	[423]
25	methyl viologen	1-butyl-3-methylimidazolium hexafluorophosphate	0.35	20	[385]
26	methyl viologen	1-butyl-3-methylimidazolium hexafluorophosphate	0.8	65	[385]
27	methyl viologen	CH_3CN	0.25	10	[422]
28	methyl viologen	CH_3CN	0.29	20	[385]
29	methyl viologen	CH_3CN	0.29	20	[422]
30	methyl viologen	CH_3CN	0.33	30	[422]
31	methyl viologen	CH_3CN	0.37	40	[422]
32	methyl viologen	CH_3CN	0.40	50	[422]
33	methyl viologen	CH_3CN	0.45	65	[385]
34	methyl viologen	CH_3CN	0.45	65	[422]
35	methyl viologen	CH_3CN/H_2O 2:8	0.14	10	[422]
36	methyl viologen	CH_3CN/H_2O 2:8	0.17	20	[422]
37	methyl viologen	CH_3CN/H_2O 2:8	0.20	30	[422]
38	methyl viologen	CH_3CN/H_2O 2:8	0.22	40	[422]
39	methyl viologen	CH_3CN/H_2O 2:8	0.25	50	[422]
40	methyl viologen	CH_3CN/H_2O 2:8	0.32	65	[422]
41	methyl viologen	CH_3CN/H_2O 3:7	0.19	10	[422]
42	methyl viologen	CH_3CN/H_2O 3:7	0.21	20	[422]
43	methyl viologen	CH_3CN/H_2O 3:7	0.24	30	[422]
44	methyl viologen	CH_3CN/H_2O 3:7	0.28	40	[422]
45	methyl viologen	CH_3CN/H_2O 3:7	0.32	50	[422]
46	methyl viologen	CH_3CN/H_2O 3:7	0.38	65	[422]
47	methyl viologen	CH_3CN/H_2O 6:4	0.2	10	[422]
48	methyl viologen	CH_3CN/H_2O 6:4	0.24	20	[422]
49	methyl viologen	CH_3CN/H_2O 6:4	0.27	30	[422]
50	methyl viologen	CH_3CN/H_2O 6:4	0.31	40	[422]
51	methyl viologen	CH_3CN/H_2O 6:4	0.33	50	[422]
52	methyl viologen	CH_3CN/H_2O 6:4	0.38	65	[422]
53	methyl viologen	CH_3CN/H_2O 8:2	0.24	10	[422]
54	methyl viologen	CH_3CN/H_2O 8:2	0.27	20	[422]
55	methyl viologen	CH_3CN/H_2O 8:2	0.32	30	[422]
56	methyl viologen	CH_3CN/H_2O 8:2	0.35	40	[422]
57	methyl viologen	CH_3CN/H_2O 8:2	0.39	50	[422]
58	methyl viologen	CH_3CN/H_2O 8:2	0.40	65	[422]
59	methyl viologen	H_2O	0.16	5	[374]
60	methyl viologen	H_2O	0.096	7	[422]
61	methyl viologen	H_2O	0.11	7	[422]
62	methyl viologen	H_2O	0.12	7	[422]
63	methyl viologen	H_2O	0.13	7	[422]
64	methyl viologen	H_2O	0.15	7	[422]

65	methyl viologen	H_2O	0.15	7	[422]
66	methyl viologen	H_2O	0.16	7	[422]
67	methyl viologen	H_2O	0.16	7	[422]
68	methyl viologen	H_2O	0.18	7	[422]
69	methyl viologen	H_2O	0.088	10	[84]
70	methyl viologen	H_2O	0.066	10	[84]
71	methyl viologen	H_2O	0.10	10	[422]
72	methyl viologen	H_2O	0.15	10	[84]
73	methyl viologen	H_2O	0.11	15	[422]
74	methyl viologen	H_2O	0.12	15	[422]
75	methyl viologen	H_2O	0.14	15	[422]
76	methyl viologen	H_2O	0.15	15	[422]
77	methyl viologen	H_2O	0.17	15	[374]
78	methyl viologen	H_2O	0.17	15	[422]
79	methyl viologen	H_2O	0.17	15	[422]
80	methyl viologen	H_2O	0.18	15	[422]
81	methyl viologen	H_2O	0.20	15	[422]
82	methyl viologen	H_2O	0.13	20	[422]
83	methyl viologen	H_2O	0.18	20	[374]
84	methyl viologen	H_2O	0.075	25	[84]
85	methyl viologen	H_2O	0.11	25	[84]
86	methyl viologen	H_2O	0.11	25	[422]
87	methyl viologen	H_2O	0.13	25	[422]
88	methyl viologen	H_2O	0.15	25	[422]
89	methyl viologen	H_2O	0.16	25	[422]
90	methyl viologen	H_2O	0.17	25	[84]
91	methyl viologen	H_2O	0.18	25	[374]
92	methyl viologen	H_2O	0.18	25	[422]
93	methyl viologen	H_2O	0.19	25	[422]
94	methyl viologen	H_2O	0.19	25	[422]
95	methyl viologen	H_2O	0.22	25	[422]
96	methyl viologen	H_2O	0.13	30	[422]
97	methyl viologen	H_2O	0.19	33	[374]
98	methyl viologen	H_2O	0.080	35	[84]
99	methyl viologen	H_2O	0.12	35	[84]
100	methyl viologen	H_2O	0.13	35	[422]
101	methyl viologen	H_2O	0.14	35	[422]
102	methyl viologen	H_2O	0.16	35	[422]
103	methyl viologen	H_2O	0.17	35	[422]
104	methyl viologen	H_2O	0.19	35	[84]
105	methyl viologen	H_2O	0.20	35	[422]
106	methyl viologen	H_2O	0.20	35	[422]
107	methyl viologen	H_2O	0.21	35	[422]

108	methyl viologen	H_2O	0.23	35	[422]
109	methyl viologen	H_2O	0.15	40	[422]
110	methyl viologen	H_2O	0.2	42	[374]
111	methyl viologen	H_2O	0.086	45	[84]
112	methyl viologen	H_2O	0.13	45	[84]
113	methyl viologen	H_2O	0.13	45	[422]
114	methyl viologen	H_2O	0.16	45	[422]
115	methyl viologen	H_2O	0.17	45	[422]
116	methyl viologen	H_2O	0.19	45	[422]
117	methyl viologen	H_2O	0.21	45	[84]
118	methyl viologen	H_2O	0.22	45	[422]
119	methyl viologen	H_2O	0.22	45	[422]
120	methyl viologen	H_2O	0.22	45	[422]
121	methyl viologen	H_2O	0.25	45	[422]
122	methyl viologen	H_2O	0.16	50	[422]
123	methyl viologen	H_2O	0.21	52	[374]
124	methyl viologen	H_2O	0.14	55	[422]
125	methyl viologen	H_2O	0.17	55	[422]
126	methyl viologen	H_2O	0.19	55	[422]
127	methyl viologen	H_2O	0.21	55	[422]
128	methyl viologen	H_2O	0.24	55	[422]
129	methyl viologen	H_2O	0.24	55	[422]
130	methyl viologen	H_2O	0.24	55	[422]
131	methyl viologen	H_2O	0.27	55	[422]
132	methyl viologen	H_2O	0.101	60	[84]
133	methyl viologen	H_2O	0.15	60	[84]
134	methyl viologen	H_2O	0.22	60	[84]
135	methyl viologen	H_2O	0.22	61	[374]
136	methyl viologen	H_2O	0.16	65	[422]
137	methyl viologen	H_2O	0.18	65	[422]
138	methyl viologen	H_2O	0.18	65	[422]
139	methyl viologen	H_2O	0.21	65	[422]
140	methyl viologen	H_2O	0.22	65	[422]
141	methyl viologen	H_2O	0.26	65	[422]
142	methyl viologen	H_2O	0.26	65	[422]
143	methyl viologen	H_2O	0.26	65	[422]
144	methyl viologen	H_2O	0.30	65	[422]
145	methyl viologen	H_2O	0.23	69	[374]
146	methyl viologen	$H_2O + CaCl_2$ 0.017 M	0.17	25	[381]
147	methyl viologen	$H_2O + CaCl_2$ 0.017 M	0.19	40	[381]
148	methyl viologen	$H_2O + CaCl_2$ 0.017 M	0.22	60	[381]
149	methyl viologen	$H_2O + CaCl_2$ 0.033 M	0.16	25	[381]
150	methyl viologen	$H_2O + CaCl_2$ 0.033 M	0.17	40	[381]

151	methyl viologen	H_2O + $CaCl_2$ 0.033 M	0.2	60	[381]
152	methyl viologen	H_2O + $CaCl_2$ 0.067 M	0.15	25	[381]
153	methyl viologen	H_2O + $CaCl_2$ 0.067 M	0.17	40	[381]
154	methyl viologen	H_2O + $CaCl_2$ 0.067 M	0.19	60	[381]
155	methyl viologen	H_2O + $CaCl_2$ 0.13 M	0.14	25	[381]
156	methyl viologen	H_2O + $CaCl_2$ 0.13 M	0.16	40	[381]
157	methyl viologen	H_2O + $CaCl_2$ 0.13 M	0.18	60	[381]
158	methyl viologen	H_2O + $CaCl_2$ 0.27 M	0.14	25	[381]
159	methyl viologen	H_2O + $CaCl_2$ 0.27 M	0.13	40	[381]
160	methyl viologen	H_2O + $CaCl_2$ 0.27 M	0.15	60	[381]
161	methyl viologen	H_2O + CsCl 0.05 M	0.16	10	[381]
162	methyl viologen	H_2O + CsCl 0.05 M	0.17	25	[381]
163	methyl viologen	H_2O + CsCl 0.05 M	0.17	35	[381]
164	methyl viologen	H_2O + CsCl 0.05 M	0.2	45	[381]
165	methyl viologen	H_2O + CsCl 0.05 M	0.2	60	[381]
166	methyl viologen	H_2O + CsCl 0.1 M	0.13	10	[381]
167	methyl viologen	H_2O + CsCl 0.1 M	0.12	25	[381]
168	methyl viologen	H_2O + CsCl 0.1 M	0.15	35	[381]
169	methyl viologen	H_2O + CsCl 0.1 M	0.18	45	[381]
170	methyl viologen	H_2O + CsCl 0.1 M	0.17	60	[381]
171	methyl viologen	H_2O + CsCl 0.2 M	0.13	10	[381]
172	methyl viologen	H_2O + CsCl 0.2 M	0.1	25	[381]
173	methyl viologen	H_2O + CsCl 0.2 M	0.16	35	[381]
174	methyl viologen	H_2O + CsCl 0.2 M	0.2	45	[381]
175	methyl viologen	H_2O + CsCl 0.2 M	0.19	60	[381]
176	methyl viologen	H_2O + CsCl 0.4 M	0.11	10	[381]
177	methyl viologen	H_2O + CsCl 0.4 M	0.09	25	[381]
178	methyl viologen	H_2O + CsCl 0.4 M	0.14	35	[381]
179	methyl viologen	H_2O + CsCl 0.4 M	0.18	45	[381]
180	methyl viologen	H_2O + CsCl 0.4 M	0.17	60	[381]
181	methyl viologen	H_2O + CsCl 0.6 M	0.08	25	[381]
182	methyl viologen	H_2O + CsCl 0.8 M	0.1	10	[381]
183	methyl viologen	H_2O + CsCl 0.8 M	0.08	25	[381]
184	methyl viologen	H_2O + CsCl 0.8 M	0.12	35	[381]
185	methyl viologen	H_2O + CsCl 0.8 M	0.14	45	[381]
186	methyl viologen	H_2O + CsCl 0.8 M	0.14	60	[381]
187	methyl viologen	H_2O + $LaCl_3$ 0.0083 M	0.12	10	[381]
188	methyl viologen	H_2O + $LaCl_3$ 0.0083 M	0.16	25	[381]
189	methyl viologen	H_2O + $LaCl_3$ 0.0083 M	0.2	35	[381]
190	methyl viologen	H_2O + $LaCl_3$ 0.0083 M	0.23	45	[381]
191	methyl viologen	H_2O + $LaCl_3$ 0.0083 M	0.24	60	[381]
192	methyl viologen	H_2O + $LaCl_3$ 0.017 M	0.11	10	[381]
193	methyl viologen	H_2O + $LaCl_3$ 0.017 M	0.2	25	[381]

194	methyl viologen	H_2O + $LaCl_3$ 0.017 M	0.21	35	[381]
195	methyl viologen	H_2O + $LaCl_3$ 0.017 M	0.16	45	[381]
196	methyl viologen	H_2O + $LaCl_3$ 0.017 M	0.24	60	[381]
197	methyl viologen	H_2O + $LaCl_3$ 0.033 M	0.12	10	[381]
198	methyl viologen	H_2O + $LaCl_3$ 0.033 M	0.17	25	[381]
199	methyl viologen	H_2O + $LaCl_3$ 0.033 M	0.19	35	[381]
200	methyl viologen	H_2O + $LaCl_3$ 0.033 M	0.16	45	[381]
201	methyl viologen	H_2O + $LaCl_3$ 0.033 M	0.21	60	[381]
202	methyl viologen	H_2O + $LaCl_3$ 0.067 M	0.09	10	[381]
203	methyl viologen	H_2O + $LaCl_3$ 0.067 M	0.17	25	[381]
204	methyl viologen	H_2O + $LaCl_3$ 0.067 M	0.19	35	[381]
205	methyl viologen	H_2O + $LaCl_3$ 0.067 M	0.19	45	[381]
206	methyl viologen	H_2O + $LaCl_3$ 0.067 M	0.22	60	[381]
207	methyl viologen	H_2O + $LaCl_3$ 0.13 M	0.09	10	[381]
208	methyl viologen	H_2O + $LaCl_3$ 0.13 M	0.16	25	[381]
209	methyl viologen	H_2O + $LaCl_3$ 0.13 M	0.17	35	[381]
210	methyl viologen	H_2O + $LaCl_3$ 0.13 M	0.2	45	[381]
211	methyl viologen	H_2O + $LaCl_3$ 0.13 M	0.22	60	[381]
212	methyl viologen	H_2O + LiCl 0.05 M	0.16	10	[381]
213	methyl viologen	H_2O + LiCl 0.05 M	0.18	25	[381]
214	methyl viologen	H_2O + LiCl 0.05 M	0.18	35	[381]
215	methyl viologen	H_2O + LiCl 0.05 M	0.18	45	[381]
216	methyl viologen	H_2O + LiCl 0.05 M	0.22	60	[381]
217	methyl viologen	H_2O + LiCl 0.1 M	0.14	10	[381]
218	methyl viologen	H_2O + LiCl 0.1 M	0.17	25	[381]
219	methyl viologen	H_2O + LiCl 0.1 M	0.16	35	[381]
220	methyl viologen	H_2O + LiCl 0.1 M	0.19	45	[381]
221	methyl viologen	H_2O + LiCl 0.1 M	0.2	60	[381]
222	methyl viologen	H_2O + LiCl 0.2 M	0.13	10	[381]
223	methyl viologen	H_2O + LiCl 0.2 M	0.15	25	[381]
224	methyl viologen	H_2O + LiCl 0.2 M	0.16	35	[381]
225	methyl viologen	H_2O + LiCl 0.2 M	0.17	45	[381]
226	methyl viologen	H_2O + LiCl 0.2 M	0.19	60	[381]
227	methyl viologen	H_2O + LiCl 0.4 M	0.12	10	[381]
228	methyl viologen	H_2O + LiCl 0.4 M	0.14	25	[381]
229	methyl viologen	H_2O + LiCl 0.4 M	0.15	35	[381]
230	methyl viologen	H_2O + LiCl 0.4 M	0.16	45	[381]
231	methyl viologen	H_2O + LiCl 0.4 M	0.18	60	[381]
232	methyl viologen	H_2O + LiCl 0.6 M	0.13	25	[381]
233	methyl viologen	H_2O + LiCl 0.8 M	0.11	10	[381]
234	methyl viologen	H_2O + LiCl 0.8 M	0.13	35	[381]
235	methyl viologen	H_2O + LiCl 0.8 M	0.14	45	[381]
236	methyl viologen	H_2O + LiCl 0.8 M	0.15	60	[381]

237	methyl viologen	H_2O + NaCl 0.05 M	0.17	25	[381]
238	methyl viologen	H_2O + NaCl 0.05 M	0.15	35	[381]
239	methyl viologen	H_2O + NaCl 0.05 M	0.19	45	[381]
240	methyl viologen	H_2O + NaCl 0.05 M	0.22	60	[381]
241	methyl viologen	H_2O + NaCl 0.1 M	0.15	10	[381]
242	methyl viologen	H_2O + NaCl 0.1 M	0.15	25	[381]
243	methyl viologen	H_2O + NaCl 0.1 M	0.15	35	[381]
244	methyl viologen	H_2O + NaCl 0.1 M	0.17	45	[381]
245	methyl viologen	H_2O + NaCl 0.1 M	0.19	60	[381]
246	methyl viologen	H_2O + NaCl 0.2 M	0.12	10	[381]
247	methyl viologen	H_2O + NaCl 0.2 M	0.12	25	[381]
248	methyl viologen	H_2O + NaCl 0.2 M	0.15	35	[381]
249	methyl viologen	H_2O + NaCl 0.2 M	0.16	45	[381]
250	methyl viologen	H_2O + NaCl 0.2 M	0.19	60	[381]
251	methyl viologen	H_2O + NaCl 0.3 M	0.12	25	[381]
252	methyl viologen	H_2O + NaCl 0.4 M	0.11	10	[381]
253	methyl viologen	H_2O + NaCl 0.4 M	0.12	25	[381]
254	methyl viologen	H_2O + NaCl 0.4 M	0.14	35	[381]
255	methyl viologen	H_2O + NaCl 0.4 M	0.16	45	[381]
256	methyl viologen	H_2O + NaCl 0.4 M	0.18	60	[381]
257	N,N-dimethylaniline	CH_3CN/H_2O	0.5	10	[423]
258	N,N-dimethylaniline	CH_3CN/H_2O	0.74	20	[423]
259	N,N-dimethylaniline	CH_3CN/H_2O	0.79	30	[423]
260	N,N-dimethylaniline	CH_3CN/H_2O	0.65	40	[423]
261	N,N-dimethylaniline	CH_3CN/H_2O	0.81	50	[423]
262	N,N-dimethylaniline	CH_3CN/H_2O	0.75	60	[423]
263	N,N,N',N'-tetramethyl-1,4-phenylenediamine	CH_3CN/H_2O	0.53	10	[423]
264	N,N,N',N'-tetramethyl-1,4-phenylenediamine	CH_3CN/H_2O	0.57	20	[423]
265	N,N,N',N'-tetramethyl-1,4-phenylenediamine	CH_3CN/H_2O	0.68	30	[423]
266	N,N,N',N'-tetramethyl-1,4-phenylenediamine	CH_3CN/H_2O	0.66	40	[423]
267	N,N,N',N'-tetramethyl-1,4-phenylenediamine	CH_3CN/H_2O	0.67	50	[423]
268	N,N,N',N'-tetramethyl-1,4-phenylenediamine	CH_3CN/H_2O	0.71	60	[423]
269	*p*-anisidine	CH_3CN/H_2O	0.72	10	[423]
270	*p*-anisidine	CH_3CN/H_2O	0.68	20	[423]
271	*p*-anisidine	CH_3CN/H_2O	0.62	30	[423]
272	*p*-anisidine	CH_3CN/H_2O	0.61	40	[423]
273	*p*-anisidine	CH_3CN/H_2O	0.58	50	[423]
274	*p*-anisidine	CH_3CN/H_2O	0.6	60	[423]
275	*p*-toluidine	CH_3CN/H_2O	0.57	10	[423]
276	*p*-toluidine	CH_3CN/H_2O	0.54	20	[423]
277	*p*-toluidine	CH_3CN/H_2O	0.65	30	[423]
278	*p*-toluidine	CH_3CN/H_2O	0.51	40	[423]
279	*p*-toluidine	CH_3CN/H_2O	0.74	50	[423]

280	*p*-toluidine	CH_3CN/H_2O	0.75	60	[423]
281	Phenothiazine	CH_3CN/H_2O	0.41	10	[423]
282	Phenothiazine	CH_3CN/H_2O	0.53	20	[423]
283	Phenothiazine	CH_3CN/H_2O	0.46	30	[423]
284	Phenothiazine	CH_3CN/H_2O	0.45	40	[423]
285	Phenothiazine	CH_3CN/H_2O	0.51	50	[423]
286	Phenothiazine	CH_3CN/H_2O	0.51	60	[423]

6.10) Tabulated values for the cage-escape yields of Ir(III), Rh(III), Os(II), Cu(I), Cr(III), Fe(III), Re(I), Co(III) and Pt(II) photosensitizers.

Table 20 gathers the cage-escape yields of Ir(III), Rh(III), Os(II), Cu(I), Cr(III), Fe(III), Re(I), Co(III) and Pr(II) photosensitizers with several quenchers and solvents. Electron transfer quenching sensitized by the listed metal photosensitizers are primarily done by triplet states with the exception of some Cr(III) and Fe(III) which are primarily doublet excited states. For a specific excited state description, see relevant reference(s).

Table 20. Cage-escape yields (ϕ_{ce}) of Ir(III), Rh(III), Os(II), Cu(I), Cr(III), Fe(III), Re(I), Co(III) and Pt(II) photosensitizers.

Entry	Photosensitizer	Quencher	Solvent	ϕ_{ce}	Ref
1	$[Co(L^{CNC})_2]^+$	methyl viologen	CH_3CN	0.02	[520]
2	$[Cr(bpy)_3]^{3+}$	1,2,4-trimethoxybenzene	CH_3CN	0.021	[349]
3	$[Cr(bpy)_3]^{3+}$	1,4-anisidine	CH_3CN	0.18	[349]
4	$[Cr(bpy)_3]^{3+}$	1,4-dimethoxybenzene	CH_3CN	0.019	[349]
5	$[Cr(bpy)_3]^{3+}$	2-aminonaphthalene	CH_3CN	0.07	[349]
6	$[Cr(bpy)_3]^{3+}$	3,3'-dimethylbenzidine	CH_3CN	0.31	[349]
7	$[Cr(bpy)_3]^{3+}$	diphenyl-1,4-phenylenediamine	CH_3CN	0.56	[349]
8	$[Cr(bpy)_3]^{3+}$	diphenylamine	CH_3CN	0.07	[349]
9	$[Cr(bpy)_3]^{3+}$	N,N-dimethylaniline	CH_3CN	0.09	[349]
10	$[Cr(bpy)_3]^{3+}$	N,N,N',N'-tetramethyl-1,4-phenylenediamine	CH_3CN	0.8	[349]
11	$[Cr(bpy)_3]^{3+}$	N,N,N',N'-tetramethylbenzidine	CH_3CN	0.35	[349]
12	$[Cr(bpy)_3]^{3+}$	phenothiazine	CH_3CN	0.16	[349]
13	$[Cr(dpphen)_3]^{3+}$	1,2-phenylenediamine	CH_3CN	0.26	[349]
14	$[Cr(dpphen)_3]^{3+}$	1,2,4-trimethoxybenzene	CH_3CN	0.017	[349]
15	$[Cr(dpphen)_3]^{3+}$	1,3,5-trimethoxybenzene	CH_3CN	0.027	[349]
16	$[Cr(dpphen)_3]^{3+}$	1,4-dimethoxybenzene	CH_3CN	0.032	[349]
17	$[Cr(dpphen)_3]^{3+}$	1,4-phenylenediamine	CH_3CN	0.61	[349]
18	$[Cr(dpphen)_3]^{3+}$	3,3'-dimethylbenzidine	CH_3CN	0.43	[349]
19	$[Cr(dpphen)_3]^{3+}$	N,N,N',N'-tetramethyl-1,4-phenylenediamine	CH_3CN	0.79	[349]

20	$[Cr(dpphen)_3]^{3+}$	N,N,N',N'-tetramethylbenzidine	CH_3CN	0.35	349
21	$[Cr(dpphen)_3]^{3+}$	triphenylamine	CH_3CN	0.039	349
22	$[Cr(dpq)_2]^{3+}$	tri-*p*-anisylamine	CH_3CN	0.13	439
23	$[Cr(dpq)_2]^{3+}$	tri-*p*-anisylamine	CH_3CN	0.13	440
24	$[Cr(dpq)_2]^{3+}$	tri-*p*-PEG_3-arylamine	CH_3CN	0.14	440
25	$[Cr(dpq)_2]^{3+}$	tri-*p*-PEG_7-arylamine	CH_3CN	0.19	440
26	$[Cr(dpq)_2]^{3+}$	Tris(4-chlorophenyl)amine	CH_3CN	0.16	440
27	$[Cr(dpq)_2]^{3+}$	Tris(4-bromophenyl)amine	CH_3CN	0.16	440
28	$[Cr(dpq)_2]^{3+}$	Tris(4-iodophenyl)amine	CH_3CN	0.18	440
29	$[Cr(dpq)_2]^{3+}$	N,N-dimethylaniline	CH_3CN	0.07	440
30	$[Cr(dpq)_2]^{3+}$	N,N-dimethyltoluidine	CH_3CN	0.08	440
31	$[Cr(dpq)_2]^{3+}$	4-methoxy-N,N'-dimethylaniline	CH_3CN	0.08	440
32	$[Cr(dpq)_2]^{3+}$	THIQ	CH_3CN	<0.07	440
33	$[Cr(dpq)_2]^{3+}$	triethylamine	CH_3CN	0.11	440
34	$[Cr(dpq)_2]^{3+}$	diisopropylethylamine	CH_3CN	0.11	440
35	$[Cr(tpe)_2]^{3+}$	4-aminomorpholine	CH_3CN	0.73	441
36	$[Cr(tpe)_2]^{3+}$	cyclohexyltrifluoroborate	CH_3CN	0.27	441
37	$[Cr(tpe)_2]^{3+}$	DABCO	CH_3CN	<0.08	441
38	$[Cr(tpe)_2]^{3+}$	DABSO	CH_3CN	<0.07	441
39	$[Cu(dpp)_2]^{+}$	benzyl viologen	CH_3CN 0.1 M $TBAPF_6$	0.57	378
40	$[Cu(dpp)_2]^{+}$	methyl viologen	CH_3CN 0.1 M $TBAPF_6$	0.95	378
41	$[Fe(btz)_3]^{3+}$	triethylamine	CH_3CN/CH_3OH 4:3	0.20	461
42	$[Fe(phtmeimb)_2]^{+}$	$[Fe(phtmeimb)_2]^{+}$	CH_3CN	0.04	460
43	$[Fe(phtmeimb)_2]^{+}$	diphenylamine	CH_3CN	0.05	444
44	$[Fe(phtmeimb)_2]^{+}$	methyl Viologen	CH_3CN	0.05	444
45	$[Fe(phtmeimb)_2]^{+}$	N,N-dimethylaniline	CH_2Br_2	0.54	51
46	$[Fe(phtmeimb)_2]^{+}$	N,N-dimethylaniline	CH_2Cl_2	0.6	51
47	$[Fe(phtmeimb)_2]^{+}$	N,N-dimethylaniline	CH_3CN	0.02	51
48	$[Fe(phtmeimb)_2]^{+}$	N,N-dimethylaniline	CH_3CN + 30% MeI	0.05	51
49	$[Fe(phtmeimb)_2]^{+}$	N,N-dimethylaniline	CH_3CN + 50% MeI	0.09	51
50	$[Fe(phtmeimb)_2]^{+}$	N,N-dimethylaniline	CH_3CN 0.1M $TBAPF_6$	0.35	51
51	$[Fe(phtmeimb)_2]^{+}$	N,N-dimethylaniline	CH_3CN 0.2M $TBAPF_6$	0.30	51
52	$[Fe(phtmeimb)_2]^{+}$	N,N-dimethylaniline	CH_3CN 1M $TBAPF_6$	0.17	51
53	$[Fe(phtmeimb)_2]^{+}$	N,N-dimethylaniline	DMF	0.01	51
54	$[Fe(phtmeimb)_2]^{+}$	N,N-dimethyltoluidine	CH_2Cl_2	0.36	51
55	$[Fe(phtmeimb)_2]^{+}$	N,N-dimethyltoluidine	CH_3CN	0.05	51
56	$[Fe(phtmeimb)_2]^{+}$	N,N-dimethyltoluidine	DMF	0.03	51
57	$[Fe(phtmeimb)_2]^{+}$	tri-*p*-tolylamine	CH_2Cl_2	0.63	51
58	$[Fe(phtmeimb)_2]^{+}$	tri-*p*-tolylamine	CH_3CN	0.07	51
59	$[Fe(phtmeimb)_2]^{+}$	tri-*p*-tolylamine	DMF	0.07	51
60	$[Fe(phtmeimb)_2]^{+}$	triethylamine	CH_2Cl_2	0.21	429
61	$[Fe(phtmeimb)_2]^{+}$	triethylamine	CH_3CN	0.01	429

62	$[Fe(phtmeimb)_2]^+$	triethylamine	DMF	0.09	429
63	$[Ir((dFCF_3)ppy)_2(dtb)]^+$	4-bromobenzene diazonium	CH_3CN	1	94
64	$[Ir((dFCF_3)ppy)_2(dtb)]^+$	4-ethylesterbenzene diazonium	CH_3CN	0.89	94
65	$[Ir((dFCF_3)ppy)_2(dtb)]^+$	4-methoxybenzene diazonium	CH_3CN	0.44	94
66	$[Ir((dFCF_3)ppy)_2(dtb)]^+$	4-nitrobenzene diazonium	CH_3CN	1	94
67	$[Ir(NBI)_2(phen)]^+$	N,N-dimethyltoluidine	CH_3CN/H_2O 2:1	0.78	63
68	$[Ir(ppy)_2(dtb)]^+$	4-bromobenzene diazonium	CH_3CN	1	94
69	$[Ir(ppy)_2(dtb)]^+$	4-ethylesterbenzene diazonium	CH_3CN	1	94
70	$[Ir(ppy)_2(dtb)]^+$	4-methoxybenzene diazonium	CH_3CN	0.43	94
71	$[Ir(ppy)_2(dtb)]^+$	4-nitrobenzene diazonium	CH_3CN	1	94
72	$[Ir(ppy)_3]$	4-bromobenzene diazonium	CH_3CN	1	94
73	$[Ir(ppy)_3]$	4-methoxybenzene diazonium	CH_3CN	0.61	94
74	$[Os(bpy)_2(das)]^{2+}$	methyl viologen	8 :5 (v/v) 0.1M $TEAClO_4$/ CH_3CN to CH_2Cl_2	0.21	82
75	$[Os(bpy)_3]^{2+}$	4-bromobenzene diazonium	CH_3CN	0.61	94
76	$[Os(bpy)_3]^{2+}$	4-ethylesterbenzene diazonium	CH_3CN	0.89	94
77	$[Os(bpy)_3]^{2+}$	4-methoxybenzene diazonium	CH_3CN	0.18	94
78	$[Os(bpy)_3]^{2+}$	4-nitrobenzene diazonium	CH_3CN	0.97	94
79	$[Os(phen)(dmpp)_2]^{2+}$	methyl viologen	8 :5 (v/v) 0.1M $TEAClO_4$/ CH_3CN to CH_2Cl_2	0.14	82
80	$[Os(phen)_2(dppm)]^{2+}$	methyl viologen	8 :5 (v/v) 0.1M $TEAClO_4$/ CH_3CN to CH_2Cl_2	0.18	82
81	$[Pt(mnt)_2]^{2-}$	1-ethyl-1'-(3-sulfonatepropyl)-3,3'-dimethyl-4,4'-bipyridinium	DMSO	1	471
82	$[Pt(mnt)_2]^{2-}$	1-ethyl-1'-(3-sulfonatepropyl)-4,4'-bipyridinium	DMSO	1	471
83	$[Pt(mnt)_2]^{2-}$	N,N'-(1,3-propenyl)-2,2'-bipyridinium	DMSO	0.11	471
84	$[Pt_2(pop)_4]^{4-}$	$[Ni(cyclam)]^{2+}$	0.01M $HClO_4$ under air	0.054	472
85	$[Pt_2(pop)_4]^{4-}$	$[Ni(cyclam)]^{2+}$	0.01M $HClO_4$ under argon	0.028	472
86	$[Re(4,4'\text{-}PO3^{2-})_2\text{-}bpy)(CO)_3(Cl)]^-$	Phenothiazine	EtOH	0.26	470
87	$[Re(4,4'\text{-}PO_3H_2)_2\text{-}bpy)(CO)_3(Cl)]^+$	Phenothiazine	EtOH	0.15	470
88	$[Re(4,4',5,5'\text{-}(CH_3)_4\text{-}bpy)(py)(CO)_3]^+$	$Co(CO_4)^-$	CH_3CN (355nm)	0.67	465
89	$[Re(4,4',5,5'\text{-}(CH_3)_4\text{-}bpy)(py)(CO)_3]^+$	$Co(CO_4)^-$	CH_3CN (532 nm)	0.04	465
90	$[Re(BP)(4\text{-}dab)(CO)_3]^+$	1,4-diazabicyclo[2.2.2]octane	CH_3CN	0.73	464
91	$[Re(BP)(5\text{-}dab)(CO)_3]^+$	1,4-diazabicyclo[2.2.2]octane	CH_3CN	0.73	464
92	$[Re(BP)(bpy)(CO)_3]^+$	1,4-diazabicyclo[2.2.2]octane	CH_3CN	0.79	464
93	$[Re(BP)(bpz)(CO)_3]^+$	1,4-diazabicyclo[2.2.2]octane	CH_3CN	0.54	464
94	$[Re(BP)(dmb)(CO)_3]^+$	1,4-diazabicyclo[2.2.2]octane	CH_3CN	0.85	464
95	$[Re(bpy)(py)(CO)_3]^+$	1,2-dihydroxybenzene	H_2O	0.37	466
96	$[Re(bpy)(py)(CO)_3]^+$	1,4-hydroquinone	H_2O	0.33	466
97	$[Re(bpy)(py)(CO)_3]^+$	2,5-dihydroxybenzoic acid	H_2O	0.37	466
98	$[Re(bpy)(py)(CO)_3]^+$	$Co(CO_4)^-$	CH_3CN (355nm)	0.65	465
99	$[Re(bpy)(py)(CO)_3]^+$	$Co(CO_4)^-$	CH_3CN (532 nm)	0.04	465

100	$[Rh(dpphen)_3]^{3+}$	1,2-dimethoxybenzene	CH_3CN/H_2O 1:1	0.52	[349]
101	$[Rh(dpphen)_3]^{3+}$	1,2-phenylenediamine	CH_3CN/H_2O 1:1	0.64	[349]
102	$[Rh(dpphen)_3]^{3+}$	1,2,4-trimethoxybenzene	CH_3CN/H_2O 1:1	0.49	[349]
103	$[Rh(dpphen)_3]^{3+}$	1,3,5-trimethoxybenzene	CH_3CN/H_2O 1:1	0.44	[349]
104	$[Rh(dpphen)_3]^{3+}$	1,4-dimethoxybenzene	CH_3CN/H_2O 1:1	0.48	[349]
105	$[Rh(dpphen)_3]^{3+}$	1,4-phenylenediamine	CH_3CN/H_2O 1:1	0.78	[349]
106	$[Rh(dpphen)_3]^{3+}$	3,3'-dimethylbenzidine	CH_3CN/H_2O 1:1	0.55	[349]
107	$[Rh(dpphen)_3]^{3+}$	diphenylamine	CH_3CN/H_2O 1:1	0.38	[349]
108	$[Rh(dpphen)_3]^{3+}$	methoxybenzene	CH_3CN/H_2O 1:1	0.58	[349]
109	$[Rh(dpphen)_3]^{3+}$	N,N,N',N'-tetramethyl-1,4-phenylenediamine	CH_3CN/H_2O 1:1	0.88	[349]
110	$[Rh(dpphen)_3]^{3+}$	N,N,N',N'-tetramethylbenzidine	CH_3CN/H_2O1:1	0.58	[349]
111	Ir_2-TAPHAT	bromide	CH_3CN	0.7	[431]
112	Ir2-TAPHAT	bromide	CH_3CN/H_2O 1:1	0.03	[431]
113	Ir_2-TAPHAT	chloride	CH_3CN	0.55	[431]
114	Ir2-TAPHAT	chloride	CH_3CN/H_2O 1:1	0.04	[431]
115	Ir_2-TAPHAT	iodide	CH_3CN	0.9	[431]
116	Ir_2-TAPHAT	iodide	CH_3CN/H_2O 1:1	0.32	[431]
117	Ir_2-TPPHZ	bromide	CH_3CN	0.81	[431]
118	Ir_2-TPPHZ	bromide	CH_3CN/H_2O 1:1	0.02	[431]
119	Ir_2-TPPHZ	chloride	CH_3CN	0.8	[431]
120	Ir_2-TPPHZ	chloride	CH_3CN/H_2O 1:1	0.02	[431]
121	Ir_2-TPPHZ	iodide	CH_3CN	0.96	[431]
122	Ir_2-TPPHZ	iodide	CH_3CN/H_2O 1:1	0.11	[431]
123	$Re(4,4'\text{-}PO_3H_2)_2\text{-bpy})(CO)_3(Cl)]^+$	phenothiazine	Surface of ZrO_2	0.42	[470]

6.11) Tabulated values for the cage-escape yields porphyrin derivatives.

Table 20 gathers the cage-escape yields of porphyrin derivatives with several quenchers and solvents. Electron transfer quenching sensitized by porphyrin derivatives occur primarily from singlet and triplet states. For a specific excited state description, see relevant reference(s).

Table 21. Cage-escape yields (ϕ_{ce}) of porphyrin derivatives

Entry	Photosensitizer	Quencher	Solvent	ϕ_{ce}	Ref
1	AlTPP	benzoquinone	ethanol	0.21	[168]
2	CdTPP	benzoquinone	ethanol	0.16	[168]
3	CrTPP	benzoquinone	ethanol	<0.002	[168]
4	CuTPP	benzoquinone	ethanol	<0.002	[168]
5	H_2TPP	benzoquinone	ethanol	0.084	[168]
6	MgTPP	benzoquinone	ethanol	0.24	[168]
7	PdTPP	benzoquinone	ethanol	0.055	[168]

8	RuTPP	benzoquinone	ethanol	0.07	168
9	Zn(OEP)	1,4-benzoquinone	hexyl alcohol	0.27	349
10	Zn(OEP)	1,4-naphthoquinone	hexyl alcohol	0.17	349
11	Zn(OEP)	2,5-dimethyl-1,4-benzoquinone	hexyl alcohol	0.22	349
12	Zn(OEP)	9,10-anthraquinone	hexyl alcohol	0.13	349
13	Zn(OEP)	tetramethyl-1,4-benzoquinone	hexyl alcohol	0.22	349
14	ZnCPP-	methyl viologen	H_2O, 0.01M Phosphate, 0.01M EDTA	0.037	521
15	$ZnMPyP^{+}$	methyl viologen	H_2O, 0.01M Phosphate, 0.01M EDTA	0.1	521
16	ZnP	methyl viologen	ethanol	ND	478
17	ZnP n=1	methyl viologen	ethanol	0.12	478
18	ZnP n=2	methyl viologen	ethanol	0.15	478
19	ZnP n=4	methyl viologen	ethanol	0.29	478
20	ZnP n=6	methyl viologen	ethanol	0.31	478
21	$ZnTCPP^{4-}$	methyl viologen	H_2O, 0.01M Phosphate, 0.01M EDTA	<0.01	521
22	$ZnTMPyP^{4+}$	methyl viologen	H_2O, 0.01M Phosphate, 0.01M EDTA	0.75	521
23	ZnTPP	benzoquinone	ethanol	0.22	168
24	$ZnTSPP^{4-}$	methyl viologen	H_2O, 0.01M Phosphate, 0.01M EDTA	<0.01	521

References

1. Muñoz-García, A. B.; Benesperi, I.; Boschloo, G.; Concepcion, J. J.; Delcamp, J. H.; Gibson, E. A.; Meyer, G. J.; Pavone, M.; Pettersson, H.; Hagfeldt, A.; Freitag, M., Dye-Sensitized Solar Cells Strike Back. *Chem. Soc. Rev.* **2021,** *50*, 12450-12550.
2. Gong, J.; Sumathy, K.; Qiao, Q.; Zhou, Z., Review on Dye-Sensitized Solar Cells (Dsscs): Advanced Techniques and Research Trends. *Renew. Sust. Energ. Rev.* **2017,** *68*, 234-246.
3. Hagfeldt, A.; Boschloo, G.; Sun, L.; Kloo, L.; Pettersson, H., Dye-Sensitized Solar Cells. *Chem. Rev.* **2010,** *110*, 6595-6663.
4. Albery, W. J., Development of Photogalvanic Cells for Solar Energy Conservation. *Acc. Chem. Res.* **1982,** *15*, 142-148.
5. McDaniel, N. D.; Bernhard, S., Solar Fuels: Thermodynamics, Candidates, Tactics, and Figures of Merit. *Dalton Trans.* **2010,** *39*, 10021-10030.
6. Powers, D. C.; Hwang, S. J.; Zheng, S.-L.; Nocera, D. G., Halide-Bridged Binuclear Hx-Splitting Catalysts. *Inorg. Chem.* **2014,** *53*, 9122-9128.
7. Pannwitz, A.; Klein, D. M.; Rodríguez-Jiménez, S.; Casadevall, C.; Song, H.; Reisner, E.; Hammarström, L.; Bonnet, S., Roadmap Towards Solar Fuel Synthesis at the Water Interface of Liposome Membranes. *Chem. Soc. Rev.* **2021,** *50*, 4833-4855.
8. Andrei, V.; Wang, Q.; Uekert, T.; Bhattacharjee, S.; Reisner, E., Solar Panel Technologies for Light-to-Chemical Conversion. *Acc. Chem. Res.* **2022,** *55*, 3376-3386.
9. Wang, Q.; Pornrungroj, C.; Linley, S.; Reisner, E., Strategies to Improve Light Utilization in Solar Fuel Synthesis. *Nat. Energy* **2022,** *7*, 13-24.
10. Bhattacharjee, S.; Rahaman, M.; Andrei, V.; Miller, M.; Rodríguez-Jiménez, S.; Lam, E.; Pornrungroj, C.; Reisner, E., Photoelectrochemical Co2-to-Fuel Conversion with Simultaneous Plastic Reforming. *Nat. Synth.* **2023,** *2*, 182-192.
11. Rahaman, M.; Andrei, V.; Wright, D.; Lam, E.; Pornrungroj, C.; Bhattacharjee, S.; Pichler, C. M.; Greer, H. F.; Baumberg, J. J.; Reisner, E., Solar-Driven Liquid Multi-Carbon Fuel Production Using a Standalone Perovskite–Bivo4 Artificial Leaf. *Nat. Energy* **2023,** *8*, 629-638.
12. Gust, D.; Moore, T. A.; Moore, A. L., Solar Fuels Via Artificial Photosynthesis. *Acc. Chem. Res.* **2009,** *42*, 1890-1898.
13. Morris, A. J.; Meyer, G. J.; Fujita, E., Molecular Approaches to the Photocatalytic Reduction of Carbon Dioxide for Solar Fuels. *Acc. Chem. Res.* **2009,** *42*, 1983-1994.
14. Ashford, D. L.; Gish, M. K.; Vannucci, A. K.; Brennaman, M. K.; Templeton, J. L.; Papanikolas, J. M.; Meyer, T. J., Molecular Chromophore–Catalyst Assemblies for Solar Fuel Applications. *Chem. Rev.* **2015,** *115*, 13006-13049.
15. Hammarström, L., Accumulative Charge Separation for Solar Fuels Production: Coupling Light-Induced Single Electron Transfer to Multielectron Catalysis. *Acc. Chem. Res.* **2015,** *48*, 840-850.
16. Brady, M. D.; Sampaio, R. N.; Wang, D.; Meyer, T. J.; Meyer, G. J., Dye-Sensitized Hydrobromic Acid Splitting for Hydrogen Solar Fuel Production. *J. Am. Chem. Soc.* **2017,** *139*, 15612-15615.
17. Kagalwala, H. N.; Chirdon, D. N.; Bernhard, S., Solar Fuel Generation. In *Iridium(Iii) in Optoelectronic and Photonics Applications*, Zysman-Colman, E., Ed. John Wiley & Sons Ltd.: Chichester, West Sussex, 2017; pp 583-615.

18. Segev, G.; Kibsgaard, J.; Hahn, C.; Xu, Z. J.; Cheng, W.-H.; Deutsch, T. G.; Xiang, C.; Zhang, J. Z.; Hammarström, L.; Nocera, D. G.*, et al.*, The 2022 Solar Fuels Roadmap. *J. Phys. D Appl. Phys.* **2022,** *55*, 323003.
19. Artero, V.; Chavarot-Kerlidou, M.; Fontecave, M., Splitting Water with Cobalt. *Angew. Chem. Int. Ed.* **2011,** *50*, 7238-7266.
20. Nguyen, D. N.; Giannoudis, E.; Straistari, T.; Fize, J.; Koepf, M.; Tran, P. D.; Chavarot-Kerlidou, M.; Artero, V., Unassisted Solar Syngas Production by a Molecular Dye-Cobalt Catalyst Assembly in a Tandem Photoelectrochemical Cell. *ACS Energy Lett.* **2024,** *9*, 829-834.
21. Wang, Q.; Domen, K., Particulate Photocatalysts for Light-Driven Water Splitting: Mechanisms, Challenges, and Design Strategies. *Chem. Rev.* **2020,** *120*, 919-985.
22. Feng, C.; Wang, F.; Liu, Z.; Nakabayashi, M.; Xiao, Y.; Zeng, Q.; Fu, J.; Wu, Q.; Cui, C.; Han, Y.*, et al.*, A Self-Healing Catalyst for Electrocatalytic and Photoelectrochemical Oxygen Evolution in Highly Alkaline Conditions. *Nature Comm.* **2021,** *12*, 5980.
23. Shaw, M. H.; Twilton, J.; MacMillan, D. W. C., Photoredox Catalysis in Organic Chemistry. *J. Org. Chem.* **2016,** *81*, 6898-6926.
24. Romero, N. A.; Nicewicz, D. A., Organic Photoredox Catalysis. *Chem. Rev.* **2016,** *116*, 10075-10166.
25. Wang, C.-S.; Dixneuf, P. H.; Soulé, J.-F., Photoredox Catalysis for Building C–C Bonds from C(Sp2)–H Bonds. *Chem. Rev.* **2018,** *118*, 7532-7585.
26. Narayanam, J. M. R.; Stephenson, C. R. J., Visible Light Photoredox Catalysis: Applications in Organic Synthesis. *Chem. Soc. Rev.* **2011,** *40*, 102-113.
27. Gehlen, M. H., The Centenary of the Stern-Volmer Equation of Fluorescence Quenching: From the Single Line Plot to the Sv Quenching Map. *J. Photoch. Photobio. C* **2020,** *42*, 100338.
28. Stern, O.; Volmer, M., Über Die Abklingungszit Der Fluoreszenz. *Physik. Z.* **1919,** *20*, 183-188.
29. Lakowicz, J. R., *Principles of Fluorescence Spectroscopy*. Springer US, New York: 2006.
30. Rehm, D.; Weller, A., Kinetics of Fluorescence Quenching by Electron and H-Atom Transfer. *Isr. J. Chem.* **1970,** *8*, 259-271.
31. Rehm, D.; Weller, A., Kinetik Und Mechanismus Der Elektronübertragung Bei Der Fluoreszenzlöschung in Acetonitril. *Berich. Bunsen. Gesell.* **1969,** *73*, 834-839.
32. Marcus, R. A.; Sutin, N., Electron Transfers in Chemistry and Biology. *BBA-Bioenergetics* **1985,** *811*, 265-322.
33. Marcus, R. A., On the Theory of Oxidation-Reduction Reactions Involving Electron Transfer. I. *J. Chem. Phys.* **1956,** *24*, 966-978.
34. Marcus, R. A., Chemical and Electrochemical Electron-Transfer Theory. *Annu. Rev. Phys. Chem.* **1964,** *15*, 155-196.
35. Lyon, R. K.; Levy, D. H., Demonstration of the "Cage" Effect. *J. Am. Chem. Soc.* **1961,** *83*, 4290-4290.
36. Rabinowitsch, E.; Wood, W. C., The Collison Mechanism and the Primary Photochemical Process in Solutions. *Trans. Faraday Soc.* **1936,** *32*, 1381-1387.
37. Rabinowitch, E., Collision, Co-Ordination, Diffusion and Reaction Velocity in Condensed Systems. *Trans. Faraday Soc.* **1937,** *33*, 1225-1233.
38. Franck, J.; Rabinowitsch, E., Some Remarks About Free Radicals and the Photochemistry of Solutions. *Trans. Faraday Soc.* **1934,** *30*, 120-130.
39. Chou, M.; Creutz, C.; Sutin, N., Rate Constants and Activation Parameters for Outer-Sphere Electron-Transfer Reactions and Comparisons with the Predictions of Marcus Theory. *J. Am. Chem. Soc.* **1977,** *99*, 5615-5623.

40. Steinfeld, J. I.; Francisco, J. S.; Hase, W. L., *Chemical Kinetics and Dynamics*. Prentice Hall Englewood Cliffs (New Jersey): 1989; Vol. 3.
41. Porter, G.; Topp, M. R., Nanosecond Flash Photolysis. *Proc. R. Soc. A* **1970,** *315*, 163-184.
42. Morton, C. M.; Zhu, Q.; Ripberger, H.; Troian-Gautier, L.; Toa, Z. S. D.; Knowles, R. R.; Alexanian, E. J., C–H Alkylation Via Multisite-Proton-Coupled Electron Transfer of an Aliphatic C–H Bond. *J. Am. Chem. Soc.* **2019,** *141*, 13253-13260.
43. Troian-Gautier, L.; Swords, W. B.; Meyer, G. J., Iodide Photoredox and Bond Formation Chemistry. *Acc. Chem. Res.* **2019,** *52*, 170-179.
44. Troian-Gautier, L.; Turlington, M. D.; Wehlin, S. A. M.; Maurer, A. B.; Brady, M. D.; Swords, W. B.; Meyer, G. J., Halide Photoredox Chemistry. *Chem. Rev.* **2019,** *119*, 4628-4683.
45. Bevernaegie, R.; Wehlin, S. A. M.; Piechota, E. J.; Abraham, M.; Philouze, C.; Meyer, G. J.; Elias, B.; Troian-Gautier, L., Improved Visible Light Absorption of Potent Iridium(Iii) Photo-Oxidants for Excited-State Electron Transfer Chemistry. *J. Am. Chem. Soc.* **2020,** *142*, 2732-2737.
46. Cerfontaine, S.; Duez, Q.; Troian-Gautier, L.; Barozzino-Consiglio, G.; Loiseau, F.; Cornil, J.; De Winter, J.; Gerbaux, P.; Elias, B., Efficient Convergent Energy Transfer in a Stereoisomerically Pure Heptanuclear Luminescent Terpyridine-Based Ru(Ii)–Os(Ii) Dendrimer. *Inorg. Chem.* **2020,** *59*, 14536-14543.
47. Cerfontaine, S.; Troian-Gautier, L.; Wehlin, S. A. M.; Loiseau, F.; Cauët, E.; Elias, B., Tuning the Excited-State Deactivation Pathways of Dinuclear Ruthenium(Ii) 2,2′-Bipyridine Complexes through Bridging Ligand Design. *Dalton Trans.* **2020,** *49*, 8096-8106.
48. Cerfontaine, S.; Wehlin, S. A. M.; Elias, B.; Troian-Gautier, L., Photostable Polynuclear Ruthenium(Ii) Photosensitizers Competent for Dehalogenation Photoredox Catalysis at 590 Nm. *J. Am. Chem. Soc.* **2020,** *142*, 5549-5555.
49. Wehlin, S. A. M.; Troian-Gautier, L.; Maurer, A. B.; Brennaman, M. K.; Meyer, G. J., Photophysical Characterization of New Osmium (Ii) Photocatalysts for Hydrohalic Acid Splitting. *J. Chem. Phys.* **2020,** *153*, 054307.
50. Xu, B.; Troian-Gautier, L.; Dykstra, R.; Martin, R. T.; Gutierrez, O.; Tambar, U. K., Photocatalyzed Diastereoselective Isomerization of Cinnamyl Chlorides to Cyclopropanes. *J. Am. Chem. Soc.* **2020,** *142*, 6206-6215.
51. Aydogan, A.; Bangle, R. E.; Cadranel, A.; Turlington, M. D.; Conroy, D. T.; Cauët, E.; Singleton, M. L.; Meyer, G. J.; Sampaio, R. N.; Elias, B.; Troian-Gautier, L., Accessing Photoredox Transformations with an Iron(Iii) Photosensitizer and Green Light. *J. Am. Chem. Soc.* **2021,** *143*, 15661-15673.
52. Bevernaegie, R.; Wehlin, S. A. M.; Elias, B.; Troian-Gautier, L., A Roadmap Towards Visible Light Mediated Electron Transfer Chemistry with Iridium(Iii) Complexes. *ChemPhotoChem* **2021,** *5*, 217-234.
53. Nicewicz, D. A.; MacMillan, D. W. C., Merging Photoredox Catalysis with Organocatalysis: The Direct Asymmetric Alkylation of Aldehydes. *Science* **2008,** *322*, 77-80.
54. Narayanam, J. M. R.; Tucker, J. W.; Stephenson, C. R. J., Electron-Transfer Photoredox Catalysis: Development of a Tin-Free Reductive Dehalogenation Reaction. *J. Am. Chem. Soc.* **2009,** *131*, 8756-8757.
55. Arias-Rotondo, D. M.; McCusker, J. K., The Photophysics of Photoredox Catalysis: A Roadmap for Catalyst Design. *Chem. Soc. Rev.* **2016,** *45*, 5803-5820.
56. Margrey, K. A.; Nicewicz, D. A., A General Approach to Catalytic Alkene Anti-Markovnikov Hydrofunctionalization Reactions Via Acridinium Photoredox Catalysis. *Acc. Chem. Res.* **2016,** *49*, 1997-2006.
57. Zhang, J.; Campolo, D.; Dumur, F.; Xiao, P.; Fouassier, J. P.; Gigmes, D.; Lalevée, J., Iron Complexes in Visible-Light-Sensitive Photoredox Catalysis: Effect of Ligands on Their Photoinitiation Efficiencies. *ChemCatChem* **2016,** *8*, 2227-2233.

58. Zhang, P.; Le, C. C.; MacMillan, D. W. C., Silyl Radical Activation of Alkyl Halides in Metallaphotoredox Catalysis: A Unique Pathway for Cross-Electrophile Coupling. *J. Am. Chem. Soc.* **2016,** *138*, 8084-8087.
59. Larsen, C. B.; Wenger, O. S., Photoredox Catalysis with Metal Complexes Made from Earth-Abundant Elements. *Chem-Eur. J.* **2018,** *24*, 2039-2058.
60. Glaser, F.; Kerzig, C.; Wenger, O. S., Multi-Photon Excitation in Photoredox Catalysis: Concepts, Applications, Methods. *Angew. Chem. Int. Ed.* **2020,** *59*, 10266-10284.
61. Ting, S. I.; Garakyaraghi, S.; Taliaferro, C. M.; Shields, B. J.; Scholes, G. D.; Castellano, F. N.; Doyle, A. G., 3d-D Excited States of Ni(Ii) Complexes Relevant to Photoredox Catalysis: Spectroscopic Identification and Mechanistic Implications. *J. Am. Chem. Soc.* **2020,** *142*, 5800-5810.
62. Sheridan, M. V.; Wang, Y.; Wang, D.; Troian-Gautier, L.; Dares, C. J.; Sherman, B. D.; Meyer, T. J., Light-Driven Water Splitting Mediated by Photogenerated Bromine. *Angew. Chem.* **2018,** *130*, 3507-3511.
63. Yang, M.; Yarnell, J. E.; El Roz, K.; Castellano, F. N., A Robust Visible-Light-Harvesting Cyclometalated Ir(Iii) Diimine Sensitizer for Homogeneous Photocatalytic Hydrogen Production. *ACS Appl. Energy Mater.* **2020,** *3*, 1842-1853.
64. Wang, Y.; Zhao, X.; Zhao, Y.; Yang, T.; Liu, X.; Xie, J.; Li, G.; Zhu, D.; Tan, H.; Su, Z., Photosensitizers Based on Ir(Iii) Complexes for Highly Efficient Photocatalytic Hydrogen Generation. *Dyes Pigments* **2019,** *170*, 107547.
65. Stoll, T.; Gennari, M.; Fortage, J.; Castillo, C. E.; Rebarz, M.; Sliwa, M.; Poizat, O.; Odobel, F.; Deronzier, A.; Collomb, M.-N., An Efficient Ruii–Rhiii–Ruii Polypyridyl Photocatalyst for Visible-Light-Driven Hydrogen Production in Aqueous Solution. *Angew. Chem. Int. Ed.* **2014,** *53*, 1654-1658.
66. Rupp, M.; Auvray, T.; Rousset, E.; Mercier, G. M.; Marvaud, V.; Kurth, D. G.; Hanan, G. S., Photocatalytic Hydrogen Evolution Driven by a Heteroleptic Ruthenium(Ii) Bis(Terpyridine) Complex. *Inorg. Chem.* **2019,** *58*, 9127-9134.
67. Pfeffer, M. G.; Müller, C.; Kastl, E. T. E.; Mengele, A. K.; Bagemihl, B.; Fauth, S. S.; Habermehl, J.; Petermann, L.; Wächtler, M.; Schulz, M.*, et al.*, Active Repair of a Dinuclear Photocatalyst for Visible-Light-Driven Hydrogen Production. *Nature Chem.* **2022,** *14*, 500-506.
68. Fischer, S.; Hollmann, D.; Tschierlei, S.; Karnahl, M.; Rockstroh, N.; Barsch, E.; Schwarzbach, P.; Luo, S.-P.; Junge, H.; Beller, M.*, et al.*, Death and Rebirth: Photocatalytic Hydrogen Production by a Self-Organizing Copper–Iron System. *ACS Catal.* **2014,** *4*, 1845-1849.
69. Fihri, A.; Artero, V.; Razavet, M.; Baffert, C.; Leibl, W.; Fontecave, M., Cobaloxime-Based Photocatalytic Devices for Hydrogen Production. *Angew. Chem. Int. Ed.* **2007,** *47*, 564-567.
70. Troian-Gautier, L.; Marcelis, L.; De Winter, J.; Gerbaux, P.; Moucheron, C., Two Ruthenium Complexes Capable of Storing Multiple Electrons on a Single Ligand - Photophysical, Photochemical and Electrochemical Properties of [Ru(Phen)2(Taphat)]2+ and [Ru(Phen)2(Taphat)Ru(Phen)2]4+. *Dalton Trans.* **2017,** *46*, 15287-15300.
71. Troian-Gautier, L.; Mugeniwabagara, E.; Fusaro, L.; Cauët, E.; Kirsch-De Mesmaeker, A.; Luhmer, M., Photo-Cidnp Reveals Different Protonation Sites Depending on the Primary Step of the Photoinduced Electron-/Proton-Transfer Process with Ru(Ii) Polyazaaromatic Complexes. *J. Am. Chem. Soc.* **2017,** *139*, 14909-14912.
72. Troian-Gautier, L.; Mugeniwabagara, E.; Fusaro, L.; Moucheron, C.; Kirsch-De Mesmaeker, A.; Luhmer, M., Ph Dependence of Photoinduced Electron Transfer with [Ru(Tap)3]2+. *Inorg. Chem.* **2017,** *56*, 1794-1803.
73. Pozza, M. D.; Mesdom, P.; Abdullrahman, A.; Prieto Otoya, T. D.; Arnoux, P.; Frochot, C.; Niogret, G.; Saubaméa, B.; Burckel, P.; Hall, J. P.*, et al.*, Increasing the Π-Expansive Ligands in Ruthenium(Ii)

Polypyridyl Complexes: Synthesis, Characterization, and Biological Evaluation for Photodynamic Therapy Applications. *Inorg. Chem.* **2023,** *62*, 18510-18523.
74. Mani, A.; Feng, T.; Gandioso, A.; Vinck, R.; Notaro, A.; Gourdon, L.; Burckel, P.; Saubaméa, B.; Blacque, O.; Cariou, K.*, et al.*, Structurally Simple Osmium(Ii) Polypyridyl Complexes as Photosensitizers for Photodynamic Therapy in the near Infrared**. *Angew. Chem. Int. Ed.* **2023,** *62*, e202218347.
75. Huang, H.; Yu, B.; Zhang, P.; Huang, J.; Chen, Y.; Gasser, G.; Ji, L.; Chao, H., Highly Charged Ruthenium(Ii) Polypyridyl Complexes as Lysosome-Localized Photosensitizers for Two-Photon Photodynamic Therapy. *Angew. Chem. Int. Ed.* **2015,** *54*, 14049-14052.
76. Raza, A.; Archer, S. A.; Fairbanks, S. D.; Smitten, K. L.; Botchway, S. W.; Thomas, J. A.; MacNeil, S.; Haycock, J. W., A Dinuclear Ruthenium(Ii) Complex Excited by near-Infrared Light through Two-Photon Absorption Induces Phototoxicity Deep within Hypoxic Regions of Melanoma Cancer Spheroids. *J. Am. Chem. Soc.* **2020,** *142*, 4639-4647.
77. Foxon, S. P.; Alamiry, M. A. H.; Walker, M. G.; Meijer, A. J. H. M.; Sazanovich, I. V.; Weinstein, J. A.; Thomas, J. A., Photophysical Properties and Singlet Oxygen Production by Ruthenium(Ii) Complexes of Benzo[I]Dipyrido[3,2-A:2′,3′-C]Phenazine: Spectroscopic and Td-Dft Study. *J. Phys. Chem. A* **2009,** *113*, 12754-12762.
78. Archer, S. A.; Raza, A.; Dröge, F.; Robertson, C.; Auty, A. J.; Chekulaev, D.; Weinstein, J. A.; Keane, T.; Meijer, A. J. H. M.; Haycock, J. W.*, et al.*, A Dinuclear Ruthenium(Ii) Phototherapeutic That Targets Duplex and Quadruplex DNA. *Chem. Sci.* **2019,** *10*, 3502-3513.
79. Lorand, J. P., The Cage Effect. In *Progress in Inorganic Chemistry*, Edwards, J. O., Ed. 1972; pp 207-325.
80. Rebbert, R. E.; Ausloos, P., The Photolysis and Radiolysis of Ch3n2ch3 and Ch3n2ch3-Cd3n2cd3 Mixtures1. *J. Phys. Chem* **1962,** *66*, 2253-2258.
81. Kornfeld, G.; Farkas, L.; Rabinowitsch, E., General Discussion. *Trans. Faraday Soc.* **1934,** *30*, 130-131.
82. Olmsted, J.; Meyer, T. J., Factors Affecting Cage Escape Yields Following Electron-Transfer Quenching. *J. Phys. Chem* **1987,** *91*, 1649-1655.
83. Georgopoulos, M.; Hoffman, M. Z., Cage Escape Yields in the Quenching of Tris (2,2'-Bipyridine)Ruthenium(Ii) by Methylviologen: Presence of Triethanolamine as a Sacrificial Electron Donor. *J. Phys. Chem* **1991,** *95*, 7717-7721.
84. Clark, C. D.; Hoffman, M. Z., Ion-Pairing Control of Excited-State Electron-Transfer Reactions. Quenching, Charge Recombination, and Back Electron Transfer. *J. Phys. Chem* **1996,** *100*, 7526-7532.
85. Sano, H.; Tachiya, M., Partially Diffusion-Controlled Recombination. *J. Chem. Phys.* **2008,** *71*, 1276-1282.
86. Eigen, M., Über Die Kinetik Sehr Schnell Verlaufender Ionenreaktionen in Wässeriger Lösung.*. *Z. Phys. Chem.* **1954,** *1*, 176-200.
87. Li, G.; Swords, W. B.; Meyer, G. J., Bromide Photo-Oxidation Sensitized to Visible Light in Consecutive Ion Pairs. *J. Am. Chem. Soc.* **2017,** *139*, 14983-14991.
88. Troian-Gautier, L.; Beauvilliers, E. E.; Swords, W. B.; Meyer, G. J., Redox Active Ion-Paired Excited States Undergo Dynamic Electron Transfer. *J. Am. Chem. Soc.* **2016,** *138*, 16815-16826.
89. De Kreijger, S.; Gillard, M.; Elias, B.; Troian-Gautier, L., Spectroscopic Techniques to Unravel Mechanistic Details in Light-Induced Transformations and Photoredox Catalysis. *ChemCatChem* **2024,** *16*, e202301100.
90. Bergeron, B. V.; Kelly, C. A.; Meyer, G. J., Thin Film Actinometers for Transient Absorption Spectroscopy: Applications to Dye-Sensitized Solar Cells. *Langmuir* **2003,** *19*, 8389-8394.

91. Yoshimura, A.; Hoffman, M. Z.; Sun, H., An Evaluation of the Excited State Absorption Spectrum of Ru(Bpy)32+ in Aqueous and Acetonitrile Solutions. *J. Photoch. Photobio. A* **1993,** *70*, 29-33.
92. Müller, P.; Brettel, K., [Ru(Bpy)3]2+ as a Reference in Transient Absorption Spectroscopy: Differential Absorption Coefficients for Formation of the Long-Lived 3mlct Excited State. *Photochem. Photobio. Sci.* **2012,** *11*, 632-636.
93. Goez, M.; von Ramin-Marro, D.; Othman Musa, M. H.; Schiewek, M., Photoionization of [Ru(Bpy)3]2+: A Catalytic Cycle with Water as Sacrificial Donor. *J. Phys. Chem. A* **2004,** *108*, 1090-1100.
94. Ripak, A.; De Kreijger, S.; Sampaio, R. N.; Vincent, C. A.; Cauët, É.; Jabin, I.; Tambar, U. K.; Elias, B.; Troian-Gautier, L., Photosensitized Activation of Diazonium Derivatives for C–B Bond Formation. *Chem Catal.* **2023**, 100490.
95. Ripak, A.; De Kreijger, S.; Elias, B.; Troian-Gautier, L., A Protocol for Determining Cage-Escape Yields Using Nanosecond Transient Absorption Spectroscopy. *STAR Protocols* **2023,** *4*, 102312.
96. Gould, I. R.; Farid, S., Concentration-Dependent Photoinduced Electron-Transfer Reactions: 1:1 and 1:2 Radical-Ion Complexes. *J. Am. Chem. Soc.* **1993,** *115*, 4814-4822.
97. Stern, O.; Volmer, M., Über Die Abklingungszit Der Fluoreszenz. *Phyik. Z.* **1919,** *20*, 183-188.
98. Benesi, H. A.; Hildebrand, J. H., A Spectrophotometric Investigation of the Interaction of Iodine with Aromatic Hydrocarbons. *J. Am. Chem. Soc.* **1949,** *71*, 2703-2707.
99. Ward, W. M.; Farnum, B. H.; Siegler, M.; Meyer, G. J., Chloride Ion-Pairing with Ru(Ii) Polypyridyl Compounds in Dichloromethane. *J. Phys. Chem. A* **2013,** *117*, 8883-8894.
100. Li, P.; Deetz, A. M.; Hu, J.; Meyer, G. J.; Hu, K., Chloride Oxidation by One- or Two-Photon Excitation of N-Phenylphenothiazine. *J. Am. Chem. Soc.* **2022,** *144*, 17604-17610.
101. Ye, Y.; Garrido-Barros, P.; Wellauer, J.; Cruz, C. M.; Lescouëzec, R.; Wenger, O. S.; Herrera, J. M.; Jiménez, J.-R., Luminescence and Excited-State Reactivity in a Heteroleptic Tricyanido Fe(Iii) Complex. *J. Am. Chem. Soc.* **2024,** *146*, 954-960.
102. Rosso, C.; Filippini, G.; Cozzi, P. G.; Gualandi, A.; Prato, M., Highly Performing Iodoperfluoroalkylation of Alkenes Triggered by the Photochemical Activity of Perylene Diimides. *ChemPhotoChem* **2019,** *3*, 193-197.
103. Tian, X.; Karl, T. A.; Reiter, S.; Yakubov, S.; de Vivie-Riedle, R.; König, B.; Barham, J. P., Electro-Mediated Photoredox Catalysis for Selective C(Sp3)–O Cleavages of Phosphinated Alcohols to Carbanions. *Angew. Chem. Int. Ed.* **2021,** *60*, 20817-20825.
104. Haimerl, J.; Ghosh, I.; König, B.; Vogelsang, J.; Lupton, J. M., Single-Molecule Photoredox Catalysis. *Chem. Sci.* **2019,** *10*, 681-687.
105. Glaser, F.; Wenger, O. S., Red Light-Based Dual Photoredox Strategy Resembling the Z-Scheme of Natural Photosynthesis. *JACS Au* **2022,** *2*, 1488-1503.
106. Glaser, F.; Schmitz, M.; Kerzig, C., Coulomb Interactions for Mediator-Enhanced Sensitized Triplet–Triplet Annihilation Upconversion in Solution. *Nanoscale* **2024,** *16*, 123-137.
107. Deetz, A. M.; Troian-Gautier, L.; Wehlin, S. A. M.; Piechota, E. J.; Meyer, G. J., On the Determination of Halogen Atom Reduction Potentials with Photoredox Catalysts. *J. Phys. Chem. A* **2021,** *125*, 9355-9367.
108. Sutherland, W., Lxxv. A Dynamical Theory of Diffusion for Non-Electrolytes and the Molecular Mass of Albumin. *London Edinburgh Philos. Mag. & J. Sci.* **1905,** *9*, 781-785.
109. Miller, C. C.; Walker, J., The Stokes-Einstein Law for Diffusion in Solution. *P. R. Soc. Lond. A-Conta.* **1924,** *106*, 724-749.
110. Einstein, A., Über Die Von Der Molekularkinetischen Theorie Der Wärme Geforderte Bewegung Von in Ruhenden Flüssigkeiten Suspendierten Teilchen. *Ann. Phys.* **1905,** *322*, 549-560.

111. Chiorboli, C.; Indelli, M. T.; Rampi Scandola, M. A.; Scandola, F., Salt Effects on Nearly Diffusion Controlled Electron-Transfer Reactions: Bimolecular Rate Constants and Cage Escape Yields in Oxidative Quenching of Tris(2,2'-Bipyridine)Ruthenium(Ii). *J. Phys. Chem* **1988,** *92*, 156-163.
112. Debye, P., Reaction Rates in Ionic Solutions. *T. Electrochem. Soc.* **1942,** *82*, 265.
113. Fuoss, R. M., Ionic Association. Iii. The Equilibrium between Ion Pairs and Free Ions. *J. Am. Chem. Soc.* **1958,** *80*, 5059-5061.
114. Turlington, M. D.; Troian-Gautier, L.; Sampaio, R. N.; Beauvilliers, E. E.; Meyer, G. J., Ligand Control of Supramolecular Chloride Photorelease. *Inorg. Chem.* **2018,** *57*, 5624-5631.
115. Turlington, M. D.; Troian-Gautier, L.; Sampaio, R. N.; Beauvilliers, E. E.; Meyer, G. J., Control of Excited-State Supramolecular Assembly Leading to Halide Photorelease. *Inorg. Chem.* **2019,** *58*, 3316-3328.
116. Montes-Navajas, P.; Garcia, H., Complexes of Basic Tricyclic Dyes in Their Acid and Basic Forms with Cucurbit[7]Uril: Determination of Pka and Association Constants in the Ground and Singlet Excited State. *J. Photoch. Photobio. A* **2009,** *204*, 97-101.
117. Grabowski, Z. R.; Rubaszewska, W., Generalised Förster Cycle. Thermodynamic and Extrathermodynamic Relationships between Proton Transfer, Electron Transfer and Electronic Excitation. *J. Chem. Soc., Faraday Trans. 1* **1977,** *73*, 11-28.
118. Deetz, A. M.; Meyer, G. J., Resolving Halide Ion Stabilization through Kinetically Competitive Electron Transfers. *JACS Au* **2022,** *2*, 985-995.
119. Sutin, N., Nuclear, Electronic, and Frequency Factors in Electron Transfer Reactions. *Acc. Chem. Res.* **1982,** *15*, 275-282.
120. Marcus, R. A., Tutorial on Rate Constants and Reorganization Energies. *J. Electroanal. Chem.* **2000,** *483*, 2-6.
121. Barbara, P. F.; Meyer, T. J.; Ratner, M. A., Contemporary Issues in Electron Transfer Research. *J. Phys. Chem* **1996,** *100*, 13148-13168.
122. Marcus, R. A., Electron Transfer Reactions in Chemistry. Theory and Experiment. *Rev. Mod. Phys.* **1993,** *65*, 599-610.
123. Piechota, E. J.; Meyer, G. J., Introduction to Electron Transfer: Theoretical Foundations and Pedagogical Examples. *J. Chem. Ed.* **2019,** *96*, 2450-2466.
124. Benniston, A. C.; Harriman, A., Charge on the Move: How Electron-Transfer Dynamics Depend on Molecular Conformation. *Chem. Soc. Rev.* **2006,** *35*, 169-179.
125. Moss, S. J.; Coady, C. J., Potential-Energy Surfaces and Transition-State Theory. *J. Chem. Ed.* **1983,** *60*, 455.
126. Schlegel, H. B., Exploring Potential Energy Surfaces for Chemical Reactions: An Overview of Some Practical Methods. *J. Comput. Chem.* **2003,** *24*, 1514-1527.
127. Brunschwig, B. S.; Sutin, N., Energy Surfaces, Reorganization Energies, and Coupling Elements in Electron Transfer. *Coord. Chem. Rev.* **1999,** *187*, 233-254.
128. Marcus, R. A., Local Approximation of Potential-Energy Surfaces by Surfaces Permitting Separation of Variables. *J. Chem. Phys.* **2004,** *41*, 610-616.
129. Lewis, N. A., Potential Energy Diagrams: A Conceptual Tool in the Study of Electron Transfer Reactions. *J. Chem. Ed.* **1980,** *57*, 478.
130. Skourtis, S. S.; Beratan, D. N.; Onuchic, J. N., The Two-State Reduction for Electron and Hole Transfer in Bridge-Mediated Electron-Transfer Reactions. *Chem. Phys.* **1993,** *176*, 501-520.
131. Di Giacomo, F., A Short Account of Rrkm Theory of Unimolecular Reactions and of Marcus Theory of Electron Transfer in a Historical Perspective. *J. Chem. Ed.* **2015,** *92*, 476-481.

132. Fawcett, W. R., *Liquids, Solutions, and Interfaces : From Classical Macroscopic Descriptions to Modern Microscopic Details*. Oxford University Press: Cary, United States, 2004.
133. Reynolds, L.; Gardecki, J. A.; Frankland, S. J. V.; Horng, M. L.; Maroncelli, M., Dipole Solvation in Nondipolar Solvents: Experimental Studies of Reorganization Energies and Solvation Dynamics. *J. Phys. Chem* **1996,** *100*, 10337-10354.
134. Hauser, A.; Enachescu, C.; Daku, M. L.; Vargas, A.; Amstutz, N., Low-Temperature Lifetimes of Metastable High-Spin States in Spin-Crossover and in Low-Spin Iron(Ii) Compounds: The Rule and Exceptions to the Rule. *Coord. Chem. Rev.* **2006,** *250*, 1642-1652.
135. Oliver, J. D.; Mullica, D. F.; Hutchinson, B. B.; Milligan, W. O., Iron-Nitrogen Bond Lengths in Low-Spin and High-Spin Iron(Ii) Complexes with Poly(Pyrazolyl)Borate Ligands. *Inorg. Chem.* **1980,** *19*, 165-169.
136. Rohmer, M.-M.; Strich, A.; Bénard, M.; Malrieu, J.-P., Metal−Metal Bond Length Variability in Co3(Dipyridylamide)4cl2: Bond-Stretch Isomerism, Crystal Field Effects, or Spin Transition Process? A Dft Study. *J. Am. Chem. Soc.* **2001,** *123*, 9126-9134.
137. McGrath, C. M.; O'Connor, C. J.; Sangregorio, C.; Seddon, J. M. W.; Sinn, E.; Sowrey, F. E.; Young, N. A., Direct Measurement of the High-Spin and Low-Spin Bond Lengths and the Spin State Population in Mixed Spin State Systems: An Fe K-Edge Xafs Study of Iron(Iii) Dithiocarbamate Complexes. *Inorg. Chem. Commun.* **1999,** *2*, 536-539.
138. Chen, K.; Costas, M.; Que, J. L., Spin State Tuning of Non-Heme Iron-Catalyzed Hydrocarbon Oxidations: Participation of Feiii–Ooh and Fev□O Intermediates. *J. Chem. Soc. Dalton* **2002**, 672-679.
139. Demadis, K. D.; Hartshorn, C. M.; Meyer, T. J., The Localized-to-Delocalized Transition in Mixed-Valence Chemistry. *Chem. Rev.* **2001,** *101*, 2655-2686.
140. Hu, K.; Blair, A. D.; Piechota, E. J.; Schauer, P. A.; Sampaio, R. N.; Parlane, F. G. L.; Meyer, G. J.; Berlinguette, C. P., Kinetic Pathway for Interfacial Electron Transfer from a Semiconductor to a Molecule. *Nature Chem.* **2016,** *8*, 853.
141. Piechota, E. J.; Troian-Gautier, L.; Sampaio, R. N.; Brennaman, M. K.; Hu, K.; Berlinguette, C. P.; Meyer, G. J., Optical Intramolecular Electron Transfer in Opposite Directions through the Same Bridge That Follows Different Pathways. *J. Am. Chem. Soc.* **2018,** *140*, 7176-7186.
142. Sampaio, R. N.; Piechota, E. J.; Troian-Gautier, L.; Maurer, A. B.; Hu, K.; Schauer, P. A.; Blair, A. D.; Berlinguette, C. P.; Meyer, G. J., Kinetics Teach That Electronic Coupling Lowers the Free-Energy Change That Accompanies Electron Transfer. *Proc. Natl. Acad. Sci. USA* **2018,** *115*, 7248-7253.
143. Lambert, C.; Nöll, G., The Class Ii/Iii Transition in Triarylamine Redox Systems. *J. Am. Chem. Soc.* **1999,** *121*, 8434-8442.
144. Robin, M. B.; Day, P., Mixed Valence Chemistry-a Survey and Classification. In *Advances in Inorganic Chemistry and Radiochemistry*, Emeléus, H. J.; Sharpe, A. G., Eds. Academic Press: 1968; Vol. 10, pp 247-422.
145. Hush, N. S., Intervalence-Transfer Absorption. Part 2. Theoretical Considerations and Spectroscopic Data. In *Progress in Inorganic Chemistry*, Cotton, F. A., Ed. John Wiley & Sons: New York, London, Sidney, 1967; pp 391-444.
146. Hush, N. S., Distance Dependence of Electron Transfer Rates. *Coord. Chem. Rev.* **1985,** *64*, 135-157.
147. Roest, M. R.; Verhoeven, J. W.; Schuddeboom, W.; Warman, J. M.; Lawson, J. M.; Paddon-Row, M. N., Solvent and Distance Dependent Charge Separation in Rigid Trichromophoric Systems. *J. Am. Chem. Soc.* **1996,** *118*, 1762-1768.
148. Paddon-Row, M. N., Investigating Long-Range Electron-Transfer Processes with Rigid, Covalently Linked Donor-(Norbornylogous Bridge)-Acceptor Systems. *Acc. Chem. Res.* **1994,** *27*, 18-25.

149. Ondersma, J. W.; Hamann, T. W., Measurements and Modeling of Recombination from Nanoparticle Tio2 Electrodes. *J. Am. Chem. Soc.* **2011,** *133*, 8264-8271.
150. DeVries, M. J.; Pellin, M. J.; Hupp, J. T., Dye-Sensitized Solar Cells: Driving-Force Effects on Electron Recombination Dynamics with Cobalt-Based Shuttles. *Langmuir* **2010,** *26*, 9082-9087.
151. Balzani, V.; Scandola, F.; Orlandi, G.; Sabbatini, N.; Indelli, M. T., The Nonadiabaticity Problem of Outer-Sphere Electron-Transfer Reactions. Reduction and Oxidation of Europium Ions. *J. Am. Chem. Soc.* **1981,** *103*, 3370-3378.
152. Beratan, D. N.; Onuchic, J. N., Adiabaticity and Nonadiabaticity in Bimolecular Outer-Sphere Charge Transfer Reactions. *J. Chem. Phys.* **1988,** *89*, 6195-6203.
153. Zusman, L. D., Outer-Sphere Electron Transfer in Polar Solvents. *Chemical Physics* **1980,** *49*, 295-304.
154. Bolton, J. R.; Archer, M. D., Basic Electron-Transfer Theory. In *Electron Transfer in Inorganic, Organic, and Biological Systems*, American Chemical Society: 1991; Vol. 228, pp 7-23.
155. Kurland, R. J.; Winkler, M. E., Ferrocynanide Carbon-13 Nmr Line Broadening as a Probe of Electron Transfer Reactions. *J. Biochem. Biophys. Methods* **1981,** *4*, 215-225.
156. Koval, C. A.; Margerum, D. W., Determination of the Self-Exchange Electron-Transfer Rate Constant for a Copper(Iii/Ii) Tripeptide Complex by Proton Nmr Line Broadening. *Inorg. Chem.* **1981,** *20*, 2311-2318.
157. Zandstra, P. J.; Weissman, S. I., Note on Measurements of Rates of Electron Transfer Processes by Broadening of Esr Lines. *J. Chem. Phys.* **2004,** *35*, 757-757.
158. Creutz, C., Mechanism of the Quenching of the Emission of Substituted Polypyridineruthenium(Ii) Complexes by Europium(Ii). *Inorg. Chem.* **1978,** *17*, 1046-1051.
159. Marcus, R. A., On the Theory of Electron-Transfer Reactions. Vi. Unified Treatment for Homogeneous and Electrode Reactions. *J. Chem. Phys.* **2004,** *43*, 679-701.
160. Roth, J. P.; Yoder, J. C.; Won, T.-J.; Mayer, J. M., Application of the Marcus Cross Relation to Hydrogen Atom Transfer Reactions. *Science* **2001,** *294*, 2524-2526.
161. Ratner, M. A.; Levine, R. D., A Thermodynamic Derivation of the Cross-Relations for Rates of Electron-Transfer Reactions. *J. Am. Chem. Soc.* **1980,** *102*, 4898-4900.
162. Koenig, T.; Fischer, H., Cage Effects. In *Free Radicals*, Kochi, J. K., Ed. Wiley: New York, 1973; Vol. 1, pp 157-189.
163. Haselbach, E.; Vauthey, E.; Suppan, P., Comparison of Photoinduced Electron Transfer Reactions of Aromatic Carbonyl Vs. Cyano Compounds with Electron Donors in Condensed Phase:The Importance. *Tetrahedron* **1988,** *44*, 7335-7344.
164. Bruce, J. M.; Dodd, N. J. F.; Gorman, A. A.; Hamblett, I.; Kerr, C. W.; Lambert, C.; McNeeney, S. P., Anthralin-Derived Transients—Ii. Formation of the Radical by Spontaneous Fragmentation of Both Singlet and Triplet States of the 10,10′-Dehydrodimer: Radical Pair Multiplicity Effects. *Photochem. Photobiol.* **1990,** *52*, 345-351.
165. Dektar, J. L.; Hacker, N. P., Triphenylsulfonium Salt Photochemistry. New Evidence for Triplet Excited State Reactions. *J. Org. Chem.* **1988,** *53*, 1833-1835.
166. Holten, D.; Gouterman, M.; Parson, W. W.; Windsor, M. W.; Rockley, M. G., Electron Transfer from Photoexcited Singlet and Triplet Bacteriopheophytin. *Photochem. Photobiol.* **1976,** *23*, 415-423.
167. Gouterman, M.; Holten, D., Electron Transfer from Photoexcited Singlet and Triplet Bacteriopheophytin—Ii. Theoretical. *Photochem. Photobiol.* **1977,** *25*, 85-92.
168. Harriman, A.; Porter, G.; Wilowska, A., Photoreduction of Benzo-1,4-Quinone Sensitised by Metalloporphyrins. *J. Chem. Soc., Faraday Trans. 2* **1983,** *79*, 807-816.

169. Schuster, D. I.; Karp, P. B., Photochemistry of Ketones in Solution Lviii: Mechanism of Photoreduction of Benzophenone by Benzhydrol. *J. Photochem.* **1980,** *12*, 333-344.
170. Johnston, L. J.; Wong, D. F., Electron Transfer Reactions of Triplet 9-Arylxanthenium and 9-Arylthioxanthenium Cations. *J. Phys. Chem* **1993,** *97*, 1589-1595.
171. Neumann, S.; Wenger, O. S.; Kerzig, C., Controlling Spin-Correlated Radical Pairs with Donor–Acceptor Dyads: A New Concept to Generate Reduced Metal Complexes for More Efficient Photocatalysis. *Chem-Eur. J.* **2021,** *27*, 4115-4123.
172. Khudyakov, I. V.; Serebrennikov, Y. A.; Turro, N. J., Spin-Orbit Coupling in Free-Radical Reactions: On the Way to Heavy Elements. *Chem. Rev.* **1993,** *93*, 537-570.
173. Takahiro, N.; Yasuhiko, S., A Striking Effect of Spin Multiplicity on the Photoinduced Electron-Transfer Reaction of a 1-Vinylnaphthalene – Pyromellitic Dianhydride System. *Chem. Lett.* **1994,** *23*, 1577-1580.
174. Satoh, S. I.; Nakajima, T.; Shirota, Y., The Effect of Spin Multiplicity on the Photochemical Reaction of a 2-Vinylnaphthalene-Dichloromaleic Anhydride System. *Research on Chemical Intermediates* **1995,** *21*, 939-949.
175. Giachino, G. G.; Kearns, D. R., Nature of the External Heavy-Atom Effect on Radiative and Nonradiative Singlet–Triplet Transitions. *J. Chem. Phys.* **1970,** *52*, 2964-2974.
176. Giachino, G. G.; Kearns, D. R., External Heavy Atom Perturbation of Vibronic Transitions in Singlet–Triplet Spectra. *J. Chem. Phys.* **1970,** *53*, 3886-3891.
177. McClure, D. S., Triplet-Singlet Transitions in Organic Molecules. Lifetime Measurements of the Triplet State. *J. Chem. Phys.* **2004,** *17*, 905-913.
178. Kasha, M., Collisional Perturbation of Spin-Orbital Coupling and the Mechanism of Fluorescence Quenching. A Visual Demonstration of the Perturbation. *J. Chem. Phys.* **1952,** *20*, 71-74.
179. McGlynn, S. P.; Sunseri, R.; Christodouleas, N., External Heavy-Atom Spin-Orbital Coupling Effect. I. The Nature of the Interaction. *J. Chem. Phys.* **1962,** *37*, 1818-1824.
180. Koziar, J. C.; Cowan, D. O., Photochemical Heavy-Atom Effects. *Acc. Chem. Res.* **1978,** *11*, 334-341.
181. Mok, K. H.; Hore, P. J., Photo-Cidnp Nmr Methods for Studying Protein Folding. *Methods* **2004,** *34*, 75-87.
182. Goez, M., Chapter 3 Photo-Cidnp Spectroscopy. In *Annual Reports on Nmr Spectroscopy*, Academic Press: 2009; Vol. 66, pp 77-147.
183. Hore, J.; Broadhurst, R. W., Photo-Cidnp of Biopolymers. *Prog. Nucl. Magn. Reson. Spectrosc.* **1993,** *25*, 345-402.
184. Goez, M., Elucidating Organic Reaction Mechanisms Using Photo-Cidnp Spectroscopy. In *Hyperpolarization Methods in Nmr Spectroscopy*, Kuhn, L. T., Ed. Springer Berlin Heidelberg: Berlin, Heidelberg, 2013; pp 1-32.
185. Kuhn, L. T., Photo-Cidnp Nmr Spectroscopy of Amino Acids and Proteins. In *Hyperpolarization Methods in Nmr Spectroscopy*, Kuhn, L. T., Ed. Springer Berlin Heidelberg: Berlin, Heidelberg, 2013; pp 229-300.
186. Okuno, Y.; Cavagnero, S., Photochemically Induced Dynamic Nuclear Polarization: Basic Principles and Applications. In *Emagres*, pp 283-314.
187. Kaptein, R., Biological Magnetic Resonance. *LJ Berliner and J. Reuben* **1982,** *5*.
188. McLauchlan, K. A.; Steiner, U. E., Invited Article. *Mol. Phys.* **1991,** *73*, 241-263.
189. Salikhov, K. M.; Sagdeev, R. Z.; Buchachenko, A. L., *Spin Polarization and Magnetic Effects in Radical Reactions*. Elsevier: Netherlands, 1984.

190. Steiner, U. E.; Ulrich, T., Magnetic Field Effects in Chemical Kinetics and Related Phenomena. *Chem. Rev.* **1989,** *89*, 51-147.
191. Ulrich, T.; Steiner, U. E.; Schlenker, W., Control of Photo-Electron-Transfer Induced Radical Production by Micellar Cages, Heavy-Atom Substituents and Magnetic Fields. *Tetrahedron* **1986,** *42*, 6131-6142.
192. Steiner, U., A Triplet Mechanism for Magnetic Field Modulation of Photochemical Quantum Yields. *Berich. Bunsen. Gesell.* **1981,** *85*, 228-233.
193. Zewail, A. H., Femtochemistry: Atomic-Scale Dynamics of the Chemical Bond Using Ultrafast Lasers (Nobel Lecture). *Angew. Chem. Int. Ed.* **2000,** *39*, 2586-2631.
194. Kumpulainen, T.; Lang, B.; Rosspeintner, A.; Vauthey, E., Ultrafast Elementary Photochemical Processes of Organic Molecules in Liquid Solution. *Chem. Rev.* **2017,** *117*, 10826-10939.
195. Liu, Y.; Turner, D. B.; Singh, T. N.; Angeles-Boza, A. M.; Chouai, A.; Dunbar, K. R.; Turro, C., Ultrafast Ligand Exchange: Detection of a Pentacoordinate Ru(Ii) Intermediate and Product Formation. *J. Am. Chem. Soc.* **2009,** *131*, 26-27.
196. Steinke, S. J.; Gupta, S.; Piechota, E. J.; Moore, C. E.; Kodanko, J. J.; Turro, C., Photocytotoxicity and Photoinduced Phosphine Ligand Exchange in a Ru(Ii) Polypyridyl Complex. *Chem. Sci.* **2022,** *13*, 1933-1945.
197. A L Harris; J K Brown, a.; Harris, C. B., The Nature of Simple Photodissociation Reactions in Liquids on Ultrafast Time Scales. *Annu. Rev. Phys. Chem.* **1988,** *39*, 341-366.
198. Booth, D.; Noyes, R. M., The Effect of Viscosity on the Quantum Yield for Iodine Dissociation. *J. Am. Chem. Soc.* **1960,** *82*, 1868-1872.
199. Lampe, F. W.; Noyes, R. M., Absolute Quantum Yields for Dissociation of Iodine in Inert Solvents. *J. Am. Chem. Soc.* **1954,** *76*, 2140-2144.
200. Chuang, T. J.; Hoffman, G. W.; Eisenthal, K. B., Picosecond Studies of the Cage Effect and Collision Induced Predissociation of Iodine in Liquids. *Chem. Phys. Lett.* **1974,** *25*, 201-205.
201. Langhoff, C. A.; Moore, B.; DeMeuse, M., Diffusive and Nondiffusive Time Scales in the Dissociation and Recombination of Molecular Iodine in Linear Alkanes. *J. Am. Chem. Soc.* **1982,** *104*, 3576-3579.
202. Waits, H. P.; Hammond, G. S., Cage Effects in Thermal Decomposition Reactions in Solution. *J. Am. Chem. Soc.* **1964,** *86*, 1911-1918.
203. Hammond, G. S.; Fox, J. R., Cage Effects in Thermal and Photochemical Decomposition of an Azo Compound. *J. Am. Chem. Soc.* **1964,** *86*, 1918-1921.
204. Hammond, G. S.; Wu, C.-H. S.; Trapp, O. D.; Warkentin, J.; Keys, R. T., The Mechanism of Decomposition of Azo Compounds. Ii. Cage Effects in the Decomposition of A,A-Azoisobutyronitrile and Related Compounds. *J. Am. Chem. Soc.* **1960,** *82*, 5394-5399.
205. Strong, R. L., The Photoproduction and Recombination of Bromine Atoms in the Liquid Phase. *J. Am. Chem. Soc.* **1965,** *87*, 3563-3567.
206. Miller, A. A.; Willard, J. E., The Exchange Reaction between Bromine and Bromotrichloromethane. *J. Chem. Phys.* **2004,** *17*, 168-175.
207. Tanner, D. D.; Meintzer, C. P.; Dionarian, N.; Singh, H.; Tsai, E. C.; Oumar-Mahamat, H., Cage Return and Solvent Viscosity and Their Importance in Determining the Kinetic Deuterium Isotope Effect Observed During Benzylic Bromination. *J. Am. Chem. Soc.* **1990,** *112*, 2736-2739.
208. Zhu, Z. R.; Harris, J. M., Photodissociation and Nongeminate Recombination of Bromine in Liquids Initiated by 532 Nm Radiation. *Chem. Phys. Lett.* **1991,** *186*, 183-188.
209. Abul-Haj, N. A.; Kelley, D. F., Geminate Recombination and Relaxation of Molecular Bromine. *Chem. Phys. Lett.* **1985,** *119*, 182-187.

210. Kong, Q.; Lee, J. H.; Lo Russo, M.; Kim, T. K.; Lorenc, M.; Cammarata, M.; Bratos, S.; Buslaps, T.; Honkimaki, V.; Ihee, H.; Wulff, M., Photolysis of Br2 in Ccl4 Studied by Time-Resolved X-Ray Scattering. *Acta Crystallogr. A* **2010,** *66*, 252-260.
211. Hippler, H.; Schubert, V.; Troe, J., Photolysis Quantum Yields and Atom Recombination Rates of Bromine in Compressed Gases. Experiments up to 7 Kbar. *J. Chem. Phys.* **1984,** *81*, 3931-3941.
212. Lee, W.; Lee, Y.; Allard, S.; Ra, J.; Han, S.; Lee, Y., Mechanistic and Kinetic Understanding of the Uv254 Photolysis of Chlorine and Bromine Species in Water and Formation of Oxyhalides. *Environ. Sci. Technol.* **2020,** *54*, 11546-11555.
213. J Schroeder; Troe, J., Elementary Reactions in the Gas-Liquid Transition Range. *Annu. Rev. Phys. Chem.* **1987,** *38*, 163-190.
214. MacDonald, L. H.; Strong, R. L., Excited States in Bromine Photoexcitation and Recombination. *J. Phys. Chem* **1991,** *95*, 6940-6945.
215. Raftery, D.; Iannone, M.; Phillips, C. M.; Hochstrasser, R. M., Hydrogen Abstraction Dynamics in Solution Studied by Picosecond Infrared Spectroscopy. *Chem. Phys. Lett.* **1993,** *201*, 513-520.
216. Brady Clark, K.; Griller, D., Cage Effect on the Photolysis of Chlorine in Solution. *Chem. Phys. Lett.* **1990,** *168*, 477-481.
217. Orr-Ewing, A. J., Taking the Plunge: Chemical Reaction Dynamics in Liquids. *Chem. Soc. Rev.* **2017,** *46*, 7597-7614.
218. Raftery, D.; Gooding, E.; Romanovsky, A.; Hochstrasser, R. M., Vibrational Product State Dynamics in Solution Phase Bimolecular Reactions: Transient Infrared Study of Cn Radical Reactions. *J. Chem. Phys.* **1994,** *101*, 8572-8579.
219. Benjamin, I., Photodissociation of Icn in Liquid Chloroform: Molecular Dynamics of Ground and Excited State Recombination, Cage Escape, and Hydrogen Abstraction Reaction. *J. Chem. Phys.* **1995,** *103*, 2459-2471.
220. Vieceli, J.; Chorny, I.; Benjamin, I., Photodissociation of Icn at the Liquid/Vapor Interface of Chloroform. *J. Chem. Phys.* **2001,** *115*, 4819-4828.
221. Winter, N.; Chorny, I.; Vieceli, J.; Benjamin, I., Molecular Dynamics Study of the Photodissociation and Photoisomerization of Icn in Water. *J. Chem. Phys.* **2003,** *119*, 2127-2143.
222. Winter, N.; Benjamin, I., Photodissociation of Icn at the Liquid/Vapor Interface of Water. *J. Chem. Phys.* **2004,** *121*, 2253-2263.
223. Johnson, M. L.; Benjamin, I., Photodissociation of Icn at the Water/Chloroform Interface. *J. Phys. Chem. A* **2009,** *113*, 7403-7411.
224. Benjamin, I., Theory and Computer Simulations of Solvation and Chemical Reactions at Liquid Interfaces. *Acc. Chem. Res.* **1995,** *28*, 233-239.
225. Benjamin, I., Chemical Reactions and Solvation at Liquid Interfaces: A Microscopic Perspective. *Chem. Rev.* **1996,** *96*, 1449-1476.
226. Winter, N. D.; Do, A. J., Molecular Dynamics Study of the Photodissociation of Icn in Ethanol: Effect of Solvent Polarity. *Journal of Solution Chemistry* **2021,** *50*, 894-919.
227. Benderskii, A. V.; Wight, C. A., Photochemistry of Ozone in Solid Mixtures with Argon. *J. Chem. Phys.* **1994,** *101*, 292-298.
228. Wang, Z.; Wasserman, T.; Gershgoren, E.; Ruhman, S., Vibrational Dephasing of I3− in Cooled Ethanol Solutions — Where Is the Inhomogeneity? *J. Mol. Liq.* **2000,** *86*, 229-236.
229. Wang, Z.; Wasserman, T.; Gershgoren, E.; Vala, J.; Kosloff, R.; Ruhman, S., Geminate Recombination of I3− in Cooled Liquid and Glassy Ethanol. *Chem. Phys. Lett.* **1999,** *313*, 155-161.

230. Gardner, J. M.; Abrahamsson, M.; Farnum, B. H.; Meyer, G. J., Visible Light Generation of Iodine Atoms and I−I Bonds: Sensitized I− Oxidation and I3− Photodissociation. *J. Am. Chem. Soc.* **2009,** *131*, 16206-16214.
231. Schutte, E.; Weakley, T. J. R.; Tyler, D. R., Radical Cage Effects in the Photochemical Degradation of Polymers: Effect of Radical Size and Mass on the Cage Recombination Efficiency of Radical Cage Pairs Generated Photochemically from the (Cpch2ch2n(Ch3)C(O)(Ch2)Nch3)2mo2(Co)6 (N = 3, 8, 18) Complexes. *J. Am. Chem. Soc.* **2003,** *125*, 10319-10326.
232. Oelkers, A. B.; Scatena, L. F.; Tyler, D. R., Femtosecond Pump−Probe Transient Absorption Study of the Photolysis of [Cp‘Mo(Co)3]2 (Cp‘ = H5-C5h4ch3): Role of Translational and Rotational Diffusion in the Radical Cage Effect. *J. Phys. Chem. A* **2007,** *111*, 5353-5360.
233. Harris, J. D.; Oelkers, A. B.; Tyler, D. R., The Solvent Cage Effect: Is There a Spin Barrier to Recombination of Transition Metal Radicals? *J. Am. Chem. Soc.* **2007,** *129*, 6255-6262.
234. Covert, K. J.; Askew, E. F.; Grunkemeier, J.; Koenig, T.; Tyler, D. R., Cage Effects in Organometallic Radical Chemistry. Fractional Cage-Recombination Efficiency for Photochemical Caged-Pair Intermediates of Cp'2m2(Co)6 (M = Molybdenum and Tungsten; Cp' = .Eta.5-C5h4ch3). *J. Am. Chem. Soc.* **1992,** *114*, 10446-10448.
235. Barry, J. T.; Berg, D. J.; Tyler, D. R., Radical Cage Effects: The Prediction of Radical Cage Pair Recombination Efficiencies Using Microviscosity across a Range of Solvent Types. *J. Am. Chem. Soc.* **2017,** *139*, 14399-14405.
236. Barry, J. T.; Tyler, D. R., Solvent Cage Effects: A Comparison of Geminate and Nongeminate Radical Cage Pair Combination Efficiencies. *Inorg. Chem.* **2020,** *59*, 13875-13879.
237. Braden, D. A.; Parrack, E. E.; Tyler, D. R., Solvent Cage Effects. I. Effect of Radical Mass and Size on Radical Cage Pair Recombination Efficiency. Ii. Is Geminate Recombination of Polar Radicals Sensitive to Solvent Polarity? *Coord. Chem. Rev.* **2001,** *211*, 279-294.
238. *Methods in Enzymology*. Academic Press: New York, 1998; Vol. 291.
239. Borfecchia, E.; Garino, C.; Salassa, L.; Ruiu, T.; Gianolio, D.; Zhang, X.; Attenkofer, K.; Chen, L. X.; Gobetto, R.; Sadler, P. J.; Lamberti, C., X-Ray Transient Absorption Structural Characterization of the 3mlct Triplet Excited State of Cis-[Ru(Bpy)2(Py)2]2+. *Dalton Trans.* **2013,** *42*, 6564-6571.
240. Antonini, E.; Brunori, M., *Hemoglobin and Myoglobin in Their Reactions with Ligands*. Amsterdam : North-Holland: 1971.
241. Jones, A. R., The Photochemistry and Photobiology of Vitamin B12. *Photochem. Photobio. Sci.* **2017,** *16*, 820-834.
242. White, J. K.; Schmehl, R. H.; Turro, C., An Overview of Photosubstitution Reactions of Ru (Ii) Imine Complexes and Their Application in Photobiology and Photodynamic Therapy. *Inorg. Chim. Acta* **2017,** *454*, 7-20.
243. Barigelletti, F.; Juris, A.; Balzani, V.; Belser, P.; Von Zelewsky, A., Excited-State Properties of Complexes of the Tris(Diimine)Ruthenium(2+) Ion Family. *Inorg. Chem.* **1983,** *22*, 3335-3339.
244. Soupart, A.; Alary, F.; Heully, J.-L.; Elliott, P. I. P.; Dixon, I. M., Recent Progress in Ligand Photorelease Reaction Mechanisms: Theoretical Insights Focusing on Ru (Ii) 3mc States. *Coord. Chem. Rev.* **2020,** *408*, 213184.
245. Soupart, A.; Alary, F.; Heully, J.-L.; Elliott, P. I. P.; Dixon, I. M., Theoretical Study of the Full Photosolvolysis Mechanism of [Ru(Bpy)3]2+: Providing a General Mechanistic Roadmap for the Photochemistry of [Ru(N^N)3]2+-Type Complexes toward Both Cis and Trans Photoproducts. *Inorg. Chem.* **2020,** *59*, 14679-14695.
246. Eastham, K.; Scattergood, P. A.; Chu, D.; Boota, R. Z.; Soupart, A.; Alary, F.; Dixon, I. M.; Rice, C. R.; Hardman, S. J. O.; Elliott, P. I. P., Not All 3mc States Are the Same: The Role of 3mccis States in the

Photochemical N∧ N Ligand Release from [Ru (Bpy) 2 (N∧ N)] 2+ Complexes. *Inorg. Chem.* **2022,** *61*, 19907-19924.
247. Geoffroy, G. L.; Hammond, G. S.; Gray, H. B., Photochemical Reductive Elimination of Oxygen, Hydrogen, and Hydrogen Chloride from Iridium Complexes. *J. Am. Chem. Soc.* **1975,** *97*, 3933-3936.
248. White, J. K.; Schmehl, R. H.; Turro, C., An Overview of Photosubstitution Reactions of Ru(Ii) Imine Complexes and Their Application in Photobiology and Photodynamic Therapy. *Inorg. Chim. Acta* **2017,** *454*, 7-20.
249. Cerfontaine, S.; Wehlin, S. A. M.; Elias, B.; Troian-Gautier, L., Photostable Polynuclear Ruthenium (Ii) Photosensitizers Competent for Dehalogenation Photoredox Catalysis at 590 Nm. *J. Am. Chem. Soc.* **2020,** *142*, 5549-5555.
250. Cerfontaine, S.; Troian-Gautier, L.; Wehlin, S. A. M.; Loiseau, F.; Cauët, E.; Elias, B., Tuning the Excited-State Deactivation Pathways of Dinuclear Ruthenium (Ii) 2, 2′-Bipyridine Complexes through Bridging Ligand Design. *Dalton Trans.* **2020,** *49*, 8096-8106.
251. Cerfontaine, S.; Troian-Gautier, L.; Duez, Q.; Cornil, J.; Gerbaux, P.; Elias, B., Mlct Excited-State Behavior of Trinuclear Ruthenium(Ii) 2,2′-Bipyridine Complexes. *Inorg. Chem.* **2021,** *60*, 366-379.
252. Li, G.; Brady, M. D.; Meyer, G. J., Visible Light Driven Bromide Oxidation and Ligand Substitution Photochemistry of a Ru Diimine Complex. *J. Am. Chem. Soc.* **2018,** *140*, 5447-5456.
253. Steinke, S. J.; Piechota, E. J.; Loftus, L. M.; Turro, C., Acetonitrile Ligand Photosubstitution in Ru(Ii) Complexes Directly from the 3mlct State. *J. Am. Chem. Soc.* **2022,** *144*, 20177-20182.
254. James, B. R., The Porphyrins. In *The Porphyrins*, Dolphin, D., Ed. Academic Press: New York, 1978; Vol. V.
255. Momenteau, M.; Reed, C. A., Synthetic Heme-Dioxygen Complexes. *Chem. Rev.* **1994,** *94*, 659-698.
256. Antonini, E., Hemoglobin and Myoglobin in Their Reactions with Ligands. *Front. Biol.* **1971,** *21*, 27-31.
257. Hastings, J. W.; Olson, J. S., Quentin H. Gibson, a Biographical Memoir. *National Academy of Sciences* **2014**, 1-26.
258. Gibson, Q. H.; Ainsworth, S., Photosensitivity of Hæm Compounds. *Nature* **1957,** *180*, 1416-1417.
259. Noble, R. W.; Brunori, M.; Wyman, J.; Antonini, E., Studies on the Quantum Yields of the Photodissociation of Carbon Monoxide from Hemoglobin and Myoglobin*. *Biochem.* **1967,** *6*, 1216-1222.
260. Chernoff, D. A.; Hochstrasser, R. M.; Steele, A. W., Geminate Recombination of O2 and Hemoglobin. *Proc. Natl. Acad. Sci. USA* **1980,** *77*, 5606-5610.
261. Noe, L. J.; Eisert, W. G.; Rentzepis, P. M., Picosecond Photodissociation and Subsequent Recombination Processes in Carbon Monoxide Hemoglobin. *Proc. Natl. Acad. Sci. USA* **1978,** *75*, 573-577.
262. Eisert, W.; Degenkolb, E.; Noe, L.; Rentzepis, P., Kinetics of Carboxymyoglobin and Oxymyoglobin Studied by Picosecond Spectroscopy. *Biophys. J.* **1979,** *25*, 455-464.
263. Scaltrito, D. V.; Fry, H. C.; Showalter, B. M.; Thompson, D. W.; Liang, H.-C.; Zhang, C. X.; Kretzer, R. M.; Kim, E.-i.; Toscano, J. P.; Karlin, K. D.; Meyer, G. J., Reversible Carbon Monoxide Photodissociation from Cu(I) Coordination Compounds. *Inorg. Chem.* **2001,** *40*, 4514-4515.
264. Laverman, L. E.; Wanat, A.; Oszajca, J.; Stochel, G.; Ford, P. C.; van Eldik, R., Mechanistic Studies on the Reversible Binding of Nitric Oxide to Metmyoglobin. *J. Am. Chem. Soc.* **2001,** *123*, 285-293.
265. Laverman, L. E.; Ford, P. C., Mechanistic Studies of Nitric Oxide Reactions with Water Soluble Iron(Ii), Cobalt(Ii), and Iron(Iii) Porphyrin Complexes in Aqueous Solutions: Implications for Biological Activity. *J. Am. Chem. Soc.* **2001,** *123*, 11614-11622.

266. Ye, X.; Demidov, A.; Champion, P. M., Measurements of the Photodissociation Quantum Yields of Mbno and Mbo2 and the Vibrational Relaxation of the Six-Coordinate Heme Species. *J. Am. Chem. Soc.* **2002,** *124*, 5914-5924.
267. Walda, K. N.; Liu, X. Y.; Sharma, V. S.; Magde, D., Geminate Recombination of Diatomic Ligands Co, O2, and No with Myoglobin. *Biochem.* **1994,** *33*, 2198-2209.
268. Fry, H. C.; Hoertz, P. G.; Wasser, I. M.; Karlin, K. D.; Meyer, G. J., Efficient Photodissociation of O2 from Synthetic Heme and Heme/M (M = Fe, Cu) Complexes. *J. Am. Chem. Soc.* **2004,** *126*, 16712-16713.
269. Babcock, G. T., How Oxygen Is Activated and Reduced in Respiration. *Proc. Natl. Acad. Sci. USA* **1999,** *96*, 12971-12973.
270. H. Michel; J. Behr; A. Harrenga, a.; Kannt, A., Cytochrome C Oxidase: Structure and Spectroscopy. *Annu. Rev. Biophys. Biomol. Struct.* **1998,** *27*, 329-356.
271. Tsukihara, T.; Aoyama, H.; Yamashita, E.; Tomizaki, T.; Yamaguchi, H.; Shinzawa-Itoh, K.; Nakashima, R.; Yaono, R.; Yoshikawa, S., Structures of Metal Sites of Oxidized Bovine Heart Cytochrome C Oxidase at 2.8 Å. *Science* **1995,** *269*, 1069-1074.
272. Fry, H. C.; Cohen, A. D.; Toscano, J. P.; Meyer, G. J.; Karlin, K. D., Photoinduced Carbon Monoxide Migration in a Synthetic Heme−Copper Complex. *J. Am. Chem. Soc.* **2005,** *127*, 6225-6230.
273. GIBSON, Q.; GREENWOOD, C., Reactions of Cytochrome Oxidase with Oxygen and Carbon Monoxide. *Biochem. J.* **1963,** *86*, 541-554.
274. Greenwood, C.; Gibson, Q. H., The Reaction of Reduced Cytochrome C Oxidase with Oxygen. *J. Biol. Chem.* **1967,** *242*, 1782-1787.
275. Szundi, I.; Liao, G.-L.; Einarsdóttir, Ó., Near-Infrared Time-Resolved Optical Absorption Studies of the Reaction of Fully Reduced Cytochrome C Oxidase with Dioxygen. *Biochem.* **2001,** *40*, 2332-2339.
276. Hill, B. C., Stopped-Flow, Laser-Flash Photolysis Studies on the Reactions of Co and O2 with the Cytochrome Caa3 Complex from Bacillus Subtilis: Conservation of Electron Transfer Pathways from Cytochrome C to O2. *Biochem.* **1996,** *35*, 6136-6143.
277. Oliveberg, M.; Malmstroem, B. G., Reaction of Dioxygen with Cytochrome C Oxidase Reduced to Different Degrees: Indications of a Transient Dioxygen Complex with Copper-B. *Biochem.* **1992,** *31*, 3560-3563.
278. Babcock, G. T.; Floris, R.; Nilsson, T.; Pressler, M.; Varotsis, C.; Vollenbroek, E., Dioxygen Activation in Enzymatic Systems and in Inorganic Models. *Inorg. Chim. Acta* **1996,** *243*, 345-353.
279. Ogura, T.; Kitagawa, T., Resonance Raman Characterization of the P Intermediate in the Reaction of Bovine Cytochrome C Oxidase. *Biochim. Biophys. Acta Bioenerg.* **2004,** *1655*, 290-297.
280. Kitagawa, T.; Ogura, T., Oxygen Activation Mechanism at the Binuclear Site of Heme–Copper Oxidase Superfamily as Revealed by Time-Resolved Resonance Raman Spectroscopy. In *Progress in Inorganic Chemistry*, 1996; pp 431-479.
281. Ogura, T.; Takahashi, S.; Hirota, S.; Shinzawa-Itoh, K.; Yoshikawa, S.; Appelman, E. H.; Kitagawa, T., Time-Resolved Resonance Raman Elucidation of the Pathway for Dioxygen Reduction by Cytochrome C Oxidase. *J. Am. Chem. Soc.* **1993,** *115*, 8527-8536.
282. Ogura, T.; Takahashi, S.; Shinzawa-Itoh, K.; Yoshikawa, S.; Kitagawa, T., Observation of the Iron(Ii)-Oxygen Stretching Raman Band for Cytochrome Oxidase Compound a at Ambient Temperature. *J. Am. Chem. Soc.* **1990,** *112*, 5630-5631.
283. Einarsdottir, O.; Dyer, R. B.; Lemon, D. D.; Killough, P. M.; Hubig, S. M.; Atherton, S. J.; Lopez-Garriga, J. J.; Palmer, G.; Woodruff, W. H., Photodissociation and Recombination of Carbonmonoxy Cytochrome Oxidase: Dynamics from Picoseconds to Kiloseconds. *Biochem.* **1993,** *32*, 12013-12024.

284. Alben, J. O.; Moh, P. P.; Fiamingo, F. G.; Altschuld, R. A., Cytochrome Oxidase (A3) Heme and Copper Observed by Low-Temperature Fourier Transform Infrared Spectroscopy of the Co Complex. *Proc. Natl. Acad. Sci. USA* **1981,** *78*, 234-237.
285. Fry, H. C.; Scaltrito, D. V.; Karlin, K. D.; Meyer, G. J., The Rate of O2 and Co Binding to a Copper Complex, Determined by a "Flash-and-Trap" Technique, Exceeds That for Hemes. *J. Am. Chem. Soc.* **2003,** *125*, 11866-11871.
286. Lucas, H. R.; Meyer, G. J.; Karlin, K. D., Co and O2 Binding to Pseudo-Tetradentate Ligand−Copper(I) Complexes with a Variable N-Donor Moiety: Kinetic/Thermodynamic Investigation Reveals Ligand-Induced Changes in Reaction Mechanism. *J. Am. Chem. Soc.* **2010,** *132*, 12927-12940.
287. Saracini, C.; Liakos, D. G.; Zapata Rivera, J. E.; Neese, F.; Meyer, G. J.; Karlin, K. D., Excitation Wavelength Dependent O2 Release from Copper(Ii)–Superoxide Compounds: Laser Flash-Photolysis Experiments and Theoretical Studies. *J. Am. Chem. Soc.* **2014,** *136*, 1260-1263.
288. Baxter, N.; Horsford, J.; Wokes, F.; Norris, F. W.; Fernandes, S. J. G., Cyanocobalamin and Hydroxocobalamin in Vitamin B12 Injections. *J. Pharm. Pharmacol.* **1953,** *5*, 723-736.
289. Hodgkin, D. C.; Pickworth, J.; Robertson, J. H.; Trueblood, K. N.; Prosen, R. J.; White, J. G., Structure of Vitamin B12 : The Crystal Structure of the Hexacarboxylic Acid Derived from B12 and the Molecular Structure of the Vitamin. *Nature* **1955,** *176*, 325-328.
290. Walker, L. A.; Shiang, J. J.; Anderson, N. A.; Pullen, S. H.; Sension, R. J., Time-Resolved Spectroscopic Studies of B12 Coenzymes: The Photolysis and Geminate Recombination of Adenosylcobalamin. *J. Am. Chem. Soc.* **1998,** *120*, 7286-7292.
291. Chen, E.; Chance, M. R., Continuous-Wave Quantum Yields of Various Cobalamins Are Influenced by Competition between Geminate Recombination and Cage Escape. *Biochemistry* **1993,** *32*, 1480-1487.
292. Chen, E.; Chance, M. R., Nanosecond Transient Absorption Spectroscopy of Coenzyme B12. Quantum Yields and Spectral Dynamics. *J. Biol. Chem.* **1990,** *265*, 12987-12994.
293. Sension, R. J.; Cole, A. G.; Harris, A. D.; Fox, C. C.; Woodbury, N. W.; Lin, S.; Marsh, E. N. G., Photolysis and Recombination of Adenosylcobalamin Bound to Glutamate Mutase. *J. Am. Chem. Soc.* **2004,** *126*, 1598-1599.
294. Sension, R. J.; Harris, D. A.; Stickrath, A.; Cole, A. G.; Fox, C. C.; Marsh, E. N. G., Time-Resolved Measurements of the Photolysis and Recombination of Adenosylcobalamin Bound to Glutamate Mutase. *J. Phys. Chem. B* **2005,** *109*, 18146-18152.
295. Jones, A. R.; Hardman, S. J. O.; Hay, S.; Scrutton, N. S., Is There a Dynamic Protein Contribution to the Substrate Trigger in Coenzyme B12-Dependent Ethanolamine Ammonia Lyase? *Angew. Chem. Int. Ed.* **2011,** *50*, 10843-10846.
296. Peng, J.; Tang, K.-C.; McLoughlin, K.; Yang, Y.; Forgach, D.; Sension, R. J., Ultrafast Excited-State Dynamics and Photolysis in Base-Off B12 Coenzymes and Analogues: Absence of the Trans-Nitrogenous Ligand Opens a Channel for Rapid Nonradiative Decay. *J. Phys. Chem. B* **2010,** *114*, 12398-12405.
297. Jones, A. R., Magnetic Field Effects in Proteins. *Mol. Phys.* **2016,** *114*, 1691-1702.
298. Chagovetz, A. M.; Grissom, C. B., Magnetic Field Effects in Adenosylcob(Iii)Alamin Photolysis: Relevance to B12 Enzymes. *J. Am. Chem. Soc.* **1993,** *115*, 12152-12157.
299. Harkins, T. T.; Grissom, C. B., Magnetic Field Effects on B₁₂ Ethanolamine Ammonia Lyase: Evidence for a Radical Mechanism. *Science* **1994,** *263*, 958-960.
300. Taylor, R. T.; Smucker, L.; Hanna, M. L.; Gill, J., Aerobic Photoiysis of Alkylcobalamins: Quantum Yields and Light-Action Spectra. *Arch. Biochem. Biophys.* **1973,** *156*, 521-533.
301. Shiang, J. J.; Walker, L. A.; Anderson, N. A.; Cole, A. G.; Sension, R. J., Time-Resolved Spectroscopic Studies of B12 Coenzymes: The Photolysis of Methylcobalamin Is Wavelength Dependent. *J. Phys. Chem. B* **1999,** *103*, 10532-10539.

302. Matthews, R. G., Cobalamin-Dependent Methyltransferases. *Acc. Chem. Res.* **2001,** *34*, 681-689.
303. Matthews, R. G.; Koutmos, M.; Datta, S., Cobalamin-Dependent and Cobamide-Dependent Methyltransferases. *Curr. Opin. Struct. Biol.* **2008,** *18*, 658-666.
304. Yoshizawa, M.; Klosterman, J. K., Molecular Architectures of Multi-Anthracene Assemblies. *Chem. Soc. Rev.* **2014,** *43*, 1885-1898.
305. v. Bünau, G., J. B. Birks: Photophysics of Aromatic Molecules. Wiley-Interscience, London 1970. 704 Seiten. Preis: 210s. *Berich. Bunsen. Gesell.* **1970,** *74*, 1294-1295.
306. Murov, S. L.; Carmichael, I.; Hug, G. L., *Handbook of Photochemistry, 2nd Edition*. Marcel Dekker, Inc.,New York: 1993.
307. Szwarc, M., Radical Anions and Carbanions as Donors in Electron-Transfer Processes. *Acc. Chem. Res.* **1972,** *5*, 169-176.
308. Kikuchi, K.; Hoshi, M.; Abe, E.; Kokubun, H., Heavy Atom Effects on Geminate and Free Radical Recombination. *J. Photoch. Photobio. A* **1988,** *45*, 1-7.
309. Kikuchi, K.; Hoshi, M.; Niwa, T.; Takahashi, Y.; Miyashi, T., Heavy-Atom Effects on the Excited Singlet-State Electron-Transfer Reaction. *J. Phys. Chem* **1991,** *95*, 38-42.
310. Sau, S. C.; Schmitz, M.; Burdenski, C.; Baumert, M.; Antoni, P. W.; Kerzig, C.; Hansmann, M. M., Dicationic Acridinium/Carbene Hybrids as Strongly Oxidizing Photocatalysts. *J. Am. Chem. Soc.* **2024,** *146*, 3416-3426.
311. Gould, I. R.; Ege, D.; Mattes, S. L.; Farid, S., Return Electron Transfer within Geminate Radical Ion Pairs. Observation of the Marcus Inverted Region. *J. Am. Chem. Soc.* **1987,** *109*, 3794-3796.
312. Gould, I. R.; Farid, S., Specific Deuterium Isotope Effects on the Rates of Electron Transfer within Geminate Radical-Ion Pairs. *J. Am. Chem. Soc.* **1988,** *110*, 7883-7885.
313. Gould, I. R.; Moody, R.; Farid, S., Electron-Transfer Reactions in the Marcus Inverted Region: Differences in Solvation and Electronic Coupling between Excited Charge-Transfer Complexes and Geminate Radical Ion Pairs. *J. Am. Chem. Soc.* **1988,** *110*, 7242-7244.
314. Gould, I. R.; Moser, J. E.; Ege, D.; Farid, S., Effect of Molecular Dimension on the Rate of Return Electron Transfer within Photoproduced Geminate Radical Ion Pairs. *J. Am. Chem. Soc.* **1988,** *110*, 1991-1993.
315. Gould, I. R.; Moser, J. E.; Armitage, B.; Farid, S.; Goodman, J. L.; Herman, M. S., Electron-Transfer Reactions in the Marcus Inverted Region. Charge Recombination Versus Charge Shift Reactions. *J. Am. Chem. Soc.* **1989,** *111*, 1917-1919.
316. Gould, I. R.; Ege, D.; Moser, J. E.; Farid, S., Efficiencies of Photoinduced Electron-Transfer Reactions: Role of the Marcus Inverted Region in Return Electron Transfer within Geminate Radical-Ion Pairs. *J. Am. Chem. Soc.* **1990,** *112*, 4290-4301.
317. Lewis, F. D.; Bedell, A. M.; Dykstra, R. E.; Elbert, J. E.; Gould, I. R.; Farid, S., Photochemical Generation, Isomerization, and Oxygenation of Stilbene Cation Radicals. *J. Am. Chem. Soc.* **1990,** *112*, 8055-8064.
318. Gould, I. R.; Young, R. H.; Moody, R. E.; Farid, S., Contact and Solvent-Separated Geminate Radical Ion Pairs in Electron-Transfer Photochemistry. *J. Phys. Chem* **1991,** *95*, 2068-2080.
319. Gould, I. R.; Farid, S., Steric Effects in Photoinduced Electron-Transfer Reactions. *J. Phys. Chem* **1993,** *97*, 13067-13072.
320. Gould, I. R.; Noukakis, D.; Gomez-Jahn, L.; Young, R. H.; Goodman, J. L.; Farid, S., Radiative and Nonradiative Electron Transfer in Contact Radical-Ion Pairs. *Chem. Phys.* **1993,** *176*, 439-456.
321. Gould, I. R.; Farid, S., Dynamics of Bimolecular Photoinduced Electron-Transfer Reactions. *Acc. Chem. Res.* **1996,** *29*, 522-528.

322. Zhou, J.; Shah, R. P.; Findley, B. R.; Braun, C. L., Long Distance Photoinduced Electron Transfer in Solutions: A Mechanism for Producing Large Yields of Free Ions by Electron Transfer Quenching. *J. Phys. Chem. A* **2002,** *106*, 12-20.
323. Burget, D.; Jacques, P.; Vauthey, E.; Suppan, P.; Haselbach, E., Marcus Inverted Region: Nature of Donor–Acceptor Pairs and Free Ion Yields. *J. Chem. Soc., Faraday Trans.* **1994,** *90*, 2481-2487.
324. Niwa, T.; Kikuchi, K.; Matsusita, N.; Hayashi, M.; Katagiri, T.; Takahashi, Y.; Miyashi, T., Solvent Effects on Photoinduced Electron-Transfer Reactions. *J. Phys. Chem* **1993,** *97*, 11960-11964.
325. Kikuchi, K.; Niwa, T.; Takahashi, Y.; Ikeda, H.; Miyashi, T., Quenching Mechanism in a Highly Exothermic Region of the Rehm-Weller Relationship for Electron-Transfer Fluorescence Quenching. *J. Phys. Chem* **1993,** *97*, 5070-5073.
326. Hino, T.; Akazawa, H.; Masuhara, H.; Mataga, N., Ionic Photodissociation of Excited Electron Donor-Acceptor Systems. Ii. Importance of the Chemical Property of Donor-Acceptor Pairs. *J. Phys. Chem* **1976,** *80*, 33-37.
327. Zanini, G. P.; Montejano, H. A.; Previtali, C. M., Photoinduced Electron-Transfer Quenching of Excited Singlet States of Polycyclic Aromatic Hydrocarbons by Organic Acceptors. *J. Chem. Soc., Faraday Trans.* **1995,** *91*, 1197-1202.
328. Lewis, F. D.; Dykstra, R. E.; Gould, I. R.; Farid, S., Cage Escape Yields and Direct Observation of Intermediates in Photoinduced Electron-Transfer Reactions of Cis- and Trans-Stilbene. *J. Phys. Chem* **1988,** *92*, 7042-7043.
329. Gould, I. R.; Noukakis, D.; Gomez-Jahn, L.; Goodman, J. L.; Farid, S., Explanation of the Driving-Force Dependence of Return Electron Transfer in Contact Radical-Ion Pairs. *J. Am. Chem. Soc.* **1993,** *115*, 4405-4406.
330. Kikuchi, K.; Katagiri, T.; Niwa, T.; Takahashi, Y.; Suzuki, T.; Ikeda, H.; Miyashi, T., Evidence for Generation of Electronically Excited Radical Ion in Very Exothermic Electron-Transfer Fluorescence Quenching. *Chem. Phys. Lett.* **1992,** *193*, 155-160.
331. Tachiya, M., Energetics of Electron Transfer Reactions in Polar Solvents. *Chem. Phys. Lett.* **1994,** *230*, 491-494.
332. Mataga, N.; Asahi, T.; Kanda, Y.; Okada, T.; Kakitani, T., The Bell-Shaped Energy Gap Dependence of the Charge Recombination Reaction of Geminate Radical Ion Pairs Produced by Fluorescence Quenching Reaction in Acetonitrile Solution. *Chem. Phys.* **1988,** *127*, 249-261.
333. Ottolenghi, M., Charge-Transfer Complexes in the Excited State. Laser Photolysis Studies. *Acc. Chem. Res.* **1973,** *6*, 153-160.
334. Masuhara, H.; Hino, T.; Mataga, N., Ionic Photodissociation of Excited Electron Donor-Acceptor Systems. I. Empirical Equation on the Relation between the Yield and the Solvent Dielectric Constant. *J. Phys. Chem* **1975,** *79*, 994-1000.
335. Yoshio, T.; Yasuzo, N.; Noboru, M., Laser Photolysis Studies on the Formation of Solvated Ion Radicals in the Pyrene–N,N-Dimethylaniline System in Various Solvents. *B. Chem. Soc. Jpn.* **1972,** *45*, 764-769.
336. Venkatraman, R. K.; Orr-Ewing, A. J., Solvent Effects on Ultrafast Photochemical Pathways. *Acc. Chem. Res.* **2021,** *54*, 4383-4394.
337. Masuhara, H.; Saito, T.; Maeda, Y.; Mataga, N., Dynamic Behaviour of Excited Charge Transfer Systems in Polar Solvents. *J. Mol. Struct.* **1978,** *47*, 243-259.
338. Harumichi, K.; Shunichi, O.; Youichi, O.; Haruo, S., Solvent Effect on Reaction Mechanism and Kinetics of Triplet Ion Pairs between Chloranil and Acenaphthene. *B. Chem. Soc. Jpn.* **1990,** *63*, 2173-2182.
339. Wega, J.; Vauthey, E., Bimolecular Photoinduced Symmetry-Breaking Charge Separation of Perylene in Solution. *Photochem. Photobio. Sci.* **2024,** *23*, 93-105.

340. Craig, B. B.; Rodgers, M. A. J., Nanosecond Laser Studies of Photophysical Processes in the Benzene + Tetracyanobenzene Molecular Complex. *J. Chem. Soc., Faraday Trans. 2* **1976,** *72*, 1259-1266.
341. Jones, G.; Chiang, S. H.; Becker, W. G.; Welch, J. A., Photosensitization of Quadricyclene Isomerization by Electron Acceptors. A Short-Circuit Nonradiative Decay Mechanism for Electron Donor-Acceptor Quenching in Polar Media. *J. Phys. Chem* **1982,** *86*, 2805-2808.
342. Lewis, F. D.; Petisce, J. R., Proton Transfer Reactions of Photogenerated Cyanoaromatic-Methylaromatic Radical Ion Pairs†. *Tetrahedron* **1986,** *42*, 6207-6217.
343. S. Jayanthi, S.; Ramamurthy, P., Photoinduced Electron Transfer Reactions of 2,4,6-Triphenylpyrylium: Solvent Effect and Charge-Shift Type of Systems. *Phys. Chem. Chem. Phys.* **1999,** *1*, 4751-4757.
344. Jayanthi, S. S.; Ramamurthy, P., Excited Singlet State Reactions of Thiopyrylium with Electron Donors: Electron Transfer, Induction of Triplet by Internal and External Heavy Atom Effect, and Comparison of Pyrylium and Thiopyrylium Reactions. *J. Phys. Chem. A* **1998,** *102*, 511-518.
345. Klimtchuk, E. S.; Irinyi, G.; Khudyakov, I. V.; Margulis, L. A.; Kuzmin, V. A., Effect of Magnetic Field on Radical Yields During the Photoreduction of Xanthene Dyes in Viscous Media. *J. Chem. Soc., Faraday Trans. 1* **1989,** *85*, 4119-4128.
346. Douglas, P.; Waechter, G.; Mills, A., Ionic Srength Effects on the Ground State Complexation and Triplet State Electron Transfer Reaction between Rose Bengall and Methyl Viologen. *Photochem. Photobiol.* **1990,** *52*, 473-479.
347. Jones, G., II; Chatterjee, S., Steric Control of Distance Parameters and the Yield of Charge Carriers in Photochemical Electron Transfer. The Quenching of Eosin Y by Hindered Phenols. *J. Phys. Chem* **1988,** *92*, 6862-6864.
348. Iwa, P.; Steiner, U. E.; Vogelmann, E.; Kramer, H. E. A., Linear Free-Enthalpy Relation for Radical Yield in Fluorescence Quenching by Electron Transfer. *J. Phys. Chem* **1982,** *86*, 1277-1285.
349. Ohno, T.; Yoshimura, A.; Shioyama, H.; Mataga, N., Energy Gap Dependence of Spin-Inverted Electron Transfer within Geminate Radical Pairs Formed by the Quenching of Phosphorescent States in Polar Solvents. *J. Phys. Chem* **1987,** *91*, 4365-4370.
350. Steiner, U., Spin-Selective Depopulation of Triplet Sublevels in Rapidly Rotating Triplet Exciplexes Detected by a Heavy-Atom-Induced Magnetic Field Effect. *Chem. Phys. Lett.* **1980,** *74*, 108-112.
351. Steiner, U. E.; Haas, W., Spin-Orbit Coupling Induced Magnetic Field Effects in Electron-Transfer Reactions with Excited Triplets: The Role of Triplet Exciplexes and Radical Pairs in Geminate Recombination. *J. Phys. Chem* **1991,** *95*, 1880-1890.
352. Gilch, P.; Linsenmann, M.; Haas, W.; Steiner, U. E., Magnetic Field Effect on the Photooxidation Efficiency of Ferrocene. *Chem. Phys. Lett.* **1996,** *254*, 384-390.
353. Steiner, U.; Winter, G., Position Dependent Heavy Atom Effect in Physical Triplet Quenching by Electron Donors. *Chem. Phys. Lett.* **1978,** *55*, 364-368.
354. Kawanishi, Y.; Kitamura, N.; Tazuke, S., Coulombic Effect on Photoinduced Electron-Transfer Reactions between Phenothiazines and Viologens. *J. Phys. Chem* **1986,** *90*, 2469-2475.
355. Periasamy, N.; Linschitz, H., Cage Escape and Spin Rephasing of Triplet Ion-Radical Pairs: Temperature-Viscosity and Magnetic Field Effects in Photoreduction of Fluorenone by Dabco. *Chemical Physics Letters* **1979,** *64*, 281-285.
356. Levin, P. P.; Kuzmin, V. A., Spin-Orbit Coupling and Paramagnetic Relaxation in Micellized Triplet Radical Pairs. Determination of Relaxation Parameters from Magnetic Field Dependences of the Decay Kinetics. *Chem. Phys. Lett.* **1990,** *165*, 302-308.
357. Harumichi, K.; Hiroshi, S.; Haruo, S., Heavy-Atom Effect on Decay Dynamics of Triplet-State Ion Pairs. Chloranil–Naphthalene (1:2) Termolecular Systems. *B. Chem. Soc. Jpn.* **1990,** *63*, 1441-1446.

358. Sul'timova, N. B.; Levin, P. P.; Chaikovskaya, O. N., Kinetics of Radical Formation and Decay in Photooxidation of 4-Halophenols Sensitized by 4-Carboxybenzophenone in Aqueous Solutions. *Russ. Chem. B+*. **2005,** *54*, 1439-1444.
359. Das, P. K.; Encinas, M. V.; Scaiano, J. C., Laser Flash Photolysis Study of the Reactions of Carbonyl Triplets with Phenols and Photochemistry of P-Hydroxypropiophenone. *J. Am. Chem. Soc.* **1981,** *103*, 4154-4162.
360. Khudyakov, I.; Levin, P.; Kuzmin, V., Kinetics of Geminate Recombination of Organic Free Radicals in Viscous Solvents. *Photochem. Photobio. Sci.* **2008,** *7*, 1540-1543.
361. Simon, J. D.; Peters, K. S., Solvent Effects on the Picosecond Dynamics of the Photoreduction of Benzophenone by Aromatic Amines. *J. Am. Chem. Soc.* **1981,** *103*, 6403-6406.
362. Ci, X.; Silveira da Silva, R.; Nicodem, D.; Whitten, D. G., Electron and Hydrogen Atom Transfer Mechanisms for the Photoreduction of O-Quinones. Visible Light-Induced Photoreactions Of .Beta.-Lapachone with Amines, Alcohols, and Amino Alcohols. *J. Am. Chem. Soc.* **1989,** *111*, 1337-1343.
363. Bock, C. R.; Meyer, T. J.; Whitten, D. G., Electron Transfer Quenching of the Luminescent Excited State of Tris(2,2'-Bipyridine)Ruthenium(Ii). Flash Photolysis Relaxation Technique for Measuring the Rates of Very Rapid Electron Transfer Reactions. *J. Am. Chem. Soc.* **1974,** *96*, 4710-4712.
364. Brennaman, M. K.; Dillon, R. J.; Alibabaei, L.; Gish, M. K.; Dares, C. J.; Ashford, D. L.; House, R. L.; Meyer, G. J.; Papanikolas, J. M.; Meyer, T. J., Finding the Way to Solar Fuels with Dye-Sensitized Photoelectrosynthesis Cells. *J. Am. Chem. Soc.* **2016,** *138*, 13085-13102.
365. Wolff, H.-J.; Burssher, D.; Steiner, U. E., Spin-Orbit Coupling Controlled Spin Chemistry of Ru(Bpy)32+ Photooxidation: Detection of Strong Viscosity Dependence of in-Cage Backward Electron Transfer Rate. *Pure Appl. Chem.* **1995,** *67*, 167.
366. Wilson, G. J.; Launikonis, A.; Sasse, W. H. F.; Mau, A. W. H., Chromophore-Specific Quenching of Ruthenium Trisbipyridine−Arene Bichromophores by Methyl Viologen. *J. Phys. Chem. A* **1998,** *102*, 5150-5156.
367. Fodor, L.; Ülveczki, A.; Horváth, A.; Steiner, U. E., Ligand Dependence of Magnetic Spin Effects on Photooxidation of [Ru(Bpy)3−N(Cn)2n](+2−2n) Type Complexes. *Inorg. Chim. Acta* **2002,** *338*, 133-141.
368. Bürßner, D.; Steiner, U. E., Spin Chemistry of Ru(Ii)-Trisdiimine Complex Photooxidation in Magnetic Fields up to 17.5 Tesla. *Coord. Chem. Rev.* **1994,** *132*, 51-56.
369. Wolff, H.-J.; Steiner, U. E., Aspects of Ligand and Electron-Acceptor Dependence of Magnetic Field Effects on Net Electron Transfer Efficiencies in Photooxidation of Ru(Ii)-Trisbipyridyl Type Complexes. *Z. Phys. Chem.* **1990,** *169*, 147-158.
370. Bürßner, D.; Wolff, H.-J.; Steiner, U. E., Magnetokinetic Probing of Extremely Fast Electron Spin Relaxation in Paramagnetic Ruthenium Complexes*. *Z. Phys. Chem.* **1993,** *182*, 297-308.
371. Steiner, U. E.; Bürßner, D., Theoretical Treatment of Magnetic Field Dependent in-Cage Backward Electron Transfer During Photooxidation of Ru(Ii) Complexes. *Z. Phys. Chem.* **1990,** *169*, 159-180.
372. Steiner, U. E.; Wolff, H. J.; Ulrich, T.; Ohno, T., Spin-Orbit Coupling and Magnetic Field Effects in Photoredox Reactions of Ruthenium(Ii) Complexes. *J. Phys. Chem* **1989,** *93*, 5147-5154.
373. Fodor, L.; Horváth, A.; Hötzer, K. A.; Walbert, S.; Steiner, U. E., Enhancement of Magnetic Field Effect in Ru(Bpy)32+/Mv2+ System by Ru(Bpy)32+-Ag+ Exciplex Formation. *Chem. Phys. Lett.* **2000,** *316*, 411-418.
374. Hötzer, K. A.; Klingert, A.; Klumpp, T.; Krissinel, E.; Bürssner, D.; Steiner, U. E., Temperature-Dependent Spin Relaxation: A Major Factor in Electron Backward Transfer Following the Quenching of *Ru(Bpy)32+ by Methyl Viologen. *J. Phys. Chem. A* **2002,** *106*, 2207-2217.

375. Glaser, F.; Kerzig, C.; Wenger, O. S., Sensitization-Initiated Electron Transfer Via Upconversion: Mechanism and Photocatalytic Applications. *Chem. Sci.* **2021,** *12*, 9922-9933.
376. Weinheimer, C.; Choi, Y.; Caldwell, T.; Gresham, P.; Olmsted, J., Effect of a Steric Spacer on Chromophoric Interactions of Ruthenium Complexes Containing Covalently Bound Anthracene. *J. Photoch. Photobio. A* **1994,** *78*, 119-126.
377. Chan, S. F.; Chou, M.; Creutz, C.; Matsubara, T.; Sutin, N., Mechanism of the Formation of Dihydrogen from the Photoinduced Reactions of Poly(Pyridine)Ruthenium(Ii) and Poly(Pyridine)Rhodium(Iii) Complexes. *J. Am. Chem. Soc.* **1981,** *103*, 369-379.
378. Ruthkosky, M.; Castellano, F. N.; Meyer, G. J., Photodriven Electron and Energy Transfer from Copper Phenanthroline Excited States. *Inorg. Chem.* **1996,** *35*, 6406-6412.
379. Kalyanasundaram, K.; Neumann-Spallart, M., Influence of Added Salts on the Cage Escape Yields in the Photoredox Quenching of Ru(Bpy)2+3 Excited States. *Chem. Phys. Lett.* **1982,** *88*, 7-12.
380. Hoffman, M. Z., Cage Escape Yields from the Quenching of Excited Tris(Bipyridyl)Ruthenium(2+) by Methylviologen in Aqueous Solution. *J. Phys. Chem* **1988,** *92*, 3458-3464.
381. Clark, C. D.; Hoffman, M. Z., Ion-Pairing Control of Excited-State Electron-Transfer Reactions Effect of Cations on Cationic Reactants. *J. Photoch. Photobio. A* **1997,** *111*, 9-13.
382. Hoselton, M. A.; Lin, C. T.; Schwarz, H. A.; Sutin, N., Kinetics and Mechanism of the Quenching of the Emission of Substituted Polypyridineruthenium(Ii) Complexes. Reactions of Rul3+, *Rul32+, and Rul33+ with the Copper(I)-Copper(Ii) Couple. *J. Am. Chem. Soc.* **1978,** *100*, 2383-2388.
383. Ohno, T.; Yoshimura, A.; Prasad, D. R.; Hoffman, M. Z., A Weak .Delta.G.Degree. Dependence of Back Electron Transfer within the Geminate Redox Pairs Formed in the Quenching of Excited Ruthenium(Ii) Complexes by Methyl Viologen. *J. Phys. Chem* **1991,** *95*, 4723-4728.
384. Mallouk, T. E.; Krueger, J. S.; Mayer, J. E.; Dymond, C. M. G., Reductive Quenching of Ruthenium Polypyridyl Sensitizers by Cyanometalate Complexes. *Inorg. Chem.* **1989,** *28*, 3507-3510.
385. Gordon, C. M.; McLean, A. J., Photoelectron Transfer from Excited-State Ruthenium() Tris(Bipyridyl) to Methylviologen in an Ionic Liquid. *Chem. Commun.* **2000**, 1395-1396.
386. Marton, A.; Clark, C. C.; Srinivasan, R.; Freundlich, R. E.; Narducci Sarjeant, A. A.; Meyer, G. J., Static and Dynamic Quenching of Ru(Ii) Polypyridyl Excited States by Iodide. *Inorg. Chem.* **2006,** *45*, 362-369.
387. Wehlin, S. A. M.; Troian-Gautier, L.; Li, G.; Meyer, G. J., Chloride Oxidation by Ruthenium Excited-States in Solution. *J. Am. Chem. Soc.* **2017,** *139*, 12903-12906.
388. Troian-Gautier, L.; Wehlin, S. A. M.; Meyer, G. J., Photophysical Properties of Tetracationic Ruthenium Complexes and Their Ter-Ionic Assemblies with Chloride. *Inorg. Chem.* **2018,** *57*, 12232-12244.
389. Wehlin, S. A. M.; Troian-Gautier, L.; Sampaio, R. N.; Marcélis, L.; Meyer, G. J., Ter-Ionic Complex That Forms a Bond Upon Visible Light Absorption. *J. Am. Chem. Soc.* **2018,** *140*, 7799-7802.
390. Swords, W. B.; Li, G.; Meyer, G. J., Iodide Ion Pairing with Highly Charged Ruthenium Polypyridyl Cations in Ch3cn. *Inorg. Chem.* **2015,** *54*, 4512-4519.
391. Casarin, L.; Swords, W. B.; Caramori, S.; Bignozzi, C. A.; Meyer, G. J., Rapid Static Sensitizer Regeneration Enabled by Ion Pairing. *Inorg. Chem.* **2017,** *56*, 7324-7327.
392. Swords, W. B.; Meyer, G. J.; Hammarström, L., Excited-State Proton-Coupled Electron Transfer within Ion Pairs. *Chem. Sci.* **2020,** *11*, 3460-3473.
393. Deetz, A. M.; Goodwin, M. J.; Kober, E. A.; Meyer, G. J., Nanosecond Intra-Ionic Chloride Photo-Oxidation. *Inorg. Chem.* **2023,** *62*, 11414-11425.
394. Previtali, C. M., Solvent Effects on Intermolecular Electron Transfer Processes. *Pure Appl. Chem.* **1995,** *67*, 127-134.

395. Sun, H.; Hoffman, M. Z., Photo-Induced Charge Separation by Ruthenium (Ii) Photosensitizers. *J. Chem. Sci.* **1993,** *105*, 487-494.
396. Senz, A.; Gsponer, H. E., Yield of Ions Produced in the Luminescence Quenching of Tris (2,2′-Bipyridine)Ruthenium(Ii) by Dichlorophenolate Ions. *J. Phys. Org. Chem.* **1995,** *8*, 706-712.
397. Turro, N. J.; Weed, G. C., Micellar Systems as Supercages for Reactions of Geminate Radical Pairs. Magnetic Effects. *J. Am. Chem. Soc.* **1983,** *105*, 1861-1868.
398. Turro, N. J.; Mattay, J., Photochemistry of Some Deoxybenzoins in Micellar Solutions. Cage Effects, Isotope Effects, and Magnetic Field Effects. *J. Am. Chem. Soc.* **1981,** *103*, 4200-4204.
399. Gould, I. R.; Zimmt, M. B.; Turro, N. J.; Baretz, B. H.; Lehr, G. F., Dynamics of Radical Pair Reactions in Micelles. *J. Am. Chem. Soc.* **1985,** *107*, 4607-4612.
400. Kleinman, M. H.; Shevchenko, T.; Bohne, C., Magnetic Field Effects on the Dynamics of Radical Pairs in Micelles: A New Approach to Understanding the "Cage Effect". *Photochem. Photobiol.* **1998,** *67*, 198-205.
401. Goez, M.; Henbest, K. B.; Windham, E. G.; Maeda, K.; Timmel, C. R., Quenching Mechanisms and Diffusional Pathways in Micellar Systems Unravelled by Time-Resolved Magnetic-Field Effects. *Chem-Eur. J.* **2009,** *15*, 6058-6064.
402. Atik, S. S.; Thomas, J. K., Photoinduced Electron Transfer in Organized Assemblies. *J. Am. Chem. Soc.* **1981,** *103*, 3550-3555.
403. Kalyanasundaram, K., Photoredox Reaction in Micellar Solutions Sensitized by Surfactant Derivative of Tris(2,2′-Bipyridyl)Ruthenium(Ii). *J. Chem. Soc. Chem. Comm.* **1978**, 628-630.
404. Abbas, A.; Oswald, E.; Romer, J.; Lenzer, A.; Heiland, M.; Streb, C.; Kranz, C.; Pannwitz, A., Initial Quenching Efficiency Determines Light-Driven H2 Evolution of [Mo3s13]2− in Lipid Bilayers. *Chem-Eur. J.* **2023,** *29*, e202302284.
405. Song, H.; Amati, A.; Pannwitz, A.; Bonnet, S.; Hammarström, L., Mechanistic Insights into the Charge Transfer Dynamics of Photocatalytic Water Oxidation at the Lipid Bilayer–Water Interface. *J. Am. Chem. Soc.* **2022,** *144*, 19353-19364.
406. Grätzel, M.; Kozak, J. J.; Thomas, J. K., Electron Reactions and Electron Transfer Reactions Catalyzed by Micellar Systems. *J. Chem. Phys.* **1975,** *62*, 1632-1640.
407. Schmehl, R. H.; Whitten, D. G., Photoinduced Redox Reactions in Aqueous Micelles. Quenching, Back-Reaction, and Competing Processes for Tetraanionic Porphyrins with Alkylviologens. *J. Phys. Chem* **1981,** *85*, 3473-3480.
408. Hackett, J. W.; Turro, C., Bimolecular Electron Transfer Quenching of Neutral *Ru(Phen)2bps by 4,4‘-Diheptyl Viologen in Water and Bound to Sds Micelles. *J. Phys. Chem. A* **1998,** *102*, 5728-5733.
409. Piechota, E. J.; Turro, C., Dynamic Orientation Control of Bimolecular Electron Transfer at Charged Micelle Surfaces. *J. Chem. Phys.* **2020,** *153*.
410. Matsuo, T., Photoinduced Electron-Transfer Reactions in Membrane and Polymer Systems for Solar Energy Conversion. *Pure Appl. Chem.* **1982,** *54*, 1693-1703.
411. Adams, R. E.; Schmehl, R. H., Micellar Effects on Photoinduced Electron Transfer in Aqueous Solutions Revisited: Dramatic Enhancement of Cage Escape Yields in Surfactant Ru(Ii) Diimine Complex/[Ru(Nh3)6]2+ Systems. *Langmuir* **2016,** *32*, 8598-8607.
412. Turro, N. J.; Khudyakov, I. V.; Gopidas, K. R., A Laser Flash Photolysis Study of Magnetic Field Effects in Photoinduced Electron Transfer between Ru (Bpy)2+3 and N,N′-Dimethylviologen in Micellar Solutions. *Chem. Phys.* **1992,** *162*, 131-143.
413. Clark, C. D.; Hoffman, M. Z., Solvent Reorganization Energy in Excited-State Electron-Transfer Reactions. Quenching and Geminate-Pair Back Electron Transfer. *J. Phys. Chem* **1996,** *100*, 14688-14693.

414. Ohno, T.; Yoshimura, A.; Mataga, N.; Tazuke, S.; Kawanishi, Y.; Kitamura, N., Backward Electron Transfers within Geminate Radical Pairs Formed by Electron-Transfer Quenching of Phosphorescent States of Tris(2,2'-Bipyrazine)Ruthenium(Ii) and Tris(4-Methyl-2-(2'-Pyridyl)Pyrimidine)Ruthenium(Ii). *J. Phys. Chem* **1989,** *93*, 3546-3551.
415. Ohno, T.; Yoshimura, A.; Mataga, N., Bell-Shaped Energy-Gap Dependence of Backward Electron Transfer Occurring within Geminate Radical Pairs Produced by Quenching of Ruthenium(Ii) Polypyridine Complexes by Aromatic Amines. *J. Phys. Chem* **1990,** *94*, 4871-4876.
416. Yonemoto, E. H.; Riley, R. L.; Kim, Y. I.; Atherton, S. J.; Schmehl, R. H.; Mallouk, T. E., Photoinduced Electron Transfer in Covalently Linked Ruthenium Tris(Bipyridyl)-Viologen Molecules: Observation of Back Electron Transfer in the Marcus Inverted Region. *J. Am. Chem. Soc.* **1992,** *114*, 8081-8087.
417. Yonemoto, E. H.; Riley, R. L.; Kim, Y. I.; Atherton, S. J.; Schmehl, R. H.; Mallouk, T. E., Photoinduced Electron Transfer in Covalently Linked Ruthenium Tris(Bipyridyl)-Viologen Molecules: Observation of Back Electron Transfer in the Marcus Inverted Region. [Erratum to Document Cited in Ca117(18):183725s]. *Journal of the American Chemical Society* **1993,** *115*, 5348-5348.
418. Sutin, N.; Creutz, C., Light Induced Electron Transfer Reactions of Metal Complexes. *Pure Appl. Chem.* **1980,** *52*, 2717-2738.
419. Mok, C. Y.; Zanella, A. W.; Creutz, C.; Sutin, N., Ground- and Excited-State Electron-Transfer Reactions: Photoinduced Redox Reactions of Poly(Pyridine)Ruthenium(Ii) Complexes and Cobalt(Iii) Cage Compounds. *Inorg. Chem.* **1984,** *23*, 2891-2897.
420. Sun, H.; Neshvad, G.; Hoffman, M. Z., Energy Gap Dependence of the Efficiency of Charge Separation Upon the Sacrificial Reductive Quenching of the Excited States of Ru(Ii)-Diimine Photosensitizers in Aqueous Solution. *Mol. Cryst. Liq.* **1991,** *194*, 141-150.
421. Sun, H.; Hoffman, M. Z., Reductive Quenching of the Excited States of Ruthenium(Ii) Complexes Containing 2,2'-Bipyridine, 2,2'-Bipyrazine, and 2,2'-Bipyrimidine Ligands. *J. Phys. Chem* **1994,** *98*, 11719-11726.
422. Sun, H.; Yoshimura, A.; Hoffman, M. Z., Oxidative Quenching of the Excited State of Tris(2,2'-Bipyridine)Ruthenium(2+) Ion by Methylviologen. Variation of Solution Medium and Temperature. *J. Phys. Chem* **1994,** *98*, 5058-5064.
423. Clark, C. D.; Hoffman, M. Z., Does Back Electron Transfer within Geminate Redox Pairs Formed in Bimolecular Quenching Follow a Marcus Bell-Shaped Energy Gap Dependence? *J. Photoch. Photobio. A* **1996,** *99*, 9-11.
424. Juris, A.; Balzani, V.; Belser, P.; von Zelewsky, A., Characterization of the Excited State Properties of Some New Photosensitizers of the Ruthenium (Polypyridine) Family. *Helv. Chim. Acta* **1981,** *64*, 2175-2182.
425. Bevernaegie, R.; Doix, B.; Bastien, E.; Diman, A.; Decottignies, A.; Feron, O.; Elias, B., Exploring the Phototoxicity of Hypoxic Active Iridium(Iii)-Based Sensitizers in 3d Tumor Spheroids. *J. Am. Chem. Soc.* **2019,** *141*, 18486-18491.
426. Deaton, J. C.; Castellano, F. N., Archetypal Iridium(Iii) Compounds for Optoelectronic and Photonic Applications. In *Iridium(Iii) in Optoelectronic and Photonics Applications*, Zysman-Colman, E., Ed. John Wiley & Sons Ltc.: Chichester, West Sussex, 2017; pp 1-69.
427. Colombo, A.; Dragonetti, C.; Guerchais, V.; Hierlinger, C.; Zysman-Colman, E.; Roberto, D., A Trip in the Nonlinear Optical Properties of Iridium Complexes. *Coord. Chem. Rev.* **2020,** *414*, 213293.
428. Henwood, A. F.; Zysman-Colman, E., Lessons Learned in Tuning the Optoelectronic Properties of Phosphorescent Iridium(Iii) Complexes. *Chem. Commun.* **2017,** *53*, 807-826.

429. Aydogan, A.; Bangle, R. E.; De Kreijger, S.; Dickenson, J. C.; Singleton, M. L.; Cauët, E.; Cadranel, A.; Meyer, G. J.; Elias, B.; Sampaio, R. N.; Troian-Gautier, L., Mechanistic Investigation of a Visible Light Mediated Dehalogenation/Cyclisation Reaction Using Iron(Iii), Iridium(Iii) and Ruthenium(Ii) Photosensitizers. *Catal. Sci. Technol.* **2021,** *11*, 8037-8051.
430. Chattapadhyay, D.; Aydogan, A.; Doktor, K.; Maity, A.; Wu, J. W.; Michaudel, Q., Harnessing Sulfur(Vi) Fluoride Exchange Click Chemistry and Photocatalysis for Deaminative Benzylic Arylation. *ACS Catal.* **2023,** *13*, 7263-7268.
431. De Kreijger, S.; Elias, B.; Troian-Gautier, L., Chloride, Bromide, and Iodide Photooxidation in Acetonitrile/Water Mixtures Using Binuclear Iridium(Iii) Photosensitizers. *Inorg. Chem.* **2023,** *62*, 16196-16202.
432. Farnum, B. H.; Jou, J. J.; Meyer, G. J., Visible Light Generation of I–I Bonds by Ru-Tris(Diimine) Excited States. *Proc. Natl. Acad. Sci. USA* **2012,** *109*, 15628-15633.
433. Farnum, B. H.; Gardner, J. M.; Marton, A.; Narducci-Sarjeant, A. A.; Meyer, G. J., Influence of Ion Pairing on the Oxidation of Iodide by Mlct Excited States. *Dalton Trans.* **2011,** *40*, 3830-3838.
434. Deetz, A. M.; Goodwin, M. J.; Kober, E. A.; Meyer, G. J., Nanosecond Intra-Ionic Chloride Photo-Oxidation. *Inorg. Chem.* **2023**.
435. DiLuzio, S.; Connell, T. U.; Mdluli, V.; Kowalewski, J. F.; Bernhard, S., Understanding Ir(Iii) Photocatalyst Structure‑Activity Relationships: A Highly Parallelized Study of Light-Driven Metal Reduction Processes. *J. Am. Chem. Soc.* **2022,** *144*, 1431-1444.
436. Hasebe, N.; Deguchi, Y.; Murayama, S.; Yoshihara, T.; Horiuchi, H.; Okutsu, T.; Tobita, S., Phosphorescence Quenching of Neutral and Cationic Iridium(Iii) Complexes by Molecular Oxygen and Aromatic Electron Acceptors. *J. Photoch. Photobio. A* **2016,** *324*, 134-144.
437. Ohno, T., Backward Electron Transfers within a Geminate Pair Formed in the Quenching of the Phosphorescent States of Rhodium(Iii) Compounds. *J. Phys. Chem* **1985,** *89*, 5709-5713.
438. Pizzocaro, C.; Bolte, M.; Hoffman, M. Z., Polymerization of Acrylamide Photosensitized by the Tris(2,2′-Bipyridine)Chromium(Iii) Ion in Aqueous Solution. *Polyhedron* **1993,** *12*, 855-858.
439. Bürgin, T. H.; Glaser, F.; Wenger, O. S., Shedding Light on the Oxidizing Properties of Spin-Flip Excited States in a Criii Polypyridine Complex and Their Use in Photoredox Catalysis. *J. Am. Chem. Soc.* **2022,** *144*, 14181-14194.
440. Wang, C.; Li, H.; Bürgin, T. H.; Wenger, O. S., Cage Escape Governs Photoredox Reaction Rates and Quantum Yields. *Nature Chem.* **2024**.
441. Sittel, S.; Sell, A. C.; Hofmann, K.; Wiedemann, C.; Nau, J. P.; Kerzig, C.; Manolikakes, G.; Heinze, K., Visible-Light Induced Fixation of So2 into Organic Molecules with Polypyridine Chromium(Iii) Complexes. *ChemCatChem* **2023,** *15*, e202201562.
442. Glaser, F.; Aydogan, A.; Elias, B.; Troian-Gautier, L., The Great Strides of Iron Photosensitizers for Contemporary Organic Photoredox Catalysis: On Our Way to the Holy Grail? *Coord. Chem. Rev.* **2024,** *500*, 215522.
443. de Groot, L. H. M.; Ilic, A.; Schwarz, J.; Wärnmark, K., Iron Photoredox Catalysis–Past, Present, and Future. *J. Am. Chem. Soc.* **2023,** *145*, 9369-9388.
444. Kjær, K. S.; Kaul, N.; Prakash, O.; Chábera, P.; Rosemann, N. W.; Honarfar, A.; Gordivska, O.; Fredin, L. A.; Bergquist, K.-E.; Häggström, L.*, et al.*, Luminescence and Reactivity of a Charge-Transfer Excited Iron Complex with Nanosecond Lifetime. *Science* **2019,** *363*, 249-253.
445. Prakash, O.; Lindh, L.; Kaul, N.; Rosemann, N. W.; Losada, I. B.; Johnson, C.; Chábera, P.; Ilic, A.; Schwarz, J.; Gupta, A. K.*, et al.*, Photophysical Integrity of the Iron(Iii) Scorpionate Framework in Iron(Iii)–Nhc Complexes with Long-Lived 2lmct Excited States. *Inorg. Chem.* **2022**.

446. Reddy Marri, A.; Marchini, E.; Cabanes, V. D.; Argazzi, R.; Pastore, M.; Caramori, S.; Gros, P. C., Record Power Conversion Efficiencies for Iron(Ii)-Nhc-Sensitized Dsscs from Rational Molecular Engineering and Electrolyte Optimization. *J. Mater. Chem. A* **2021,** *9*, 3540-3554.
447. Marri, A. R.; Marchini, E.; Cabanes, V. D.; Argazzi, R.; Pastore, M.; Caramori, S.; Bignozzi, C. A.; Gros, P. C., A Series of Iron(Ii)-Nhc Sensitizers with Remarkable Power Conversion Efficiency in Photoelectrochemical Cells**. *Chem-Eur. J.* **2021,** *27*, 16260-16269.
448. Marchini, E.; Darari, M.; Lazzarin, L.; Boaretto, R.; Argazzi, R.; Bignozzi, C. A.; Gros, P. C.; Caramori, S., Recombination and Regeneration Dynamics in Fenhc(Ii)-Sensitized Solar Cells. *Chem. Commun.* **2020,** *56*, 543-546.
449. Leis, W.; Argüello Cordero, M. A.; Lochbrunner, S.; Schubert, H.; Berkefeld, A., A Photoreactive Iron(Ii) Complex Luminophore. *J. Am. Chem. Soc.* **2022,** *144*, 1169-1173.
450. Woodhouse, M. D.; McCusker, J. K., Mechanistic Origin of Photoredox Catalysis Involving Iron(Ii) Polypyridyl Chromophores. *Journal of the American Chemical Society* **2020,** *142*, 16229-16233.
451. Rosemann, N. W.; Chábera, P.; Prakash, O.; Kaufhold, S.; Wärnmark, K.; Yartsev, A.; Persson, P., Tracing the Full Bimolecular Photocycle of Iron(Iii)–Carbene Light Harvesters in Electron-Donating Solvents. *J. Am. Chem. Soc.* **2020,** *142*, 8565-8569.
452. Kandori, H.; Kemnitz, K.; Yoshihara, K., Subpicosecond Transient Absorption Study of Intermolecular Electron Transfer between Solute and Electron-Donating Solvents. *J. Phys. Chem* **1992,** *96*, 8042-8048.
453. Castner, E. W.; Kennedy, D.; Cave, R. J., Solvent as Electron Donor: Donor/Acceptor Electronic Coupling Is a Dynamical Variable. *J. Phys. Chem. A* **2000,** *104*, 2869-2885.
454. van Willigen, H.; Jones, G.; Farahat, M. S., Time-Resolved Epr Study of Photoexcited Triplet-State Formation in Electron-Donor-Substituted Acridinium Ions. *J. Phys. Chem* **1996,** *100*, 3312-3316.
455. Martinho, J. M. G., Heavy-Atom Quenching of Monomer and Excimer Pyrene Fluorescence. *J. Phys. Chem* **1989,** *93*, 6687-6692.
456. Benniston, A. C.; Harriman, A.; Rostron, J. P., The Effect of Solvent Polarity on the Photophysical Properties of 4-Cyano-(4′-Methylthio)Diphenylacetylene: A Prototypic Donor–Acceptor System. *Phys. Chem. Chem. Phys.* **2005,** *7*, 3041-3047.
457. Benniston, A. C.; Harriman, A.; Li, P.; Rostron, J. P.; van Ramesdonk, H. J.; Groeneveld, M. M.; Zhang, H.; Verhoeven, J. W., Charge Shift and Triplet State Formation in the 9-Mesityl-10-Methylacridinium Cation. *J. Am. Chem. Soc.* **2005,** *127*, 16054-16064.
458. Schwarz, J.; Ilic, A.; Johnson, C.; Lomoth, R.; Wärnmark, K., High Turnover Photocatalytic Hydrogen Formation with an Fe(Iii) N-Heterocyclic Carbene Photosensitiser. *Chem. Commun.* **2022,** *58*, 5351-5354.
459. Rosemann, N. W.; Lindh, L.; Bolaño Losada, I.; Kaufhold, S.; Prakash, O.; Ilic, A.; Schwarz, J.; Wärnmark, K.; Chábera, P.; Yartsev, A.; Persson, P., Competing Dynamics of Intramolecular Deactivation and Bimolecular Charge Transfer Processes in Luminescent Fe(Iii) N-Heterocyclic Carbene Complexes. *Chem. Sci.* **2023,** *14*, 3569-3579.
460. Kaul, N.; Lomoth, R., The Carbene Cannibal: Photoinduced Symmetry-Breaking Charge Separation in an Fe(Iii) N-Heterocyclic Carbene. *J. Am. Chem. Soc.* **2021,** *143*, 10816-10821.
461. Ilic, A.; Schwarz, J.; Johnson, C.; de Groot, L. H. M.; Kaufhold, S.; Lomoth, R.; Wärnmark, K., Photoredox Catalysis Via Consecutive 2lmct- and 3mlct-Excitation of an Fe(Iii/Ii)–N-Heterocyclic Carbene Complex. *Chem. Sci.* **2022,** *13*, 9165-9175.
462. Takeda, H.; Koike, K.; Morimoto, T.; Inumaru, H.; Ishitani, O., Photochemistry and Photocatalysis of Rhenium(I) Diimine Complexes. In *Advances in Inorganic Chemistry*, Eldik, R. v.; Stochel, G., Eds. Academic Press: 2011; Vol. 63, pp 137-186.

463. Kuramochi, Y.; Ishitani, O.; Ishida, H., Reaction Mechanisms of Catalytic Photochemical Co2 Reduction Using Re(I) and Ru(Ii) Complexes. *Coord. Chem. Rev.* **2018,** *373*, 333-356.
464. Lucia, L. A.; Schanze, K. S., Cage Escape Yields for Photoinduced Bimolecular Electron Transfer Reactions of Re(I) Complexes. *Inorg. Chim. Acta* **1994,** *225*, 41-49.
465. Lucia, L. A.; Abboud, K.; Schanze, K. S., Outer Sphere Metal-to-Ligand Charge Transfer in Organometallic Ion Pairs. *Inorg. Chem.* **1997,** *36*, 6224-6234.
466. Rodenberg, A.; Orazietti, M.; Mosberger, M.; Bachmann, C.; Probst, B.; Alberto, R.; Hamm, P., Quinones as Reversible Electron Relays in Artificial Photosynthesis. *ChemPhysChem* **2016,** *17*, 1321-1328.
467. Bachmann, C.; Probst, B.; Guttentag, M.; Alberto, R., Ascorbate as an Electron Relay between an Irreversible Electron Donor and Ru(Ii) or Re(I) Photosensitizers. *Chem. Commun.* **2014,** *50*, 6737-6739.
468. Rodenberg, A.; Orazietti, M.; Probst, B.; Bachmann, C.; Alberto, R.; Baldridge, K. K.; Hamm, P., Mechanism of Photocatalytic Hydrogen Generation by a Polypyridyl-Based Cobalt Catalyst in Aqueous Solution. *Inorg. Chem.* **2015,** *54*, 646-657.
469. Probst, B.; Guttentag, M.; Rodenberg, A.; Hamm, P.; Alberto, R., Photocatalytic H2 Production from Water with Rhenium and Cobalt Complexes. *Inorg. Chem.* **2011,** *50*, 3404-3412.
470. Oppelt, K.; Fernández-Terán, R.; Pfister, R.; Hamm, P., Geminate Recombination Versus Cage Escape in the Reductive Quenching of a Re(I) Carbonyl Complex on Mesoporous Zro2. *J. Phys. Chem. C* **2019,** *123*, 19952-19961.
471. Kisch, H.; Duemler, W.; Chiorboli, C.; Scandola, F.; Salbeck, J.; Daub, J., Charge-Transfer Complexes of Metal Dithiolenes. Ix. Photoinduced Electron Transfer within Metal Dithiolene-Viologen Ion Pairs Studied by Flash Photolysis. *J. Phys. Chem* **1992,** *96*, 10323-10326.
472. Mackay, I.; Cai, L. Z.; Kirk, A. D.; McAuley, A., Quenching of Triplet State Tetrakis(M-Pyrophosphito-Pp')Diplatinate(Ii) by Nickel(Ii) Macrocyclic and Tris-Diimine Complexes. *Inorg. Chem.* **1999,** *38*, 3628-3633.
473. Harriman, A.; Porter, G.; Searle, N., Reversible Photo-Oxidation of Zinc Tetraphenylporphine by Benzo-1,4-Quinone. *J. Chem. Soc., Faraday Trans. 2* **1979,** *75*, 1515-1521.
474. Gore, B. L.; Harriman, A.; Richoux, M.-C., Influence of Ionic Strength on the Efficiency of Charge Separation. *J. Photochem.* **1982,** *19*, 209-214.
475. Hurst, J. K.; Thompson, D. H. P.; Connolly, J. S., Photooxidation of Tetraanionic Sensitizer Ions by Dihexadecyl Phosphate Vesicle-Bound Viologens. *J. Am. Chem. Soc.* **1987,** *109*, 507-515.
476. Limburg, B.; Bouwman, E.; Bonnet, S., Effect of Liposomes on the Kinetics and Mechanism of the Photocatalytic Reduction of Methyl Viologen. *J. Phys. Chem. B* **2016,** *120*, 6969-6975.
477. Turro, N. J., Molecular Structure as a Blueprint for Supramolecular Structure Chemistry in Confined Spaces. *Proc. Natl. Acad. Sci. USA* **2005,** *102*, 10766-10770.
478. Harriman, A.; Porter, G.; Wilowska, A., Photoredox Properties of Zinc Porphyrin–Viologen Complexes. *J. Chem. Soc., Faraday Trans. 2* **1984,** *80*, 191-204.
479. Mandal, K.; Hoffman, M. Z., Solution Medium Control of the Photoredox Yield in the Ru(Bpy)32+/Methyl Viologen/Edta System. *J. Phys. Chem* **1984,** *88*, 185-187.
480. Hoffman, M. Z., Cage Escape Yields from the Quenching of Excited Tris(Bipyridyl)Ruthenium(2+) by Methylviologen in Aqueous Solution [Erratum to Document Cited in Ca109(2):14476r]. *J. Phys. Chem* **1991,** *95*, 2606-2606.
481. Yonemoto, E. H.; Saupe, G. B.; Schmehl, R. H.; Hubig, S. M.; Riley, R. L.; Iverson, B. L.; Mallouk, T. E., Electron-Transfer Reactions of Ruthenium Trisbipyridyl-Viologen Donor-Acceptor Molecules: Comparison of the Distance Dependence of Electron Transfer-Rates in the Normal and Marcus Inverted Regions. *J. Am. Chem. Soc.* **1994,** *116*, 4786-4795.

482. McNaught, A. D.; Wilkinson, A., Compendium of Chemical Terminology: Iupac Recommendations. *the Gold book* **1997**.
483. Bard, A. J.; Faulkner, L. R.; White, H. S., *Electrochemical Methods: Fundamentals and Applications*. John Wiley & Sons: 2022.
484. Marcus, R. A., Nobel Lecture. Nobelprize.Org. Nobel Prize Outreach <Https://Www.Nobelprize.Org/Prizes/Chemistry/1992/Marcus/Lecture/. **1992**.
485. Kerr, J. A., Bond Dissociation Energies by Kinetic Methods. *Chem. Rev.* **1966,** *66*, 465-500.
486. Anne, A.; Fraoua, S.; Grass, V.; Moiroux, J.; Savéant, J.-M., The Role of Homolytic Bond Dissociation Energy in the Deprotonation of Cation Radicals. Examples in the Nadh Analogues Series. *J. Am. Chem. Soc.* **1998,** *120*, 2951-2958.
487. Richards, B. S.; Hudry, D.; Busko, D.; Turshatov, A.; Howard, I. A., Photon Upconversion for Photovoltaics and Photocatalysis: A critical review. *Chem. Rev.* **2021,** *121*, 9165-9195.
488. Pfund, B.; Steffen, D. M.; Schreier, M. R.; Bertrams, M.-S.; Ye, C.; Börjesson, K.; Wenger, O. S.; Kerzig, C., Uv Light Generation and Challenging Photoreactions Enabled by Upconversion in Water. *J. Am. Chem. Soc.* **2020,** *142*, 10468-10476.
489. Wang, C.; Reichenauer, F.; Kitzmann, W. R.; Kerzig, C.; Heinze, K.; Resch-Genger, U., Efficient Triplet-Triplet Annihilation Upconversion Sensitized by a Chromium(Iii) Complex Via an Underexplored Energy Transfer Mechanism. *Angew. Chem. Int. Ed.* **2022,** *61*, e202202238.
490. Uji, M.; Zähringer, T. J. B.; Kerzig, C.; Yanai, N., Visible-to-Uv Photon Upconversion: Recent Progress in New Materials and Applications. *Angew. Chem. Int. Ed.* **2023,** *62*, e202301506.
491. Glaser, F.; Schmitz, M.; Kerzig, C., Coulomb Interactions for Mediator-Enhanced Sensitized Triplet–Triplet Annihilation Upconversion in Solution. *Nanoscale* **2024**.
492. Wenger, O. S., Photoactive Complexes with Earth-Abundant Metals. *J. Am. Chem. Soc.* **2018,** *140*, 13522-13533.
493. Sinha, N.; Wenger, O. S., Photoactive Metal-to-Ligand Charge Transfer Excited States in 3d6 Complexes with Cr0, Mni, Feii, and Coiii. *J. Am. Chem. Soc.* **2023,** *145*, 4903-4920.
494. Kitzmann, W. R.; Bertrams, M.-S.; Boden, P.; Fischer, A. C.; Klauer, R.; Sutter, J.; Naumann, R.; Förster, C.; Niedner-Schatteburg, G.; Bings, N. H.*, et al.*, Stable Molybdenum(0) Carbonyl Complex for Upconversion and Photoredox Catalysis. *J. Am. Chem. Soc.* **2023,** *145*, 16597-16609.
495. Kitzmann, W. R.; Heinze, K., Charge-Transfer and Spin-Flip States: Thriving as Complements. *Angew. Chem. Int. Ed.* **2023,** *62*, e202213207.
496. Chan, A. Y.; Ghosh, A.; Yarranton, J. T.; Twilton, J.; Jin, J.; Arias-Rotondo, D. M.; Sakai, H. A.; McCusker, J. K.; MacMillan, D. W. C., Exploiting the Marcus Inverted Region for First-Row Transition Metal–Based Photoredox Catalysis. *Science* **2023,** *382*, 191-197.
497. Kunnus, K.; Guo, M.; Biasin, E.; Larsen, C. B.; Titus, C. J.; Lee, S. J.; Nordlund, D.; Cordones, A. A.; Uhlig, J.; Gaffney, K. J., Quantifying the Steric Effect on Metal–Ligand Bonding in Fe Carbene Photosensitizers with Fe 2p3d Resonant Inelastic X-Ray Scattering. *Inorg. Chem.* **2022,** *61*, 1961-1972.
498. Moonshiram, D.; Gimbert-Suriñach, C.; Guda, A.; Picon, A.; Lehmann, C. S.; Zhang, X.; Doumy, G.; March, A. M.; Benet-Buchholz, J.; Soldatov, A.*, et al.*, Tracking the Structural and Electronic Configurations of a Cobalt Proton Reduction Catalyst in Water. *J. Am. Chem. Soc.* **2016,** *138*, 10586-10596.
499. Zhao, J.; De Kreijger, S.; Troian-Gautier, L.; Yu, J.; Hu, W.; Zhang, X.; Elias, B.; Moonshiram, D., Deciphering the Photophysical Kinetics, Electronic Configurations and Structural Conformations of Iridium–Cobalt Hydrogen Evolution Photocatalysts. *Chem. Commun.* **2022,** *58*, 8057-8060.
500. Chen, L. X.; Shaw, G. B.; Novozhilova, I.; Liu, T.; Jennings, G.; Attenkofer, K.; Meyer, G. J.; Coppens, P., Mlct State Structure and Dynamics of a Copper(I) Diimine Complex Characterized by

Pump−Probe X-Ray and Laser Spectroscopies and Dft Calculations. *J. Am. Chem. Soc.* **2003,** *125*, 7022-7034.
501. Canton, S. E.; Zhang, X.; Zhang, J.; van Driel, T. B.; Kjaer, K. S.; Haldrup, K.; Chabera, P.; Harlang, T.; Suarez-Alcantara, K.; Liu, Y.*, et al.*, Toward Highlighting the Ultrafast Electron Transfer Dynamics at the Optically Dark Sites of Photocatalysts. *J. Phys. Chem. Lett.* **2013,** *4*, 1972-1976.
502. Canton, S. E.; Kjær, K. S.; Vankó, G.; van Driel, T. B.; Adachi, S.-i.; Bordage, A.; Bressler, C.; Chabera, P.; Christensen, M.; Dohn, A. O.*, et al.*, Visualizing the Non-Equilibrium Dynamics of Photoinduced Intramolecular Electron Transfer with Femtosecond X-Ray Pulses. *Nature Comm.* **2015,** *6*, 6359.
503. Marian, C. M., Spin–Orbit Coupling and Intersystem Crossing in Molecules. *Wires. Comput. Mol. Sci.* **2012,** *2*, 187-203.
504. Inada, T. N.; Miyazawa, C. S.; Kikuchi, K.; Yamauchi, M.; Nagata, T.; Takahashi, Y.; Ikeda, H.; Miyashi, T., Effects of Molecular Charge on Photoinduced Electron-Transfer Reactions. *J. Am. Chem. Soc.* **1999,** *121*, 7211-7219.
505. Ford, W. E.; Rodgers, M. A. J., Electron Transfer Reactions Mediated by Acridine Triplet State in Aqueous Solutions — Triplet Energy Transfer from Ru(Bipy)32+ and Photosensitized Electron Transfer from Para-Substituted Phenols to Methyl Viologen. *J. Photoch. Photobio. A* **1991,** *59*, 73-80.
506. Borsarelli, C. D.; Montejano, H. A.; Cosa, J. J.; Previtali, C. M., Medium Effects on the Photochemical Reaction between Pyrene and Indole. A Laser Flash Photolysis Study. *J. Photoch. Photobio. A* **1995,** *91*, 13-19.
507. Shigeya, N.; Nobuyoshi, S.; Hiroki, K.; Yoshizo, S.; Takashi, T.; Hiroshi, K., Free Radicals Produced from the Derivatives of Pyrylium Salts in Solution by Photoillumination. *B. Chem. Soc. Jpn.* **1985,** *58*, 2600-2607.
508. Manoj, N.; Gopidas, K. R., Photophysical and Electron-Transfer Properties of a Few 2,6-Dimethyl-4-Arylpyrylium Derivatives. *J. Photoch. Photobio. A* **1999,** *127*, 31-37.
509. Manoj, N.; Ajit Kumar, R.; Gopidas, K. R., Photophysical and Electron Transfer Studies of a Few 2,6-Dimethyl-4-(Alkylphenyl)Pyrylium and Thiopyrylium Derivatives. *J. Photoch. Photobio. A* **1997,** *109*, 109-118.
510. Bignozzi, C. A.; Scandola, F., Cyano-Bridged Ruthenium(Ii)/Platinum(Ii) Complexes: Synthesis, Photophysical Properties, and Excited-State Redox Behavior. *Inorg. Chem.* **1984,** *23*, 1540-1545.
511. Shan, B.; Schmehl, R., Photochemical Generation of Strong One-Electron Reductants Via Light-Induced Electron Transfer with Reversible Donors Followed by Cross Reaction with Sacrificial Donors. *J. Phys. Chem. A* **2014,** *118*, 10400-10406.
512. Ülveczky, A.; Horváth, A., Photooxidation of Ru (Bpy) (Cn)42− and Ru (Dmbpy) (Cn)42−. *Inorg. Chim. Acta* **1995,** *236*, 173-176.
513. Akasheh, T. S.; Al-Rawashdeh, N. A. F., Efficient Production of Methyl Viologen Cation Radicals Using Ruii Systems. *J. Photoch. Photobio. A* **1990,** *54*, 283-292.
514. Shioyama, H.; Masuhara, H.; Mataga, N., Radical Yield in Electron Transfer Quenching of the Excited Tris(2,2′-Bipyridine)Ruthenium(Ii) Complex. *Chem. Phys. Lett.* **1982,** *88*, 161-165.
515. Darwent, J. R.; Kalyanasundaram, K., Electron-Transfer Reactions of Quinones, Hydroquinones and Methyl Viologen, Photosensitized by Tris(2,2′-Bipyridine)-Ruthenium(Ii). *J. Chem. Soc., Faraday Trans. 2* **1981,** *77*, 373-382.
516. Khnayzer, R. S.; McCusker, C. E.; Olaiya, B. S.; Castellano, F. N., Robust Cuprous Phenanthroline Sensitizer for Solar Hydrogen Photocatalysis. *J. Am. Chem. Soc.* **2013,** *135*, 14068-14070.

517. Shan, B.; Baine, T.; Ma, X. A. N.; Zhao, X.; Schmehl, R. H., Mechanistic Details for Cobalt Catalyzed Photochemical Hydrogen Production in Aqueous Solution: Efficiencies of the Photochemical and Non-Photochemical Steps. *Inorg. Chem.* **2013,** *52*, 4853-4859.
518. Shylin, S. I.; Pavliuk, Mariia V.; D'Amario, L.; Fritsky, I. O.; Berggren, G., Photoinduced Hole Transfer from Tris(Bipyridine)Ruthenium Dye to a High-Valent Iron-Based Water Oxidation Catalyst. *Faraday Discuss.* **2019,** *215*, 162-174.
519. Lecomte, J.-P.; Kirsch-De Mesmaeker, A.; Feeney, M. M.; Kelly, J. M., Ruthenium(Ii) Complexes with 1,4,5,8,9,12-Hexaazatriphenylene and 1,4,5,8-Tetraazaphenanthrene Ligands: Key Role Played by the Photoelectron Transfer in DNA Cleavage and Adduct Formation. *Inorg. Chem.* **1995,** *34*, 6481-6491.
520. Sinha, N.; Pfund, B.; Wegeberg, C.; Prescimone, A.; Wenger, O. S., Cobalt(Iii) Carbene Complex with an Electronic Excited-State Structure Similar to Cyclometalated Iridium(Iii) Compounds. *J. Am. Chem. Soc.* **2022,** *144*, 9859-9873.
521. Richoux, M.-C.; Harriman, A., Influence of Electrostatic Forces Upon the Efficiency of Charge Separation for the Zinc Porphyrin/Methyl Viologen System. *J. Chem. Soc., Faraday Trans. 1* **1982,** *78*, 1873-1885.

For TOC Use Only